SYNTHESIS AND CHARACTERIZATION OF MODIFIED LEAD CALCIUM TITANATE CERAMICS AND LASER ABLATED THIN FILMS

A

Thesis Submitted for the

Award of the Degree of

DOCTOR OF PHILOSOPHY

By

SARABJIT SINGH

to the

School of Physics & Materials Science

Thapar Institute of Engineering & Technology

(Deemed University)

Patiala - 147004

April - 2005

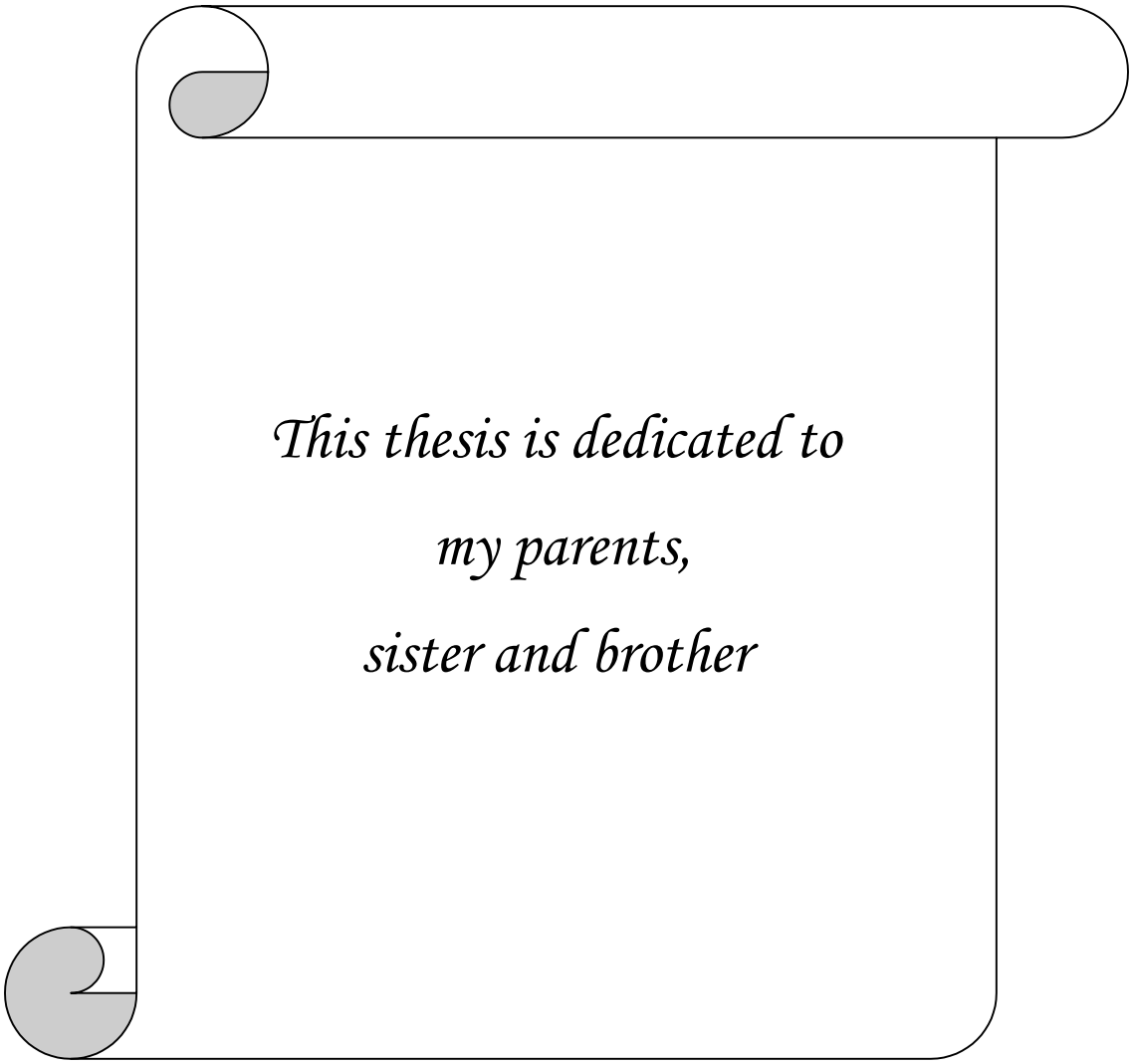
This thesis is dedicated to
my parents,
sister and brother

CERTIFICATE

This is to certify that the work embodied in this thesis entitled "***Synthesis and Characterization of Modified Lead Calcium Titanate Ceramics and Laser Ablated Thin Films***" which is being submitted by **Mr. Sarabjit Singh** in fulfillment of the requirements for the award of the degree of **Doctor of Philosophy** in **School of Physics and Materials Science** of **Thapar Institute of Engineering and Technology (Deemed University), Patiala** is a record of candidate's own work carried out by him under our supervision and guidance. The matter presented in this thesis has not been submitted in part or full for the award of any degree in any other university or institute.

19/4/05

Professor K.K. Raina
Dean Research and Sponsored Projects
School of Physics and Materials Science
Thapar Institute of Engineering and Technology
(Deemed University)
Patiala - 147004
INDIA
rainatietp@yahoo.com

19.4.2005

Dr. Chandra Prakash
Scientist 'E'
Head, Electroceramics Group
Solid State Physics Laboratory
Lucknow Road, Timarpur
Delhi - 110054
INDIA
prakash@ssplnet.org

ACKNOWLEDGEMENTS

Behind the work compiled in these pages lie the steady encouragement, fruitful guidance and constant enthusiasm of my research supervisors **Dr. Chandra Prakash** and **Prof. K.K. Raina**. I owe the greatest debt of gratitude to them for suggesting the research problem followed by meticulous suggestions, ever-willing help and the freedom extended to me during the period of my research.

I take the privilege to express my deep sense of gratitude to **Dr. H.P. Vyas,** Director, S.S.P.L., Delhi for his kind support and providing me a lot of opportunity for the interaction with national and international scientists in the various conferences and seminars held during the tenure of my Ph.D. I am thankful to **Prof. Vikram Kumar**, former Director, S.S.P.L., Delhi for giving me the opportunity to join the flourishing Electroceramics group. I must acknowledge **Prof. S.C. Saxena**, Director T.I.E.T., Patiala for granting me the permission to register for Ph.D. programme in his meritorious institute. I am also thankful to **Prof. N.K. Verma**, Head of the Department, S.P.M.S., T.I.E.T., Patiala for giving constant encouragement throughout my Ph.D. period.

I acknowledge my deep indebtedness to **Dr. O.P. Thakur**, Sc. 'D', SSPL, Delhi for constant inspiration during the research period. I have always found him to be ready to help at any moment, may be either in the field of research or in any day-to-day problem.

I feel proud to have the distinction of being one of the research fellows of the leading "Electroceramics Group" actively engaged in the area of ferroelectric materials. I feel that I have learnt a lot not only in the field of research but have also added new experiences to my life, which has really given me the confidence and positive attitude that broadened my vision. I express my loyal venerable thanks and heartfelt gratitude to my group members, **Dr.** (**Mrs.) L. Radhapiyari Devi**, Sc. 'C', **Mr. Sanjay Pandey**, Sc. 'C', **Mr. Sandeep Mahajan**, JRF and **Mr. Madan Thakur**, Technician for their kind co-operation and unclenched support during my stay in the group. Also, I thank the families of members of this group for making me feel homely throughout my research work. Help extended by **Mr**. **D.S. Rawal** and **Mr. Devendra Verma** for SEM, by **Mr. Anshu Goyal** for XRD and by **Mr. K. Zimik** for AFM is thankfully acknowledged.

My deep sense of gratitude to **Dr. M. Vijayakumar**, Sc. 'F', D.M.R.L., Hyderabad for motivating me to take the research as one of the goal of my life.

Financial support in the form of research fellowship through the Defence Research and Development Organisation (D.R.D.O.), Ministry of Defence is greatly acknowledged. I am particularly thankful to the whole scientific and technical staff of the sister research group of S.S.P.L. for their co-operation throughout my research work.

I am also thankful to all my friends especially **Jay Prakash, Ramesh, Karnail, Shweta, Mita, Pawan, Pankaj, Parveen, Mamta, Rajesh, Divya**, **Upendra** and **Vanya** for helping me in various ways.

I am deeply indebted to my parents for their moral support and encouragement.

Sarabjit Singh

Solid State Physics Laboratory
(Defence R & D Organisation)
Lucknow Road, Delhi - 110054
(sarabjit6@rediffmail.com)

PREFACE

Lead titanate ($PbTiO_3$) [usually referred as PT] ceramics exhibit many attractive properties. These attributes make them attractive for devices in many electronic applications in the form of bulk, thin film, composite and single crystal. Because of simple perovskite structure, PT has been widely used as a model system to understand various phenomena related to cubic to tetragonal phase transition, which takes place at about 490^oC from high temperature cubic phase (Pm3m) to a tetragonal (P4mm) ferroelectric phase and is accompanied by an abrupt anomaly in electric permittivity, the spontaneous polarization, specific heat etc. In its tetragonal form, the lattice anisotropy (c/a) is 1.063. On cooling through Curie temperature (T_c), large anisotropy of this ceramic material becomes fragile. In addition, it is difficult to pole it due to high coercive force. However, if PT is doped with isovalent or aliovalent dopants, the c/a ratio decreases and then modified PT can be synthesized using standard processes. Among the dopants, the substitution of alkaline and rare earth metals for lead results in the higher electromechanical anisotropy (k_t/k_p). This large ratio of thickness to lateral electromechanical-coupling coefficient in PT is useful in high frequency transducer geometries where lateral coupling between elements is not desired.

The addition of calcium or samarium (as dopants or modifiers) into PT results in a higher k_t/k_p ratio as compared to lead zirconate titanate (PZT) ceramics. This property widely makes it possible that PT based materials can be used for high-frequency applications such as Surface Acoustic Wave (SAW) devices and piezoelectric transformers. Moreover, in the calcium modified lead titanate (PCT) materials, substitution of Ca^{2+} results in decreasing cubic to tetragonal phase transformation temperature and with suitable amount it can be brought down to room temperature. Lowering of T_c results in material (PCT ceramics) with higher dielectric constant and larger remnant polarization at room temperature. Because of these remarkable characteristics, we believe that modified PCT ceramics might be a potential candidate in many electrical and electronic applications. It is generally considered that about 24 mol% concentration of calcium allows cracking to be avoided while still having good ferroelectric properties suitable for many applications. Also 2 mol% Mn^{4+} ion substitution in PT ceramics improves the densification. Hence various modified compositions of PCT ceramics (with the

substitution of Sm, La and Ta) were prepared to investigate the further improvement on various properties of PCT ceramics with fixed amount of Ca (24 mol%) and Mn (2 mol%).

In the present work, an attempt has been made to prepare modified lead calcium titanate ceramics and simultaneously characterize them for various physical properties like structural, dielectric, ferroelectric and piezoelectric etc. Thus following compositions were prepared and processed using conventional dry ceramic technique:

1. $Pb_{0.76-x}Sm_xCa_{0.24}Mn_{0.02}Ti_{0.98}O_3$.
2. $Pb_{0.76-x}La_xCa_{0.24}Mn_{0.02}Ti_{0.98}O_3$.
3. $Pb_{0.76-3x/2}Sm_xCa_{0.24}Mn_{0.02}Ti_{0.98}O_3$.
4. $Pb_{0.76-3x/2}La_xCa_{0.24}Mn_{0.02}Ti_{0.98}O_3$.

In all the above series, x was varied from 0 to 0.1 in steps of 0.02.

5. $Pb_{0.76}Ca_{0.24}Mn_{0.02}Ti_{0.98-5x/4}Ta_xO_3$; x = 0-0.04 (in steps of 0.01).

New developments and innovative ideas in the materials processing have often led to the improved and novel material with interesting and useful properties, and/or new technologies which are faster, better, cheaper and greener (e.g. recent innovations in the areas of microwave processing and mechanochemical alloying of ceramics). Keeping these advantages in mind, some selected compositions were prepared using microwave sintering and mechanochemical alloying techniques and significant improvement in properties was achieved. Review of literature reveals that very few results are reported for the PCT ceramics using these novel techniques.

Hence we also made an attempt to prepare the following compositions:

6. $Pb_{0.76-3x/2}Sm_xCa_{0.24}Mn_{0.02}Ti_{0.98}O_3$; x = 0-0.08 (in steps of 0.02).
7. $Pb_{0.76-x}Sm_xCa_{0.24}Mn_{0.02}Ti_{0.98}O_3$; x = 0.06.

The composition (6) was prepared using microwave sintering while composition (7) by mechano-chemical alloying.

PCT thin films have been previously prepared by various methods involving RF sputtering and Sol-Gel. The pulsed laser deposition (PLD) technique has been recently used to prepare multicomponent oxides due to the congruence between the film and target compositions. In particular, it has been successfully applied to prepare ferroelectric thin film oxides including PZT films. PLD has the potential of providing highly oriented and pyrochlore-free PT perovskite phase. In the present study, thin film of one typical

composition ($Pb_{0.66}Sm_{0.08}Ca_{0.24}Mn_{0.02}Ti_{0.98}O_3$) was also attempted by laser ablation technique and characterized to study various structural and electrical properties.

The research work carried out for this Ph.D. thesis has been divided in eight chapters as summarized below briefly: -

In **Chapter I**, we describe a brief review of the research and development work that has been carried out till recently in solid ferroelectric materials in general and lead calcium titanate based ceramics in particular. The aim of carrying out the present work including the criteria of selection of various compositions, herein studied, scope of these investigations have also been discussed.

Chapter II deals with various methods of sample preparation and characterization techniques used for studying physical properties (like structural, dielectric, ferroelectric and piezoelectric) of modified PCT ceramics. The ceramic samples were prepared both in bulk and thin film form. For bulk preparation, three techniques namely conventional dry ceramic method, microwave sintering and mechanochemical alloying were used. Thin films were prepared by pulsed laser deposition technique. The details of experimental techniques, various characterization equipments and their working details are also given in this chapter.

Results and discussion of concerning structural properties of all the individual series prepared by conventional dry ceramic technique is given in **chapter III**. Theoretical explanation of experimental results for single-phase formation of polycrystalline materials and their crystal structure, density, variation of lattice parameters (calculated form the X-ray diffractrometry study) and microstructural analysis (like grain size and shape) are discussed. This chapter also includes the detailed study of sintering behaviour of the green sample (during entire heat treatment) using dilatometer.

In **chapter IV**, we present the studies of electrical (dielectric and ferroelectric) properties of the samples synthesized by conventional dry ceramic technique. The dielectric constant (ε') and loss ($\tan\delta$) have been investigated over a wide frequency (100 Hz - 1 MHz) and temperature (25^oC - 450^oC) range. The effect of substituents (viz; La, Sm and Ta) on the Curie temperature has been studied. Temperature variation of dielectric behaviour provided an insight to study the diffusivity (γ) trend. The Curie temperature was also observed by studying the thermal expansion behaviour of the sintered samples

using dilatometer. The results have been interpreted on the basis of theoretical models and hysteresis behaviour of the samples.

Chapter V discusses the piezoelectric properties [like piezoelectric charge coefficients (d_{33}, d_{31}), voltage coefficients (g_{33}, g_{31}), piezoelectric anisotropy (d_{33}/d_{31}, g_{33}/g_{31}), thickness electromechanical coupling coefficient (k_t), planar electromechanical coupling coefficient (k_p) and electromechanical anisotropy (k_t/k_p)] at room temperature in all the samples synthesized by conventional dry ceramic technique. The effects of various substituted elements and their composition on the behaviour of these properties is explained.

The results obtained using microwave sintering and mechano-chemical alloying processes for some of the selected compositions in order to study structural, electrical and piezoelectric properties have been discussed in **chapter VI**. These novel processes were adopted to observe the advantages of modified PCT ceramics and a comparison of the properties with those obtained by conventional techniques. Different mechanisms have been given to explain the observed behaviour of the various properties in our samples.

Chapter VII describes the experimental details of the PLD technique, thin film deposition using this method and the characterization of structural and electrical properties of the films. The targets were prepared by using conventional dry ceramic technique. The studied properties include perovskite-phase formation, microstructure, P-E loop, I-V and C-V characteristics. The results have been discussed in detail.

The work has been finally concluded in **chapter VIII**. It highlights the suitability of the composition to give desired properties and can be explored for various device applications. Recommendations for the future work have also been given in this chapter.

LIST OF PUBLICATIONS

In Journals

1. Influence of Ta Substitution on Structural and Dilatometric Behaviour of PCT Ceramics, **Sarabjit Singh**, O.P. Thakur, Chandra Prakash and K.K. Raina, *Ferroelectrics (Lett. Section),* 31 (2004) 141-148.
2. Electrical Properties of Tantalum Modified PCT Ceramics, **Sarabjit Singh**, O.P. Thakur, Chandra Prakash and K.K. Raina, *J. Pure & Appl. Ultrasonics,* 26 (2004) 35-39.
3. Improved Properties of Sm Substituted PCT Ceramics using Microwave Sintering, **Sarabjit Singh**, O.P. Thakur, D.S. Rawal, Chandra Prakash and K.K. Raina, *Mater. Lett.,* 59 (2005) 768-772.
4. Dilatometric and Dielectric Behavior of Sm Modified PCT Ceramics, **Sarabjit Singh**, O.P. Thakur, Chandra Prakash and K.K. Raina, *Physica B,* 355 (2005) 280-285.
5. Improved Piezoelectric Properties via Mechano-chemical Activation in Modified PCT Ceramics, **Sarabjit Singh**, O.P. Thakur, Chandra Prakash and K.K. Raina, *Mater. Chem. & Phys*. (in press)
6. Dielectric and Piezoelectric Properties of Microwave Processed Sm Substituted PCT Ceramics, **Sarabjit Singh**, O.P. Thakur and Chandra Prakash, *Journal of Physics D: Appl. Phys.* (in press)
7. Structural and Electrical Properties of Lanthanum Substituted Lead Titanate Ceramics, **Sarabjit Singh**, O.P. Thakur, Chandra Prakash and K.K. Raina, *Phase Transitions.* (in press)
8. Sintering Behaviour of Samarium Modified Lead Calcium Titanate Ceramics, **Sarabjit Singh**, O.P. Thakur, Chandra Prakash and K.K. Raina, *Ferroelectrics.* (in press)
9. Influence of Ta Substitution on the Dielectric Behaviour of PCT Ceramics, **Sarabjit Singh**, O.P. Thakur and Chandra Prakash, *Ferroelectrics.* (in press)

10. Structural, Thermal, Dielectric, Ferroelectric and Piezoelectric Behaviour of Modified $PbTiO_3$ Ceramics, **Sarabjit Singh**, O.P. Thakur, Chandra Prakash, *J. Mater. Sci.* (communicated)
11. Dielectric Behaviour and Improved Anisotropy in Piezoelectric Properties of Modified Lead Titanate Ceramics, **Sarabjit Singh**, O.P. Thakur, Chandra Prakash and K.K. Raina. (to be communicated)
12. Growth and Characterization of Laser Ablated Sm Modified PCT Thin Films, **Sarabjit Singh**, O.P. Thakur, S.K. Pandey, Chandra Prakash and K.K. Raina. (to be communicated)

In Conferences

1. Dielectric and Ferroelectric Properties of Lead Titanate Substituted with Calcium and Samarium, **Sarabjit Singh**, O.P. Thakur, Chandra Prakash and K.K. Raina, *Proceedings of National Conference on Advances in Condensed Matter Physics* (ACMP-2005), Feb 11-12, 2005, T.I.E.T., Patiala, pp. 239-243.
2. Influence of Lanthanum on the Dielectric Properties of Ca-modified PT Ceramics, **Sarabjit Singh**, O.P. Thakur, Chandra Prakash and K.K. Raina, *International Conference on Smart Materials, Structures and Systems*, July 28-30, 2005 (abstract accepted).

(Other Publications- not included in the thesis)

In Journals

1. Influence of Liquid Phase Additives on Structural and Sintering Behaviour of Samarium Modified Lead Titanate Ceramics, **Sarabjit Singh**, O.P. Thakur and Chandra Prakash, *J. Electroceramics*, 11 (2003) 67-72.
2. Study of Lead Magnesium Niobate–Lead Titanate Ceramics for Piezo-Actuator Applications, Pawan Kumar, **Sarabjit Singh**, O.P. Thakur, Chandra Prakash and T.C. Goe1, *Jpn. J. Appl. Phys. Part* 1, 43 (2004) 1501-1506.
3. Synthesis, Structural and Electrical Properties of La Modified PZT System, **Sarabjit Singh**, O.P. Thakur and Chandra Prakash, *Defence Science Journal.* (in press)

4. Structural and Electrostrictive Behaviour in PMN-PT (68:32) Ceramics, Pawan Kumar, Seema Sharma, **Sarabjit Singh**, O.P. Thakur, Chandra Prakash and T.C. Goel, *Ferroelectrics*. (in press)

In Conferences

1. Structural and Thermal Properties of Modified Lead Titanate Doped with Bi^{3+} and Li^{1+}, **Sarabjit Singh**, O.P. Thakur, A.R. James and Chandra Prakash, *Materials Research Society of India (MRSI) Hyderabad*, Feb 9-10, 2002.

2. Electrical Properties of PLZT (7/60/40) Ceramics: Sintered in Air and Oxygen, **Sarabjit Singh**, O.P. Thakur and Chandra Prakash, *National Seminar on Ferroelectric and Dielectrics* (NSFD)-XII, IISC Bangalore (India), Dec 16-18, 2002.

3. Dielectric Properties of PLZT system, **Sarabjit Singh**, O.P. Thakur, Chandra Prakash and K.K. Raina, *National Conference on Materials & Related Technologies (NCMRT) Proceedings*, November 19-20, 2003, TIET, Patiala (India), pp 111-115.

4. Phase Formation and Dielectric Behaviour Study of PMN-PT (68:32) Bulk and Thin Films, Pawan Kumar, Seema Sharma, T.C. Goel, **Sarabjit Singh**, O.P. Thakur and Chandra Prakash, *National Conference on Materials & Related Technologies Proceedings*, November 19-20, 2003, TIET, Patiala (India), pp 23-28.

5. Electrical Properties of Samarium Modified Lead Titanate Ceramics with Liquid Phase Additives, **Sarabjit Singh,** O.P. Thakur and Chandra Prakash, *National Seminar on Ferroelectric and Dielectrics (*NSFD)-XIII, Nov 23-25, 2004, Delhi University, Delhi (India).

TABLE OF CONTENTS

CHAPTER II EXPERIMENTAL ASPECTS

LIST OF FIGURES

CHAPTER IV

CHAPTER V

CHAPTER VI

CHAPTER VII

LIST OF TABLES

CHAPTER VI

CHAPTER VII

Chapter I

INTRODUCTION

1.1 Background

Field of ceramics has been identified as one of the primary fields where processing improvements and more advanced products can be anticipated. Most of the industrialized countries of the world have invested heavily in the manufacturing (processing) of new ceramic materials; this has led to the production of lower priced ceramics with better properties. Due to the large variety of chemical, electrical, biological and mechanical properties that ceramics presently exhibit, there is almost no social and industrial application without ceramics. Table 1.1 gives the brief description of various classes of ceramics and fields of application.

Table - 1.1

Classes of Ceramics and Fields of Application

Materials Group	Property	Application
Traditional Ceramics	Compressive Strength	Bricks
	Density + Strength	Ceramic Hollow Ware
	Density + Wear Resistance	Structural Clay Products
	Heat and Corrosion Resistance	Refractories
Structural Ceramics	Hardness	Grinding Grits and Disks
	Strength + Toughness	Engineering Ceramics
	Biocompatibility, Bioactivity	Bioceramics
	Nuclear Properties	Nuclear Ceramics
	Corrosion Resistance, Catalytic Properties	Chemocermics
Functional Ceramics	Electric Resistivity, Dielectric Properties	Electroceramics
	Magnetic Susceptibility	Magnetoceramics
	Anisotropic Optical properties	Optoceramics

In the electronic and manufacturing industries, as well as in technologies that require materials sustaining extremely high temperatures and corrosive environments, high-tech ceramics play the role of key materials; novel technologies, processes and machines are finally made possible only by means of especially tailored ceramics [1-3].

Ceramics are different from glasses and single crystals as they are composed of an aggregate of randomly oriented crystallites intimately bonded together to form a solid. Although crystallites possess an ordered internal structure like a crystal but ceramics have an isotropic character and are polycrystalline materials. The area of interest of the present work is the electronic ceramics, which are highly specialized class of materials, termed as electroceramics. Their properties are predominantly controlled by their composition in addition to processing conditions & complexities of shape. Various types of electronic ceramics are insulators, ferrites, capacitors, PTC materials, ferroelectrics, pyroelectrics, piezoelectrics, electro-optic materials etc.

From the analysis of symmetry elements [4], it is found that symmetry operations can be combined in 32 different ways, resulting 32 crystal classes. Out of these 32, only eleven crystal classes have a center of symmetry and 21 are non-centro symmetric. Out of the remaining 21 non centro-symmetric classes, 20 show the phenomenon of piezoelectricity. The remaining one non-centro symmetric class left does not show any piezoelectric effect because of the combined effect of symmetry elements [5]. Piezoelectric effect is the phenomenon of creation of electric polarization on the application of external stress and vice-versa. Some piezoelectric crystals (10 out of 20) posses spontaneous polarization and are called polar crystals. These polar crystals are also known as pyroelectric crystals and give pyroelectric effect i.e. the appearance of an electric charge at the surface of the polar material with change in temperature i.e. under uniform heating or cooling. Current generated due to these electrical charges is called the pyroelectric current. If the direction of the pyroelectric current (or spontaneous polarization) in pyroelectric crystals can be reversed by the application of high electric field then these materials are known as ferroelectrics. As all pyroelectric materials are polar, and ferroelectrics are a sub-group of these pyroelectric materials; all ferroelectrics are pyroelectrics and piezoelectrics both [6]. These crystals show large dielectric constant and high electro-mechanical coupling

factor. Polycrystalline ceramics of these materials also show the ferroelectric effect after poling.

1.1.1 An Introduction to Ferroelectricity

Ferroelectricity, which at the time was called Seignette-electricity, was reported for the first time by Joseph Valasek, who worked at the university of Minnesota in Minneapolis, in his work "Piezoelectricity and Allied Phenomena in Rochelle Salt" at the meeting of the Americal Physical Society in Washington, in 1920 [4, 7, 8].

Since the discovery of ferroelectricity in single-crystal materials (Rochelle salt) in 1921 and its subsequent extension into the realm of polycrystalline ceramics (barium titanate, $BaTiO_3$) during the early to mid-1940s, there has been a continuous succession of new materials and technology developments that have lead to a significant number of industrial and commercial applications that can be directly credited to this most unusual phenomenon. Among these applications are high dielectric constant capacitors, piezoelectric sonar and ultrasonic transducers, radio and communication filters, pyroelectric security surveillance devices, medical diagnostic transducers, stereo tweeters, buzzers, gas ignitors, positive temperature coefficient (PTC) sensors and switches, ultrasonic motors, electrooptic light valves, thin-film capacitors, and ferroelectric thin film memories. Several excellent articles on the history of ferroelectricity have been written [9-12].

1.1.2 General Features of Ferroelectrics

1.1.2a Definition

The materials which possess the spontaneous polarization even in the absence of an electric field and the direction of spontaneous polarization can be changed by an applied electric field are called ferroelectric materials and the phenomena is called ferroelectricity [13].

1.1.2b Ferroelectric Curie Point and Phase Transitions

Ferroelectric Curie point (T_c) is an important characteristic of ferroelectrics. When the temperature decreases through the Curie point, a ferroelectric crystal undergoes a structural phase transition from a paraelectric phase to a ferroelectric phase. When the temperature is above T_c, the crystal does not exhibit ferroelectricity; on the other hand, when the temperature is below T_c, the crystal exhibits ferroelectricity.

When the temperature is in the vicinity of the Curie point, thermodynamic properties (such as dielectric, elastic, optical, and thermal properties) of a ferroelectric crystal show anomalies and the structure of the crystal changes. For example, dielectric constant in most ferroelectric crystals has a very high value near their Curie point. This phenomenon is usually called the 'dielectric anomaly'. In most ferroelectrics, the temperature dependence of the dielectric constant above the Curie point (in the paraelectric region) can be described fairly accurately by a simple law called Curie-Weiss law:

$$\varepsilon' = A/(T-T_0) \qquad \textbf{…1.1}$$

where, ε' is the dielectric constant, A is the Curie constant and T_0 is the Curie Weiss temperature, which defines the paraelectric phase. In the case of a first order phase transition, $T_0 < T_c$, while for the second-order phase transition, $T_0 = T_c$. This anomaly exhibited in the dielectric behaviour of a material with variation in temperature is a characteristic feature of ferroelectric material. In fact, both the dielectric anomaly and Curie-Weiss law are predicted in the thermodynamic theory of transition. The dielectric anomaly is not a definite proof of ferroelectricity, which is normally confirmed by hysteresis loop.

1.1.2c Ferroelectric Domains and Hysteresis Loop Behavior

Ferroelectric domains are the regions of uniformly oriented spontaneous polarization within the material. Onset of the spontaneous polarization at T_c, leads to the formation of a surface charge. These surface charges produce an electric field, called depolarizing field, E_d. The depolarizing field may be very strong of the order of several kV/cm,

rendering the single–domain state of the ferroelectric energetically unfavorable [14, 15]. The electrostatic energy associated with the depolarizing field may be minimized if

(i) The ferroelectric splits into domains with oppositely oriented polarization.

(ii) The depolarizing charge is compensated for by electrical conduction through the material or by charges from the material surrounding.

Splitting of a ferroelectric crystal into domains may also occur due to the influence of mechanical stresses [16].

(a)

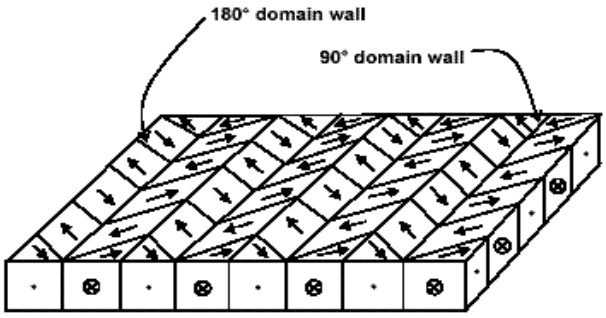

(b)

Fig. 1.1: Ferroelectric (a) Domains and (b) Domain walls

The walls, which separate domains with oppositely oriented polarization, are called 180^o walls and those, which separate regions with mutually perpendicular polarization, are called 90^o walls [17]. The 180^o and 90^o domain walls are shown in fig. 1.1. Both 90^o and 180^o walls may reduce the effects of depolarizing fields but only the formation of 90^o walls may minimize the elastic energy [18]. The 90^o domain wall motion results in large deformation and their movements require higher fields. The types of domain walls that can occur in a ferroelectric material depend on the symmetry of both the non-ferroelectric and ferroelectric phases of the material. Ferroelectric domain walls are much narrower than domain walls in ferromagnetic materials.

Hysteresis loop is the most important property of ferroelectric materials and measured by the behavior of polarization reversal or switching by an applied external electric field in the material. The domain-wall switching in a ferroelectric material, results in a ferroelectric hysteresis loop, shown in fig. 1.2. This hysteresis loop can be observed experimentally by using a Sawyer-Tower circuit [19]. As shown in fig. 1.2, at small values of the ac electric field, the polarization increases linearly with the field amplitude and in this region, the field is not strong enough to switch the domains with the unfavourable direction of the polarization (AB). As the field is increased, the polarization of domains with an unfavourable direction of polarization starts to switch in the direction of field and rapidly increasing the measured charge density. The polarization reversal takes place by the growth of existing antiparallel domains, by domain-wall motion and by nucleation and growth of new antiparallel domains [14, 20]. The polarization response in this region is strongly nonlinear and once all the domains are aligned, the ferroelectricity again behaves linearly (CD). With the decrease in field strength (DE), some domains back–switch, but at zero field the polarization is non-zero and to reach a zero polarization state, the field must be reversed. Further increase of the field in the negative direction (EFG) causes a new alignment of dipoles and saturation.

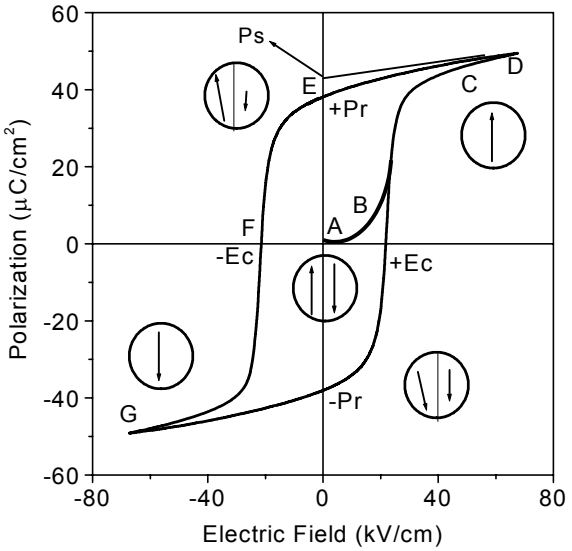

Fig. 1.2: Polarization versus electric field loop behavior of a ferroelectric material.

The field strength is then reduced to zero and reversed to complete the cycle. The value of polarization at zero field is called the remnant polarization, P_r and the field necessary to bring polarization to zero is called the coercive field, E_c. The spontaneous polarization, P_s, is usually taken as the intercept of the polarization axis, tangent to the saturated polarization. In polycrystalline materials, true spontaneous polarization equal to that of a single crystal can never be reached and here it is more correct to speak of saturated rather than of spontaneous polarization [21]. Generally, an ideal hysteresis loop is symmetrical. In some materials the coercive field, spontaneous and remnant polarizations and the shape of the loop may be affected by a number of factors including the thickness, the presence of charged defects, mechanical stresses, preparation conditions and pinning centers [22]. Polarization-electric field (P-E) hysteresis loop is also a function of temperature and usually the area of the loop shrinks with the increase in temperature until a phase transition takes place [23]. At this point no P-E loop is observed and this temperature is called Curie temperature T_c.

1.1.2d Poling

Poling is a process during which a high electric field is applied on the ferroelectric ceramic samples to force the domains to reorient in the direction of the applied electric field. The poling is possible only in ferroelectric materials and poling steps are shown in fig 1.3. Pyroelectric or piezoelectric polycrystalline materials, with randomly oriented grains cannot be poled as they lack more than one equilibrium state of the polarization vector.

Before poling, the ferroelectric ceramic does not possess any piezoelectric and pyroelectric properties owing to the random orientation of the ferroelectric domains in the ceramics. For domain reorientation, a poling field must be applied on the sample and maintained for a certain length of time. For a given field and poling time, better domain rearrangement results at higher temperature, but lower than T_c. This happens because with the increase in poling temperature, crystalline anisotropy and coercive field, E_c, of the ferroelectric materials decreases [23]. Also, with increasing temperature, space charges, which act against domain motion, decreases in ceramic materials. However, when the poling temperature is too high, problems arise as the electrical conductivity

increases and the consequent increase in leakage current would result in sample breakdown during the period of poling. Sample is allowed to cool to room temperature with the field applied and field is removed at room temperature. After poling, a remnant polarization and remnant strain are maintained within the material, and it starts exhibiting piezoelectric and pyroelectric effects [23].

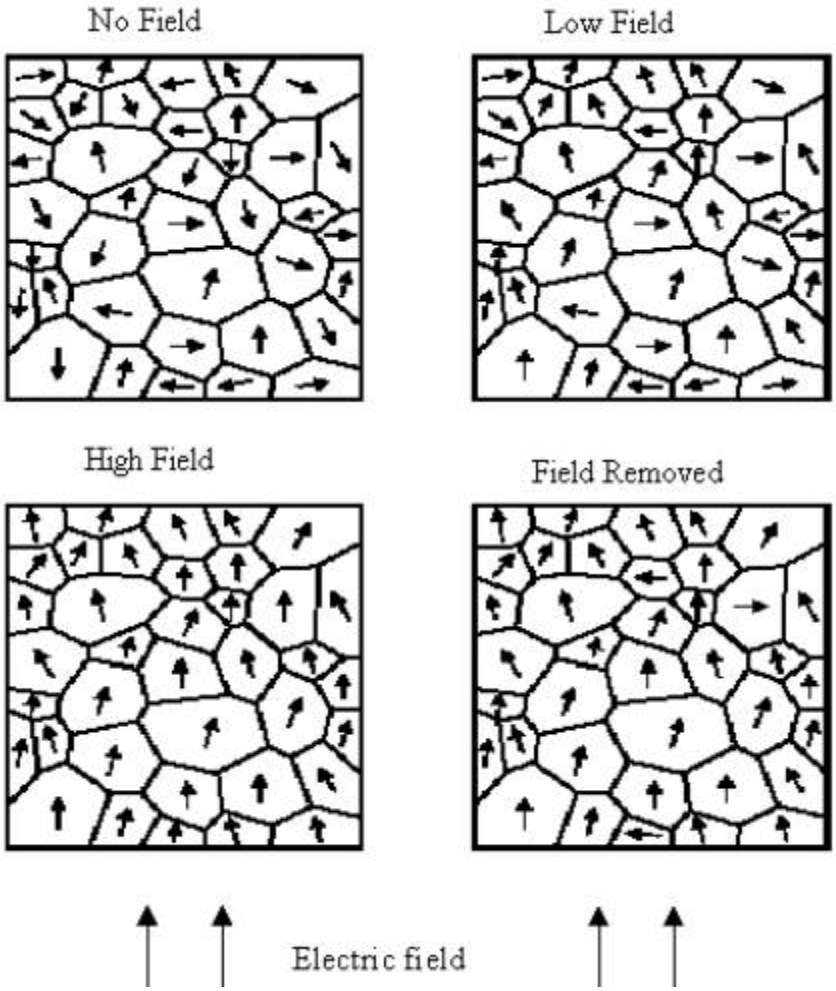

Fig. 1.3: Poling steps of a ferroelectric material

1.1.3 Piezoelectricity

Piezoelectricity stems from the Greek word piezo, which means pressure. It follows that a piezoelectric material develops a potential across its boundaries when subjected to a mechanical stress (or pressure), called direct piezoelectric effect. This property is

exploited to make sensors. Conversely, when an electric field is applied to the material, a mechanical deformation ensues, called converse piezoelectric effect and the material can be used to make actuator. Thus the piezoelectric material can be used as sensor and actuator both and hence often called as smart material. These materials are being used extensively in smart systems, which consist of a sensor, actuator and control system. Ferroelectricity is a subgroup of piezoelectricity. It is a linear effect that is related to the microscopic structure of the solid. The microscopic origin of the piezoelectric effect is the displacement of ionic charges within a crystal structure. In the absence of the external stress, the charge distribution within the crystal is symmetric and the net electric dipole moment is zero. However, when an external stress is applied, the charges are displaced and the charge distribution is no longer symmetric. A net polarization develops and results in an internal electric field. A material can only be piezoelectric if the unit cell has no center of inversion.

1.1.3a Piezoelectric Parameters and Relations

The piezoelectric parameters that are of interest when considering the electromechanical effects in piezoelectric materials are the piezoelectric charge coefficients (d_{31}, d_{33}), the piezoelectric voltage coefficients (g_{31}, g_{33}) and the piezoelectric/electromechanical coupling factors (k_{31}, k_{33}, k_p and k_t).

The application of stress (T) to a piezoelectric material produces a polarization (P), which is given by

$$P = d \cdot T \qquad \textbf{…1.2}$$

where d is the direct piezoelectric coefficient.

The application of an electric field to a piezoelectric material produces strain (S), which is linearly proportional to the applied electric field (E) and given by

$$S = d \cdot E \qquad \textbf{…1.3}$$

where d is converse piezoelectric coefficient.

Piezoelectric constants are defined as partial derivatives evaluated at constant stress (T), constant field (E), constant displacement (D) and constant strain (S) and these boundary conditions can be thought as free, short circuit, open circuit and clamped response, respectively. These constants are defined as [23].

$$d = \left(\frac{\partial S}{\partial E}\right)_T = \left(\frac{\partial D}{\partial T}\right)_E \quad \textbf{…1.4}$$

$$g = \left(-\frac{\partial E}{\partial T}\right)_D = \left(-\frac{\partial S}{\partial D}\right)_T \quad \textbf{…1.5}$$

$$e = \left(\frac{\partial T}{\partial E}\right)_S = \left(\frac{\partial D}{\partial S}\right)_E \quad \textbf{…1.6}$$

$$h = \left(-\frac{\partial T}{\partial D}\right)_S = \left(-\frac{\partial E}{\partial S}\right)_D \quad \textbf{…1.7}$$

where d and g are the piezoelectric strain coefficients, whereas e and h are the piezoelectric stress coefficients.

1.1.3b Piezoelectric Charge Coefficient (d)

When a piezoelectric material is subjected to stress, electric charge is generated on the surfaces. The charge generated per unit force is called piezoelectric charge coefficient and is denoted by ‘d’ which is measured in pC/N. Piezoelectric charge coefficient is a directional property and is usually specified with subscripts to identify the conditions under which it is determined e.g., d_{33} and d_{31}. In these piezoelectric charge coefficients, first subscript corresponds to the direction of the applied stress and second corresponds to the direction of the faces of the ceramic on which charges are developed.

1.1.3c Hydrostatic Charge Coefficient (d_h)

It corresponds the effect of development of charge when a pressure is applied on the material. Hydrostatic charge coefficient (d_h) is related to d_{33} and d_{31} piezoelectric charge constants by the relation

$$d_h = d_{33} + 2d_{31} \qquad \textbf{…1.8}$$

and is measured in Coulomb/Newton (C/N) units.

1.1.3d Piezoelectric Voltage Constant (g)

It gives the field produced by a stress in a piezoelectric material. Its usual units are meter volts / Newton and 'g' constant is related to the 'd' constant by the permittivity

$$g = d / (\varepsilon' \varepsilon_o) \qquad \textbf{…1.9}$$

where g is called the piezoelectric voltage coefficient, ε' and ε_o are the dielectric constant of the material and permittivity of the free space, respectively. Corresponding to d_{33} and d_{31} piezoelectric constants, there exist g_{33} and g_{31} piezoelectric voltage coefficients.
High 'g' constant is desirable in materials intended to generate voltages in response to a mechanical stress, as in a phonograph pickup.

1.1.3e Hydrostatic Voltage Coefficient (g_h)

It gives the field produced by a pressure. It is related to the g_{33} and g_{31} piezoelectric charge coefficients by the relation

$$g_h = g_{33} + 2g_{31} \qquad \textbf{…1.10}$$

and its usual units are meter volts/Newton.

1.1.3f Electromechanical Coupling Factor (k)

Most powerful measurement of the strength of the piezoelectric effect is the electromechanical coupling factor k, which reflects the efficiency of a material. It gives us the measure of the part of the applied electrical energy converted into mechanical energy or vice-versa and measured by resonance method [24].

$$k^2 = \frac{\text{Mechanical energy converted into electrical energy}}{\text{Input Mechanical energy}}$$

or

$$k^2 = \frac{\text{Electrical energy converted into mechanical energy}}{\text{Input electrical energy}}$$

Depending on the mode of energy conversion, there exist various electromechanical coupling factors, for example k_p, k_t and k_{33}. Here, k_p is planar coupling coefficient, related to the energy conversion, when the applied electric field is perpendicular to the generated mechanical vibrations, which are along the plane. k_t is thickness coupling factor related to the energy conversion, when the applied electric field is in the direction of generated mechanical vibrations and which are along the thickness in the material. Large k_t and small k_p in a piezoelectric material exhibits huge anisotropy behavior. Due to large anisotropy, transverse modes get suppressed resulting in the prevention of pickups due to transverse mode.

1.1.4 Types of Ferroelectric Materials

There are several types of ferroelectric materials that are grouped together according to their structure. The four main types of structures include the corner sharing oxygen octahedra, compounds containing hydrogen bonded radicals, organic polymers and ceramic polymer composites [26]. The corner sharing oxygen octahedra include the

perovskite type compounds (ABO_3 type structure, for example PCT, PZT, PT, PMN, $K_xNa_{1-x}NbO_3$, BT etc.), the tungsten bronze type ferroelectric crystals; have a structure similar to tetragonal tungsten bronze K_xWO_3 ($x < 1$), for example $PbNb_2O_6$ etc., bismuth oxide layer structured ferroelectrics (eg. $Bi_4Ti_3O_{12}$, $PbBi_2Nb_2O_9$ etc.).

1.1.5 Lead Titanate [$PbTiO_3$, (PT)] Ceramics

In the search for new perovskite-type ferroelectrics (of general formula ABO_3) that followed the discovery of barium titanate, Shirane, Hoshino and Suzuki [26, 27] studied lead titanate ($PbTiO_3$) ceramic and reported its ferroelectricity on the basis of the structural analogy between both compositions.

1.1.5a Crystal Structure

Lead titanate is a ferroelectric material with a high Curie temperature (490^oC) at which the phase transition from the cubic paraelectric phase (above Curie temperature) to the tetragonal ferroelectric phase (below Curie temperature) occurs. Lead titanate is having perovskite-type structure. This oxide ceramic has the general chemical formula ABO_3, where O is oxygen, A represents a cation with a larger ionic radius and B a cation with a smaller ionic radius. Fig. 1.4 shows a cubic ABO_3 (e.g., A is Pb and B is Ti in $PbTiO_3$) perovskite-type unit cell.

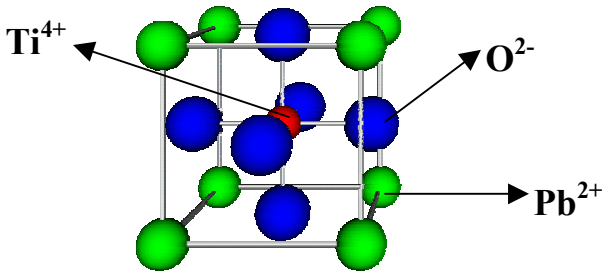

Fig. 1.4: Cubic structure of lead titanate.

The packing situation of this structure may be characterized by a tolerance factor, t, which is defined by the following equations:

$$R_A + R_O = t\sqrt{2}\,(R_B + R_O)$$

or

$$t = (R_A + R_O)/\sqrt{2}\,(R_B + R_O) \qquad \ldots 1.19$$

where R_A, R_B and R_O are the ionic radii of A, B and O ions respectively. When t is equal to 1, the packing is said to be ideal. When t is larger than 1, there is too large a space available for B ion, and therefore this ion can move inside its octahedron. In general, to form a stable perovskite structure, one requires that $0.9 < t < 1.1$.

1.1.5b Applications

Lead titanate is a well-known ferroelectric material with high Curie point and low dielectric constant, which make them attractive for high-temperature and high frequency transducer applications. These applications include surface acoustic wave (SAW) devices, actuators and piezoelectric transducer [28-30]. It is a good ferroelectric for infra-red (IR) detectors, high frequency filters and opto-electronic devices. Ferroelectric lead titanate thin films, grown directly on a semiconductor such as Si, form a very promising combination for nonvolatile memory devices as well as piezoelectric and pyroelectric sensor applications [31]. Lead titanate is being used widely in hydrophone applications. A hydrophone is the element of a sonar system used to detect the ultrasound. The sensitivity of a hydrophone is determined by the hydrostatic voltage coefficient, g_h, which relates the voltage appearing across the transducer to the applied pressure. Another useful parameter is the hydrostatic charge coefficient, d_h, which relates the charge develops to the applies stress. A useful figure of merit for hydrophone piezoceramics is reflected in the product $d_h x g_h$ since the maximum energy obtainable form a material is proportional to this product. For hydrophone applications, it is not sufficient to have a high d_{33} coefficient, and it is because of this that dense lead zirconate titanate (PZT) is far from ideal material for hydrophones. Although PZT has a high mechanical coupling coefficient and a high d_{33} coefficient, the hydrostatic coefficient, d_h is small because d_{33} and d_{31} have opposite sign and d_{31} is nearly half the value of d_{33}. In PZT, the g_h coefficient is also small because the permittivity is large [23]. Another drawback with PZT ceramics is that

these ceramics have a low Q_M, which is unsuited to the detection of sharp pulses and leads to a troublesome ringing effect [13]. For PT, d_{31} is roughly 10% of d_{33}. Therefore the d_h of PT ceramics is about twice that of PZT ceramics despite the fact that the d_{33} of PZT (Navy type I) [32] is four times larger. The large anisotropy of lead titanate consequently allows transducer designs with simple flat plates of piezoelectric material as opposed to the hollow cylindrical or spherical geometries commonly used with PZT ceramics. This is important for wide area array (for very low frequency) and high-pressure hydrophone designing where cylindrical or spherical geometries are impractical. These materials may also have some uses in underwater projectors, but the applications would be much more specialized. In the last decades or so, several manufacturers in U.S. and Japan have developed conventional ceramics with superior sensitivity under quasi-hydrostatic stress.

1.2 Review of Modified Lead Titanate Ceramics

The ferroelectric phase transition in Lead Titanate at 490^{o}C has attracted continuing interest since it was first investigated in detail by Shirane and Hoshino [33] in 1951. Above T_c, the material has a simple cubic structure with lead atoms at the corners of the cubic unit cell, the titanium is at the body center position and oxygens are at the face-centered positions. Below T_c, the structure is tetragonal with the atoms distorted from the cubic arrangement by small relative displacements along the (polar) tetragonal c axis exhibiting a large tetragonality (c/a = 1.064). This is the same structural change as occurs at the corresponding transition in $BaTiO_3$, but both the unit cell and atomic displacements display a substantial larger tetragonal distortion than they do in $BaTiO_3$. This has been one of the sources of interest in $PbTiO_3$.

Pure $PbTiO_3$ ceramics are generally too fragile and porous to be polarized [34]. Many attempts have been made to produce dense $PbTiO_3$ ceramics with good piezoelectric properties by adding additives or forming solid solutions [35-38]. Outstanding improvement in various properties is achieved, by modifying the ceramics to an extent that they become very promising piezoelectric materials for high temperature and high frequency applications because of their high Curie temperature and low dielectric constant [33]. Modified PT ceramics show usually large anisotropy in electromechanical

factors [37, 28] and a large anisotropic piezoelectric coupling [39, 40]. In the line with the present objective of the thesis, an exhaustive literature survey on modified PT ceramics is presented here. This literature survey not only highlights the various modifications attempted by various researchers and to mention the updated research activities in this important field but also to recognize the possible potential applications for which this material is of crucial significance. Although the literature collected and referred during the present studies also included several papers on PZT ceramics, modified PZT ceramics, $BaTiO_3$ ceramics, $PbTiO_3$ single crystals and solid solutions etc., of which the works on PZT based ceramics were extensively utilized, but it is neither practically possible nor desirable to present review of all of them in the present context, so the review here is restricted to modified $PbTiO_3$ ceramics and further to calcium modified PT ceramics only.

Subba Rao [35] has reported replacement of Ti^{4+} by Nb^{5+} or Ta^{5+} resulting in creation of cation vacancies, which facilitate material transport and aid sintering giving ceramics of upto 91% theoretical density. These niobium or tantalum modified (2 - 5%) ceramics have peak dielectric constant of the order of 10,000 and dielectric loss less than 0.1 in the range 25^oC - 525^oC.

In one of the earliest studied on the effect of additives on properties of $PbTiO_3$, Tien and Carlson [41] have attempted several additives and dense polycrystalline specimens are achieve. A very high d_{33} value of 130 pC/N has been reported for specimens containing one mole percent CaF_2 which had a dielectric constant of 160 at room temperature.

In a significant report by Yashihiro Matsuo et al. [42] on 0.1 to 2 mol% MnO_2 doped ceramics, the temperature range suitable for sintering is found to become broader with increasing MnO_2. The grain has been reported to increase with increasing sintering temperature. It has also been found that the addition of 2 mol% MnO_2 results in high mechanical strength, high electrical resistivity of the order of 10^{13} ohm-cm, small dielectric constant of 250, dissipation factor of 0.75 and a small planar coupling coefficient of around 4%.

From a subsequent report by Matsuo et al. [43], it was seen that the disruption of sintered ceramics is strongly influenced by their grain size. For grain size > 10 μm, a complete disruption of the fired compacts has been observed, while with grain size of 3 μm,

mechanically string ceramics were obtained. This was attributed to intergranular cracking or grain separation due to grain boundary stresses setup by incompatible expansion of the individual grains owing to different coefficients of thermal expansion in different crystallographic directions. The authors suggested that mechanically strong PT results from additives, which serve as a grain growth inhibiter.

Ueda et al. [36] have investigated the effect of adding $Bi_{2/3}TiO_3$, $PbZn_{1/3}Nb_{2/3}O_3$ or their derivatives in $PbTiO_3$ and high density. High resistivity ceramics having a dielectric constant about 200 and k_{33}, k_{31} as 0.35 & 0.068 respectively are reported.

In another report by Ikegami et al. [28] on hot pressed lanthanum modified ceramics extensive piezoelectric and electromechanical studies provide a k_t value of 0.51 and k_p value of 0.077 indicating a large electromechanical anisotropy in the ceramic system.

Hennings [44] and Rosenstein [45] investigated the range of existence of perovskite phases in the system $PbO\text{-}TiO_2\text{-}La_2O_3$ by means of X-ray diffraction, chemical analysis and microscopic analysis. Depending on the partial pressure, conversion of A-site vacancies into B-site vacancies by taking up PbO from vapour phase has been suggested. Strong evidence in favour of lanthanum incorporation at A-site is reported.

Ueda [46] performed detailed investigation on $PbTiO_3$ system with several additives and found that grain size is a major factor influencing piezoelectric and related properties.

In a series of lead titanates containing defects, the phase transition, which extends over a temperature interval, is interpreted by Shirasaki et al., [47]. According to a model, in which micro regions in the crystal differ in composition and therefore have different Curie temperature. The electrical conductivity mechanism in $PbTiO_3$ ceramics has been extensively studied by Prokopalo [48-50], It has been reported that the conductivity is due to p-type carriers. In addition to electronic process, the contribution of ionic mechanism is recognized. The motion of oxygen vacancies is suggested to have important contribution to electrical conduction in lead titanate. Electrical aging was attributed to redistribution of oxygen vacancies. Effect of several dopants on conductivity was investigated and lanthanum doping is found to creation of donor levels.

From a series of detailed reports by Keizer, Burgraff and co-workers [51-54], the effect of lanthanum incorporation and grain size on the dielectric behaviour, Curie temperature (T_c) and lattice parameters suggests that the increase of lanthanum concentration causes

the Curie temperature to decrease, and for any lanthanum concentration, a decease in grain size makes the Curie temperature shift to lower temperatures and decreases the sharpness of ferroelectric-paraelectric transition (FPT). At lanthanum concentration below 23 mol%, the FPT is not found to be broadened and has a Curie-Weiss behaviour is monophasic, homogeneous coarse-grained material.

The ferroelectric properties of lead titanate ceramics modified by (La = Mn) have been investigated by Carl [38] under quasi-static driving fields. Information about the reorientation processes was obtained from lateral switching strain and hysteresis loop measurements with low-frequency fields. It was shown that microcracking is the cause of the degradation effects found in hysteresis loop of PLMT (lead lanthanum manganese titanate) specimens during 10 - 50 Hz excitation.

New piezoelectric ceramics with zero temperature coefficients of surface wave delay time were developed by Ito et al. [55]. These lanthanum, niobium, manganese and indium modified ceramics have a temperature coefficient less than $1x10^{-6}/^{o}C$. The electromechanical coupling factor of 0.1, mechanical quality factor of 1400 and a dielectric constant of 225 was reported [56] have suggested these ceramics to be potential materials for high frequency surface acoustic wave (SAW) devices. The SAW propagation loss mechanism in the frequency range 30 MHz to 300 MHz is attributed to Rayleigh Scattering loss caused by grains and to dissipative loss caused by internal friction. Properties, such as velocities and electromechanical coupling factors for bulk wave and SAW are found to vary monotonically with ionic sizes of the rare earths [58]. Then rare earths on the other hand, the temperature coefficient of SAW delay time is found to be minimum for neodymium doping. The studies on the effect of substrate strain upon SAW velocities, by Takeuchi et al., [59] reveals a strong non-linearity and a large SAW velocity strain coefficient (~ 10).

Nagatsuna et al. [60] have extensively studied the elastic, piezoelectric, dielectric and thermal properties of lead titanate ceramics partially substituted with Nd, Mn and In and found that Nd and In substitutions in these ceramics cause positive temperature coefficients of almost all stiffness constants and negative thermal expansion coefficients which results in zero temperature coefficient of delay time. In another technologically very important report by Takeuchi et al. [61], because of near zero temperature

coefficient of SAW delay time, fabrication of a high frequency SAW filter using $(Pb,Nd)(Ti,In,Mn)O_3$ ceramics is reported. Also, due to a high electromechanical anisotropy ratio around 15, a 7.5 MHz linear array ultrasonic probe employing these ceramics is developed for medical use and is reported therein.

Dielectric and pyroelectric properties of a PT ceramic series modified by Mn, Nb and Ca is reported by Yukuan et al. [62]. It was suggested that for MnO_2 concentrations less than 0.8 mol%, the manganese ions exist as Mn^{3+} and for MnO_2 doping concentrations above 0.8 mol% as Mn^{2+} and thus contributing a space charge effect which dielectrically hardens the ceramic. Takeuchi et al. [39] examined electromechanical properties of PT ceramics modified by the partial substitution of rare earths at A-site. It was found that Sm substitution dramatically increased the ratio of electromechanical coupling factor of the thickness dilatational mode to that of the planar extensional mode and can be very useful material in array transducer applications. The coupling coefficient between thickness and lateral modes in a rectangular strip resonator was found to be less than one tenth that of PZT ceramics.

Yamamoto et al. reported the investigated dielectric and electromechanical properties of complete tetragonal range of lanthanum modified PT ceramics [63]. These hot pressed, single dopant ceramics exhibits a decrease in tetragonality, Curie point, remnant polarization and coercive field while the planar and thickness mode electromechanical factors exhibits a maximum of 15 mol% La composition, the reported values being 0.49 and 0.29, respectively. The internal stress in the ceramics was found to increase with increasing c/a ratio in the tetragonal region. In another report by the same research group [64], the fracture toughness of hot pressed $Pb_{0.85}La_{0.15}TiO_3$ ceramics with c/a ratio = 1.028 and a grain size of 3 μm, was determined by the micro-indentation technique. The compressional internal stress just after thermal depolarization was found to be 140 MN/m^2 and linearly decreased with logarithm of aging time, which is caused by the stress release during domain rearrangements.

The effect of cobalt and tungsten on the electromechanical properties of lead calcium titanate with 24 mol% calcium was studied by Yamashita et al. [65]. Mechanical quality factor, Q_M was reported to be 18 for these ceramics. Ichinose et al. [66] applied this calcium modified lead titanate ceramics for infrared sensors and found it to be

appreciable for use as a human body sensor. The success of calcium modified lead titanate ceramics does not seems to be limit or saturate, as another technologically very significant report was published by Underwater sound reference detachment of U.S. Navel research laboratory by Rittenmyer et al. [67] ceramics. These ceramics were found to be useful for electroacoustic transducer applications. This material was found to have d_h and g_h coefficients with hydroacoustic figure of merit reaching a value of ~ $2650x10^{-15}$ m^2/N. The reports mentioned the results of two prototype underwater transducers, which were designed and constructed for low frequency operations (1 - 100 kHz) and high frequency operations (200 kHz - 2 MHz).

Another research group attracted to investigate the calcium modified PT ceramics (PCT) further. In their first work, [68] on PCT ceramics, dielectric and thermal expansion measurements as a function of temperature suggest that the phase transition in these ceramics is of diffusive character and their exist a local polarization which disappear at 460^oC much above the Curie temperature.

Detailed investigations of the dielectric berhaviour of the $Pb,Ca(TiO_3)$-$Pb(Co,W)O_3$ system had been carried out by Mukherjee et al. [69]. A first order phase transition was observed at 225^oC. Observations concerning plot of imaginary impedance as a function of real impedance was described by a model with a resonant circuit and a temperature dependent load. The origin of large anisotropy in electromechanical coupling factors in samarium and calcium modified lead titanate systems was investigated by Damjanovic et al., [70] by the variation of d_{31}, $S_{ii}E$ and $\varepsilon_{33}T$ as a function of temperature. A minimum in the planar coupling factor was explained by the change of sign of the piezoelectric coefficient, d_{31}. Dielectric, piezoelectric and microstructural properties of PCT ($Pb_{1-x}Ca_x)TiO_3$ (x = 0.12 - 0.5) ceramics were investigated as a function of calcium content by Yamamoto et al. [71]. It was found that k_t/k_p was changed by calcium amount. Absence of 90^o domains was observed with the calcium content of 0.42 to 0.5 mol, in spite of having the strong piezoelectricity. Also superlattice structure appeared for $x > 0.35$.

The pyroelectric characteristics [72] and dielectric and thermal properties of PT ceramics modified by Ca-La-Bi and La-Bi [73] for improved IR detector performance were studied by Deb. The figures of merit FI and FV for calcium-modified ceramics were found to be

$1.02x10^{-8}$ and $2.44x10^{-11}$ respectively, suggesting them to be promising materials for both transverse mode and pyroelectric/CCD arrays.

Large electromechanical anisotropy was observed in lead titanate ceramics modified by 24 mol% calcium with cobalt and tungsten and by 8 mol% rare earth elements with manganese, prepared by Duran et al. [74, 75]. The hydrostatic figure of merit for hydrophone applications was ~ 2200 in case of calcium modified lead titanate.

Influence of calcium on the ferroelectricity if modified lead titanate ceramics was studied by Mendiola et al. [76] with a composition of $Pb_{1-x}Ca_x(Co_{0.5}W_{0.5})_{0.4}Ti_{0.96}O_3$ by varying x from 24 to 40 mol%. It was concluded that diminishing of tetragonality with increasing the calcium amount causes the decrease of coercive field, which favours the 90^o domain reorientations. Also the minimum poling reversal effects on piezoelectricity were justified by the moderate strains produced by poling. One more report by Pardo et al. [77] in the above series concluded that with appropriate microstructure in a ceramic, a $k_p = 0$ may be achieved if poling can achieve a high percentage 90^o domain reorientation [78]. In another paper by this group [79] it was found that with increasing calcium i.e. decreasing tetragonality, both the reorientation and relaxation of 90^o domains increases. The relaxation rate was found to increase with intensity of the poling field as well as substitution ratio [80].

In a report by King et al. [81], the strain induced ferroelectric domain structure was found to be absent in $(Pb_{1-x}Ca_x)TiO_3$ when $x \geq 0.39$ because the c/a ratio approaches unity. A simple model was presented to predict the conditions under which the ferroelectric strain-induced domain structure is absent.

Piezoelectric and dielectric properties of calcium and samarium modified PT ceramics for hydroacoustic applications were studied by Rittenmyer et al. [32]. The results showed that the piezoelectric sensitivity changes little with the addition of samarium after a certain concentration is reached, whereas the dielectric constant can be substantially varied over the range of substitution that was investigated. In contrast the addition of calcium into lead titanate produces a minimum in the dielectric constant for 15% calcium substitution and causes the voltage sensitivity of the material to reach a maximum for the compositions with about 20% calcium.

Takahashi [29] did an extensive study on the large anisotropy in modified lead titanate ceramics and their applications. A large k_t (0.56) and small k_p (0.4) in calcium modified lead titanate provided a large anisotropy ratio of 12 for this composition. It was suggested that the vanishingly small value of k_p could be achieved if 90^o domain rotation exceeds 20% though it is not always observed and depends on grain size, measuring temperature and a special agreement of 180^o and 90^o domains. Using Ca substituted PT ceramics; an ultrasonic high-resolution NDT array probe for metal flaw detection was designed, fabricated and analyzed. Further due to high hydrostatic figure of merit of 2067, this material was composed with $PbNb_2O_6$, which was considered to be the best material for hydrophones.

In a report by Frutos and Jimenez [82] on the spatial distribution of polarization in calcium modified lead titanate ceramics, it was confirmed that when crystalline anisotropy increases, the reorientation of 90^o domains predominantly takes place near the surface. Another report by Frutos et al. [83], d_{33} values arise mainly from 180^o domains polarization, but a contribution due to high internal stresses caused by poling electric fields have to be taken into account.

A method to increase the figure of merit of infrared detectors was proposed for calcium modified lead titanate ceramics with a composition of $Pb_{0.76}Ca_{0.24}[Ti_{0.96}(W_{0.5}Co_{0.5})_{0.04}]O_3$ by Mendiola et al. [84]. In their work, by subjecting the modified PCT ceramics to electric poling reversal upto 10 times, a controlled microcracking state was caused, with a considerable decrease of the dielectric permittivity and a moderate decrease of the pyroelectric coefficient. Therefore, an increase of the voltage response Vrms close to 50% was obtained.

A discussion on the concentration and temperature dependence of the lattice parameters of calcium modified lead titanate ceramics was given by Windsch et al. [85]. They showed that the temperature dependence of the lattice parameters for a sample with 24 mol% Ca reveals a second order transition near to tricritical behaviour. Different models were used to describe the pure ferroelectrics and substantially mixed ferroelectrics.

In their work of Jimenez et al. [86], extrinsic contributions to the low frequency piezoelectric properties of Ca/Sm modified lead titanate ceramics were discussed. They concluded that the behaviour of piezoelectric ceramics, with high piezoelectrical

anisotropy and tetragonal distortion at very low frequencies, must be attributed to their microstructural states (grain and microcrack sizes) and to the space charge that comes into play during poling processes.

In a study by Ranjan et al. [87], the superlattice reflections observed for the first time in the room temperature powder neutron diffraction patterns of $(Pb_{0.5}Ca_{0.5})TiO_3$ were shown to arise due to an orthorhombic distortion resulting from tilted TiO_6 octahedra and off-center location of Pb^{2+}/Ca^{2+}.

The voltage gain characteristics of piezoelectric transformer using lead calcium titanate ceramics modified by cobalt and tungsten were studied by Jeong et al. [88]. Maximum voltage gain of piezoelectric transformer was 0.72 and 0.86 at resonant frequency of second thickness extensional vibration mode at loading resistance 100 and 200 ohms, respectively.

Chu and Chen [89] were studied the effect of calcium on the piezoelectric and dielectric properties of samarium modified lead titanate ceramics by varying the amount of calcium from 11 mol% to 17 mol% in $(Pb_{0.88-x}Ca_xSm_{0.08})(Ti_{0.98}Mn_{0.02})O_3$ system. They observed that the coupling coefficient, k_t was 0.57 as Ca = 13-15 mol%, which can be used for high-temperature and high frequency applications. Another research group [90] studied the effects of cation-site vacancies on the characteristics of cubic-to-tetragonal displacive transitions in lanthanum modified lead titanate ceramics (PLT) with A (PLT-A) and B (PLT-B) site compensation using Raman scattering and in-situ XRD measurements. The suitability of amount of excess PbO in the Bi-modified lead titanate ceramics was reported by Amarande et al. [91]. The effects of excess PbO were related with the dielectric and piezoelectric properties. A decrease in maximum permittivity and shift in its temperature towards lower temperature side with the increase of samarium concentration was observed in PSmST (S = Sn) compounds [92]. A piezoelectric anisotropy (k_t/k_p) of 15 was observed by Liou et al. [93] for the system; $(Pb_{0.76}Ca_{0.24})[(Fe_{2/3}W_{1/3})_{0.04}Ti_{0.96}]O_3$ with 1 wt% MnO_2. Both the sintering temperature and sintering time were varied and the maximum value of k_t/k_p was observed at 1150^{o}C for 7 hrs sintering. A non-linear increase in the value of d_{33} with the increase in the amount of samarium in lead titanate ceramics was observed by Tickoo et al. [94]. Also transition temperature decreases with the increase of samarium amount. Another research

group [95] studied the effects of strontium on the dielectric and piezoelectric properties of samarium modified lead titanate ceramics. A decrease in lattice anisotropy and transition temperature was observed with increase in the amount of strontium. The compound with Sr = 15 mol% reported to give $k_t \sim 0.55$ with temperature coefficient of frequency, –30 ppm/^oC. Chu and Chen [96] showed the effects of sintering temperature on the piezoelectric and dielectric properties of Cd additive samarium modified lead titanate ceramics. For 2 mol% Cd and sintering temperature of 1150^oC, the authors reported the best properties ($k_t = 0.562$, $k_p = 0.038$ and $\varepsilon' = 224$) out of the rest amounts of cadmium and sintering temperature. Gomez et al. [97] showed that a good infrared detector to operate at high temperatures could be obtained from the $Pb_{0.88}Ln_{0.08}Ti_{0.98}Mn_{0.02}O_3$ (Ln = La, Sm, Eu) ferroelectric ceramics system as they show high peak pyroelectric coefficient at T_c.

Very recently Chen et al. [98] reported the comparison of the piezoelectric properties of microwave sintered PCT ceramics modified by cobalt and tungsten with conventionally sintered. Chu and Chen [99] reported the doping effects of strontium on the dielectric and piezoelectric properties of calcium additive samarium modified lead titanate ceramics prepared by conventional dry ceramic technique with composition, $(Pb_{0.73-x}Ca_{0.15}Sr_xSm_{0.08})(Ti_{0.98}Mn_{0.02})O_3$; x = 0.05 - 0.1. The maximum value of k_t was observed to be 0.565 with $k_p = 0.05$ and TCF = 14.5 ppm/^oC for x = 0.06.

Materials prepared as thin layers are nowadays of great interest for research laboratories and industries, due to their possible integration in novel multifunctional devices that have prospective use in microelectronic technology. Ferroelectric thin films are of great interest because of their applications as ferroelectric nonvolatile memories and in other integrated technologies. A large number of the work related to ferroelectric thin films is based on modified lead titanate because of the possibility to tailor the material performance for specific applications. Recent developments in micro-mechanical systems have opened new potential applications of ferroelectric thin layers in actuators and infrared sensors [100-102].

Several modifications of these materials have been studied with the aim of obtaining improved properties to make them potentially useful in specific applications [103-106]. Lanthanum modified PT films (PLT) have also been the subject of various studies in

recent past [107-116]. Lee et al. [107] have studied the electrical properties of lead lanthanum titanate thin-film capacitors. Venkateswarlu et al. [108] have grown PLT thin films on Pt-coated Si substrates by the laser ablation technique. They have observed that these films are suitable for DRAM applications. The variation of band-gap energy with lanthanum doping has been correlated with the observed microstructure of PLT films by Bhasker et al. [109]. Lanthanum graded heterostructure thin films have also been prepared on platinum substrates and their electrical properties have been compared with those of conventional thin films [110]. Rodrigues and Eiras [111] have deposited PLT thick films by dip coating. Majumder et al. [112] have studied the absorption coefficient and band-gap energy of PLT films. These films have been shown to be attractive candidates for non-volatile memory [113], pyroelectric detectors [114], electro-optic modulators [115] and microwave devices [116]. Calcium modified lead titanate thin films, due to their excellent pyroelectric and good piezoelectric properties, have received attentions of various workers [117-122]. Yamaka et al. [117] have prepared PCT films and found that the films have good pyroelectric properties. Seifert et al. [118] have investigated the fatigue, microstructure, pyroelectric and electromechanical properties of PCT films. Mendiola et al. [119] have reported the effect of processing parameters on the ferroelectric properties of PCT films. Rioboo et al [120] have measured the elastic properties of sol-gel derived PCT films. Kholkin et al. [121] have made PCT thin films with remnant polarization of 38 $\mu C/cm^2$ and piezoelectric coefficient of 70 pm/V, which are comparable to that of bulk ceramics. PCT thin films on Pt/MgO substrates prepared by multiple cathode RF-magnetron sputtering method have good ferroelectric properties [122]. In case of thin films of PCT, the substitution of Ca^{2+} for Pb^{2+} reduces the tetragonal (c/a) ratio of the PT unit cell and facilitates ferroelectric switching [123-126]. PCT has been reported to have high piezoelectric anisotropy [127-128, 32] and even in thin film form, it has d_{33} almost as high as in the case of bulk.

Recently, many studies have been carried out on the fabrication of Ca-modified lead titanate thin films by using Sol-Gel process [125] and RF sputtering [129]. Martin et al. [130] reported the influence of deposition parameters and substrate on the quality of Pulsed-Laser-Deposited (PLD) $Pb_{1-x}Ca_xTiO_3$; x = 0.24, ferroelectric film. Films deposited on $Pt/TiO_2/SiO_2/(100)Si$ substrates were polycrystalline and the orientation

disorder reported to increase with the film thickness. Also crystalline quality of the film was reported to increase with the use of high laser fluence (10 J/cm^2). Paik et al. [131] prepared the PCT thin films using sol-gel process and studied the photocurrent properties of the film capacitors. The band gap energy of the film was reported to be equal to 3.1 eV. In a study by Wang et al. [132] on the pyroelectric properties of PCT thin film detectors, increase in the voltage sensitivity was observed with an increase of Ca content in the low-frequency region ($f < 10$ Hz) reported. The results obtained by the study done by Pontes et al. [133] showed a strong dependence of the morphological, structural and electrical properties of the PCT thin films on the calcium concentration. Chopra et al. [134] prepared the PCT thin films by sol-gel process by varying the amount of calcium. The results indicated the better value of voltage responsivity and detectivity along with smaller value of loss tangent for PCT (76/24).

1.3 Objectives of the Present Work

Present work entails the following objectives: -

- To prepare modified lead calcium titanate ceramics (Bulk form) with;
    - Sm and La substitution at A site.
    - Ta substitution at B site.
- To systematically characterize these ceramics for various structural, electrical and piezoelectric properties.
- To prepare and characterize thin films of typical composition.
- To study the effects of novel processing techniques (Microwave sintering, Mechano-chemical alloying) on structural, electrical and piezoelectric properties of some typical compositions.
- To understand the composition-property relationships in the modified lead calcium titanate ceramics.

References

1. D.W. Richerson, Modern Ceramic Engineering, Marcel Dekker, New York, 1992.
2. J.S. Reed, Principles of Ceramic Processing, John Wiley and Sons, Inc., New York, 1995.
3. I.D. Marinescu, H.K. Tonshoff and I. Inasaki, Handbook of Ceramic Grinding and Polishing, Noyes Publications, USA.
4. W.G. Cady (1946), Piezo Electricity, McGraw Hill, New York, Revised Edition by Dover Publications, New York, 1964.
5. I.S. Zheludev, Sov. Phys.-Cryst., **5** (1960) 328.
6. C.S. Brown, R.C. Kell, R. Taylor and A. Thomas, Proc. IEEE part B, **109** (1962) 99.
7. J. Valasek, Ferroelectrics, **2** (1971) 239.
8. J. Fousek, Proceedings of ISAF'94 (R. K. Pandey, M. Liu and A. Safari, eds.), University Park, PA, 1994, p. 1.
9. G. Busch, Ferroelectrics, **74** (1987) 267.
10. W. Kanzig, Ferroelectrics, **74** (1987) 285.
11. L.E. Cross and R.E. Newnham, History of Ferroelectrics, pp. 289-305 in Ceramics and Civilization, Vol. III, High-Technology Ceramics-Past, Present and Future, American Ceramic Society, Westerville, OH, 1987.
12. G. Busch, Ferroelectrics, **71** (1987) 43.
13. A.J. Moulson and J.M. Herbert, Electroceramics, Chapman and Hall, 1990, U.K.
14. M.E. Lines and A.M. Glass, Principles and Applications of Ferroelectrics and Related Materials, Oxford, Clarendon (1979).
15. J.C. Burfoot and G.W. Taylor, Polar Dielectrics and Their Applications, London: Macmillan (1979).
16. G. Arlt, J. Mater. Sci., **25** (1990) 2655.
17. S. Stemmer, S.K. Streiffer, F. Ernst and M. Ruhle, Phil. Mag. A, **71** (1995) 713.

18. R.E. Newnham, Structure–Property Relations, Berlin Springer, 1975.
19. C.B. Sawyer and C.H. Tower, Phys. Rev., **35** (1930) 269.
20. V. Shur and E. Rumyantsev, J. Korean Phys. Soc., **32** (1988) S727.
21. D. Damjanovic, Rep. Prog. Phys., **61** (1998) 1267.
22. R. Ramesh, S. Aggarwal and O. Auciello, Mater. Sci. Engg. B, **32** (2001) 191.
23. B. Jaffe, W. Cook and H. Jaffe, Piezoelectric Ceramics, Academic Press, London (1971).
24. P.R. Chowdhary and S.B. Deshpande, Ind. J. Pure. Appl. Phys., **17** (1979) 571.
25. A. Safari, R.K. Panda and V.F. Janas, Ferroelectric ceramics: Processing, properties and applications, Review article.
26. G. Shirane, H. Hoshino and K. Suzuki, J. Phys. Soc. Jpn., **5** (1950) 453.
27. G. Shirane, H. Hoshino and K. Suzuki, Phys. Rev., **80** (1950) 1105.
28. S. Ikegami, I. Ueda and T. Nagata, J. Acoust. Soc. Am., **50** (1971) 1060.
29. T. Takahashi, Ceram. Bull., **69** (1990) 691.
30. O. Ohnishi, H. Kishie, A. Iwamoto, Y. Sasaki, T. Zaitsu and T. Inoue, IEEE Ultrason. Symp., **1** (1992) 483.
31. V.R. Palkar, S.C. Purandare, P. Ayyub and R. Pinto, J. Appl. Phys., **87** (2000) 462.
32. K.M. Rittenmyer and R.Y. Ting, Ferroelectrics, **110** (1990) 171.
33. G. Shirane and S. Hoshino, J. Phys. Soc. Japan, **6** (1951) 265.
34. B. Jaffe, R.S. Roth and S. Marzullo, J. Res. Nat. Bull. Stand., **55** (1955) 239.
35. E.C. Subbarao, J. Am. Ceram. Soc., **40**, (1960) 119.
36. I. Ueda and S. Ikegami, Jpn. J. Appl. Phys., **7** (1968) 236.
37. S. Ikegami and I. Ueda, J. Phys. Soc. Jap. Suppl., **28** (1970) 331.
38. K. Carl, Ferroelectrics, **9** (1975) 23.
39. H. Takeuchi, S. Jyomura, E. Yamamoto and Y. Ito, J. Acoust Soc. Am., **72** (1982) 1114.
40. H. Takeuchi, Jpn. Appl. Phys. Suppl., **24** (1985) 36.
41. T.Y. Tien and W.G. Carlson, J. Am. Ceram. Soc., **12** (1962) 567.
42. Y. Matsuo, M. Fujimura and H. Sasaki, J. Am. Ceram. Soc., **48** (1965) 111.

43. Y. Matsuo and H. Sasaki, J. Am. Ceram. Soc., **49** (1966) 229.
44. D. Hennings, Mater. Res. Bull., **6** (1971) 329.
45. D. Hennings and C. Rosenstein, Mater. Res. Bull., **7** (1972) 1505.
46. I. Ueda, Jpn. J. Appl. Phys., **11** (1972) 450.
47. S.I. Shirasaki, K. Takahashi and K. Kakegawa, J. Am. Ceram. Soc., **56** (1973) 430.
48. O.I. Prokopalo, Ferroelectrics, **5** (1973) 99.
49. O.I. Prokopalo, Ferroelectrics, **7** (1974) 333.
50. O.I. Prokopalo, Bull. Acad. Sci. USSR, **39** (1975) 84.
51. K. Keizer and A.J. Burggraaf, Phys. Stat. Solidi (a), **26** (1974) 561.
52. K. Keizer and A.J. Burggraaf, Mater. Res. Bull., **10** (1975) 521.
53. K. Keizer and A.J. Burggraaf, Ferroelectrics, **14** (1976) 671.
54. K. Keizer, G.J. Lansink and A.J. Burggraaf, J. Phys. Chem. Solids, **39** (1978) 59.
55. Y. Ito, H. Takeuchi, S. Jyomura and K. Nagatsuma, Appl. Phys. Letter., **35** (1979)
595.
56. Y. Ito, H. Takeuchi, K. Nagatsuma, S. Jyomura and S. Ashida, Jpn. J. Appl. Phys., **19** (1980) L-487.
57. S. Jyomura, K. Nagatsuma and H. Takeuchi, J. Appl. Phys., **52** (1981) 4472.
58. Y. Ito, K. Nagatsuma, H. Takeuchi and S. Jyomura, J. Appl. Phys., **52** (1981) 4479.
59. H. Takeuchi and H. Yamauchi, J. Appl. Phys., **52** (1981) 6147.
60. K. Nagatsuma, Y. Ito, D.S. Jyomura and S. Ashida, Ferroelectrics, **41** (1982) 169.
61. H. Takeuchi, S. Jyomura, Y. Ito and K. Nagatsuma, Ferroelectrics, **51** (1983) 71.
62. X.U. Yuhiaan, L. Zhungyuang and Z. Xiujuan, Ferroelectrics, **37** (1981) 615.
63. T. Yamamoto, H. Igarashi and K. Okazaki, J. Am. Ceram. Soc., **66** (1983) 363.
64. K. Okazaki, H. Igarashi and T. Yamamoto, Ferroelectrics, **49** (1983) 81.

65. Y. Yamashita and T. Takahashi, Ferroelectrics, **54** (1984) 131.
66. N. Ichinose, Y. Hirao, M. Nakamoto and Y. Yamashita, Jpn. J. Appl. Phys., Suppl, **24** (1985) 463.
67. K.M. Rittenmyer, R.Y. Ting and T. Henriquez, J. Acoust. Soc. Am., **79** (1986) 2073.
68. B. Jimenez, J.D. Frutose and C. Alemany, J. Phys. Chem. Solids, **48**, (1987) 877.
69. B.K. Mukhergee, H.D. Weiderick, N. Maffei and E.S. Prasad, IEEE Ultrasonics Symposium 1987, p-757.
70. D. Damjanovic, T.R. Gururaja and L.E. Cross, Ceram. Bull., **66** (1987) 699.
71. T. Yamamoto, M. Saho, K. Okazaki and E. Goo, Jpn. J. Appl. Phys., **26** (1987) 57.
72. K.K. Deb, Ferroelectrics, **82** (1988) 45.
73. K.K. Deb, Ferroelectrics, **88** (1988) 167.
74. P. Duran, J.F. Fdezlozano, F. Capel and C. Moure, J. Mater. Sci., **23** (1988) 4463.
75. P. Duran, J.F. Fdezlozano, F. Capel and C. Moure, J. Mater. Sci., **24** (1989) 447.
76. J. Mendiola, B. Jimenez, C. Alemany, L. Pardo and L.D. Olmo, Ferroelectrics, **94** (1989) 183.
77. L. Pardo, J. Mendiola, A.M. Gonzalez and J.D. Frutose, Ferroelectrics, **94** (1989) 189.
78. J. Mendiola, C. Alemany, L. Pardo and A. Gonzalez, Ferroelectrics, **94** (1989) 209.
79. J. Mendiola, L. Pardo, F. Carmona and A.M. Gonzalez, Ferroelectrics, **109** (1990) 125.
80. L. Pardo, F. Carmona, A.M. Gonzalez, C. Alemany and J. Mendiola, Ferroelectrics, **126** (1992) 329.
81. G. King and E.K. Goo, J. Am. Ceram. Soc., **73** (1990) 1534.
82. J.D. Frutos and B. Jimenez, Ferroelectrics, **126** (1992) 341.
83. J.D. Frutos, M.L. Calzada, B. Jimenez and E. Menendez, Ferroelectrics, **126**

(1992) 347.

84. J. Mendiola, C. Alemany and J.D. Frutos, Sens. and Actuat. A, **37-38** (1993) 516.

85. W. Windsch, H. Braeter, L. Pardo, B. Jimenez, J. Mendiola and J. A. Gonzalo, Ferroelectrics, **173** (1995) 283.

86. B. Jimenez, J.M. Vicente and R. Jimenez, J. Phys. Chem. Solids, **57** (1996) 389.

87. R. Ranjan, N. Singh, D. Pandey, V. Siruguri, P.S.R. Krishna, S.K. Paranjpe and A. Banerjee, Appl. Phys. Lett., **70** (1997) 3221.

88. Y.H. Jeong, S.H. Lee, J.H. Yoo and C.Y. Park, Sens. and Actuat., **77** (1999) 126.

89. S.Y. Chu and C.H. Chen, Sens. and Actuat. A, **89** (2001) 210.

90. T.Y. Kim, H.M. Jang and S.M. Cho, Solid State Commun., **119** (2001) 527.

91. L. Amarande, C. Miclea and C. Tanasoiu, J. Europ. Ceram. Soc., **22** (2002) 1269.

92. B.P. Das, R.N.P. Choudhary and P.K. Mahapatra, Bull. Mater. Sci., **25** (2002) 517.

93. Y.C. Liou, L. Wu, J.L. Huang and C.H. Yu, Jpn. J. Appl. Phys., **41** (2002) 1477.

94. R. Tickoo, R.P. Tandon, K.K. Bamzai and P.N. Kotru, Mater. Sci. Engg. B, **103** (2003) 145.

95. T.Y. Chen, S.Y. Chu, S.J. Wu and Y.D. Juang, Ferroelectrics, **282** (2003) 37.

96. S.Y. Chu and T.Y. Chen, Mater. Lett., **57** (2003) 2780.

97. E.S. Gomez, R.G. Ballesteros and V.C. Rivas, Mater. Charact., **50** (2003) 349.

98. C.S. Chen, S.K. Lin, C.C. Chou and C.S. Chen, Integ. Ferroelectrics, **53** (2003) 443.

99. S.Y. Chu and T.Y. Chen, Sens. and Actuat. A, **116** (2004) 10.

100. E. Cattan, T. Haccart, G. Velu, D. Remiens, C. Bergaud and L. Nicu, Sens. and Actuat., **74** (1999) 60.

101. T. Kanda, T. Morita, M.K. Kurosawa and T. Higuchi, Sens. and Actuat., **83** (2000) 67.
102. D.L. Polla, Microelectron. Engg., **29** (1995) 51.
103. M. Kochli, C. Wuethrich, K. Brooks, B. Willing, M. Forster, P. Muralt, N. Setter and P. Ryser, Sens. and Actuat. A, **61** (1997) 147.
104. D.S. Paik, A.V. Prasadarao and S. Komarneni, Mater. Lett., **32** (1997) 97.
105. A. Kholkin, A. Seifert and N. Setter, Appl. Phys. Letter., **72** (1998) 3374.
106. S.R. Shannigrahi, R.N.P. Choudhary and H.N. Acharya, J. Appl. Phys., **85** (1999) 1713.
107. S.J. Lee, M.S. Jang, C.R. Cho, K.Y. Kang and S.K. Han, Jpn. J. Appl. Phys., **34** (1995) 6133.
108. P. Venkateswarlu, S.S.N. Bharadwaja and S.B. Krupanidhi, Thin Solid Films, **389** (2001) 84.
109. S. Bhasker, S.B. Majumder, M. Jain, P.S. Dobal and R.S. Katiyar, Mater. Sci. Engg. B, **87** (2001) 178.
110. S. Bhasker, S. B. Majumder, R. R. Das, P. S. Dobal and R. S. Katiyar, Mater. Sci. Engg. B, **86** (2001) 172.
111. J.B. Rodrigues and J.A. Eiras, J. Europ. Ceram. Soc., **22** (2002) 2927.
112. S.B. Majumder, M. Jain and R.S. Katiyar, Thin Solid Films, **402** (2002) 90.
113. J.C. Shin, J.M. Lee, S.K. Hong, H.J. Cho, K.S. Kim, C.S. Hwang and H.J. Kim, J. Vac. Sci. Technol. A, **16** (1998) 2591.
114. W. Ren, Y. Liu, X. Wu, L. Zhang and X. Yao, Integ. Ferroelectrics, **15** (1997) 271.
115. A.L. Ding, W.G. Luo, P.S. Qiu, J.W. Feng and R.T. Zhang, J. Mater. Res. **13** (1998) 1266.
116. L.A. Bassora and J.A. Eras, Ferroelectrics, **223** (1995) 285.
117. E. Yamaka, H. Watanabe, H. Kimura, H. Kanaya and H. Ohkuma, J. Vac. Sci. Technol. A, **6** (1988) 2921.
118. A. Seifert, P. Muralt and N. Setter, Appl. Phys. Lett., **72** (1998) 2409.
119. J. Mendiola, P. Ramos and M.L. Kalzada, J. Phys. Chem. Solids, **59** (1998) 1571.

120. R.J.J. Rioboo, M.L. Calzada, J.K. Kruger and P. Alnot, J. Appl. Phys., **85** (1999) 7349.
121. A.L. Kholkin, M.L. Calzada, P. Ramos, J. Mendiola and N. Setter, Appl. Phys. Lett., **69** (1996) 3602.
122. H. Maiwa and N. Ichinose, Jpn. J. Appl. Phys., **36** (1997) 5825.
123. N. Nagao, T. Takeuchi and K. Iijima, Jpn. J. Appl. Phys., **32** (1993) 4065.
124. A. Tsuzuki, H. Murakami, K. Kani. K. Watari and Y. Torii, J. Mater. Sci. Lett., **10** (1991) 125.
125. R. Sirera, M.L. Calzada, F. Carmana and B. Jimenez, J. Mater. Sci. Lett., **13** (1994) 1804.
126. M.L. Calzada, M.J. Martin, P. Ramos, J. Mendiola, R. Sirera, M.F. DaSilva and J.C. Soares, J. Phys. Chem. Solids, **58** (1997) 1033.
127. Y. Yamashita, K. Yokoyama, H. Honda and T. Takahashi, Jpn. J. Appl. Phys. Suppl., **20** (1981) 183.
128. K. Uchino and K.Y. Oh, J. Am. Ceram. Soc., **74** (1991) 1131.
129. E. Yamaka, H. Watanabe, H. Kimura, H. Kanaya and H. Ohkuma, J. Vac. Sci. Technol., A, **6** (1988) 2921.
130. M.J. Martin, J. Mendiola and C. Zaldo, J. Am. Ceram. Soc., **81** (1998) 2542.
131. Y. Paik, Y.S. Yang, H.J. Joo, M.S. Jang and S. Yi, J. Koren Phys. Soc., **35** (1999) S1235.
132. C.M. Wang, Y.T. Huang, Y.C. Chen, M.S. Lee, C.C. Cheng and M.C. Kao, Jpn. J. Appl. Phys., **39** (2000) 4064.
133. F.M. Pontes, D.S.L. Pontes, E.R. Leite, E. Longo, E.M.S. Santos, S. Mergulhao, A. Chiquito, P.S. Pizani, F. Lanciotti, Jr. and J.A. Varela, J. Appl. Phys., **91** (2002) 6650.
134. S. Chopra, A.K. Tripathi, T.C. Goel and R.G. Mendiratta, Mater. Sci. Engg. B, **100** (2003) 180.

Chapter II

EXPERIMENTAL ASPECTS

This chapter presents a brief background of the various methods of sample preparation and characterization techniques used for studying properties (like structural, dielectric, ferroelectric and piezoelectric) of modified PCT ceramics. The details of experimental techniques, various characterization equipments and their working details are also given in this chapter. The ceramic samples were prepared both in bulk and thin film form. For bulk sample, three techniques namely conventional dry ceramic method, microwave sintering and mechano-chemical alloying were used. Thin films were prepared by pulsed laser deposition technique.

The properties of ferroelectric materials are strongly influenced by preparation methodology. There may be excellent compositional control of the material with improper processing, but the properties of the resulting ceramics are not necessarily good. Generally, in lead based materials, depending on the processing steps, there can be development of unwanted pyrochlore phase in the material. Therefore, it is important to understand the various process intricacies taking place during material synthesis. A study of calcination and sintering parameters is therefore essential. The properties that characterize a ferroelectric material for various applications include: phase and microstructure, dielectric constant and loss, ferroelectric and piezoelectric. Discussion on each one of the processes and the parameters is presented in following sections. Also a brief description about the synthesis and characterization parameters adopted for the material synthesis (bulk and thin films) and also for the study of various physical properties (structural, dielectric, ferroelectric and piezoelectric) of modified PCT ceramics is given at the end of this chapter.

2.1 Material Synthesis

Modified PCT samples were prepared both in bulk and thin film forms. For the preparation of bulk samples, three techniques namely conventional dry ceramic method; microwave sintering and mechano-chemical alloying were used. Thin films were prepared by pulsed laser deposition technique. In the following sections, first bulk synthesis of modified PCT ceramics in bulk form is discussed followed by thin film deposition process.

2.1.1 Synthesis of Bulk Materials

Conventional Dry Ceramic Method

A solid-state reaction is a direct reaction between starting reagents (usually powders) at high temperature. High temperature provides the necessary energy for the reaction to occur. Solid-state reaction is usually slow because during the reaction, a large amount of bonds break, and the ions migrate through a solid unlike gas phase and solution reactions. The limiting factor in solid state reaction is usually diffusion. So the rate-controlling step in a solid-state reaction is the diffusion of the cations through the product layer. Solid-state reaction occurs much more quickly with increasing temperature and reaction does not normally occur until the reaction-temperature reaches at least 2/3 of the melting point of one of the reactants.

In solid state reaction method, raw materials are weighed out according to the stoichiometry of the compound with due consideration for impurity and moisture contents. Raw materials are mechanically mixed and then grinding operations are performed to control the particle size and to make mixture homogeneous. For this purpose milling operation is performed which can reduce the particle size to 1-10 μm range [1]. An attempt to reduce the size of the particles further may affect the homogeneity and purity of the material. Distilled water is usually used as wetting medium as it is available with adequate purity at low cost and is non-inflammable. Next step is the solid state reaction between the constituents of starting materials at suitable temperature. This process is called firing or calcination. During calcination, control over stoichiometry is essential, and for it, volatile constituents have to be compensated. Calcination causes the constituents to interact by inter diffusion of their ions and

resulting in a homogeneous body. Hence, it is considered that calcination is the part of the mixing process. Calcination also controls the shrinkage during sintering. After calcination powder is compacted to give desired shape, known as green body, and this green body is densified through sintering process. A general discussion on calcination and sintering is given in the coming sections. Also, in lead based ceramics, density of the materials greatly affects the materials properties [2]. Density of the material depends on the technique used for shaping of the material, as some green body formation techniques do not require addition of binder, which is detrimental to the densification of the material. Hence, a general discussion on the shaping of the material is also presented.

2.1.1a Calcination

Calcination is a chemical reaction process during which either the partial or complete phase of the compound is formed. It also helps in removing the unwanted gases and products during the decomposition of the constituent compounds. Calcination also helps in homogenizing the materials and reducing the shrinkage during the subsequent sintering process of the finally shaped samples.

In general, four physical processes are involved in the calcination of the raw materials:

(i) Linear expansion of the particles ($< 400^0$C) (ii) Solid phase reaction (400-750^0C) (iii) Contraction of product (750-850^0C) and (iv) Grain growth ($> 850^0$C).

Synthesis of the phase of a compound takes place by solid-phase reaction, which involves the chemical reaction through atomic diffusion among grains at temperature below the melting points of the raw materials [3]. Usually, the calcination temperature is chosen high enough to cause reaction, but low enough to facilitate subsequent grinding. In the materials, having volatile constituents, the calcination temperature must be kept low enough to avoid loss of the volatile parts.

2.1.1b Shaping

Calcined powders are ball-milled again to give suitable shaping to the powder. Generally, an organic binder is incorporated into the powder, for giving sufficient

strength to green samples, so that handling between shaping and sintering may not be difficult. One of the most important requirements of the binder is that it should be possible to remove the binder from the pressed shapes without any disruptive effect. Various shaping methods are:

a) Uniaxial Pressing
b) Isostatic Pressing
c) Calendering
d) Extrusion
e) Jiggering
f) Injection Moulding
g) Silk Screening
h) Slip Casting
i) Band Casting

Among these different shaping techniques, in the present study dry pressing and isostatic pressing techniques have been used. In next sections, these two shaping techniques are discussed.

2.1.1c Uniaxial Pressing

Uniaxial pressing is used to make compacts of small sizes with simple shapes of the calcined powder. It is carried out in a die having movable top. A cavity is formed at the bottom in lower portion. This cavity is filled with free flowing granulated powder and then it is struck with the top of the die. With the help of the top-punch, pressure in the range of 70-75 MPa is applied. A lot of care at various levels of mixing is needed while using this pressing technique, as samples prepared by this technique show the mechanical cracks and layering after sintering. Highly polished die and punch surfaces help to reduce wall friction and tools are made of hardened steels to minimize wear and maintain surface finish. The process is shown in fig. 2.1.

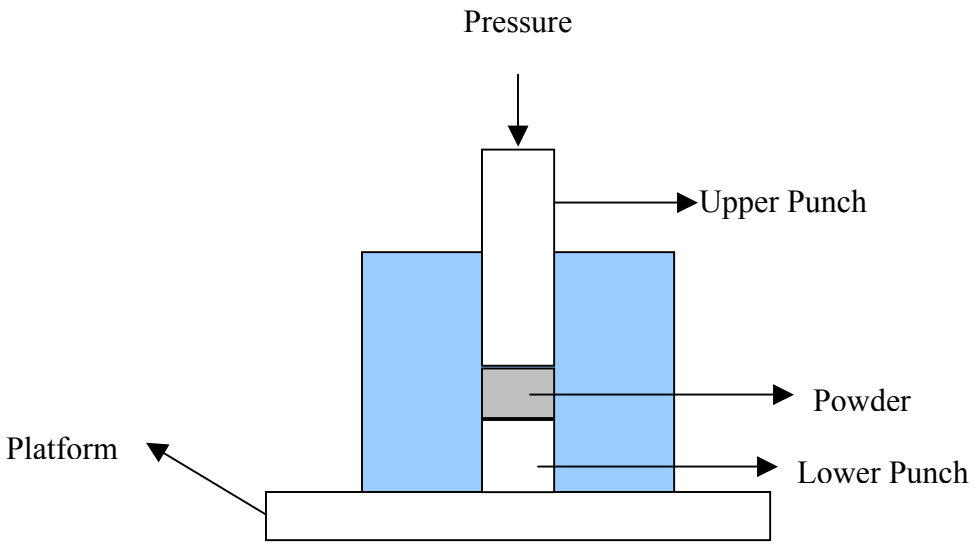

Fig. 2.1: Unidirectional pressing

2.1.1d Isostatic Pressing

Isostatic pressing is used to form samples of larger size. Many of the difficulties encountered in dry pressing are overcome by using isostatic pressing. In this technique, the calcined powder is filled in a flexible mould and the mould is immersed in liquid filled in pressure chamber of the press. More and more liquid is pumped to apply pressure. Pressure of the range 20-275 MPa can be applied using this method. This method is based on the Pascal's Law. Any change in the hydrostatic pressure is distributed uniformly through out the liquid.

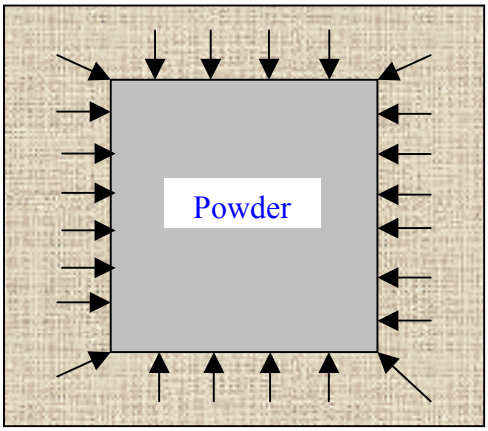

Fig. 2.2: Principle of Isostatic Pressing

Therefore, calcined powder in the flexible container receives a uniform pressure from all directions as shown in fig. 2.2. This results in higher and uniform density of the green body.

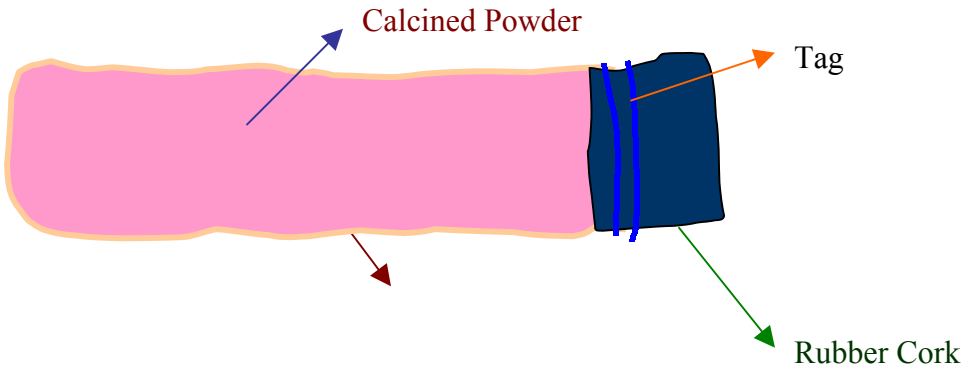

Stage 1: Filling of powder

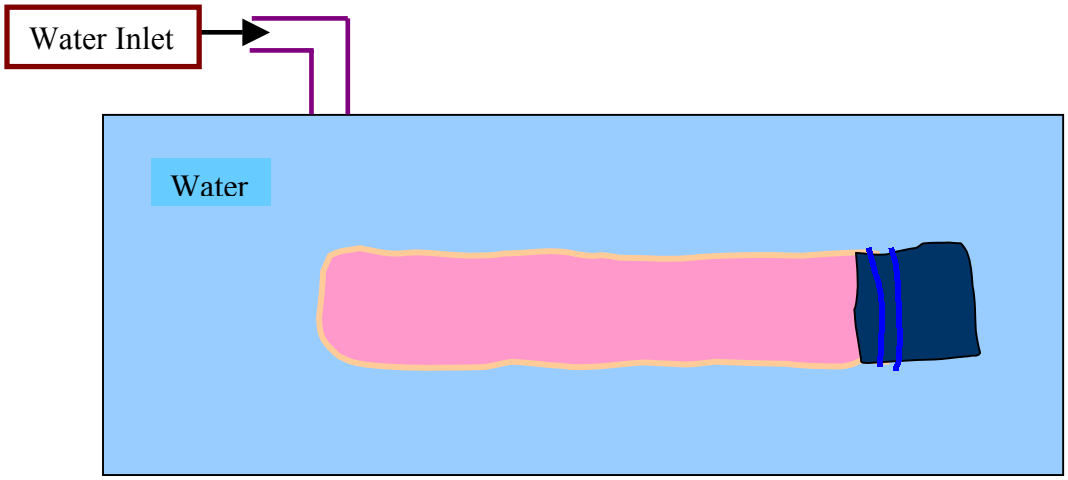

Stage 2: During Pressing

Stage 3: Sintered rod after machining

Fig. 2.3: Different stages of Cold Isostatic Pressing

The advantage of this method is that one can achieve high degree of reproducibility with intricate shapes and sizes, which are otherwise very difficult to obtain. Also, risk of having pores associated with granules is minimum and binder is not required in this process. In the present work, all the bulk samples (green form) were prepared in the form of rod using Cold Isostatic Press (CIP). The schematic of this process is shown in fig. 2.3. First of all, a rubber mold was filled with fine calcined powder and then sealed with a rubber cork. Then this assembly was put in the chamber (filled with water) and the pressure was applied by pumping more and more water in the chamber and resulting in uniform pressure in all directions (i.e. also known as isostatic pressing) to get green rod with higher and uniform density. This green rod was sintered (discussed in next section) for further densification followed by machining to get the desired diameter. Several thin slices were cut from the machined rod for further characterization.

2.1.1e Sintering

Sintering is the process in which the green compacts are consolidated into strong and dense polycrystalline aggregates. During sintering at an appreciable temperature, the atomic motion is more violent and the area between grains in contact increases due to the thermal expansion of the grains and finally only one interface between two grains remains. This corresponds to a state with much lower surface energy. In this state, the atoms on the grain surfaces are affected by neighboring atoms in all directions, which results in densified ceramic [3].

At the beginning of the sintering process, but rather at high temperature, the lattice distortion and internal strain are reduced by atomic diffusion and this is frequently called as 'the recovery process'. With the further increase in temperature, a recrystallization process takes place through atomic diffusion. During recrystallization, new crystal nuclei form and grow at grain boundaries and in other regions inside the grain with higher free energies. Meanwhile, some grains grow by swallowing up other smaller grains. In the recrystallization stage, grain growth is usually realized through the motion of grain boundaries. In general, higher the sintering temperature, larger the grains would grow, as the grain growth is caused by atomic diffusion, which increases

with the increase in sintering temperature. However, the density of a ceramic is affected by the sintering temperature and time in a more complex fashion. If the sintering temperature is too high or the sintering time is too long, the density of the lead based ceramics will be reduced owing to PbO evaporation at high temperatures. Since, the grain growth is caused by atomic diffusion, it follows that a higher sintering temperature and a larger hold time would result in larger grains.

The oxide ceramics should be sintered in an oxidizing atmosphere or in air and a reducing atmosphere must be avoided. Therefore, no organic substances should be mixed with the semifinished products, as they can produce a reducing atmosphere (i.e. CO) during sintering. Furthermore, in lead based ferroelectric ceramics, evaporation of PbO occurs above 800^{o}C and these Pb vacancies greatly affect the material properties [4]. In order to avoid lead loss, sintering is done in closed alumina (Al_2O_3) ceramic crucible by putting $PbZrO_3$ powder along with the material to be sintered for maintaining lead rich atmosphere.

2.1.2 Microwave Processing

Microwave processing of ceramics is fast emerging as a new field of ceramic processing and material synthesis. Excellent reviews have been written on the developments in this rapidly growing field [5-7]. Microwaves are electromagnetic radiation with wavelengths ranging from 1 m to 1 mm in free space with a frequency range 300 MHz to 300 GHz, respectively. Today microwaves at the 2.45 GHz frequency are used almost universally for industrial and scientific applications.

Microwaves also obey the laws of optics and can be transmitted, absorbed or reflected, depending on the material type, as shown in figure below. The interaction of microwaves with different materials is shown in fig. 2.4.

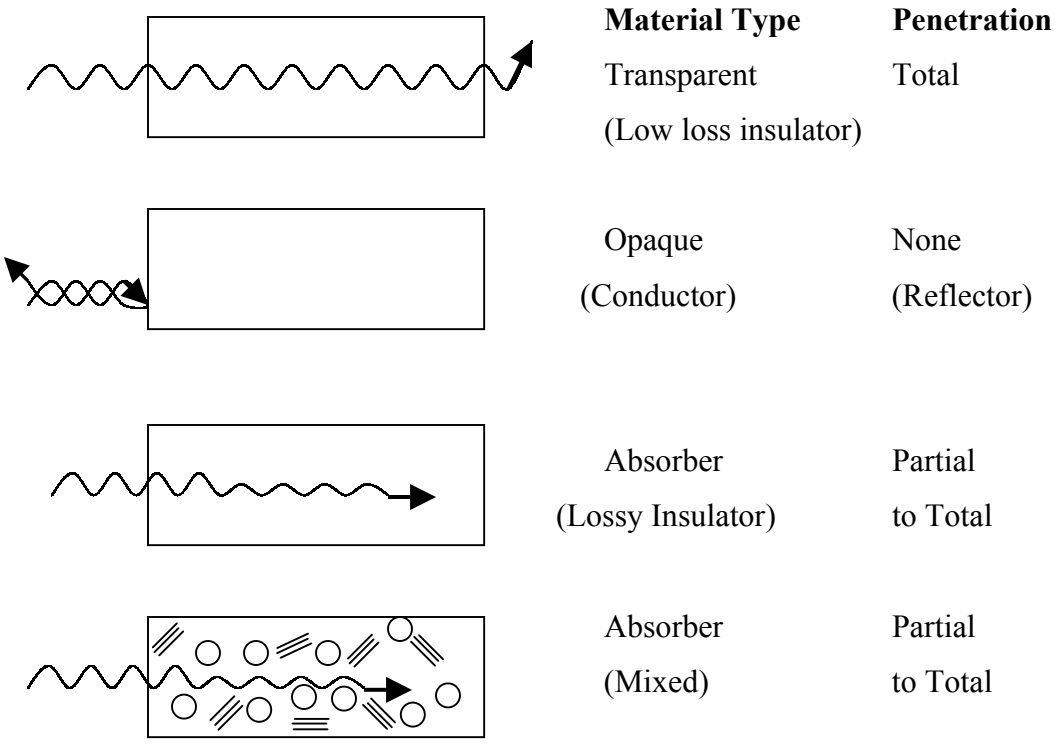

Fig. 2.4: Interaction of microwaves with different types of materials

In the microwave process, the heat is generated internally within the material instead of originating from external sources, and hence there is an inverse heating profile. The heating is very rapid as the material is heated by energy conversion rather than by energy transfer, which occurs in conventional techniques. Microwave heating depends on the material being processed, and there is almost 100% conversion of the absorbed electromagnetic energy into heat, largely within the sample itself, unlike with conventional heating where there are significant thermal losses. The degree of interaction (or absorption) of microwaves by a dielectric material is related to the material's complex permittivity, ε* (F/m), which is composed of a real part (ε', dielectric constant) and an imaginary part (ε", dielectric loss factor) by

$$\varepsilon^* = \varepsilon' - j\varepsilon'' = \varepsilon_0(\varepsilon'_r - j\varepsilon''_{eff}) \qquad \textbf{…(2.1)}$$

where $j = (-1)^{1/2}$, ε_0 is the permittivity of free space ($\varepsilon_0 = 8.854 \times 10^{-12}$ F/m), ε'_r is the relative dielectric constant, and ε''_{eff} is the effective relative dielectric loss factor.

When microwaves penetrate and propagate through a dielectric material, the internal electric fields generated within the affected volume induce translational motions of free or bound charges (e.g., electrons or ions) and rotate charge complexes such as dipoles. The resistance of these induced motions due to inertial, elastic and frictional forces, which are frequency dependent, causes losses and attenuates the electric field. As a consequence of these losses, volumetric heating results.

Microwave heating has many advantages over conventional heating methods [8-12]; some of these advantages include, time and energy saving, very rapid heating rates (> 400^{o}C/min), considerably reduced processing time and temperature, fine microstructures and hence improved mechanical properties, environment friendly, and so on.

Various characteristics and advantages for microwave processing of ceramics are given below: -

Characteristic	Advantages over conventional heating processes
Direct coupling (absorbing) of microwave creates volumetric (bulk) heating	• Potential to heat large sections uniformly • Reversed thermal gradients: surface cooler than interior • Process materials at lower surface temperatures • Rapid removal of water, binders and gases without rupture or cracking • Internal stresses reduction by lower thermal gradients • Heat in clean (pure) environment; air, controlled atmospheres, vacuum, or pressure • Control partial pressure of reactive gases for selective oxidation/reduction of certain phases • Improvement of product quality, uniformity, and yields

	• Instantaneous response to microwave power changes • Low thermal mass; precise and automated temperature control
Dielectric losses (and heating) accelerate very rapidly with increasing temperatures above critical temperature (T_{crit})	• Ability to heat "transparent" materials above T_{crit} • Very rapid processing (2-50 times faster than conventional) • Densify materials rapidly with minimum grain growth (accelerated sintering) • Reduce process cost (time, energy and labor) • Ability of heat ceramics well above 2000^{o}C (in air, vacuum, or control atmosphere)
Microwaves are polarized and coherent; location of maximum electric and magnetic fields can be controlled.	• Capability of high energy concentration in short time and in selected regions • Frequency and power level optimization for a given material, size and shape • Potential for process automation, flexibility, efficiency and energy savings • Precise heating of selected regions, i.e., brazing or sealing of joints, fiber drawing, and plasma generation • Acceleration of sintered and diffusion due to high electrical fields; thus densification at lower temperatures
Differential microwave coupling of phase, additives, and constituents leads to selective heating	• Synthesis of new materials and microstructure • Heating of selected zones (Brazing and sealing) • Enhanced coupling of microwave transparent materials • Use of fugitive coupling materials for pre heating of otherwise transparent materials • Use of microwave coupling materials as shapes or containers to heat more transparent materials

	• Superior control over state of oxidation through selective heating of phases and control over oxygen partial pressure.

2.1.3 Mechano-chemical Alloying

Mechano-chemical alloying (MCA) process, which was initially invented for ceramic strengthened alloys, [13] has been successfully employed to synthesize a wide range of nano-sized ceramic powders such as ZrO_2, Fe_2O_3, YBCO superconductor, ferrite and ferroelectrics [14-16]. The intrinsic characteristic of this process is that the solid state reaction is activated via mechanical energy instead of heat energy (high temperature). Several advantages can be listed for this mechanical synthesis process. Firstly, it uses low-cost and widely available oxides as the starting materials and skips the calcination step at an intermediate temperature, leading to a simpler process. Secondly, no heat source is needed and it takes place at a temperature close to room temperature in a sealed container, thus effectively alleviating the loss in lead content. Furthermore, the mechanically derived powders possess higher sinterability than those of the powders synthesized by conventional solid-state reaction.

2.2 Ferroelectric Thin Film Processing

Ferroelectric thin films and their applications have gained a lot of attention in the last few years as they possess prominent properties such as high remnant polarization (P_r), large dielectric constant (ε'), good pyroelectric, piezoelectric and electro-optic effects. Today, there exist several methods, both physical and chemical, for preparing thin films. The physical methods can be divided into thermal evaporation and sputtering and the chemical methods can be divided into vapor and liquid phase, which gives rise to different thin film deposition techniques. These different thin film-processing techniques can be grouped as follows:

Physical Vapor Deposition (PVD):

- Sputtering (rf-magnetron, dc, ion beam)

- Evaporation (e-beam, resistance, molecular beam epitaxy)
- Pulsed Laser Deposition (PLD)

Chemical Vapor Deposition (CVD):

- MOCVD (metal-organic CVD)
- PECVD (plasma-enhanced CVD)
- LPCVD (low-pressure CVD)
- MOD (metallorganic decomposition, sol-gel)

As the number of components in a material increase, the degree of complexity for most techniques also increases dramatically. Only PLD, and to some extent sputtering, can be described as techniques with which it is relatively "easy" to produce a target stoichiometry, because both techniques use erosion of a target material to produce the deposition flux. In all other methods, the deposition flux is produced from separate sources, each carrying one of the components of the film. PLD and sputtering have a relatively narrow range to the average energy per atom, but only PLD has an instantaneous value of the deposition rate that can exceed 10,000 Å/s. This fact sets PLD apart from all the other methods. Also the fact that PLD does operate under high background gas pressure is an advantage of the technique over the others that is particularly useful for the insitu production of multicomponent oxides such as high Tc superconducting oxides and complex ferroelectric materials.

In the present work, among several thin film deposition techniques, Pused Laser Deposition (PLD) process has been used for PCT thin film preparation. PLD is one of the most important applications of the interaction of high-powered laser light with condensed material. It has become increasingly popular within research laboratories as a method of producing thin films of novel materials ever since laser pulses in the nanosecond regime became available in the late 1970s and even more so since its success in the growth of commercial curate superconductor thin film devices in the late 1980s.

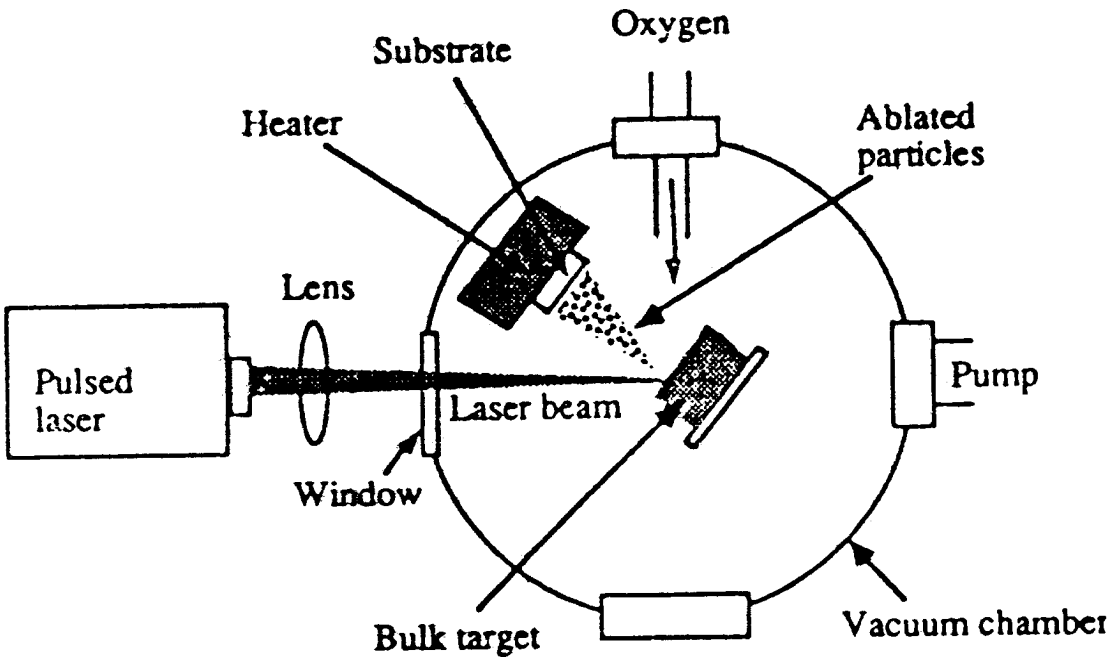

Fig. 2.5: Principle of PLD Technique

Pulsed laser deposition is a growth technique in which photonic energy is coupled to the bulk staring material via electronic processes [17]. The principle of PLD is shown in fig. 2.5. An intense laser pulse passes through an optical window of a vacuum chamber and is focused onto a solid surface (Target), where it is partially absorbed. Above a certain power density, significant material removal occurs in the form of an ejected luminous plume. The threshold power density needed to produce such a plume depends on the target material, its morphology, and the laser pulse wavelength and duration, but might be of the order of 10-500 $MWcm^{-2}$ for ablation using ultraviolet (UV) excimer laser pulses of 10 ns duration. Material from the plume is then allowed to recondense on a substrate, where film growth occurs. The growth process may be supplemented by a passive or reactive gas or an ion source, which may affect the ablation plume species in the gas phase or the surface reaction, in which case one talks about reactive PLD. The physical processes in the PLD are highly complex and interrelated, and depend on the laser pulse parameters and the properties of the target material.

Laser ablation for thin film growth has many advantages: (i) the energy source (laser) is outside the vacuum chamber which, in contrast to vacuum-installed devices, provides a much greater degree of flexibility in materials use and geometrical arrangements; (ii) almost any condensed matter material can be ablated; (iii) the pulsed nature of PLD means that film growth rates may be controlled to any desired amount; (iv) the amount of evaporated source material is localized only to that area defined by the laser focus; (v) under optimal conditions, the ratios of the elemental components of the bulk and film are the same, even for chemically complex systems; (vi) the kinetic energy of the ablated species lie mainly in a range that promotes surface mobility while avoiding bulk displacements; (vii) the ability to produce species with electronic states far from chemical equilibrium opens up the potential to produce novel or metastable materials that would be attainable under thermal conditions.

If one were to set out the properties of the ideal deposition method for a broad set of materials, PLD would stand out as perhaps the most promising choice from the selection available today.

2.3 Characterization Techniques and Studied Parameters

Detailed description of various characterization techniques is given in this section. It includes the details of instruments, their operating principles and various parameters for studying structural, electrical and piezoelectric properties.

2.3.1 Structural Characterization

2.3.1a X-ray Diffraction (XRD)

The X-ray diffraction technique is used for the structural/phase analysis of the material under investigation. The basic principle is that for a fixed wavelength (λ), the constructive interference occurs for a fixed set of an interplaner spacing (d) and incidence angle (θ) [fig. 2.6 & 2.7]. According to Bragg's condition of diffraction:

$$\lambda = 2d \sin\theta. \qquad \textbf{…(2.2)}$$

For cubic system, d is given by

$$\frac{1}{d^2} = \frac{h^2 + k^2 + l^2}{a^2} \qquad \text{…(2.3)}$$

Combining the above two equations we get a relation, which predict the diffraction angle for any set of planes for a given 'λ' if the following condition is satisfied,

$$\text{Sin}^2\theta = \frac{^2}{4a^2}(h^2 + k^2 + l^2) \qquad \text{…(2.4)}$$

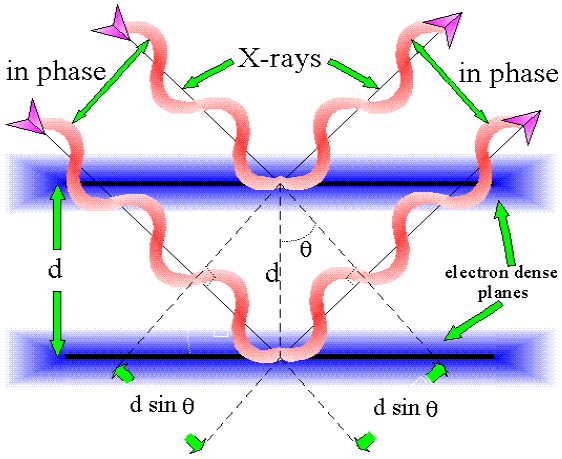

Fig. 2.6: Basic principle involved in diffraction of X- ray beam from assembly of lattice-atoms

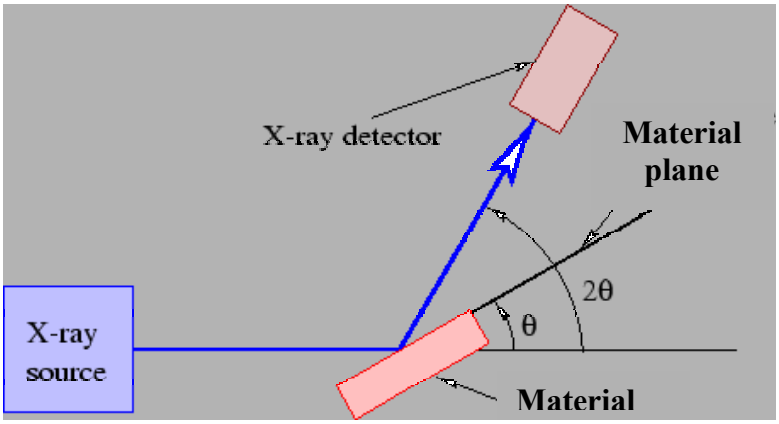

Fig. 2.7: Schematic diagram of Bragg's diffraction

Similarly, the relation for a tetragonal system is

$$\sin^2\theta = \frac{\lambda^2}{4}\left(\frac{h^2+k^2}{a^2}+\frac{l^2}{c^2}\right) \qquad \textbf{…(2.5)}$$

It is seen that diffraction directions are determined by the shape and size of the unit cell. This is an important point. All we can possibly determine about an unknown crystal by the measurement of the directions of diffracted beams are the shape and size of its unit cell. The intensities of diffracted beams are determined by the positions of the atoms within the unit cell and it follows that we must measure intensities if we are to obtain any information about the atom positions. It is also found for many crystals, that there are particular atomic arrangements, which reduce the intensities of some diffracted beams to zero. In such cases, there is simply no diffracted beam at the angle predicated by the equations of the type eqs. (2.3) and (2.4). It is in this sense that equations of this kind predict all possible diffracted beams [18].

While indexing for cubic structure, it has to be kept in mind that for simple cubic and simple tetragonal all (h k l) values are permissible, yet reflections corresponding to ($h^2+k^2+l^2$) values equal to 7, 15, 23…. are all absent. The reflection peaks for bcc satisfy the condition h+k+l = 2n. For fcc structure, the reflection peaks are found to have (h k l) values either all even or all odd. The average grain size of the sample can be calculated from the width of the peak by using the relation:

$$B = \frac{K\lambda}{LCos\theta} \qquad \textbf{…(2.6)}$$

Where B is the broadening of line expressed in the unit of 2θ, K is a constant ~ 1 in most case and L is the average length of the crystallites; and λ and θ have their usual meanings. Generally, X-ray diffraction provides information about the:

(a) Long range order structure

(b) Phase composition

(c) Crystallinity, crystal size and shape

(d) Micro-stress and strain

(e) Texture (crystal orientation)

2.3.1b Density

The bulk density (d_{ex}) was measured by the method based on the Archimedes principle and is given by:

$$d_{ex} = (W_a / W_a\text{-}W_w)\ g/cc \qquad \textbf{…(2.7)}$$

where d_{ex} is the density of the sample. Here, W_a and W_w are the weights of the material in air and in water, respectively.

Theoretical density (d_{th}) was computed from the lattice parameters using the relation,

$$d_{th} = (Z \cdot M)/(N \cdot V)\ g/cc \qquad \textbf{…(2.8)}$$

where Z is the number of molecules in a unit cell and is equal to 1 for the present system, M is the molecular weight, N is the Avogadro's number and V is the unit cell volume.

Relative density (d_{rel}) was computed using the relation,

$$d_{rel} = [(d_{th}\text{-}d_{ex})/d_{th}] \times 100\ (\%) \qquad \textbf{…(2.9)}$$

2.3.1c Scanning Electron Microscope (SEM)

The scanning electron microscope was used to determine the average crystallite size and the surface morphology of the bulk and thin films. It gives information about the grain evolution and grain size in the bulk and thin films. It also gives the information about the inter-granular and the intra-granular pores and the distribution of grains in the bulk samples. SEM measurements are based on the principle of irradiating the specimen with a finely focused electron beam. The secondary electrons, backscattered electrons, auger electrons, characteristic x-rays and several other radiations are released from the specimen. Generally, the secondary electrons are collected to form the image in the SEM mode.

2.3.1d Atomic Force Microscope (AFM)

The Atomic Force Microscope (AFM) is being used as a tool to solve processing and materials problems in a wide range of technologies affecting the electronics, telecommunications, biological, chemical, automotive, aerospace, and energy industries. The materials being investigated include thin and thick film coatings, ceramics, composites, glasses, synthetic and biological membranes, metals, polymers, and semiconductors. The AFM is being applied to studies of phenomena such as abrasion, adhesion, cleaning, corrosion, etching, friction, lubrication, plating, and polishing. By using AFM one can not only image the surface in atomic resolution but also measure the force at nano-newton scale.

Principle wise in AFM, an atomically sharp tip is scanned over a surface with feedback mechanisms that enable the piezo-electric scanners to maintain the tip at a constant force (to obtain height information), or height (to obtain force information) above the sample surface. Tips are typically made from Si_3N_4 or Si, and extended down from the end of a cantilever. The nanoscope AFM head employs an optical detection system in which the tip is attached to the underside of a reflective cantilever. A diode laser is focused onto the back of a reflective cantilever. As the tip scans the surface of the sample, moving up and down with the contour of the surface, the laser beam is deflected off the attached cantilever into a dual element photodiode. The photodetector measures the difference in light intensities between the upper and lower photodetectors, and then converts to voltage. Feedback from the photodiode difference signal, through software control from the computer, enables the tip to maintain either a constant force or constant height above the sample. In the constant force mode, the piezo-electric transducer monitors real time height deviation. In the constant height mode, the deflection force on the sample is recorded. The latter mode of operation requires calibration parameters of the scanning tip to be inserted in the sensitivity of the AFM head during force calibration of the microscope. Depending on the AFM design, scanners are used to translate either the sample under the cantilever or the cantilever over the sample. By scanning in either way, the local height of the sample is measured. Three dimensional topographical maps of the surface are then constructed by plotting the local sample height versus horizontal probe tip position. Compared with Scanning

Electron Microscope (SEM), AFM provides extraordinary topographic contrast direct height measurements and unobscured views of surface features (no coating is necessary). AFM images show critical information about surface features with unprecedented clarity. On one hand, the AFM can resolve very tiny features, even single atoms, that were previously unseen. On the other hand, the AFM can examine a field of view larger than 125 microns (0.005 inch), so that one can make comparisons with other information, e.g. features seen in the light microscope or hazes seen by eye. The AFM can also examine rough surfaces, since its vertical range is more than 5 microns.

2.3.1e Dilatometric Measurements

Dilatometric thermal expansion measurements are generally employed to determine the thermal strain generated during the course of heating. The use of this technique has mainly been confined for the study of monophasic materials, alloys and composites. The information about phase transitions in materials, sintering behaviour, thermal expansion coefficients (α) and their anisotropies are obtained from this technique.

Here in the present work, Orton dilatometer (fig. 2.8) is used to study the shrinkage behaviour of the green sample. The system is interfaced to PC and is designed to automatically measure the percent linear change and temperature of the test sample under controlled heating and cooling rates. The sample rests in an alumina sample holder assembly within the furnace. The sample holder is rigidly connected to the body of LVDT. The alumina pushrod freely moves in the tube of sample holder assembly and is in contact with the LVDT probe. The pushrod moves with the sample as it expands or contracts displacing the LVDT core. The displacement is converted in the form of electrical output by LVDT and after proper conditioning, PC collects the data. The thermocouple is kept in the vicinity of the sample. During operation, power to the furnace is controlled by a programmable PID controller interfaced to PC.

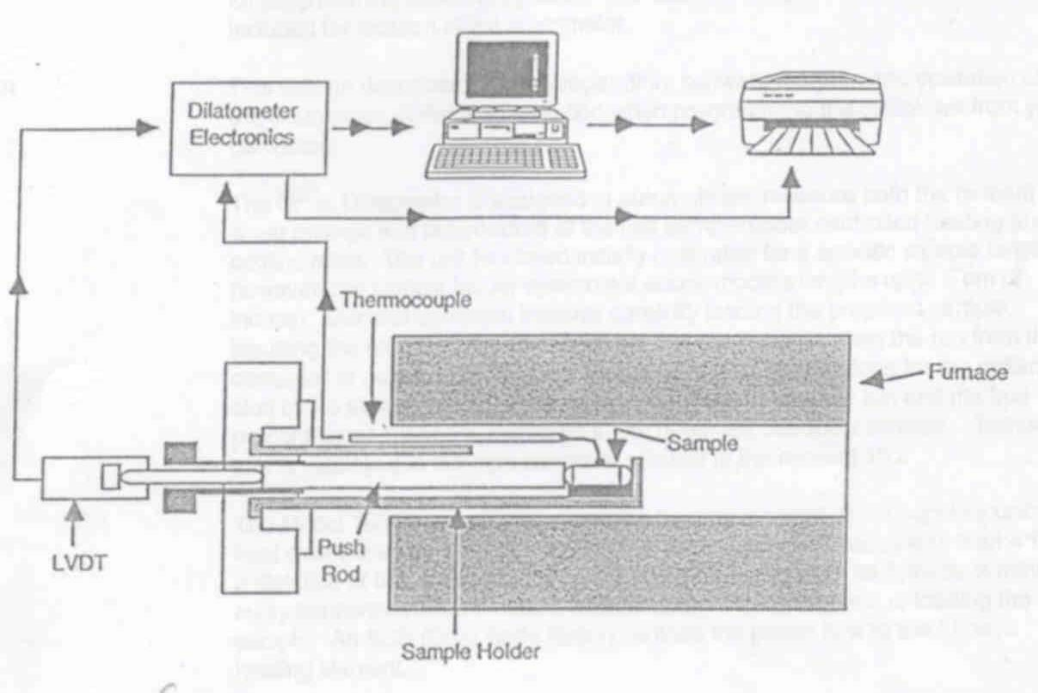

Fig. 2.8: Block diagram of Orton Dilatometer

This model uses a silicon carbide heating element, which supplies uniform heat over the sample length. The max temperature range is 1600^{o}C. Temperature is measured using platinum-platinum/10% rhodium thermocouple made from reference grade metals. The computer interface is user-friendly software program designed to increase the ease of operation and provide more analysis option then is available with the standard unit.

2.3.2 Electrical Characterization

2.3.2a Dielectric Properties

Ferroelectric materials are very often good dielectrics. For most applications of ferroelectric materials, the dielectric constant (ε') and dielectric loss (tanδ) are important practical parameters, and studies of the dielectric properties provide a great deal of information about the suitability of the material for various applications.

Dielectric Constant (ε')

For a given substance, the ratio of the capacity of a condenser with that substance as dielectric to the capacity of the same condenser with a vacuum for dielectric is called dielectric constant of the substance. It is a measure, therefore, of the amount of electrical charge a given substance can withstand at a given electric field strength.

The capacitance, C for a parallel plate capacitor is given by

$$C = \varepsilon_0 A/t \qquad \textbf{…2.10}$$

Where ε_0 is the permittivity of free space and is equal to 8.854×10^{-12} F/m, A is the area of electrode and t is the separation between two electrodes.

When a dielectric (electrical insulator) fills the space between the plates, the capacitance of the capacitor is increased by a factor ε', which is called the dielectric constant of the dielectric material. Therefore, for a parallel plate capacitor with a dielectric between the capacitor plates, the capacitance, C is given by

$$C = \varepsilon'\varepsilon_0 A/t \qquad \textbf{…2.11}$$

Thus the energy stored in a capacitor of a given volume at a given voltage is increased by the factor of the dielectric constant when the dielectric material is present.

For an alternating electric field, the dielectric constant can be written as

$$\varepsilon_r = \varepsilon' - i\varepsilon'' \qquad \textbf{…2.12}$$

where ε'is the real component of the dielectric constant, in phase with the applied field. ε" is the imaginary component, 90^o out of phase with the applied field, caused by either resistive leakage or dielectric absorption. For normal substances, the value of ε_r is low, usually under 5 for organic materials and under 20 for most inorganic materials. Generally, ferroelectric ceramics have much higher ε_r, typically several hundreds to several thousands [19].

Dielectric Loss (tanδ)

The charging current in an ideal dielectric leads the applied voltage by π/2 radians (90^o). However, in real dielectrics in addition to the charging current associated with the storage of electric charge by the dipoles, a loss current must also be considered. The loss current arises from the long-range migration of charges, e.g., dc ohmic conduction and the dissipation of energy associated with the rotation or oscillation of dipoles [19]. As the dielectric is not loss free, it is generally represented by a complex dielectric constant, defined in equation 2.12**.** The total current in the real dielectric is a complex quantity which leads the voltage by an angle (90-δ), where δ is called the loss angle. Dielectric loss (tanδ) also known as dissipation factor is defined as tanδ = ε"/ ε'. The inverse of the loss tangent, Q = (1/tanδ), is used as a figure of merit in high frequency applications.

Curie Temperature (T_c)

It is the temperature above which the spontaneous polarization (P_s) of the ferroelectric materials vanishes and it goes into paraelectric state. It is also known as Curie point, denoted as T_c. When the temperature increases through the Curie point, a ferroelectric crystal undergoes a structural phase transition from a ferroelectric (non-centrosymmetric) to paraelectric phase (symmetric) and above T_c the material does not exhibit ferroelectricity. When the temperature is in the vicinity of T_c, thermodynamic properties including dielectric, elastic, optical and thermal constants show an anomalous behavior [3]. If there are two or more ferroelectric phases in a material, the Curie point only specifies the temperature at which a ferroelectric - paraelectric phase transition occurs.

2.3.3 Electrical Measurements

2.3.3a Electrode Deposition

For any application or characterization, the ceramic material is to be made in the form of parallel plate capacitor. For this purpose, flat parallel surfaces of the ceramic material are coated with metal. It is very important and crucial to achieve a good

adhesion between the ferroelectric ceramic pellet and metallic electrode, since any residual air gap between the two acts as a capacitor in series with the material disk and obviously leads to an erroneous measured capacitance, which is lower than the actual capacitance of the ceramic. Thus, to study the electrical properties of the bulk and thin films of modified PCT ceramics, the electrical contacts were made by depositing gold electrodes on both bulk and thin films using Desk II TSC Cold Sputter/Etch Unit.

The sintered pellets were polished to a smooth finish and cleaned thoroughly using an ultrasonicator. Care was taken to ensure that the pellets faces were parallel. The flat surfaces of pellets were coated with gold using sputtering, which gives the metal-insulator-metal structure to the pellets. The pellets act as dielectric medium between the two parallel metallic plates. Now, the samples are ready for electrical measurements. In case of thin films, bottom electrodes of the films on Pt/Si substrates were created by etching the films in 10% HF solution. Gold dots of 500 μm dia were deposited on thin films surfaces by sputtering method. Thickness of the films was measured by using a tale-step method.

For Bulk Samples

Dielectric measurements of the bulk samples were carried out using computerized measurement set up. This system consists of a LCR meter model HP 4284A interfaced to a PC via IEEE 488, programmable temperature chamber connected to PC via RS 485, measurement jig and software, shown in fig. 2.9. Signal of 1V rms was applied to the sample. Measurements of the samples were done as a function of frequency and temperature. Data were recorded at the interval of two degrees. Software calculates dielectric constant, ε', using the relation

$$\varepsilon' = C \times t / (\varepsilon_0 \times A) \qquad \textbf{...2.13}$$

where C is the measured capacitance, t is thickness, A is the area of cross section and ε_o is the permittivity of the free space, (= 8.854 x 10^{-12} F/m). The frequencies were varied from 100 Hz to 1 MHz and temperature was varied from 25^{o}C to 225^{o}C. Peak in the dielectric constant versus temperature behavior gives the Curie temperature, T_c.

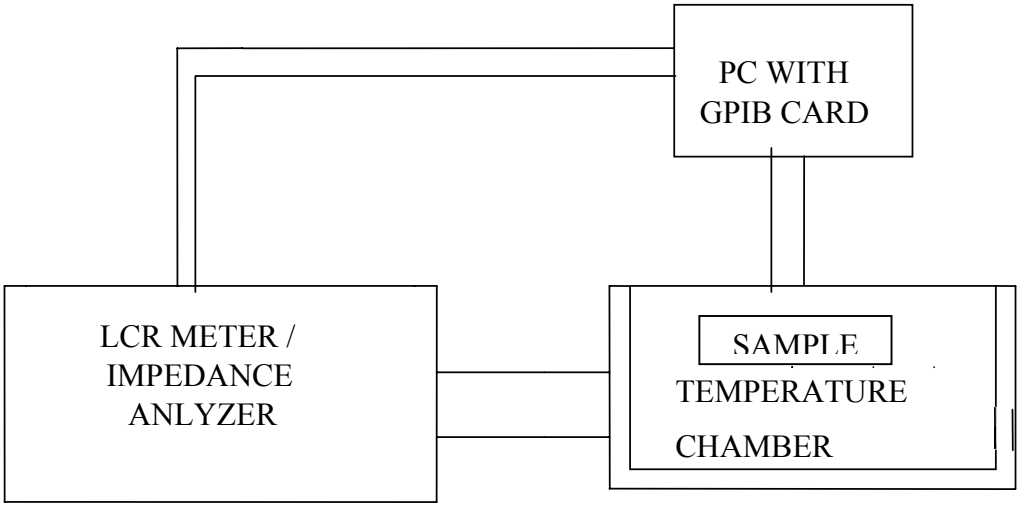

Fig. 2.9: Dielectric measurement setup for bulk samples

2.3.4 Hysteresis Measurements

Bulk System

Ferroelectric hysteresis (P-E) loops at room temperature for all the bulk samples were recorded using an Automatic PE Loop Tracer of M/S AR Imagetronics. The system consists of a PC, Software, programmable voltage source (up to 5 kV) and Silicon oil bath. The measurement is based on modified Sawyer Tower circuit, shown in fig. 2.10, operating at 50 Hz.

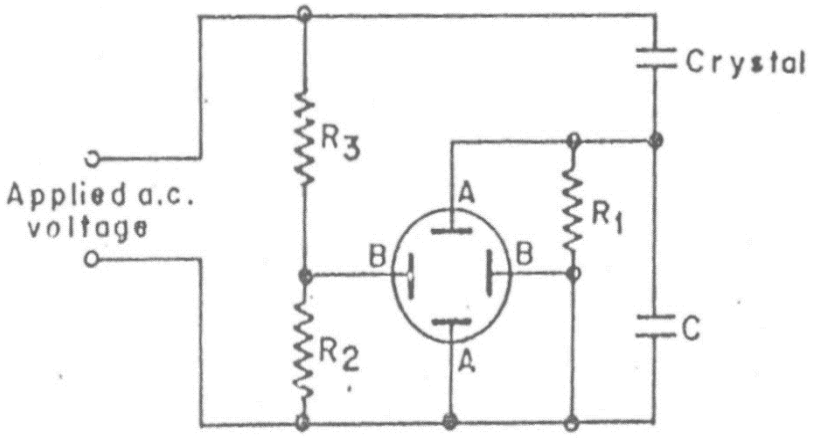

Fig. 2.10: Sawyer - Tower circuit for P - E loop measurements of bulk samples

For measurement, specimen was kept in a spring-loaded jig and immersed in silicon oil. The loop is recorded by the system and the software computes all the parameters e.g. P_s, P_r and E_c. Software has the facility of cycling and averaging of the data points.

Thin Films

The RT66A Standardized Ferroelectric Test System of MIS Radiant Technology was used for characterizing the thin films for hysteresis (P-E) loops. It combines the features of a function generator, an electrometer and a digital oscilloscope in a single package and the tester is controlled by the PC. The user specifies the operations that the tester is to perform from a menu-driven interface. The RT66A software then executes the appropriate hardware commands, collects and processes the data and then displays the results on screen. A block diagram of the RT66A test unit is shown in fig. 2.11. The user interacts with the test unit through the host computer that runs the graphical user interface, sends commands to the test units, and processes the measured data. The host computer communicates with the test unit through the data translation DT2811 interface board. The DT2811 exercises full control over all functions in the test unit.

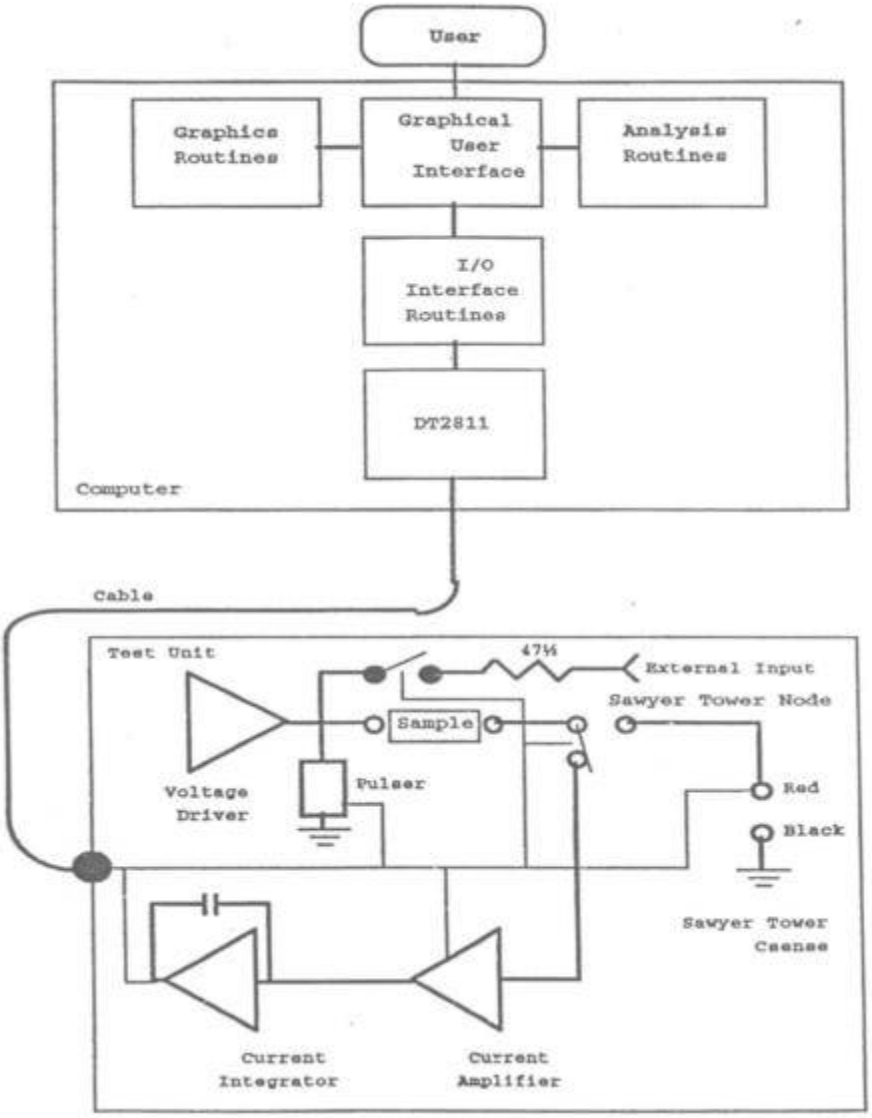

Fig. 2.11: RT66A test unit block diagram for P - E loop measurements of thin films

2.3.5 Piezoelectric Property Measurements of Bulk Samples

Piezoelectric Constants (d_{33} and d_{31})

Piezoelectric charge coefficients, d_{33} and d_{31} were been directly measured using a Piezometer System (Model PM 35, Take Control, U.K.). A brief description of this system is given below: -

Piezometer System

The PM35 (fig. 2.12) is a model in a range of instruments from Take control for measuring the properties of piezoelectric materials. By a simple, direct measurement, the PM35 gives an indication of d_{33} coefficient of all type of piezoelectric materials. The PM35 system consists of two units-force head and the PM35 system electronics unit. The later item provides the facility to store measurements. The block diagram shows the principle of operation of piezometer system. The piezoelectric sample under test is clamped within the jaws of the force head unit for testing. It is then subjected to an oscillating force and the charge developed by the sample is measured in order to determine the d_{33} coefficient.

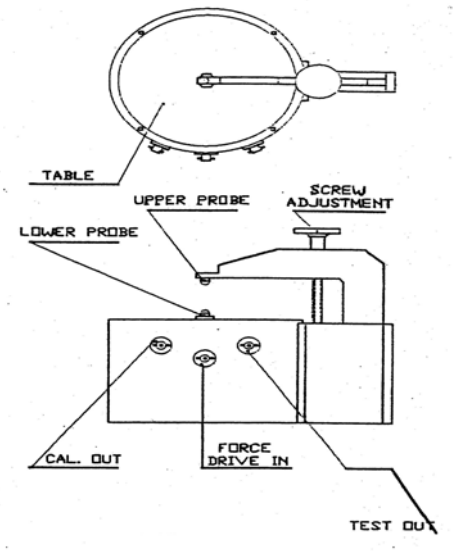

Fig. 2.12: Block diagram of P35 Piezometer System

Conventionally, d_{33} is defined as charge per unit force, both in the direction of polarization of a piezoelectric material i.e.

$$d_{33} = (\partial D_3)/(\partial T_3)_E \qquad \textbf{…2.14}$$

where D is the dielectric displacement vector and T is the applied stress vector. (The 3-axis is by convention the axis of polarization of piezoelectric materials-plastics and Ceramics).

Principle of operation:

$$d_{33} = CV/F \qquad \textbf{…2.15}$$

Where C is capacitance, V is voltage and F is force

The shunt capacitance C connected in parallel with the test specimen should be at least 10 to 100 times larger than the test sample in order to provide the correct boundary condition (constant E) for the d_{33} measurement.

Parameters:

Quasi-static force: 0. 2 N, Frequency: 20-300 Hz

Piezoelectric charge developed is collected on the shunt capacitance. This is converted to voltage reading using tube electrometer (0.1 to 10 V range) to give d_{33} directly.

$$Q_{total} = V_{observed} \times (C_{shunt} + C_{sample})$$

The value of d_{33} is displayed along with polarity.

The -ve sign indicates negative charge is generated at upper electrode as the specimen is compressed.

The +ve sign indicates the upper electrode is connected to the +ve terminal of the poling source.

A force of 0.1 Newton at a frequency of 97 Hz is applied on the electroded surfaces of poled piezoelectric ceramic samples. Force is applied by a mechanical probe, which also supports the sample and provides electrical connections to the two surfaces of the samples. The piezoelectric voltage generated is fed to an electronic driver, which after processing displays d_{33} on a microprocessor controlled digital monitor in pC/N. Stress is applied only on a small area and piezoelectric charge is generated only on the area under stress i.e. d_{33} is a point property. Another charge coefficient d_{31}, where applied force is perpendicular to the direction of poling was also measured, using a probe specially meant for this purpose.

Planar (k_p) and Thickness (k_t) Coupling Coefficients

Electromechanical coupling factors were determined by the resonance–antiresonance method using impedance-frequency data from an impedance analyzer (HP4294A) and piezoelectric resonance analysis program (PRAP) software.

2.4 Parameters Adopted for Material Synthesis in the Present Work

2.4.1 Bulk Sample Preparation and Characterization

2.4.1a Conventional Dry Ceramic Method

PCT compositions (modified by Sm, La and Ta) were prepared by using conventional Dry Ceramic Technique. To study the effect of cations on A site and to study the effect of different vacancies, Sm and La modified series were prepared in two different formulations as listed below and numbered as series A, B, C and D.

1. $Pb_{0.76-x}Sm_xCa_{0.24}Mn_{0.02}Ti_{0.98}O_3$ - Series A
2. $Pb_{0.76-3x/2}Sm_xCa_{0.24}Mn_{0.02}Ti_{0.98}O_3$ - Series B
3. $Pb_{0.76-x}La_xCa_{0.24}Mn_{0.02}Ti_{0.98}O_3$ - Series C
4. $Pb_{0.76-3x/2}La_xCa_{0.24}Mn_{0.02}Ti_{0.98}O_3$ - Series D

In all the above series, x was varied from 0 to 0.1 in steps of 0.02.

To study the effect of cation on B site, following composition was selected and named as series E.

5. $Pb_{0.76}Ca_{0.24}Mn_{0.02}Ti_{0.98-5x/4}Ta_xO_3$; x = 0-0.04 (in steps of 0.01) - Series E

Stoichiometric amounts of the raw materials in powder form (Aldrich, AR grade) of various oxides [(i) PbO, Sm_2O_3, CaO, MnO_2 and TiO_2, for compositions 1 & 2; (ii) PbO, La_2O_3, CaO, MnO_2 and TiO_2, for compositions 3 & 4; and (iii) PbO, Ta_2O_5, CaO, MnO_2 and TiO_2, for composition 5] were mixed and processed further in accordance to the given flow chart.

The mixture of raw materials was grinded for 4 hours in planetary ball mill using distilled water as the wetting agent and zirconia balls as a grinding media. After drying the slurry in oven, grinded powder was calcined at 850^{o}C for 4 hours in air followed by ball milling for 4 hours and drying. Excess PbO (2 mol%) was added to counteract the volatization of lead oxide during sintering. All the calcined powders were sieved and compacted in the form of rods using Cold Isostatic Press (CIP) (M/S Autoclave Engineers) (as shown in fig. 2.3) at a pressure of 200 MPa. These rods were sintered in a closed alumina crucibles with a heating rate of 5^{o}C/min at 1150^{o}C for 4 hours in a box furnace. A lead rich atmosphere was maintained with $PbZrO_3$ powder in order to further minimize the lead loss during firing. Sintered rods were machined to get the smooth surface and desired diameter (fig. 2.3). Sintered rods were ground to 8 mm diameter using cylindrical grinder equipped with diamond tools. These rods were sliced to make discs of thickness ~ 0.5 mm using precision diamond saw.

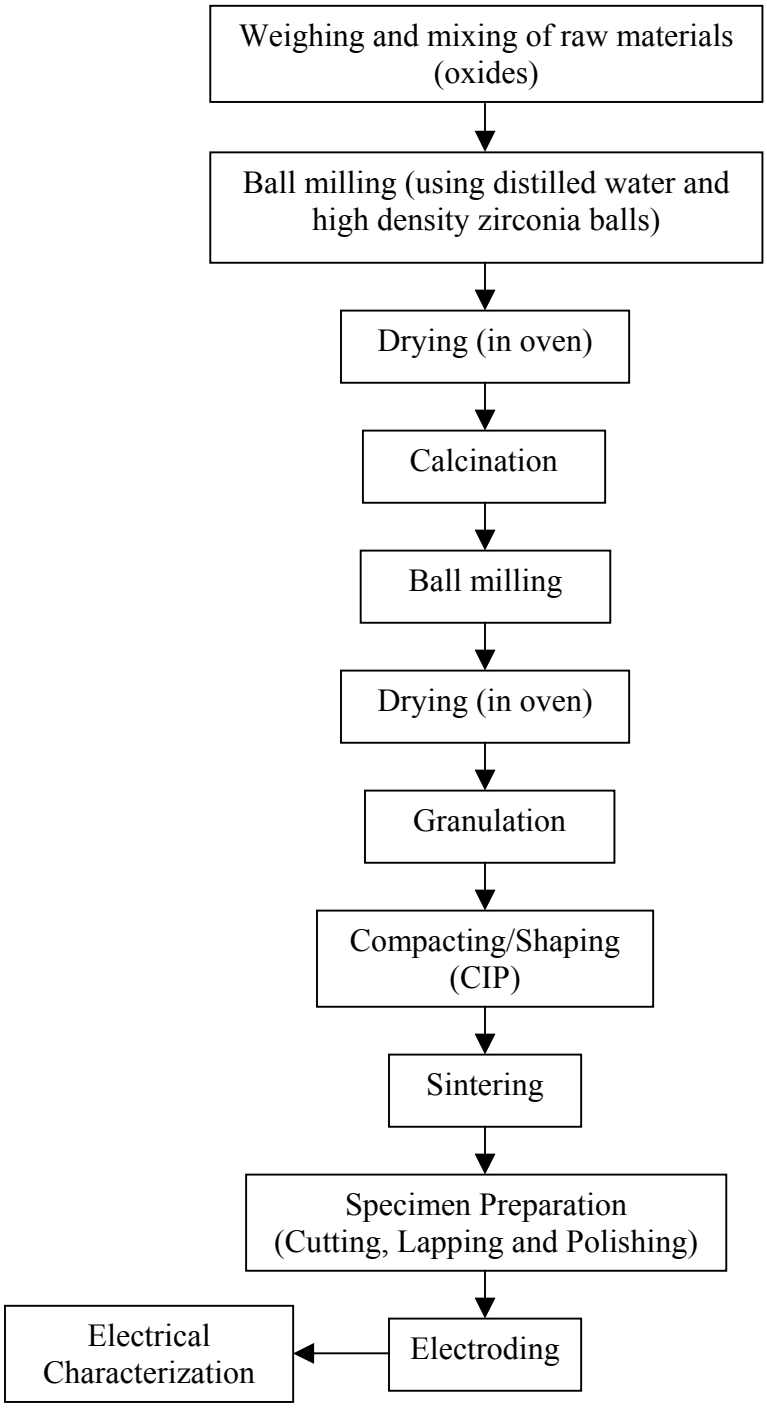

Flow Chart for Conventional Dry Ceramic Method

2.4.1b Microwave Processing

Samples with compositional formula $Pb_{0.76-3x/2}Sm_xCa_{0.24}Ti_{0.98}Mn_{0.02}O_3$ with x ranging from 0 to 0.08 in steps of 0.02 were prepared by mixing stoichiomertic amounts of PbO, CaO, TiO_2, MnO_2 and Sm_2O_3 (Aldrich, AR Grade). The powder mixture was ball milled for 4 hours in distilled water using zirconia balls as grinding media and dried in oven. The dried powder was calcined at 850°C for 4 hours in a conventional furnace. The reacted powder was ball milled again and isostatically pressed in rod form at a pressure of 200 MPa using Cold Isostatic Press (M/S Autoclave Engineers) for a homogeneous and better compaction of green rod. Microwave sintering (MS) of green rods of PCT ceramics was carried out in a modified microwave kitchen oven (2.45 GHz, 1.2 kW). The schematic of the system is depicted in fig. 2.13. Sintering was done at an optimized temperature of 1100°C for 30 minutes and the total cycle time was 135 minutes.

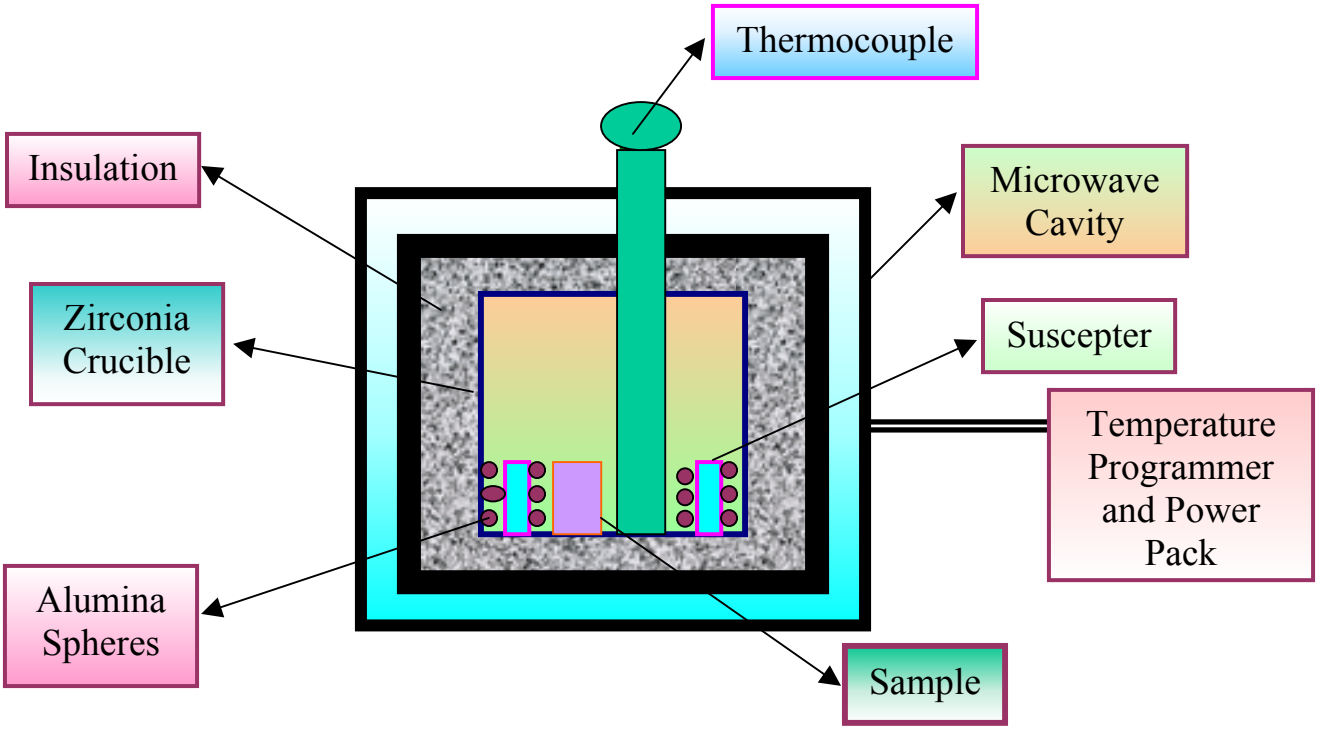

Fig. 2.13: Schematic of the microwave sintering system.

The heating rate was kept at 20°C/minute (by automatic controlling the input power to the microwave oven). Thermocouple was kept close to the sample. Cooling rate was maintained at 10°C/minute up to 800^{0}C followed by natural cooling. Sintered rods were ground to 8 mm diameter using cylindrical grinder equipped with diamond tools. These rods were sliced to make discs of thickness ~ 0.5 mm using precision diamond saw.

2.4.1c Mechano-chemical Alloying

Starting materials PbO, Sm_2O_3, TiO_2, MnO_2 and CaO (Aldrich) in the form of powders were used to prepare nominal composition $Pb_{0.70}Sm_{0.06}Ca_{0.24}Ti_{0.98}Mn_{0.02}O_3$ (PSCT). Excess PbO (2 mol%) was taken to compensate the lead loss during sintering at the elevated temperature. For mechano-chemical process, 50 grams of the powder was placed in a tungsten carbide coated jar with 80 zirconia balls (high density and high purity) of dia 10mm and subjected to dry grinding, using a planetary ball mill at a speed of 800 rpm for 30 minutes. The schematic of mechano-chemical alloying is shown in the fig. 2.14. Particle size of both the powders was measured using Micron photo sizer measuring unit (Model No. SKC-2000). The synthesized powders were pressed into rods using Cold Isostatic Press (M/S Autoclave Engineers) at a pressure of 200 Mpa and sintered at 1150°C for 4 hours in a conventional furnace.

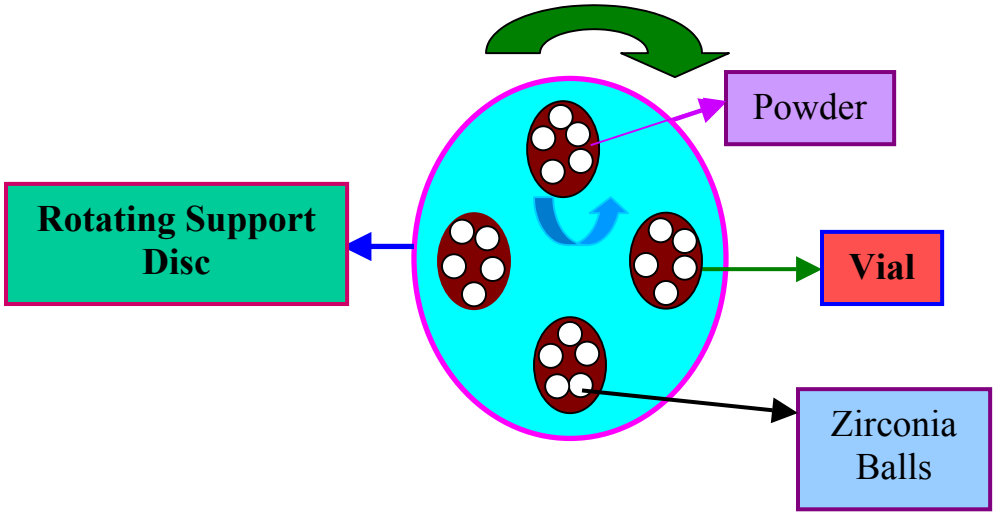

Fig. 2.14: Schematic of Mechano-chemical alloying Process

Sintered rod was grounded to 8 mm diameter using cylindrical grinder equipped with diamond tools. These rods were sliced to make discs of thickness ~ 0.5 mm using precision diamond saw.

2.4.2 Characterization

The samples prepared by Conventional Dry Ceramic technique, Microwave Processing and Mechano-chemical Alloying were characterized for structural, dielectric and piezoelectric properties. Density of sintered rods was measured by Archimedes method. The phase identification for sintered body with the substitution of Sm was carried out using XRD [PW 3020 Phillips Diffractometer interfaced with MPD Control (PW3710)] with Cu K_α (λ = 1.5405Å) radiation. The diffraction angle, 2θ, was varied from 20^o to 60^o. All the Lattice parameters ('c' and 'a') and tetragonality (c/a) were calculated by XLAT software using 2θ and hkl values. Microstructural study for the fractured surfaces of the samples was done using SEM (LEO 1430, Japan). Sintering behavior of the green samples was studied by using dilatometer (Orton, 1600D) with the variation of temperature from room temperature to 1150^{o}C. For electrical characterization, flat faces of sliced discs were gold sputtered using Turbo Sputter Coater. Measurement of dielectric constant (ε') and dissipation factor (tanδ) as a function of frequency and temperature were carried out using LCR meter (HP4284A) interfaced with a PC using IEEE-488 interface and programmable (RS-485) temperature chamber. The details are given in the electrical measurements section. Ferroelectric hysteresis (P-E) loops at room temperature for all the bulk samples were recorded using an Automatic PE Loop Tracer of M/S AR Imagetronics. The details are given in hysteresis measurements section. Piezoelectric properties were studied on the electrically poled discs. Poling was done at 150^{o}C by an applied dc field of 50 kV/cm for 30 min in a silicon oil bath. Piezoelectric charge coefficients, d_{33} and d_{31} have been directly measured using a Piezometer System (Model No. PM 35, Take Control, U.K.). The measurements of electromechanical coupling coefficients (k_t and k_p) were carried out as per IEEE standards using an impedance analyzer HP4294A and PRAP software.

2.4.3 Thin Film Preparation

A stoichiometric target of samarium modified lead calcium titanate ceramics (PCST) prepared by the solid-state reaction (conventional dry ceramic process) was used to deposit thin films by laser ablation on a platinised Si substrate. Platinum was used as bottom electrode. A KrF Excimer Laser, Lambda Physik Complex 201 (248 nm, 650 mJ, 25 ns) was used. Laser pulses with varying energy (50-250) mJ/shot were focused on to the target rotating at 10 rpm. The distance between the target and the substrate inside the vacuum chamber was ~ 5 cm. Oxygen (O_2) was used as reactive gas inside the chamber during deposition. Details of deposition conditions are given in table 2.1. A metal-ferroelectric-metal (MFM) structure was made by depositing a gold electrode of diameter 500 μm on top of the film by cold d.c. sputtering unit (Model No. Desk II TSC).

2.4.4 Thin Film Characterization

The thickness of the films was measured by using a surface profilometer (Model DEKTAK-3) after making a physical step by chemical etching. X-ray data was recorded using a Philips thin film diffractometer (Model PW 3020) fitted with glazing angle attachment using Cu(Kα) (λ = 1.5404 Å) to analyze the crystal structure with pure perovskite phase. The morphology of the films was characterized using atomic force microscopy (AFM, NT-MDT Solver P47H) in the resonant mode. Hysteresis loops were recorded using an automatic P-E loop tracer (RT-66A) of Radiant Technologies Inc. The I-V characteristics were studied using a DC power supply and a Keithley electrometer. The C-V characteristics of the films were measured at 100 kHz using a HP4294A impedance analyzer.

Table - 2.1

Deposition parameters for PSCT thin films

Substrate	$Pt/TiO_2/SiO_2/Si$ <100>
Target	$Pb_{0.66}Sm_{0.08}Ca_{0.24}Mn_{0.02}Ti_{0.98}O_3$
Target diameter	~1 inch
Substrate target distance	~5 cm
Substrate (heater) temperature	450^oC, 650^oC
Base Vacuum	3×10^{-6} torr
O_2 Pressure	9×10^{-3} torr
Laser Source	KrF Excimer, 650 mJ, 25 ns, 10 Hz
Laser energy used	(50-250) mJ/pulse
Repetition rate	5 Hz
Deposition time	30 min
Energy fluence	~ 1.2 J/cm^2
Post-deposition ex situ anneal	450^oC-650^oC/2 hrs

References

1. A.J. Moulson and J.M. Herbert, Electroceramics, Chapman and Hall, 1990, U.K.
2. M.H. Lente, A.L. Zanin, S.B. Assis, I.A. Santos, J.A. Eiras and D. Garcia, J. Eur. Ceram. Soc., **24 (**2004) 1529.
3. Y. Xu, Ferroelectric Materials and Their Applications, Elsevier Science Pub. Co. New York, USA (1991).
4. A.H. Webster, T.B. Weston and N.E.H. Bright, J. Am. Ceram. Soc. Bull., **50** (1967) 490.
5. W.H. Sutton, Am. Ceram. Soc. Bull., **68** (1989) 376.
6. D.E. Clark, W.H. Sutton and D.A. Lewis, Ceram. Trans., **80** (1997) 61.
7. J. Jacob, L.H.L. Chia and F.Y.C. Boey, J. Mater. Sci., **30** (1995) 5321.
8. R. Roy, S. Komarneni and J.L. Yang, J. Am. Ceram. Soc., **68** (1985) 392.
9. S. Komarneni and R. Roy, Mater. Lett., **4** (1986) 107.
10. Jr. W.B. Snyder, W.H. Sutton, M.F. Iskander and D.L. Johnson, Materials Research Society Proceedings, vol. 189, 1990, USA.
11. R.L. Beatty, W.H. Sutton and M.F. Iskander, Materials Research Society Proceedings, vol. 269, 1992, USA.
12. D.E. Clark, W.R. Tinga and Jr. J.R. Laia, Ceram. Trans., **36** (1993) 110.
13. A. Calka, A.P. Radlinski, Mater. Sci. Engg. A, **134** (1991) 1350.
14. J.Z. Jiang, F.W. Poulsen, S. Morup, J. Mater. Res., **14** (1999) 1343.
15. J.Z. Jiang, R. Lin, W. Lin, K. Nielsen, S. Morup, K. Dam-Johansen and R. Clasen, J. Phys. D: Appl. Phys., **30** (1997) 1458.
16. M. Simoneau, G.L. Esperance, J.L. Trudeau, R. Schultz, J. Mater. Res., **9** (1994) 535.
17. D.B. Chrisey and G.K. Hubler, Pulsed Laser Deposition of Thin Films, John Wiley and Sons, Inc., New York).
18. A.R. Verma and N. Srivastava, Crystallography for Solid State Physics, Wiley Eastern Limited, (1982).
19. B. Jaffe, W. Cook and H. Jaffe, Piezoelectric Ceramics, Academic Press, London (1971).

Chapter III

STRUCTURAL PROPERTIES

In the field of electroceramics and their processing for specific applications, one of the central paradigms is that ferroelectric-piezoelectric properties of these polycrystalline materials by the microstructure control. By bringing about a change in the microstructure of a composition, its bulk properties can be vastly changed. Microstructure and other related physical characteristics like density, porosity etc. of the modified $PbTiO_3$ are strongly affected by the processing parameters especially sintering temperature. Another significant role is played by the PbO component, which is volatile at the requisite sintering temperatures for $PbTiO_3$ ceramics. Ceramics of La-$PbTiO_3$ (PLT) [1], Lead Zirconate Titanate (PZT) [2] and PZT containing bismuth [3] have been prepared by hot pressing. Improvement in the microstructure, density, ferroelectric, piezoelectric and electro-mechanical properties is reported in the case of PZT and its modified composition by Mountvala [4].

As the entire piezo and ferroelectric behaviour of the ceramics is greatly influenced by their density after sintering, so one should first try to get the samples with higher green density so that good amount of percentage relative density achieved after sintering. Also sintering temperature and duration play a very important role in the development of microstructure and densification. Hence all the powders were first isostatically pressed into the rod form and then sintered at 1150^{o}C for 4 hrs to get sufficiently dense samples as at 1150^{o}C, maximum density (6.80 g/cc, ~ 95% relative density) of the pure PCT ceramics was achieved. Sintering temperature and duration were optimized after several experiments. Various researchers [5, 6] have also reported a density of ~ 95% of the theoretical during the sintering of PCT ceramics with 24 mol% Ca around 1050-1150^{o}C with the variation of dwelling time (3-5 hrs) and observed good ferroelectric and piezoelectric properties.

The experimental results of the structural properties of various series prepared by conventional dry ceramic technique are discussed in this chapter. These properties include the study of sintering behaviour of green samples using dilatometer, which

includes the temperature zone of maximum shrinkage, the amount of maximum shrinkage (%) and the dwelling time, perovskite phase evolution in relation with sintering behaviour, crystal structure, variation of density, lattice parameters (calculated form the XRD analysis) and grain size (obtained from microstructural analysis) with the substitution of samarium, lanthanum and tantalum in lead calcium titanate ceramics. Different series were named as series A, B, C, D and E and the compositional formula of individual series as given below: -

1. $Pb_{0.76-x}Sm_xCa_{0.24}Mn_{0.02}Ti_{0.98}O_3$ - Series A
2. $Pb_{0.76-3x/2}Sm_xCa_{0.24}Mn_{0.02}Ti_{0.98}O_3$ - Series B
3. $Pb_{0.76-x}La_xCa_{0.24}Mn_{0.02}Ti_{0.98}O_3$ - Series C
4. $Pb_{0.76-3x/2}La_xCa_{0.24}Mn_{0.02}Ti_{0.98}O_3$ - Series D

In all the above series, x was varied from 0 to 0.1 in steps of 0.02.

To study the effect of cation on B site, following composition was selected: -

$Pb_{0.76}Ca_{0.24}Mn_{0.02}Ti_{0.98-5x/4}Ta_xO_3$; x = 0 - 0.04 (in steps of 0.01) - Series E

3.1 X-ray Diffraction (XRD) Study

The XRD patterns of the modified PCT series are given in figures 3.1-3.5.

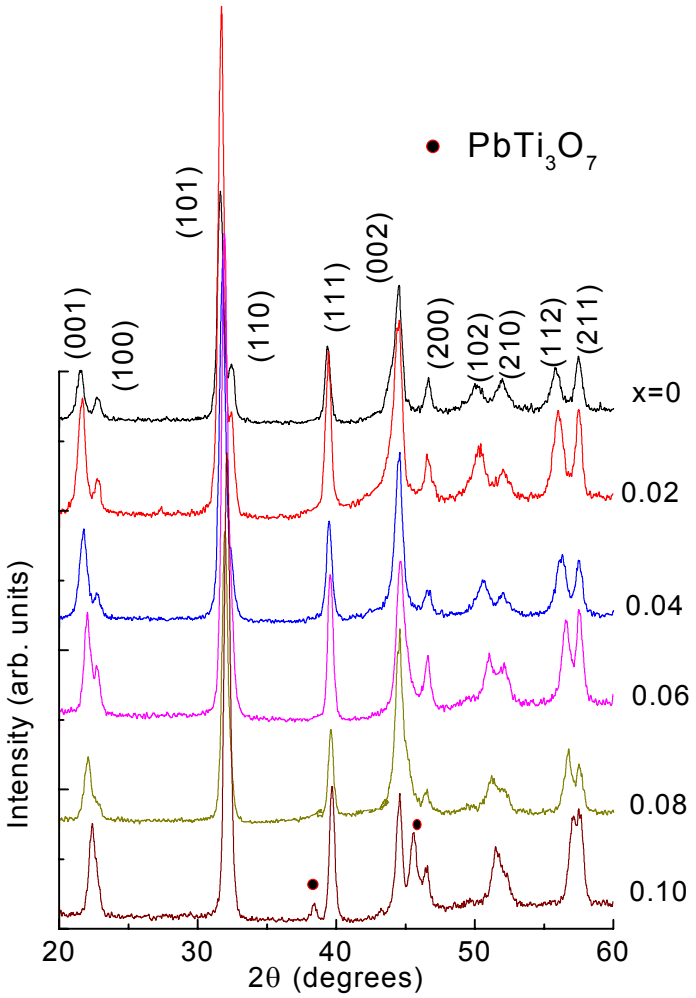

Fig. 3.1: The XRD patterns for the samples of series A

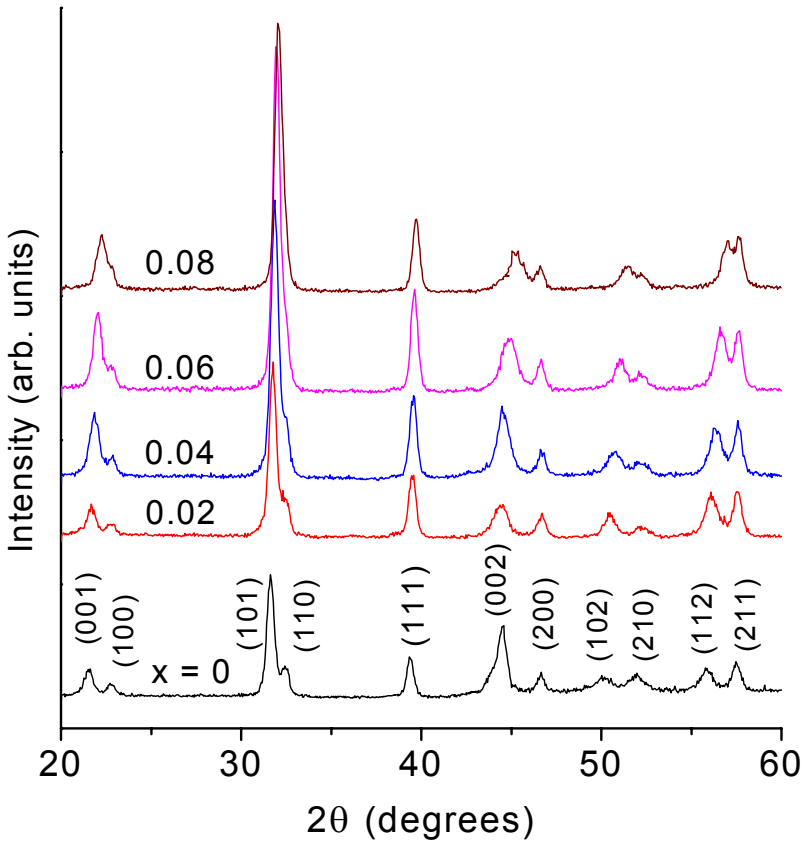

Fig. 3.2: The XRD patterns for the samples of series B

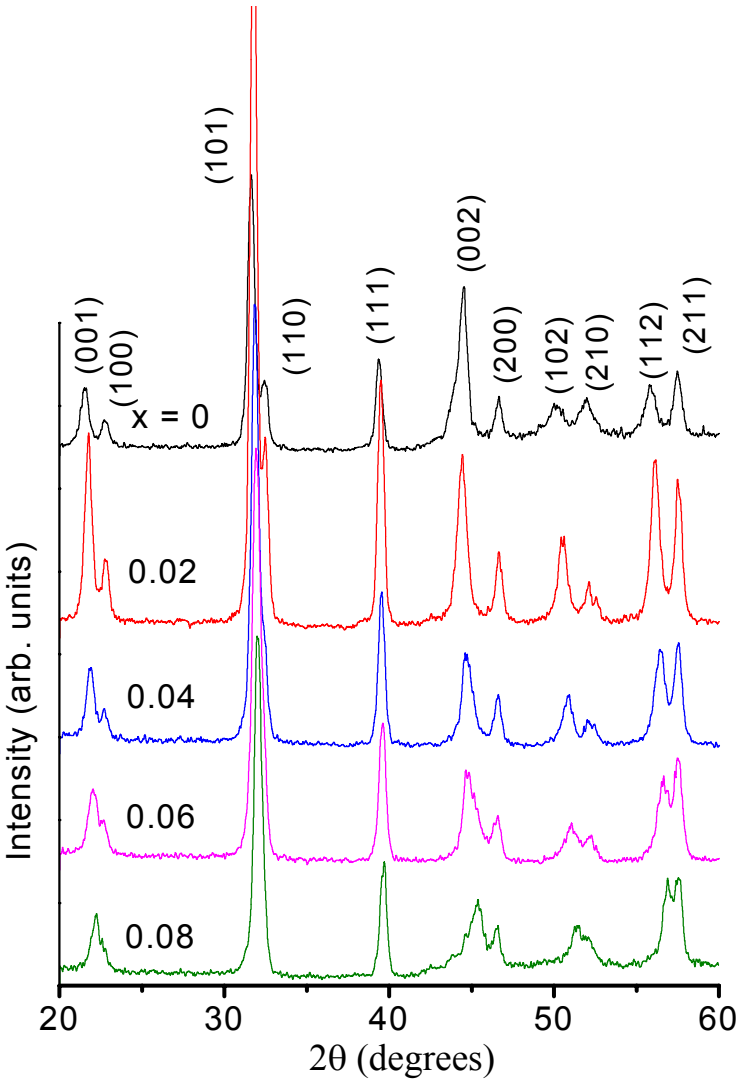

Fig. 3.3: The XRD patterns for the samples of series C

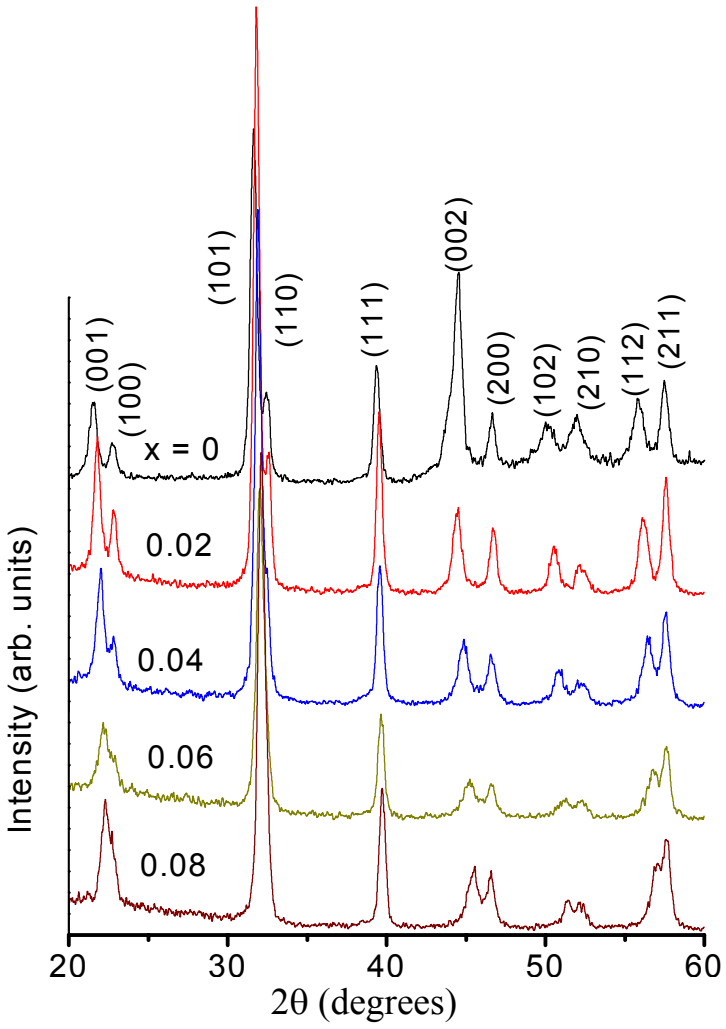

Fig. 3.4: The XRD patterns for the samples of series D

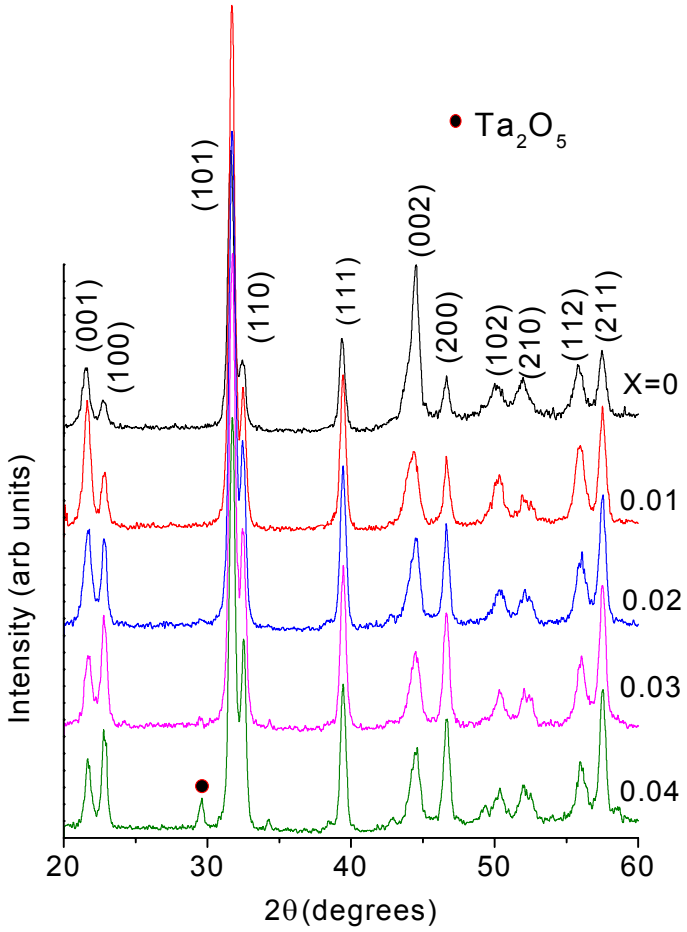

Fig. 3.5: The XRD patterns for the samples of series E

The phase formation for the present samples was confirmed by comparing the patterns with standard JCPDS file (6-0452) for $PbTiO_3$. The analysis showed all the samples to be single-phase with tetragonal structure except 10 mol% Sm and La as they reflect additional peaks of $PbTi_3O_7$ (JCPDS file, 21-949). These additional peaks are indicated in fig. 3.1. Also XRD pattern of 4 mol% Ta concentration showed extra peak of Ta_2O_5. Additional peaks could not be removed by raising sintering temperature and time. Hence further measurements were limited to 8 mol% of Sm and La substituted series and 3 mol% for Ta series. XRD analysis shows all the samples to be single-phase with tetragonal structure. The lattice parameters ('c' and 'a'), tetragonality (c/a) and unit cell volume (V) were calculated from XRD data using standard software "XLAT". The variation of 'c' and 'a' for all the series is given in table 3.1.

Table - 3.1

Lattice parameters (c, a) of the sintered samples of different series

	Series A		Series B		Series C		Series D		Series E		
x	c (Å)	a (Å)	c (Å)	a (Å)	c (Å)	a (Å)	c (Å)	a (Å)	x	c (Å)	a (Å)
0	4.099	3.879	4.099	3.879	4.099	3.879	4.099	3.879	0	4.099	3.879
0.02	4.09	3.88	4.076	3.888	4.075	3.890	4.074	3.890	0.01	4.093	3.890
0.04	4.08	3.89	4.065	3.887	4.040	3.896	4.039	3.895	0.02	4.087	3.891
0.06	4.046	3.898	4.026	3.893	4.023	3.898	4.007	3.896	0.03	4.084	3.892
0.08	4.011	3.90	3.986	3.897	3.990	3.903	3.989	3.899	-	-	-

In all the five series, the variation of lattice constants as a function of Sm, La and Ta is similar. It is seen that there is relative decrease of 'c' and relative increase of 'a' as the amount of substituent increases. However, the decrease in 'c' is much more pronounced than the increase in 'a' for all the series except the series E where this change is very less. The c/a ratio, which is a measure of crystal tetragonality, is observed to decrease with the increase in substitution level (Sm, La and Ta). The values are given in table 3.2.

Table - 3.2

Variation of Tetragonality (c/a) with different x

c/a						
	Series A	Series B	Series C	Series D	Series E	
x					x	
0	1.057	1.057	1.057	1.057	0	1.057
0.02	1.055	1.048	1.047	1.047	0.01	1.052
0.04	1.049	1.045	1.037	1.037	0.02	1.050
0.06	1.037	1.034	1.032	1.028	0.03	1.048
0.08	1.028	1.023	1.028	1.023	-	-

The decrease in tetragonality is more (from 1.057 to 1.023) in case of Sm and La substituted samples as compared to Ta substituted samples, where the decrease is only up to 1.048 from 1.057. This decrease in tetragonality confirms the approachness of the compounds towards cubic structure [7-11]. Also if we compare series A with series B and also series C with series D, then it was observed that there is relatively more difference in c/a ratio in case of Sm substitution but La substitution by two different formulas does not give any significant change. Relatively less decrease in the c/a ratio was observed in the tantalum substituted PCT ceramics as compared to Sm and La substituted ceramics resulting in the reduction of the mechanical strength. This difference in the values of c/a ratio of the series E may be probably due to the poor incorporation of Ta into the lattice and its influence on the distribution of vacancies in PCT ceramics.

3.2 Density

A study of the variation of density with the substitution of various elements (Sm, La and Ta) is presented here in this section. The values of experimental density (measured by Archimedes Principle), theoretical (XRD) density and relative density of all the sintered samples (rods) of individual series are given in tables 3.3 and 3.4. For series A, B and C, experimental and relative density showed an increasing trend. For series D, beyond 6 mol% La concentration, there is a decrease in the experimental density because of the large continuous reduction in the theoretical density for 8 mol% La samples.

Table - 3.3

Variation of experimental (d_{ex}, g/cc) and theoretical density (d_{th}, g/cc) with different x

	Series A		Series B		Series C		Series D		Series E		
x	d_{ex}	d_{th}	d_{ex}	d_{th}	d_{ex}	d_{th}	d_{ex}	d_{th}	x	d_{ex}	d_{th}
0	6.80	7.150	6.80	7.150	6.80	7.150	6.80	7.150	0	6.80	7.150
0.02	6.84	7.137	6.82	7.110	6.82	7.155	6.83	7.122	0.01	6.56	7.192
0.04	6.90	7.130	6.83	7.051	6.85	7.162	6.86	7.071	0.02	6.07	7.244
0.06	6.94	7.124	6.86	7.012	6.90	7.147	6.88	7.022	0.03	5.77	7.282
0.08	7.03	7.120	6.88	6.981	6.98	7.146	6.83	6.941	-	-	-

Table - 3.4

Variation of relative density (d_{rel}, %) with different x

d_{rel}						
	Series A	Series B	Series C	Series D	Series E	
x					x	
0	95.1	95.1	95.1	95.1	0	95.1
0.02	95.8	95.9	95.3	95.9	0.01	91.2
0.04	96.7	96.8	95.6	97.0	0.02	83.9
0.06	97.4	97.8	96.5	97.9	0.03	79.3
0.08	98.7	98.4	97.6	98.4	-	-

The theoretical density is seen to continuously decrease in all the series with increasing incorporation of Sm and La in PCT lattice, as inferred from table 3.3. This behaviour has been attributed to the replacement of Pb by Sm and La [12] because of the fact that the atomic weight of lead is much more than that of lanthanum and samarium so the molecular weight decreases as La and Sm modification increases. This clearly shows (table 3.4) that for the Sm and La substituted series, the percentage of theoretical density

constantly increases with the incorporation of Sm and La in PCT ceramics. Thus, higher samarium and lanthanum substituted PCT ceramics are seen to be relatively denser.

The role of excess PbO is again invoked to explain the increase of experimental density with increasing samarium and lanthanum substitution. Among other reasons, one possible reason is that as La and Sm ions, which replace Pb ions, increase, more and more Pb ions become surplus in the $PbTiO_3$ lattice. This metallic lead is oxidized into PbO and this volatile PbO helps in filling the pores by providing a liquid phase along grain boundaries in which material transport is facilitated resulting in better densification with increasing Sm and La content. Another reason for increasing density is that with increasing Sm and La substitution, the tetragonality of the PCT crystal lattice is reduced, which leads to a reduction in internal stresses, thus allowing crystallites in grains to accommodate more closely to form a denser micro-structure in which inter granular strains are also reduced due to less crystal anisotropy.

The theoretical density increases (table 3.4) and relative density decreases (table 3.4) with the increase in the tantalum amount in PCT ceramics where Ta replaces Ti in the B-site making modified PCT ceramics less dense. Thus it can be concluded that the substitution of Sm and La is favourable for PCT ceramics whereas tantalum substitution is unfavourable for getting the dense PCT ceramics. Also no significant change in the relative density was observed if we prepare the Sm or La substituted series with two different formulas as can be seen from the values given in table 3.4.

3.3 Microstructural Study

The grain size in lead titanate is greatly influenced upon the species and content of additives and is one of the important factors influencing the poling behaviour, ferroelectric and piezoelectric properties. The microstructures of the freshly fractured sintered samples of all the compositions are shown in figures 3.6-3.10. Average grain size was measured by linear intercept method and is given in table 3.5. It can be seen from the micrographs that the samples show uniform grain growth and grain compaction with well-defined grain boundaries with the increase in substitution of Sm and La in PCT ceramics. A drastic reduction in the crystal tetragonality with increasing amount of Sm

and La and the role played by PbO, as already discussed, may be attributed to the observed microstructural compaction.

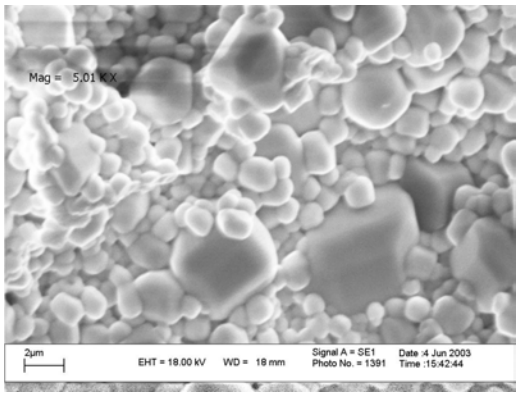

x = 0

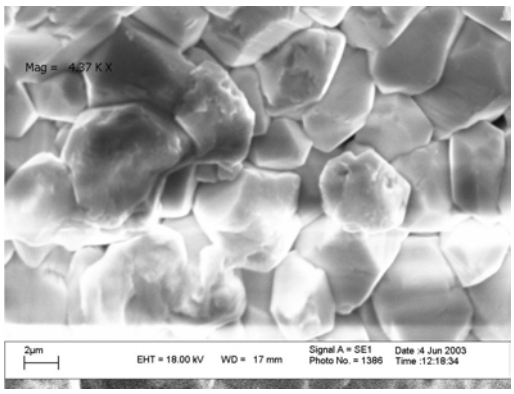

x = 0.02

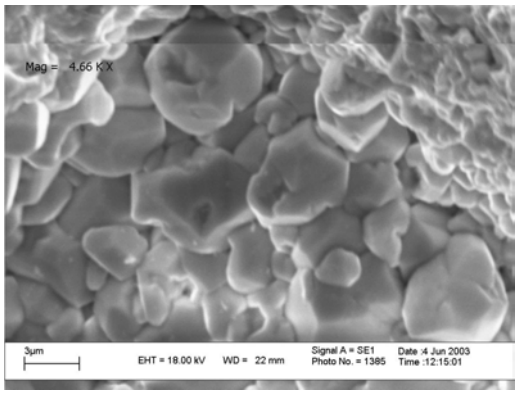

x = 0.04

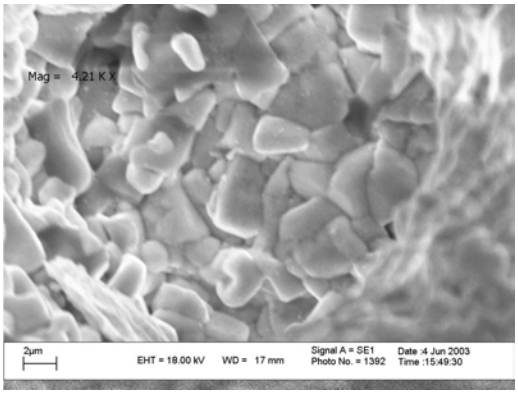

x = 0.06

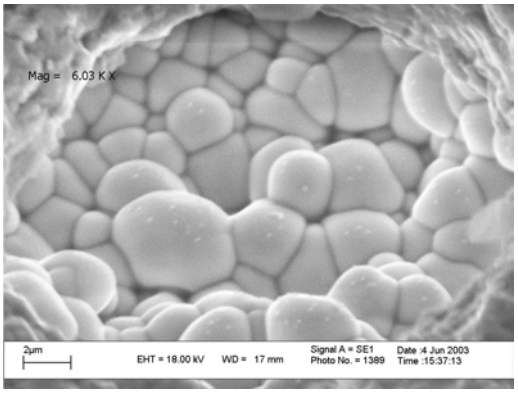

x = 0.08

Fig. 3.6: The Scanning Electron Micrographs for the fractured surfaces of the samples of series A

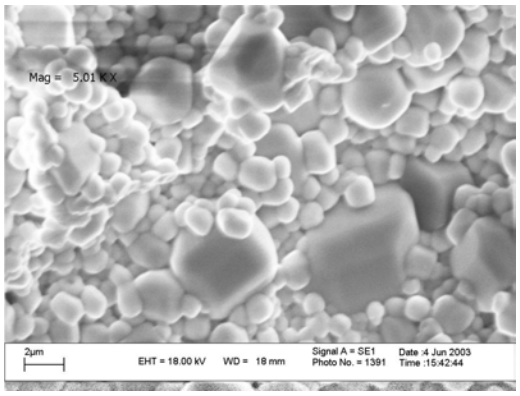

x = 0

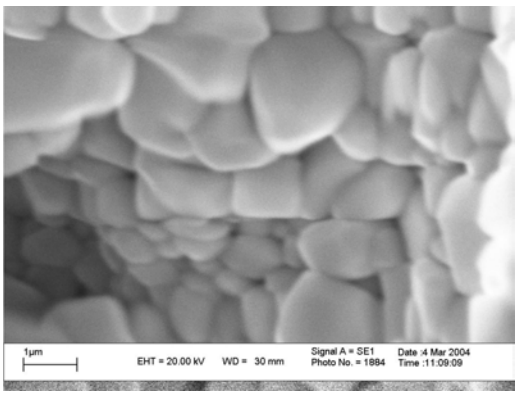

x = 0.02

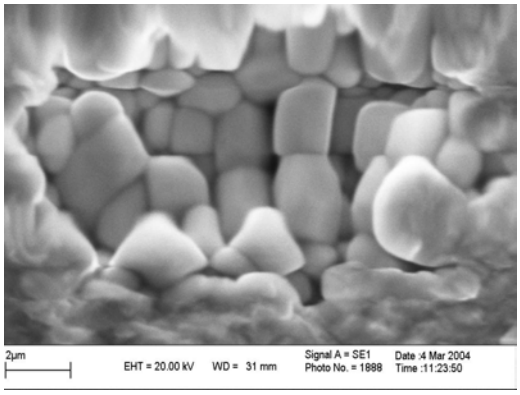

x = 0.04

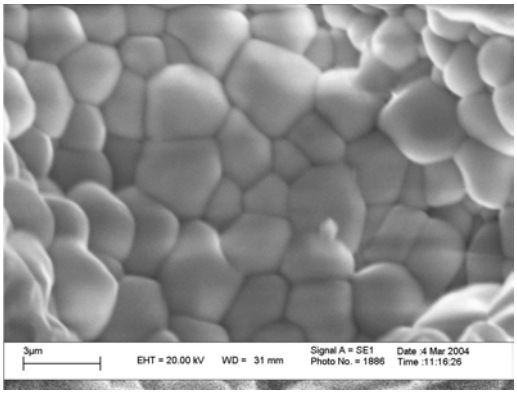

x = 0.06

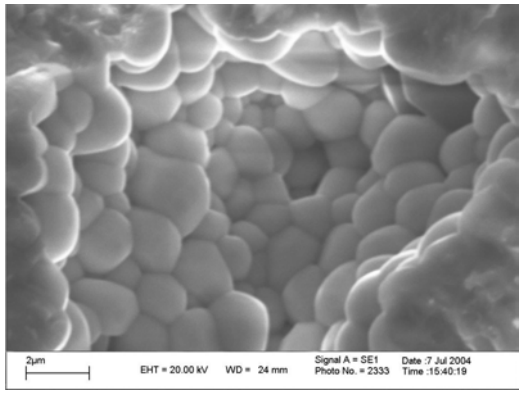

x = 0.08

Fig. 3.7: The Scanning Electron Micrographs for the fractured surfaces of the samples of series B

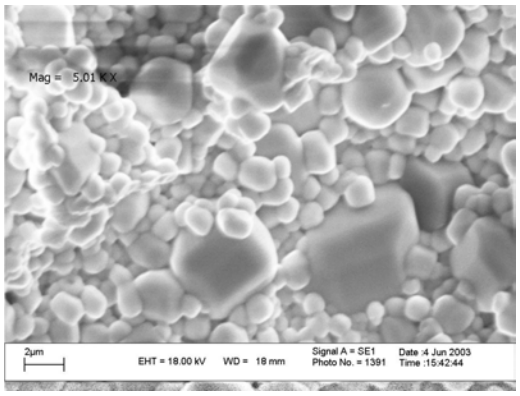

x = 0

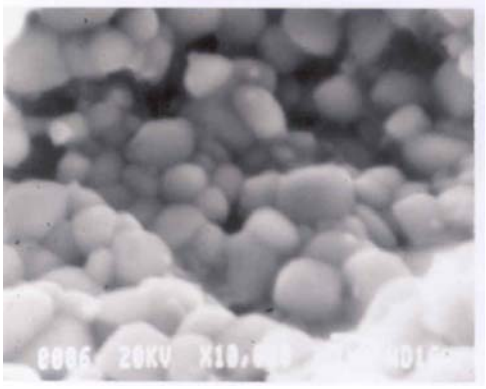

x = 0.02

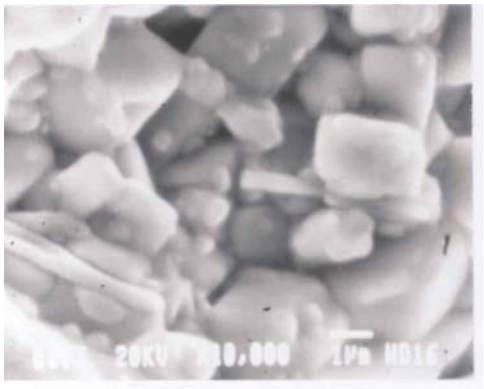

x = 0.04

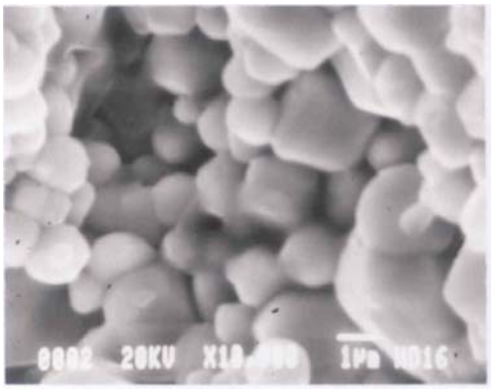

x = 0.06

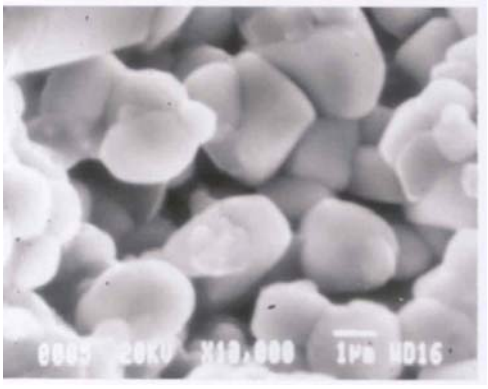

x = 0.08

Fig. 3.8: The Scanning Electron Micrographs for the fractured surfaces of the samples of series C

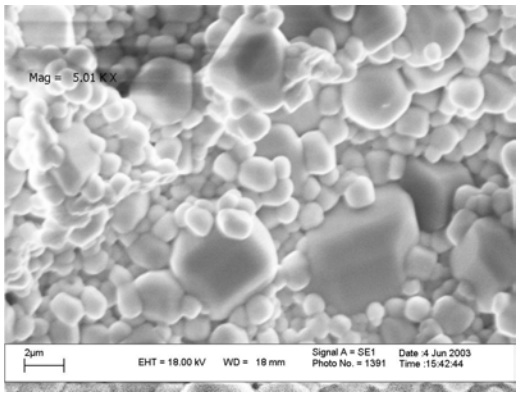

x = 0

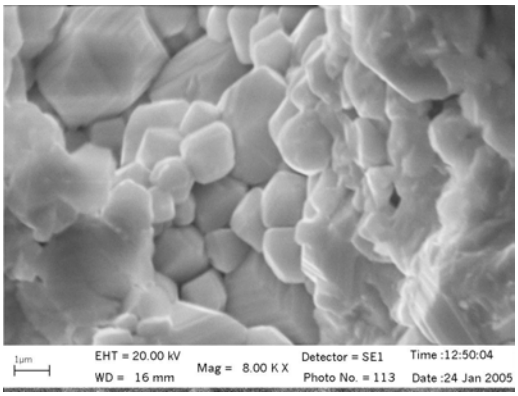

x = 0.02

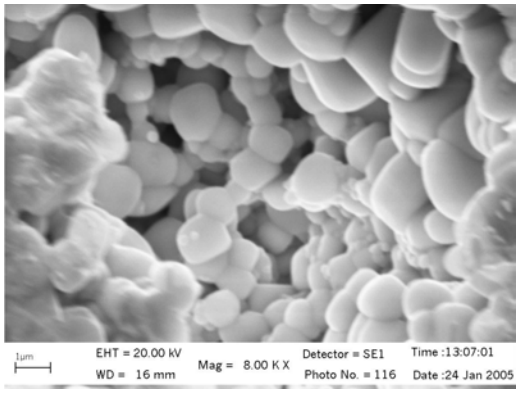

x = 0.04

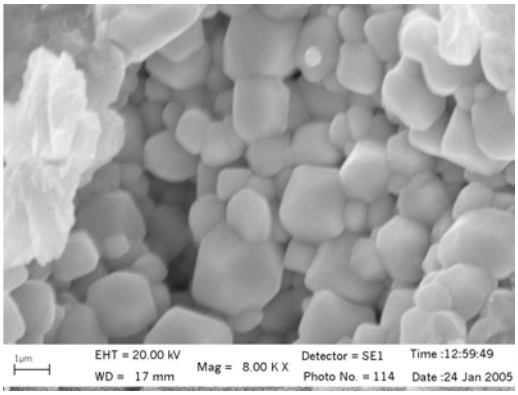

x = 0.06

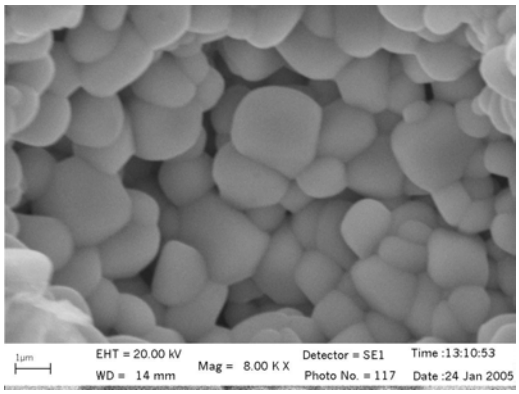

x = 0.08

Fig. 3.9: The Scanning Electron Micrographs for the fractured surfaces of the samples of series D

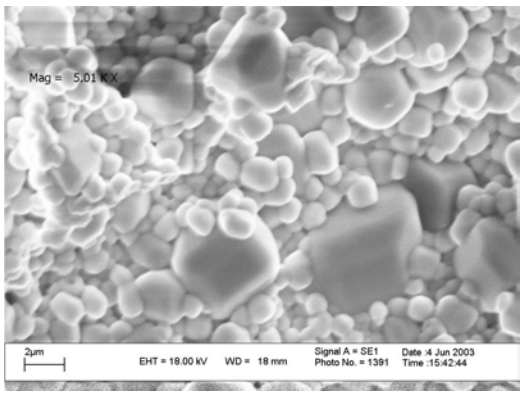

x = 0

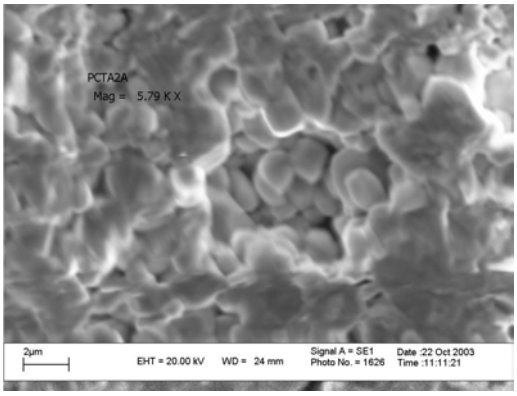

x = 0.01

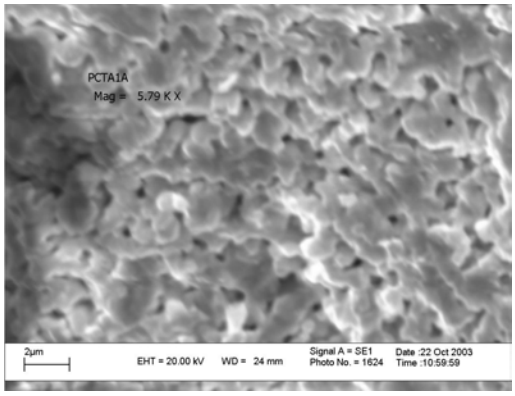

x = 0.02

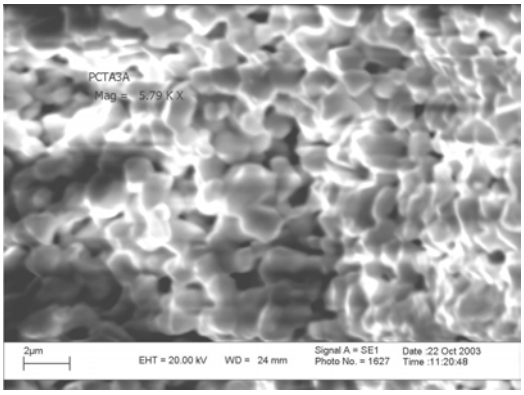

x = 0.03

Fig. 3.10: The Scanning Electron Micrographs for the fractured surfaces of the samples of series E

For the series A and B, grain size first increases for 2 mol% Sm substitution followed by the decrease with further substitution of samarium up to 6 mol% and then again increases for 8 mol%. The average grain size estimated to be 1.2-3.2 µm for series A and 1.2-2.2 µm for series B. For series C and D, grain size first increases up to 2 mol% La and then decreases for 4 mol% followed by further increase up to 8 mol%. The average grain size estimated to be 1.2-2.5 µm for series C and 1.2-2.3 µm for series D. The increase in grain size up to 2 mol% may be due to the complete dissolution of samarium in perovskite

lattice. The microstructural analysis for series E showed that as the Ta concentration increases, grain size first increases from 1.2 μm to 1.4 μm for 1 mol% followed by the decrease up to 0.9 μm for 3 mol%. Also the samples look like more porous as we increase the amount of tantalum, which is in good agreement with density results where we found a decrease in density with increase in tantalum amount.

Table - 3.5

Variation of average grain size with different x

Average Grain Size (μm)						
	Series A	Series B	Series C	Series D	Series E	
x					x	
0	1.2	1.2	1.2	1.2	0	1.2
0.02	3.2	2.0	2.0	1.8	0.01	1.4
0.04	3.0	1.8	1.5	1.5	0.02	1.1
0.06	2.2	2.0	1.8	2.0	0.03	0.9
0.08	2.8	2.2	2.5	2.4	-	-

3.4 Dilatometric (Sintering) Behaviour

Figures 3.11-3.15 show the typical dilatometric plots of one of the discs (cut from green rods) for individual series.

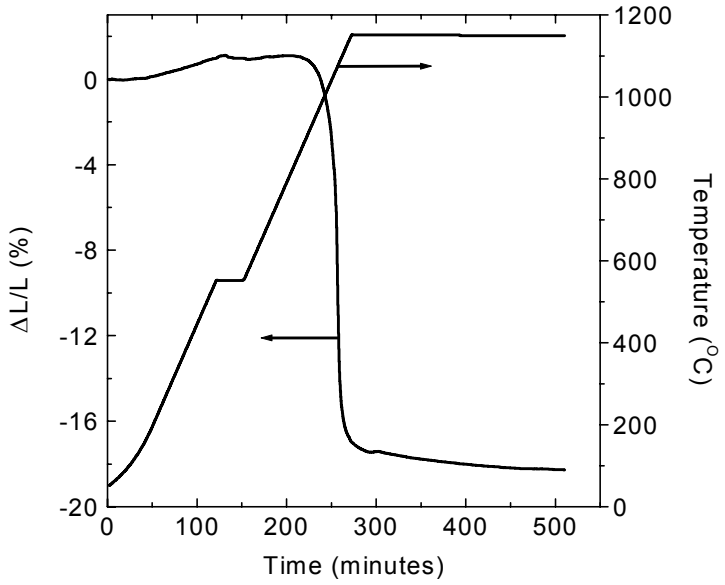

Fig. 3.11: Typical shrinkage behaviour for one of the green compact (x = 0.06) of series A

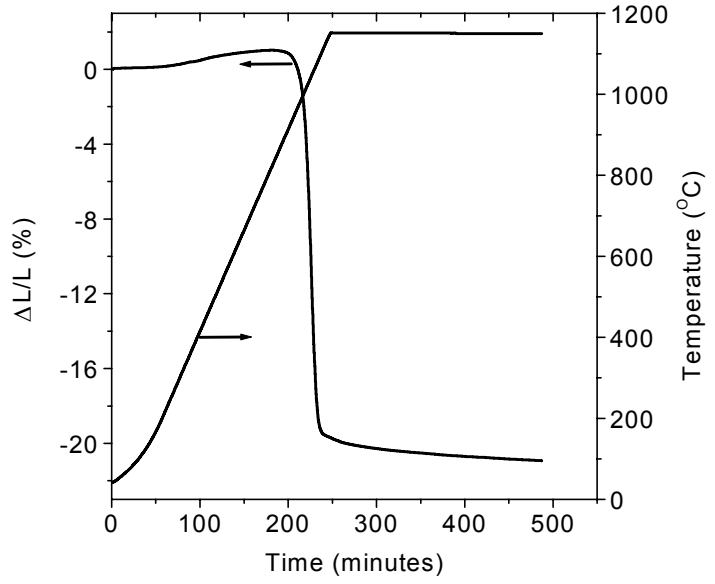

Fig. 3.12: Typical shrinkage behaviour for one of the green compact (x = 0.06) of series B

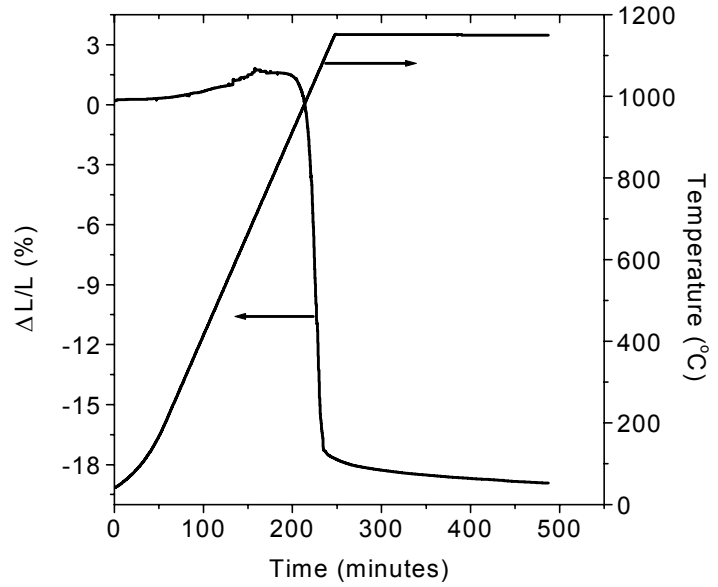

Fig. 3.13: Typical shrinkage behaviour for one of the green compact (x = 0.06) of series C

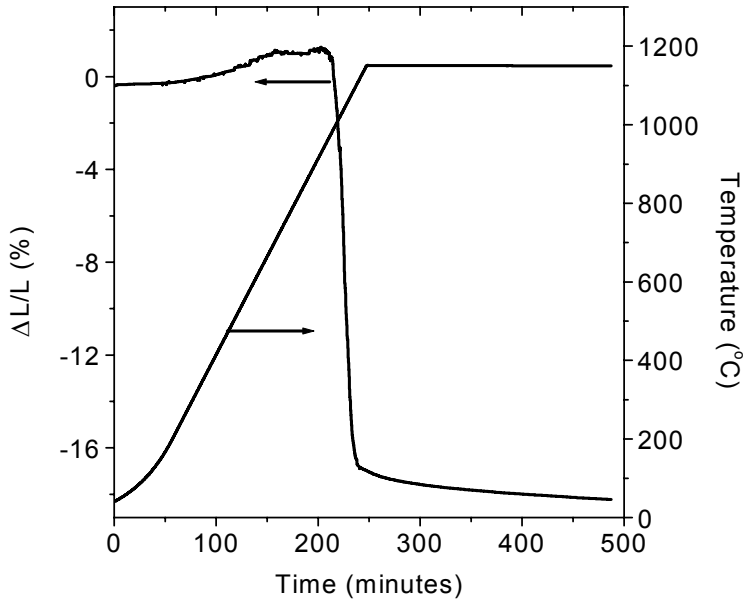

Fig. 3.14: Typical shrinkage behaviour for one of the green compact (x = 0.06) of series D

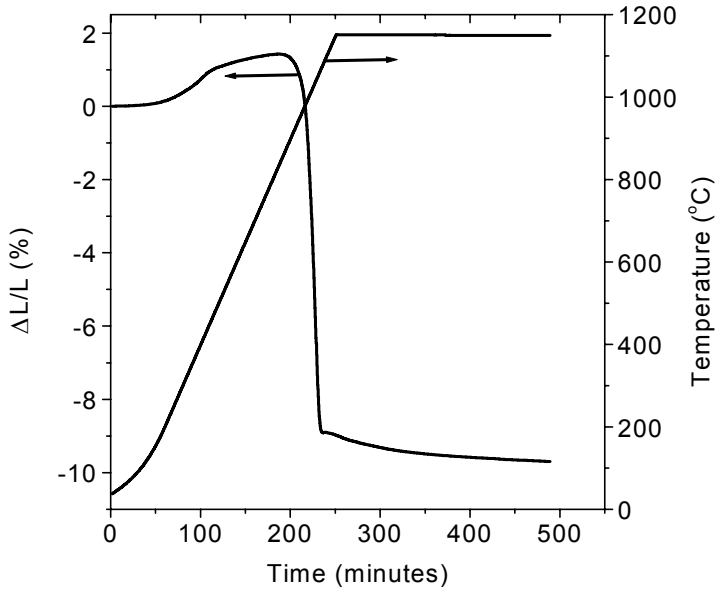

Fig. 3.15: Typical shrinkage behaviour for one of the green compact (x = 0.01) of series E

In all the plots, up to ~ 825-850^{o}C, the thermal expansion is nearly constant and the curve reaches a maximum at about 900^{o}C. Then shrinkage starts at a faster rate with increasing temperature till ~ 1080-1100^{o}C followed by slow shrinkage till 1150^{o}C. Relatively more shrinkage (~ 16-20%) was observed for the Sm and La substituted PCT samples as compared to the shrinkage (~ 10%) observed in Ta substituted sample. Shrinkage also keeps on continuing when sample is held at 1150^{o}C for 240 minutes. In order to better understand the shrinkage behaviour, the derivatives (shrinkage rate) of figures 3.11-3.15 were plotted in figures 3.16-3.20, respectively. They clearly indicate that the maximum shrinkage occurs between 900^{o}C and 1100^{o}C.

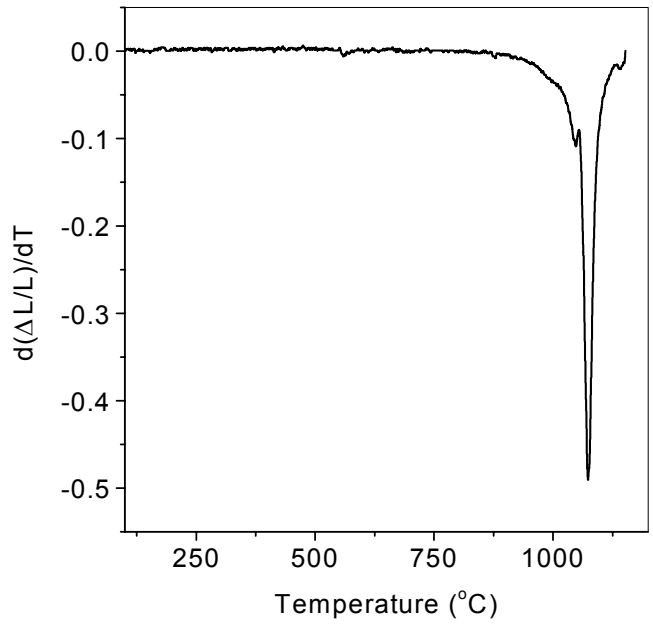

Fig. 3.16: A typical shrinkage rate for one of the green compact (x = 0.06) from series A

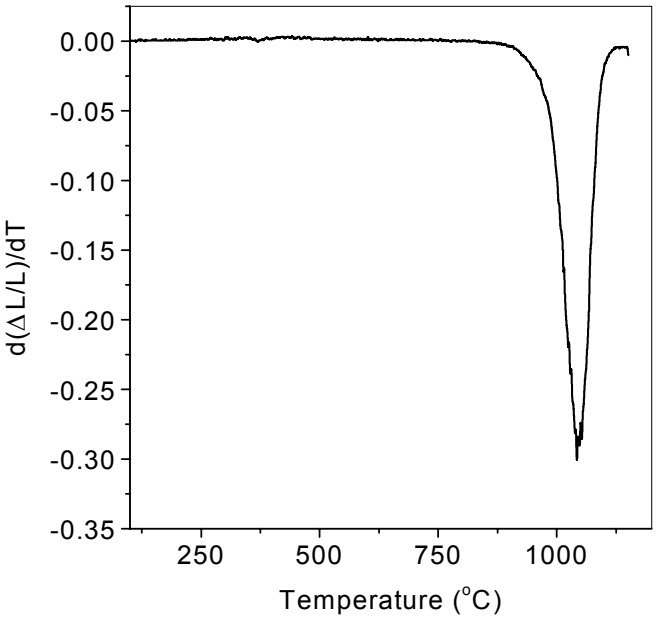

Fig. 3.17: A typical shrinkage rate for one of the green compact (x = 0.06) from series B

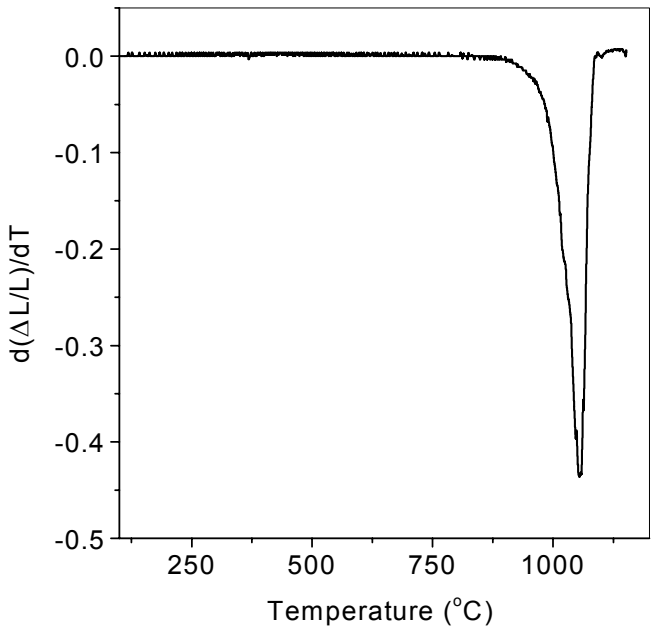

Fig. 3.18: A typical shrinkage rate for one of the green compact (x = 0.06) from series C

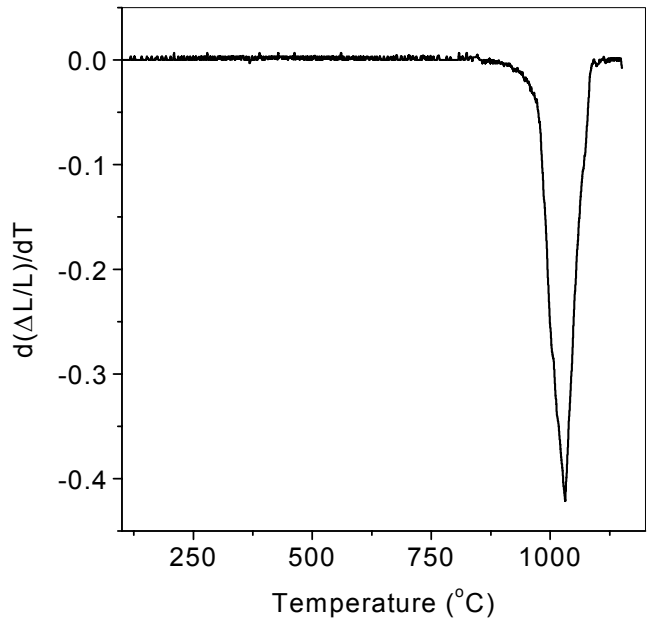

Fig. 3.19: A typical shrinkage rate for one of the green compact (x = 0.06) from series D

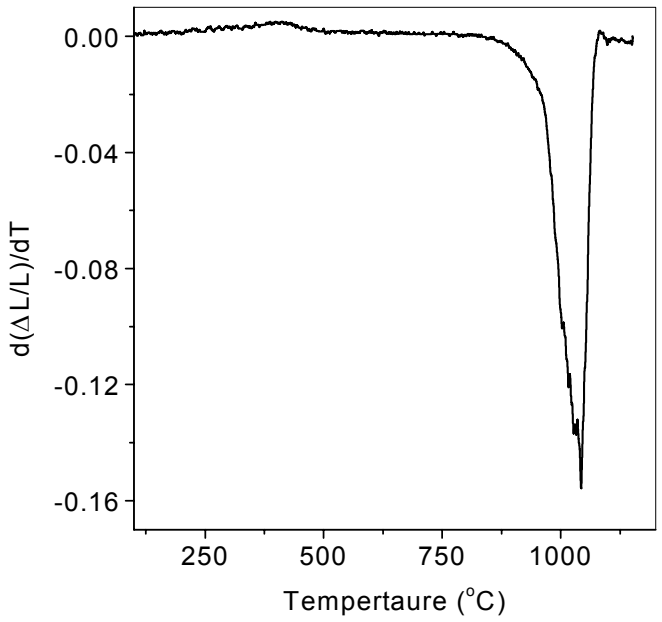

Fig. 3.20: A typical shrinkage rate for one of the green compact (x = 0.01) from series E

Further, in order to see the change during isothermal schedule of 240 min, this part was separately drawn for each plot and is shown in fig. 3.21-3.25. The logarithmic representation of this part allows the dominating shrinkage mechanism to be verified (fig. 3.26-3.30).

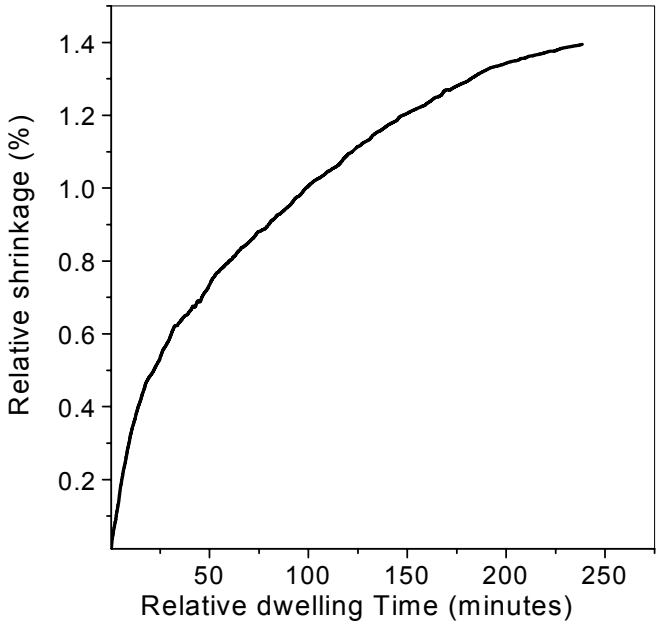

Fig. 3.21: Plot of relative shrinkage vs. relative dwelling time for fig. 3.11

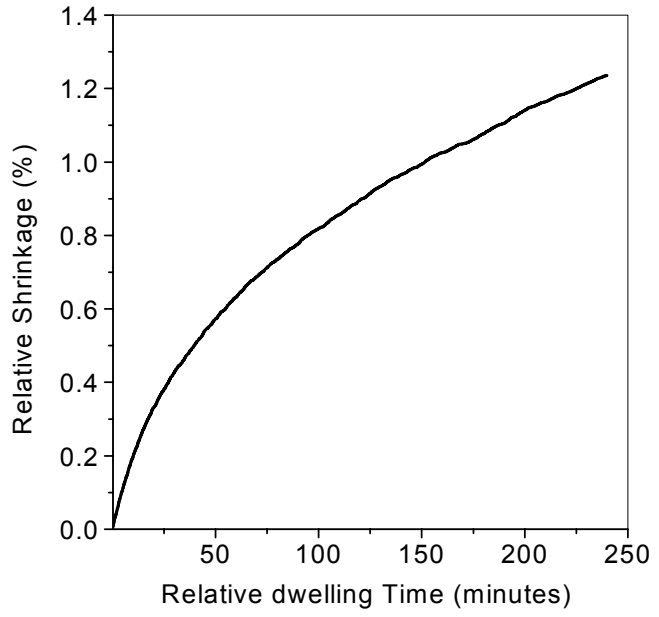

Fig. 3.22: Plot of relative shrinkage vs. relative dwelling time for fig. 3.12

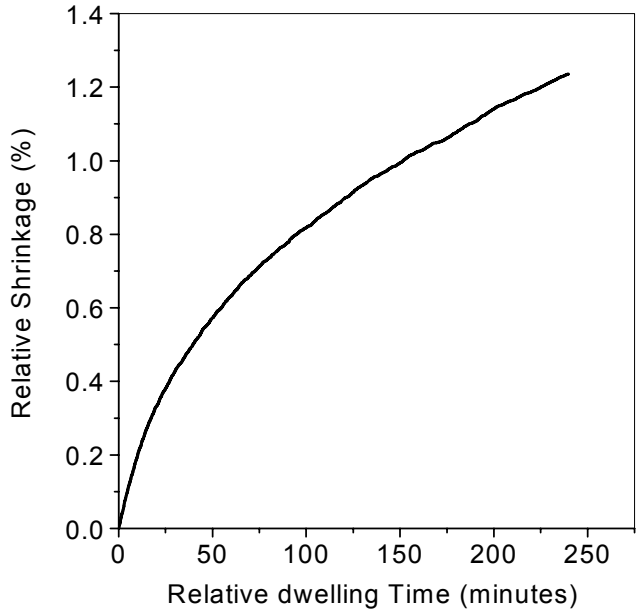

Fig. 3.23: Plot of relative shrinkage vs. relative dwelling time for fig. 3.13

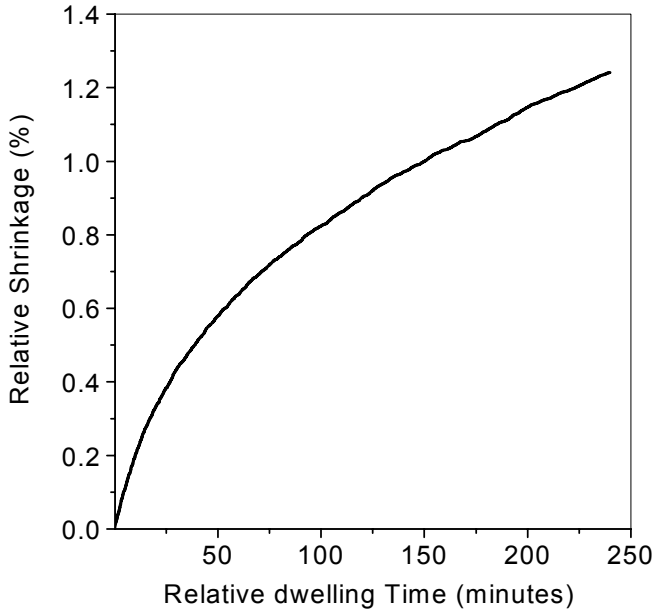

Fig. 3.24: Plot of relative shrinkage vs. relative dwelling time for fig. 3.14

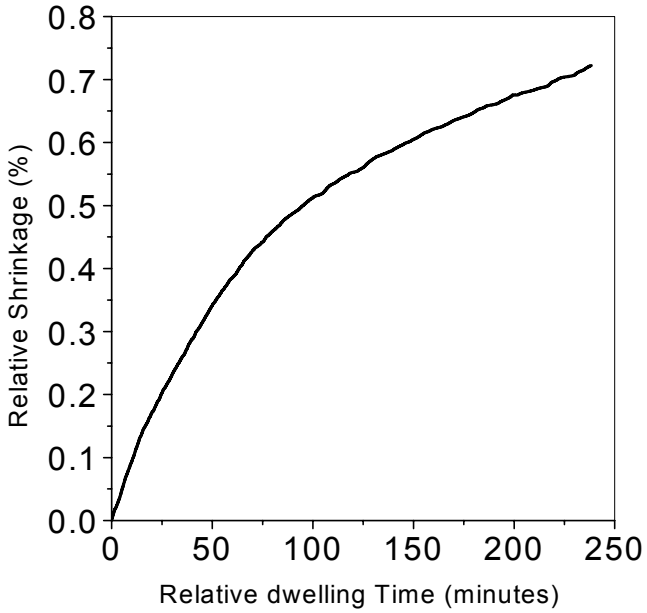

Fig. 3.25: Plot of relative shrinkage vs. relative dwelling time for fig. 3.15

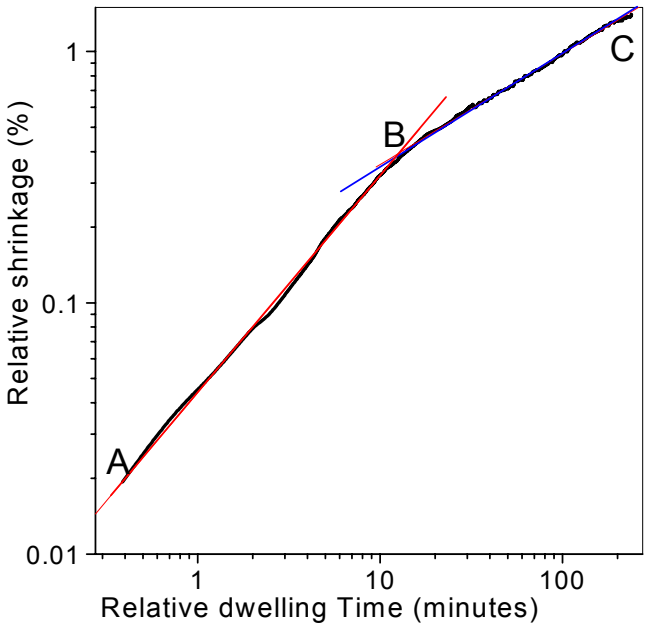

Fig. 3.26: A logarithmic plot of fig. 3.16

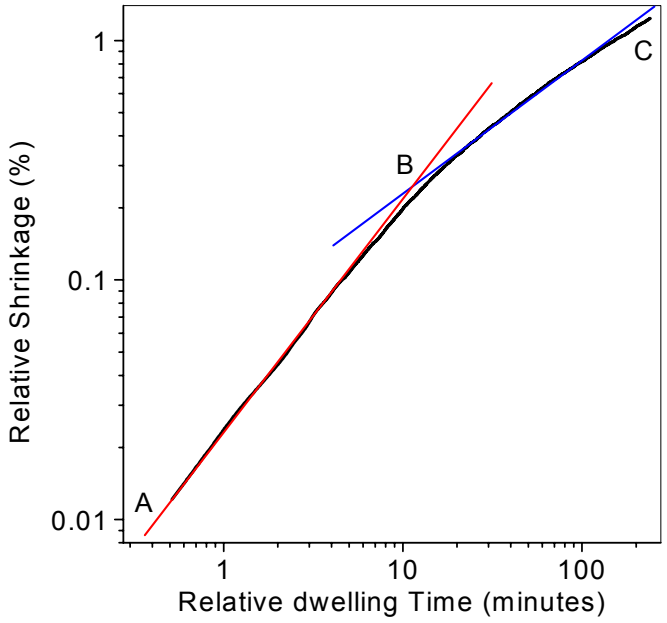

Fig. 3.27: A logarithmic plot of fig. 3.17

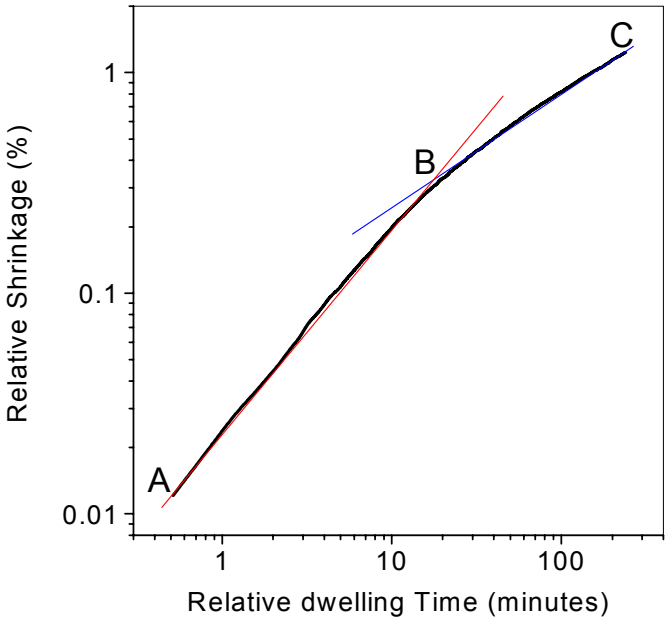

Fig. 3.28: A logarithmic plot of fig. 3.18

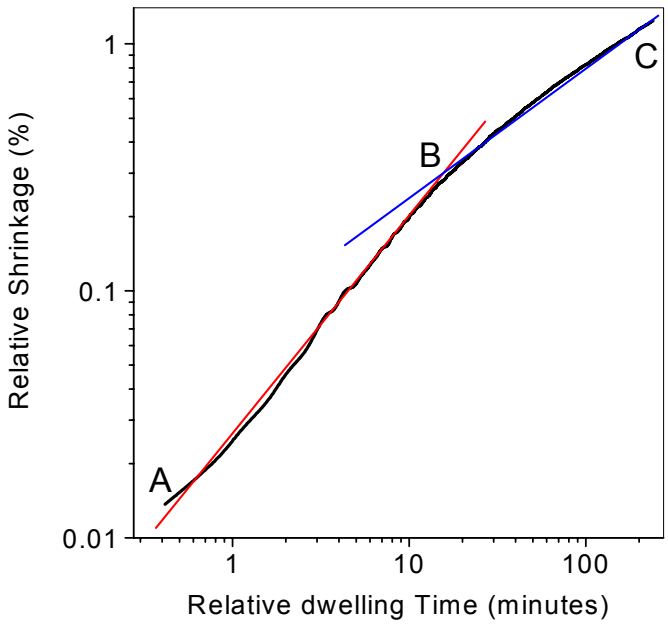

Fig. 3.29: A logarithmic plot of fig. 3.19

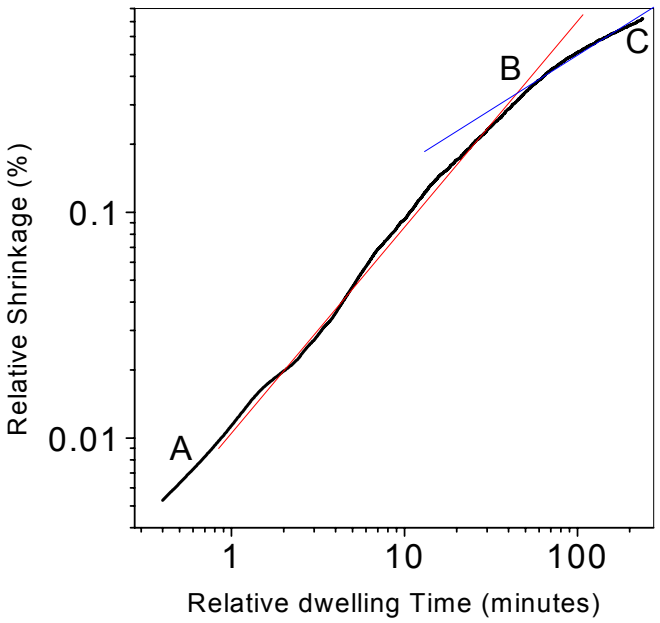

Fig. 3.30: A logarithmic plot of fig. 3.20

Figures clearly indicate that there are two distinct temporal sections in the isothermal shrinkage. In the first period, up to 10 minutes, the major part of the total isothermal shrinkage occurs. The slopes of this segment (AB) and further second segment (BC) were calculated and the values are given in table 3.6. These different slopes are an indication of different shrinkage mechanisms for the isothermal period.

According to the general sintering equation [13]

$$(\Delta L/L_o)^{m/2} = -(H/(2^m R^n))t \qquad \textbf{…3.1}$$

where $\Delta L/L_o$ is the relative shrinkage, H is a constant depending on substance and mechanism, R is the radius of the particles, t is time, n is the grain size exponent and m is the shrinkage exponent (for viscous flow: m = 2; for volume diffusion from the grain boundary: m = 5 and for grain boundary diffusion: m = 6).

The calculated values for shrinkage exponent, m for different series are given in table 3.6.

Table - 3.6

Values of slopes and shrinkage exponent, m calculated from dilatometric plots (fig. 3.21-3.25)

	Slope		m	
	Segment AB	Segment BC	Segment AB	Segment BC
Series A	0.92	0.40-0.45	2.2	5.0-4.5
Series B	1.0	0.40-0.51	2.0	5.0-4.0
Series C	1.0	0.40-0.50	2.0	5.0-4.0
Series D	0.91	0.39-0.42	2.2	5.1-4.8
Series E	0.90	0.39-0.45	2.2	5.1-4.4

As the value of m is approximately 2 for first segment (AB), thus a slope in the isothermal sintering curve corresponds to viscous flow of matter for all the compositions

and as the value of m varies nearly between 4.5-5 for second segment (BC), the slope of this region thus indicates that volume diffusion from the grain boundaries is the dominating mechanism of sintering in this period of isothermal shrinkage.

Also it was observed that shrinkage was almost constant after 200 min soaking period, which implies that the soaking for 240 min is sufficient for getting dense samples. Therefore, dilatometric study can be one of the tools for optimizing the sintering temperature and soaking duration.

3.5 The Perovskite Phase Progression Study Using Dilatometer and XRD

The typical dilatometric behaviour of the green sample was related with the XRD study (at room temperature) in order to study some reactional changes, which were observed during the heat treatment of the green sample up to 850^{o}C. The shrinkage behaviour is illustrated in fig. 3.31, which indicates the onset of shrinkage around 850^{o}C and much higher near 1100^{o}C. Up to 850^{o}C, the sample undergoes normal expansion. Some change in the expansion behaviour was observed around 450^{o}C, 550^{o}C and 700^{o}C as shown in inset. These changes were further investigated by the room temperature XRD study. The XRD patterns obtained for the powders heated at 450^{o}C, 550^{o}C for 5 min were recorded and are shown in fig. 3.32. XRD Patterns show the onset of the formation of perovskite phase at 450^{o}C and the peaks corresponding to perovskite phase become dominant at 550^{o}C and also with the soaking time (4 hrs). The change in the expansion behaviour thus can be explained on the basis of the signature of phase progression during heating of the powder as recorded by XRD technique [14]. At the early stage of the reaction, interdiffusion of cation and the vacancies in between the reacting materials takes place, leading to the formation of product at the contact point of reactants. Also the formed product has different lattice parameters compared to the reactants. This change in lattice parameter causes strain at the interface between reactant and the product, leading to the fracture at the interface. In this process, fine particles with lot of voids in between are produced, resulting in thermal expansion of the compact at reaction initiation temperature. Also the difference in the XRD patterns for the samples heat-treated at 550, 650, 750 and 850^{o}C for 4hrs were recorded and the results are shown in fig. 3.33. It can

be seen that the powder heated at 850^{o}C for 4 hrs shows the complete perovskite phase formation, so it is thus used in this study as calcination temperature.

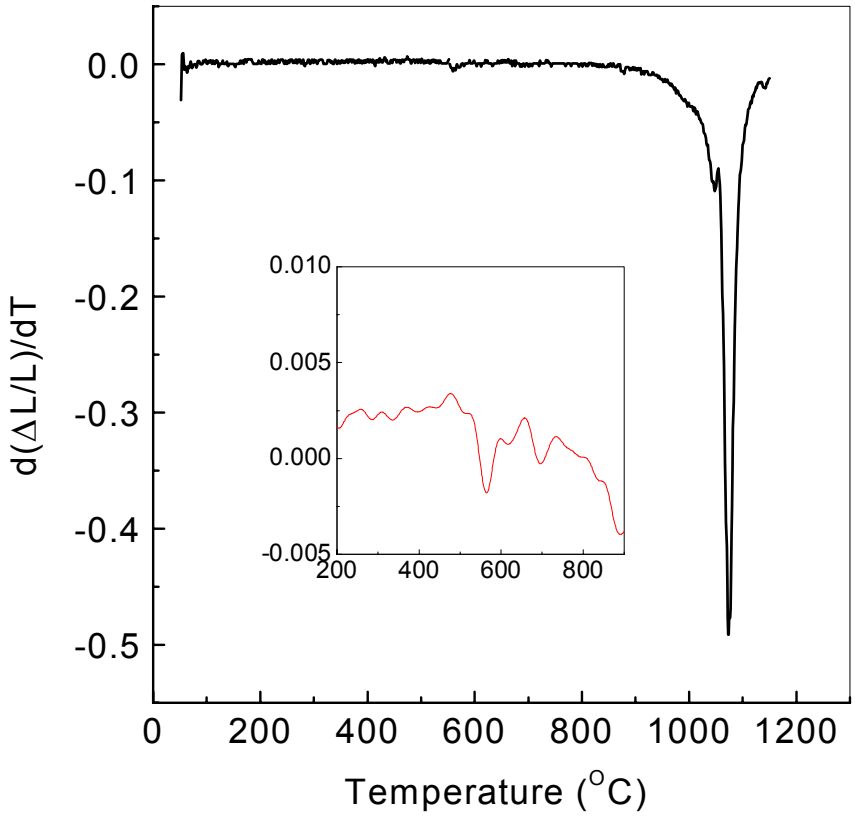

Fig. 3.31: A typical shrinkage rate of green compact

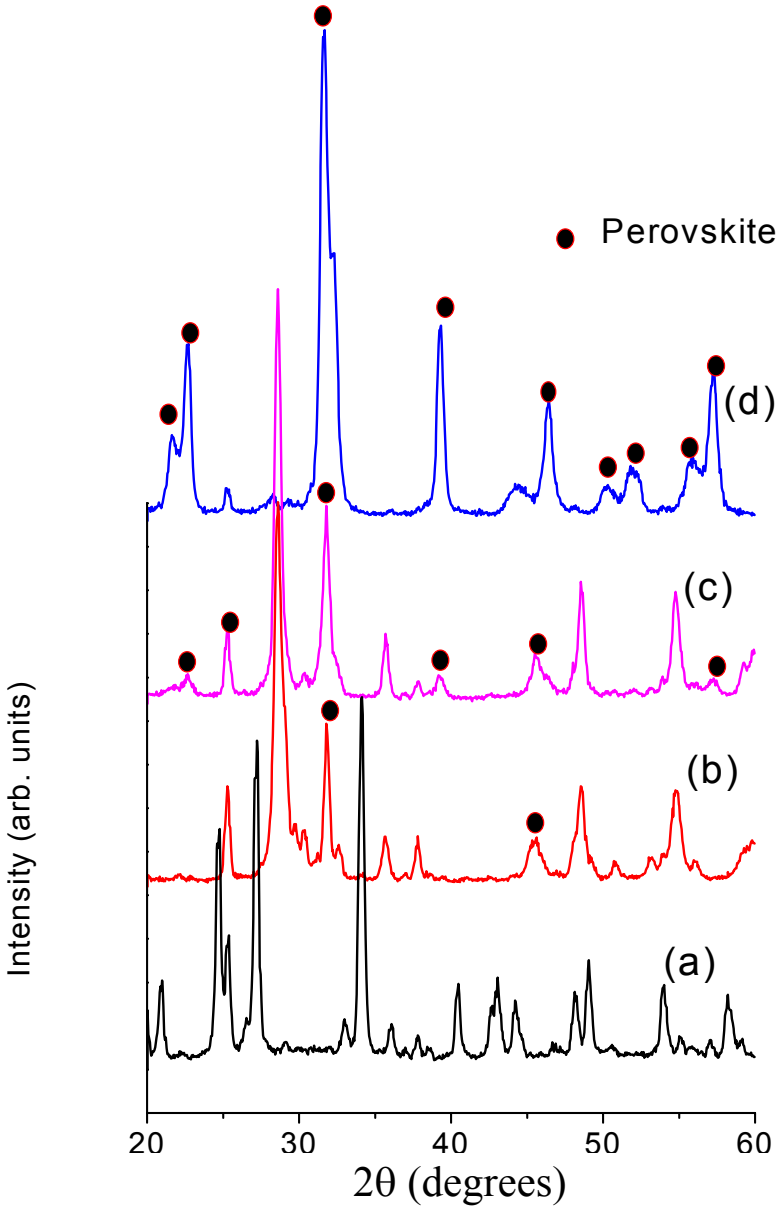

Fig. 3.32: XRD patterns for the powders (a) green (as mixed) and heated at (b) 450°C/5 min (b) 550°C/5 min and (c) 550°C/4 hrs

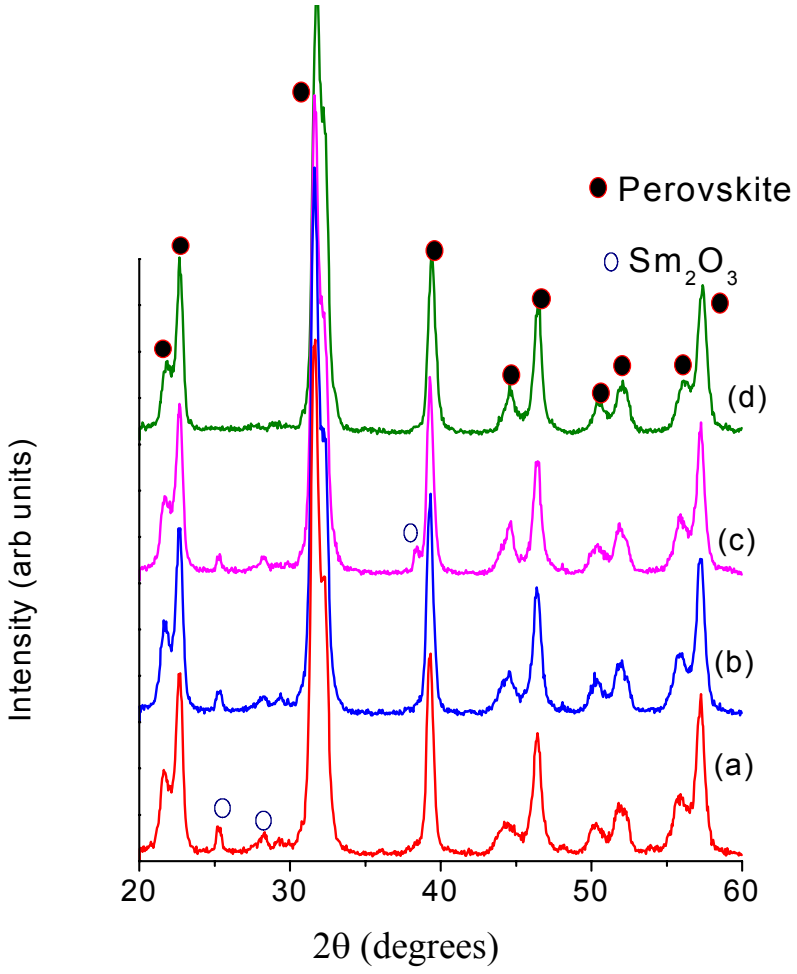

Fig. 3.33: XRD patterns for the powders heated at (a) 550°C, (b) 650°C, (c) 750°C and (d) 850°C for 4 hrs

References

1. T. Yamamoto, H. Igarashi and K. Okazaki, J. Am. Ceram. Soc., **66** (1983) 363.
2. D.A. Northrop, J. Am. Ceram. Soc., **51** (1968) 357.
3. G.H. Haertling, Am. Ceram. Soc. Bull., **43** (1964) 875.
4. J. Mountvala, Am. Ceram. Soc. Bull., **42** (1963) 120.
5. D. Damjanovic, T.R. Gururaja and L.E. Cross, Ceram. Bull., **66** (1987) 699.
6. J. Mendiola, B. Jimenez, C. Alemany, L. Pardo and L.D. Olmo, Ferroelectrics, **94** (1989) 183.
7. H. Takeuchi, S. Jyomura, E. Yamamoto and Y. Ito, J. Acoust Soc. Am., **72** (1982) 1114.
8. H. Takeuchi, D. Damjanovic, T.R. Gururaja, S.J. Jang and L.E. Cross, in proceedings of the Sixth ISAF IEEE, 1986 pp. 402.
9. J. Shenglin, Z. Xuli, W. Xiaozhen, and W. Xianghong, Piezoelect. Acoust., **17** (1995) 26.
10. I. Ueda and S. Ikegami, Jpn. J. Appl. Phys., **7** (1968) 236.
11. Y. Yamashita, K. Yokoyama, H. Honda and T. Takahashi, Jpn. J. Appl. Phys. Suppl., **20** (1981) 183.
12. D. Hennings and K.H. Hardtl, Phy. Stat. Solid (a), **3** (1990) 465.
13. D. Voltzke and H.P. Abicht, Solid State Sciences, **2** (2000) 149.
14. V.V. Bhat, M.V.R. Rao and A.M. Umerji, Mater. Res. Bull., **38** (2003) 1081.

Chapter IV

DIELECTRIC AND FERROELECTRIC PROPERTIES

In this chapter, the studies of electrical (dielectric and ferroelectric) properties of the samples of all the series (mentioned in section 2.4.1a) prepared by conventional dry ceramic technique are given. The dielectric constant (ε') and loss (tanδ) have been investigated over a wide frequency (100 Hz - 1 MHz) and temperature (25^{o}C - 450^{o}C) range. The effect of substituents (Sm, La and Ta) on the dielectric behaviour and Curie temperature was studied. Temperature dependence of dielectric behaviour provides an insight to study the diffusivity (γ) trend. The Curie temperature was also determined by studying the thermal expansion behaviour of the sintered samples using dilatometer. Ferroelectric properties include the study of polarization vs. electric field (P-E) hysteresis loops.

The results of our investigations are discussed below: -

4.1 Variation of ε' and tanδ with Frequency at Room Temperature

Fig. 4.1-4.5 show the frequency dependence of dielectric constant and loss at room temperature for the PCT series modified by the substitution of Sm, La and Ta.

Firstly, both (ε' and tanδ) show decreasing trend with increase in frequency. The fall in dielectric constant arises from the fact that polarization does not occur instantaneously with the application of the electric field because of inertia. The delay in response towards the impressed alternating electric field leads to loss and decline in dielectric constant. At low frequencies, all types of polarization contribute. As frequency is increased, those with large relaxation times cease to respond and hence the decrease in dielectric constant. While studying the behaviour of dielectric constant with frequency, it is important to note that at lower frequencies, the contribution from the space charge polarization is maximum, which reduces slowly with the increase of frequency. The space charge arises from the charge accumulation at grain boundaries and at the electrode interface, mainly due to vacancies of lead and oxygen. Since with the increase of frequency, these dipoles due to space charge do not respond at higher frequencies resulting in decrease in the

dielectric constant. The same type of frequency dependent dielectric behaviour is found in many ferroelectric ceramics [1, 2]. The behaviour of tanδ also follows the same reasoning.

Secondly, dielectric constant shows an increasing trend as we increase the amount of various substituents (Sm, La and Ta) in pure PCT ceramics. This increase in dielectric constant probably comes from the decrease in Curie temperature, T_c, with the incorporation of Sm, La and Ta in PCT system (the behaviour of Curie temperature (T_c) is discussed in the next section). In contrast to increase of dielectric constant, the loss factor (tanδ) shows a decreasing trend with increasing amount of Sm and La in PCT ceramics, whereas it increases for Ta substitution. This trend of loss may be due to the increase in density or decrease in porosity with the increase of the Sm and La substitution and an opposite trend in case of Ta, as discussed in the previous chapter (section 3.2).

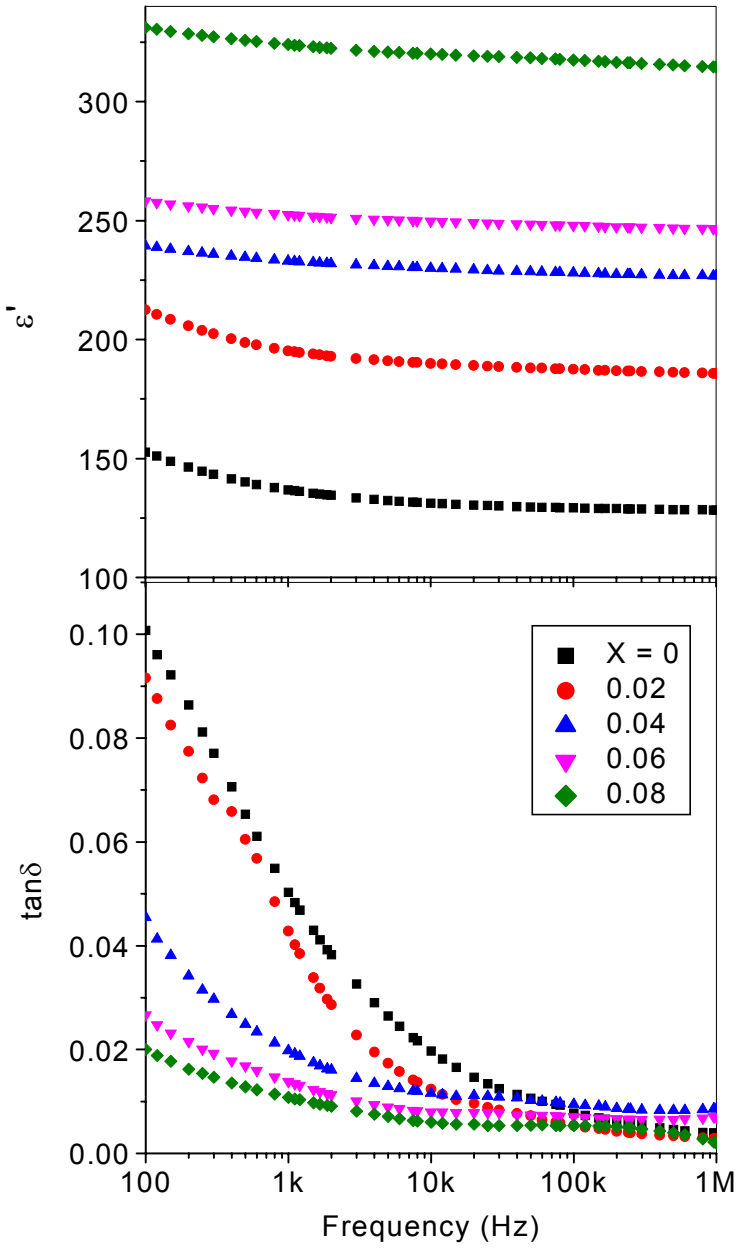

Fig. 4.1: Variation of ε' and tanδ with frequency at room temperature for series A

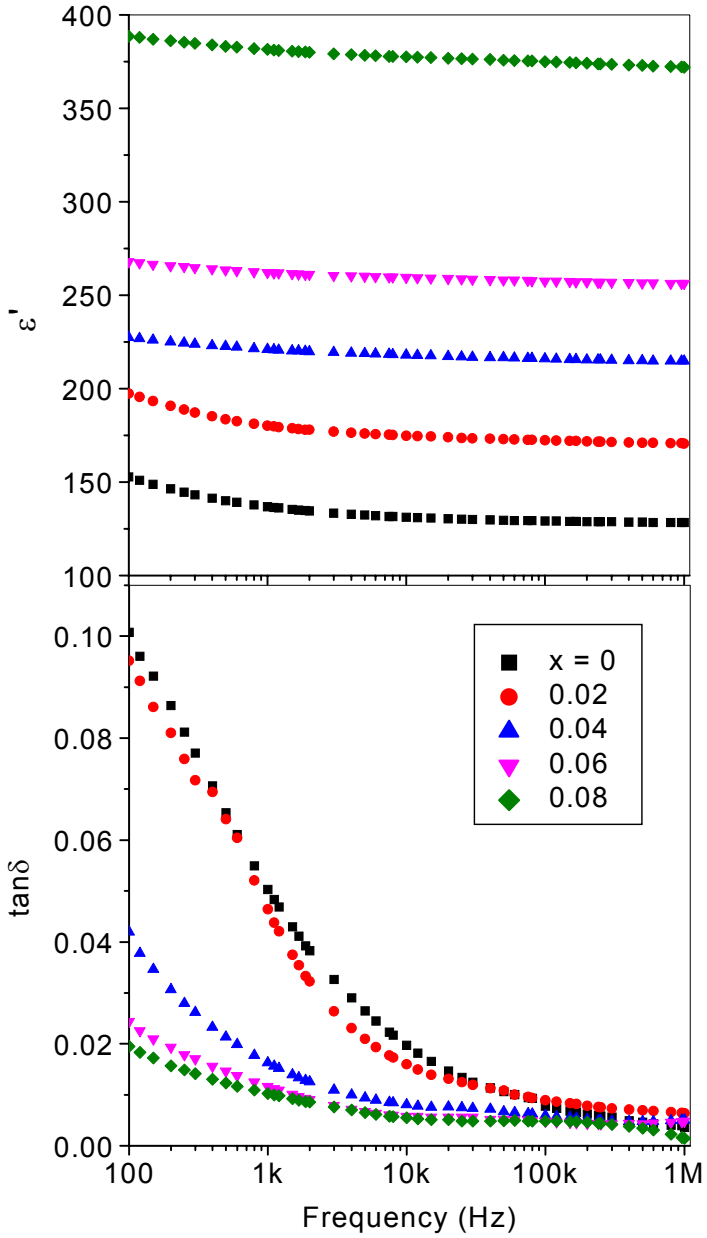

Fig. 4.2: Variation of ε' and tanδ with frequency at room temperature for Series B

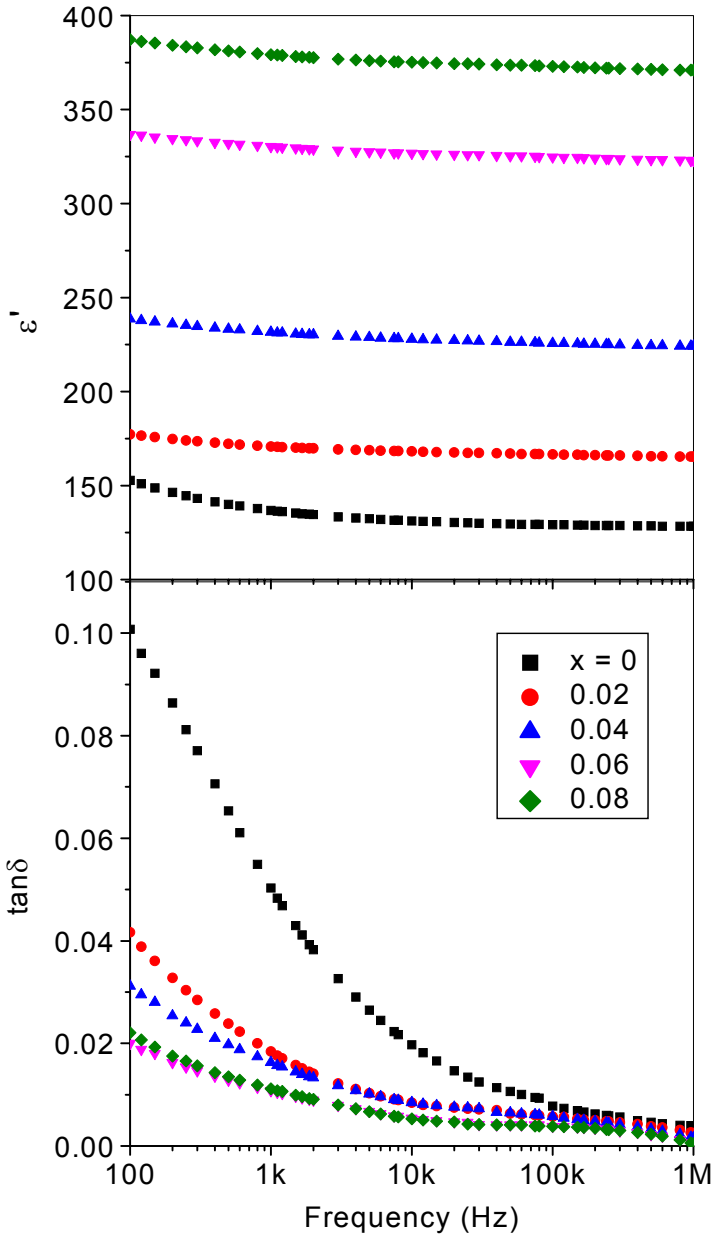

Fig. 4.3: Variation of ε' and tanδ with frequency at room temperature for series C

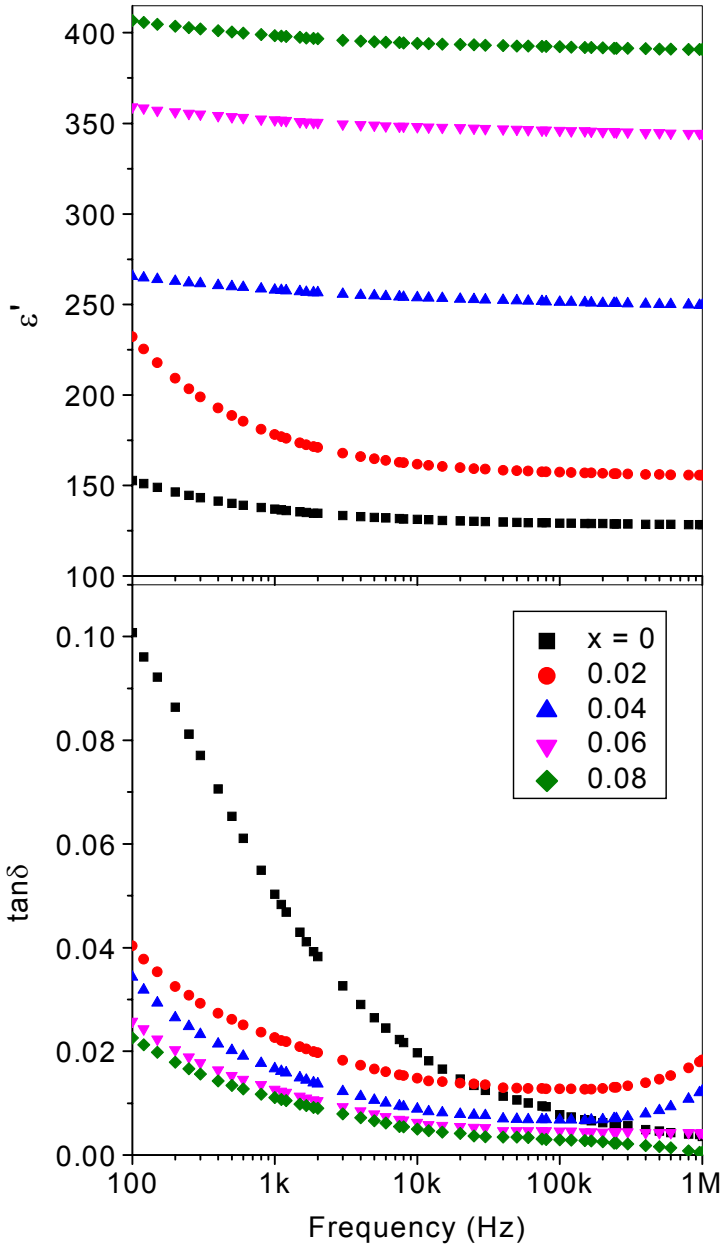

Fig. 4.4: Variation of ε' and tanδ with frequency at room temperature for series D

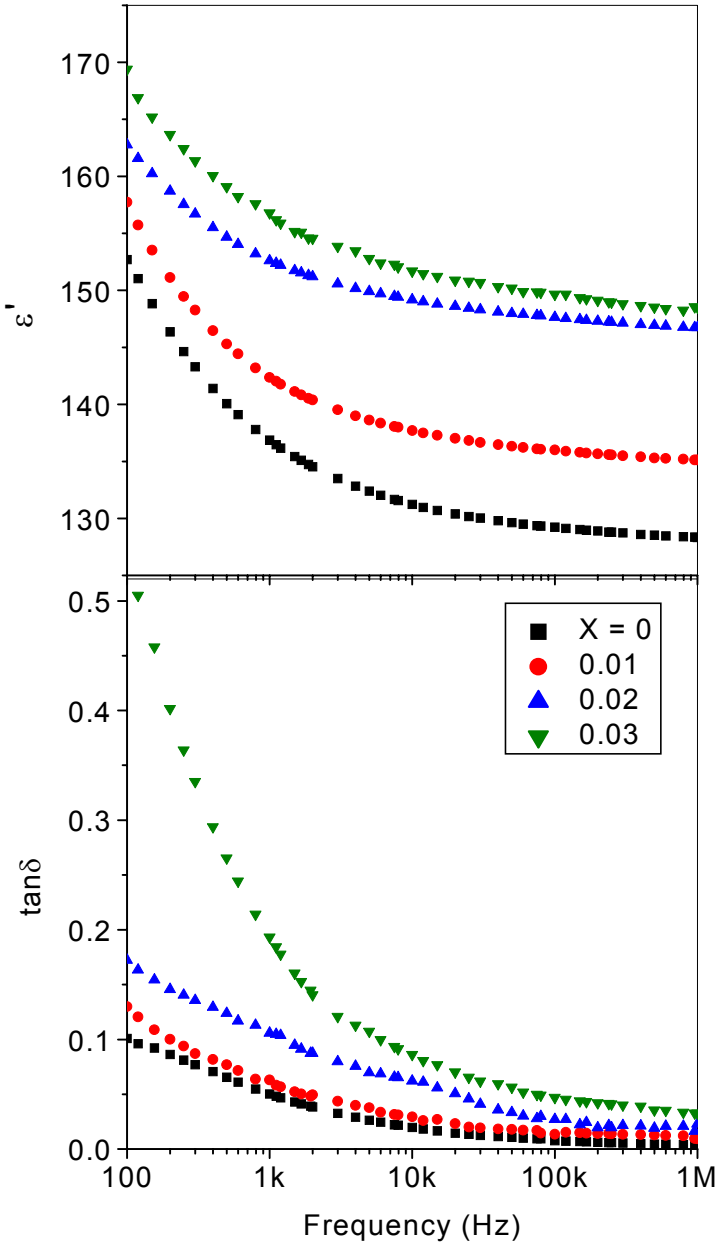

Fig. 4.5: Variation of ε' and tanδ with frequency at room temperature for series E

4.2 Temperature Variation of ε' and tanδ at Different Frequencies

The temperature variation of dielectric constant and loss was studied for all the series at three selected frequencies (1 kHz, 10 kHz and 100 kHz) and the results for one typical composition of each series are shown in fig. 4.6-4.10. For series A to series D, the plots are given for 6 mol% Sm and La substituted PCT ceramics and for series E, it is given for 3 mol% Ta substitution. As typical of normal ferroelectrics, dielectric constant increases gradually with increment in the temperature due to interfacial polarization becoming more dominant as compared to the dipolar polarization and passes through a maximum (Curie temperature, T_c) and then decreases due to the phase transition from ferroelectric to the paraelectric phase. The decrease of tanδ at the phase transition is due to the reduction in the domain wall contribution to loss. The dispersive loss at high temperature is probably due to the localized ionic mobility. Curie transition temperature is found to decrease with the increase in the amount of Sm, La and Ta in PCT ceramics. This trend is shown in fig. 4.11-4.15 in which the behaviour of dielectric constant and loss is given at one frequency (10 kHz). The obtained values are given in table 4.1 for all the series. This can be attributed to the decrease in crystal tetragonality caused by the substituting elements (discussed in previous chapter in section 3.1), which reduces the internal stress and which in turn reduces the transition temperature [3]. Also if we compare the two series of Sm (series A and B) and two series of La (series C and D) with each other, then it is observed that the change in Curie temperature is significant for the Sm substituted series as compared to the La substituted series, which may be due to the significant change in the lattice anisotropy as in case of Sm substitutes series, this change is significant as described in the section 3.1.

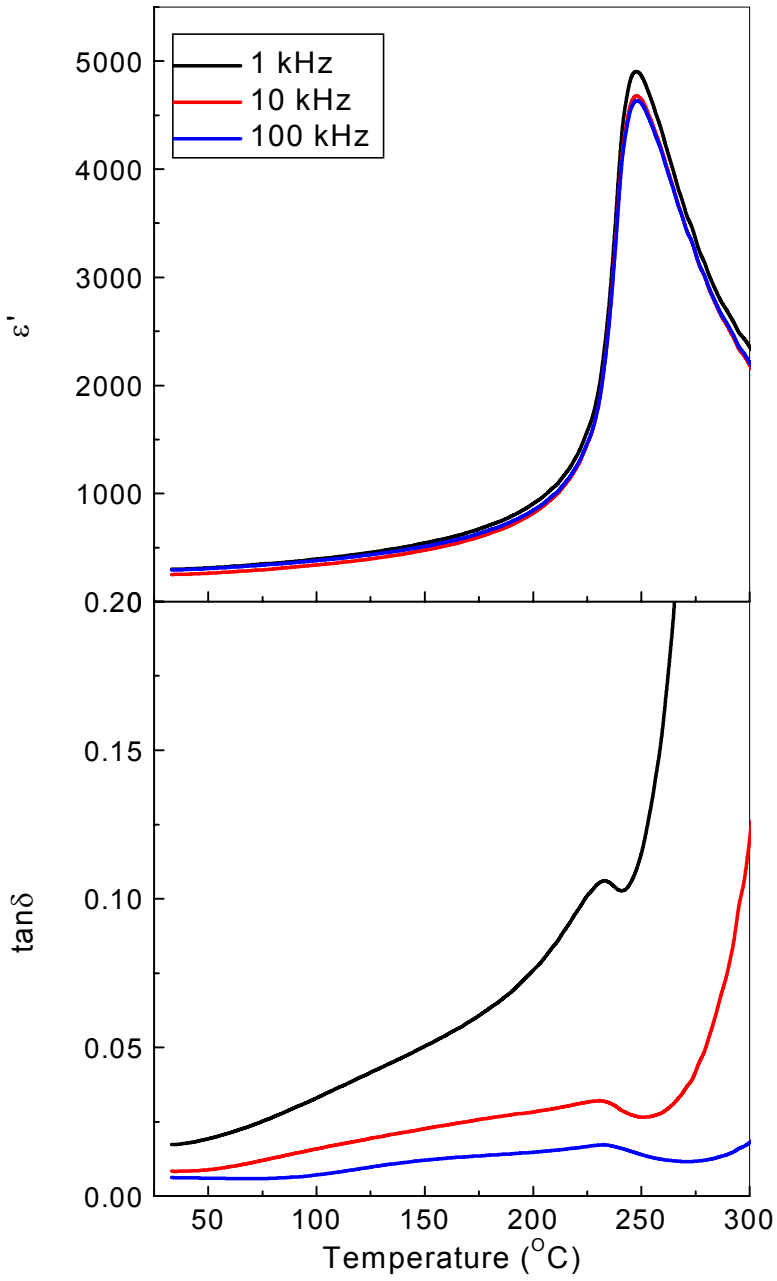

Fig. 4.6: Temperature variation of ε' and tanδ for the sample (x = 0.06) of series A at different frequencies

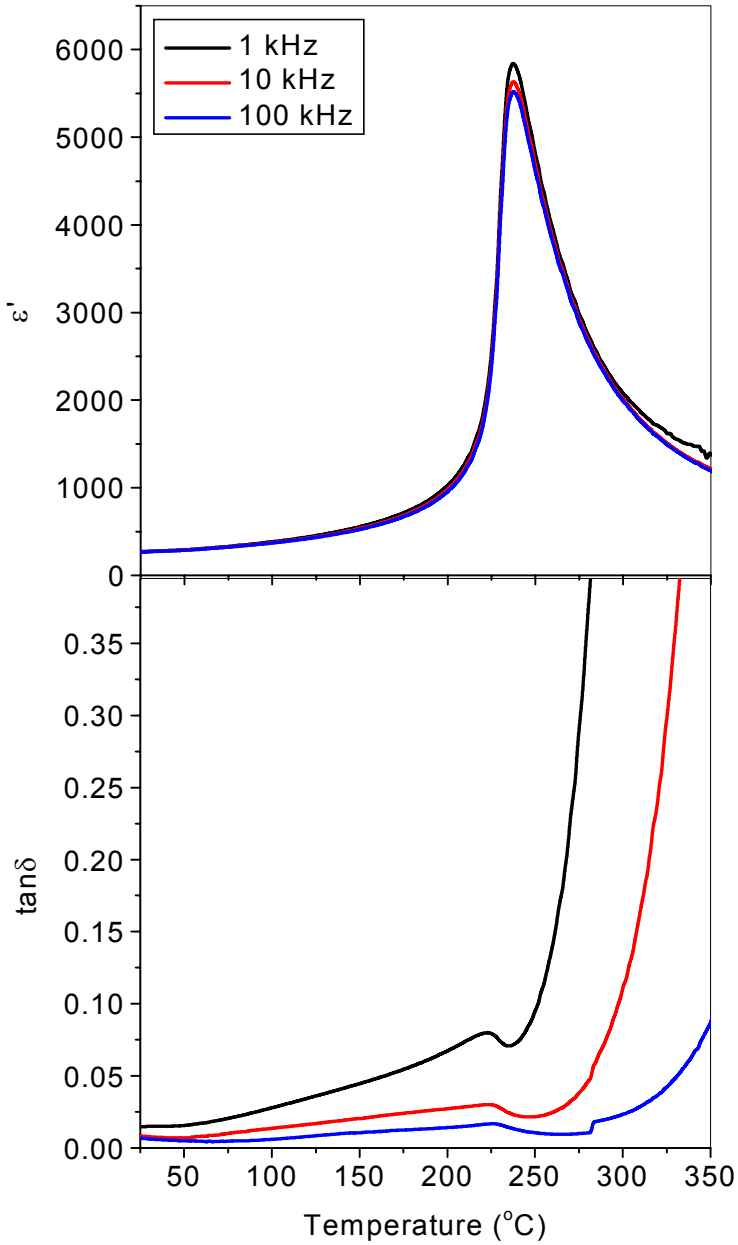

Fig. 4.7: Temperature variation of ε' and tanδ for the sample (x = 0.06) of series B at different frequencies

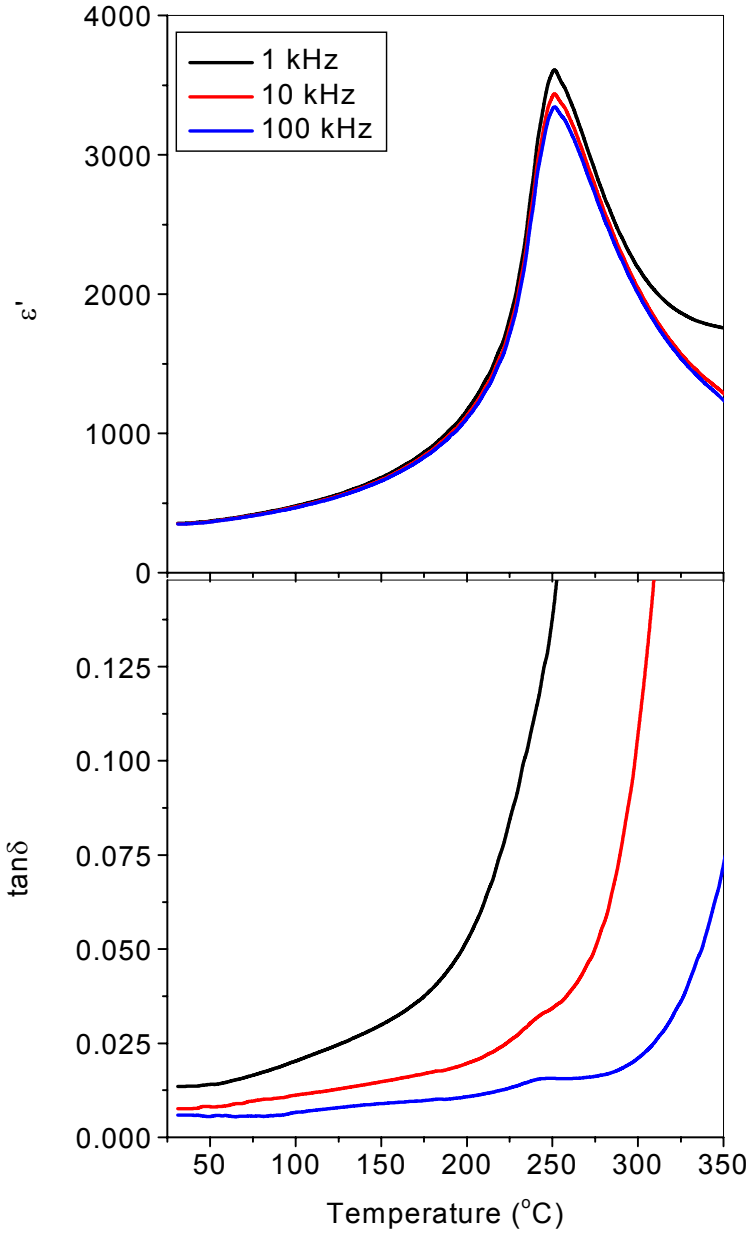

Fig. 4.8: Temperature variation of ε' and tanδ for the sample (x = 0.06) of series C at different frequencies

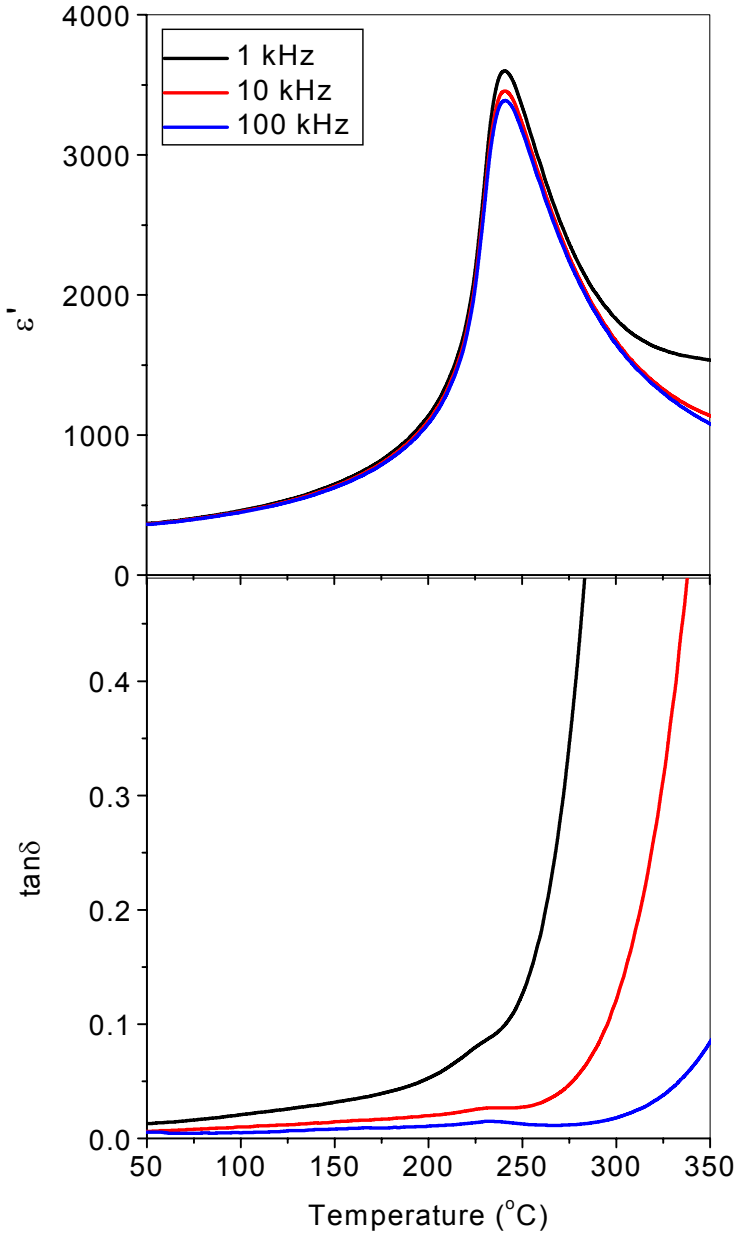

Fig. 4.9: Temperature variation of ε' and tanδ for the sample (x = 0.06) of series D at different frequencies

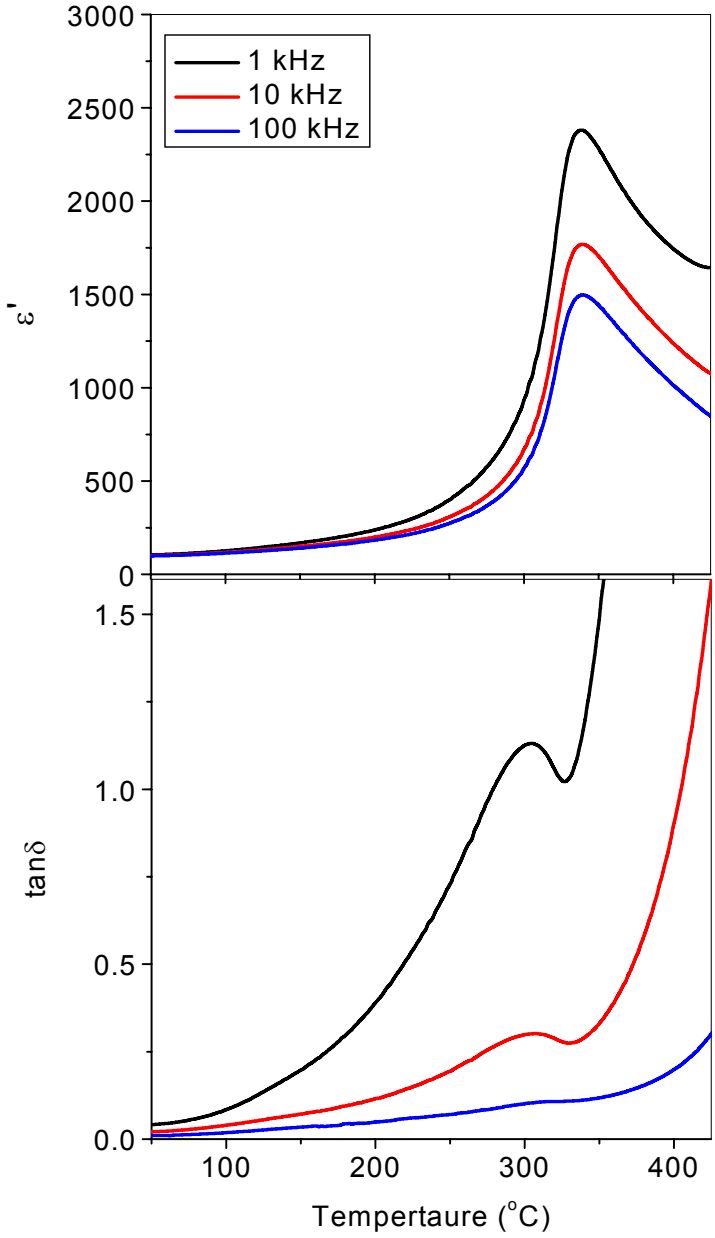

Fig. 4.10: Temperature variation of ε' and tanδ for the sample (x = 0.03) of series E at different frequencies

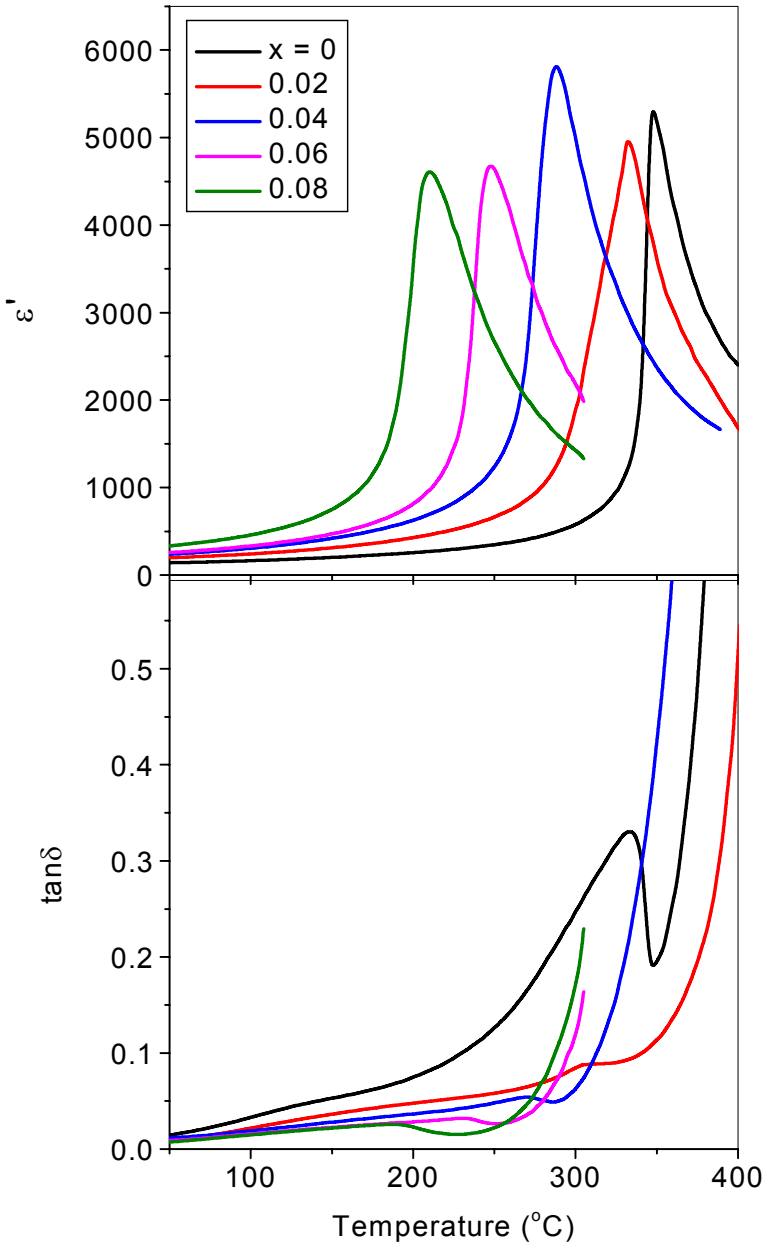

Fig. 4.11: Temperature variation of ε' and tanδ for series A at 10 kHz

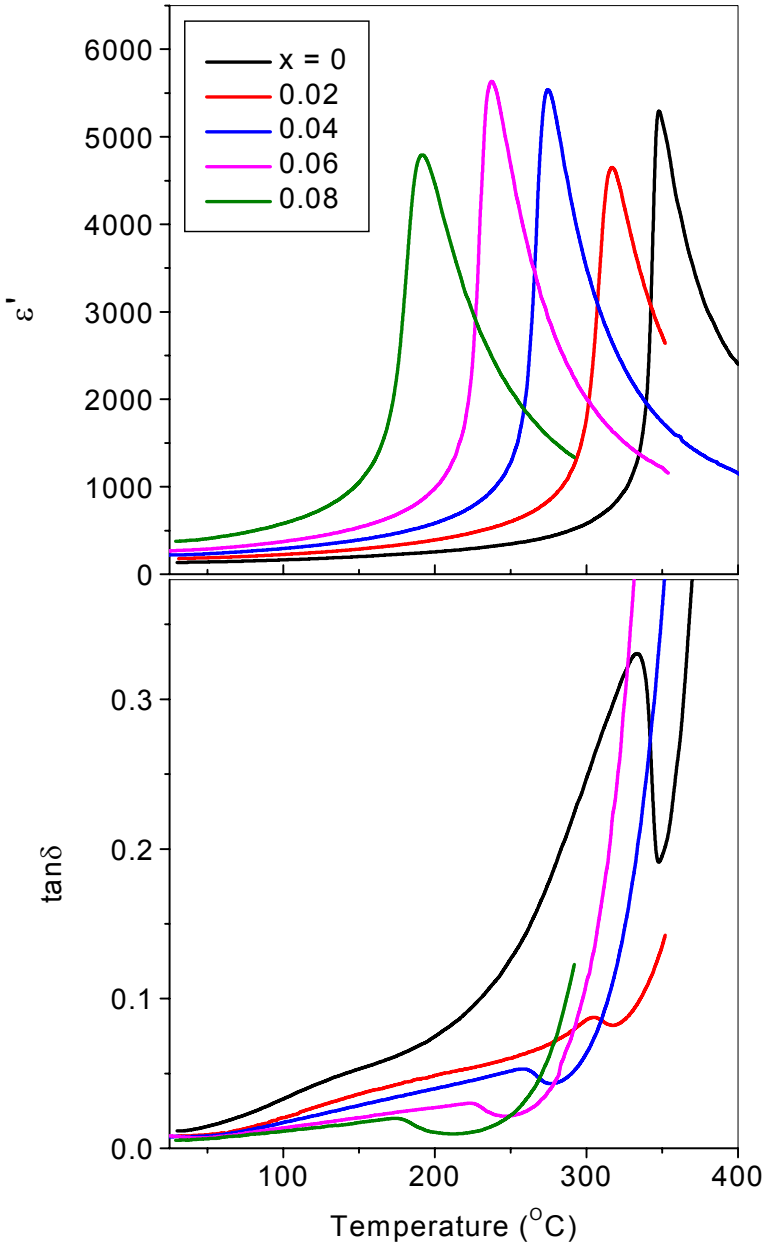

Fig. 4.12: Temperature variation of ε' and tanδ for series B at 10 kHz

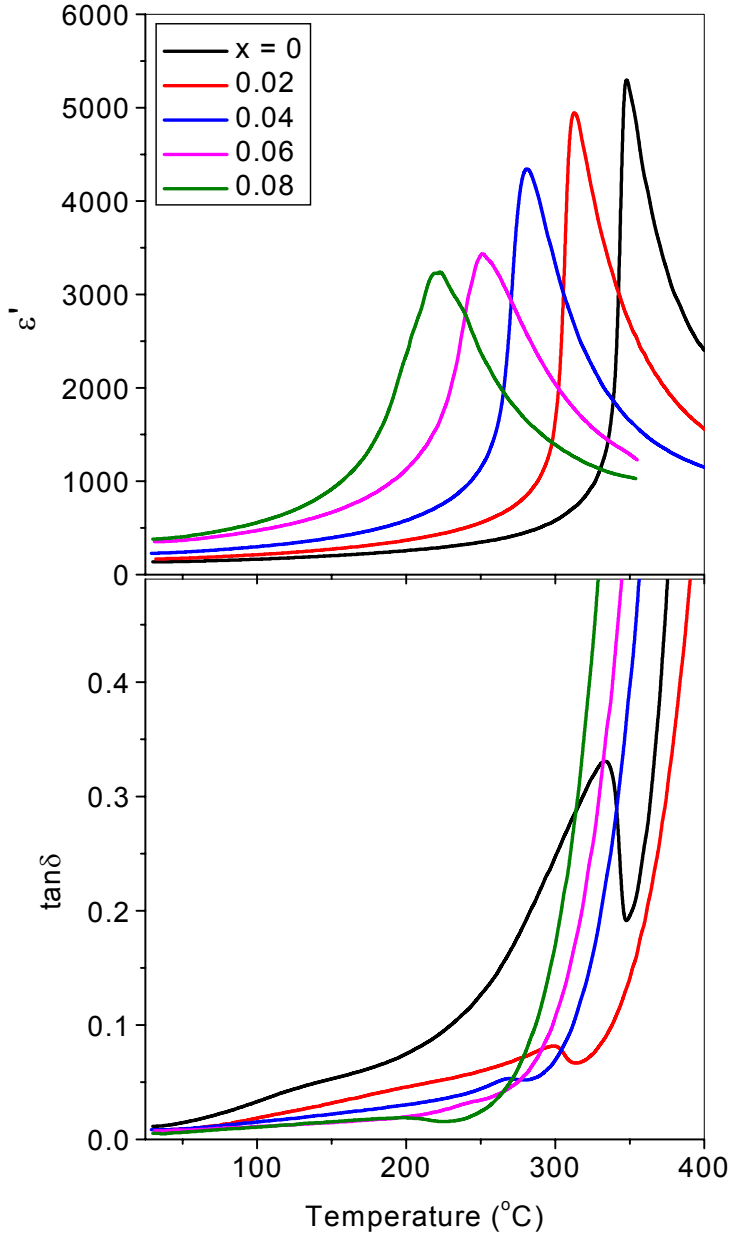

Fig. 4.13: Temperature variation of ε' and tanδ for series C at 10 kHz

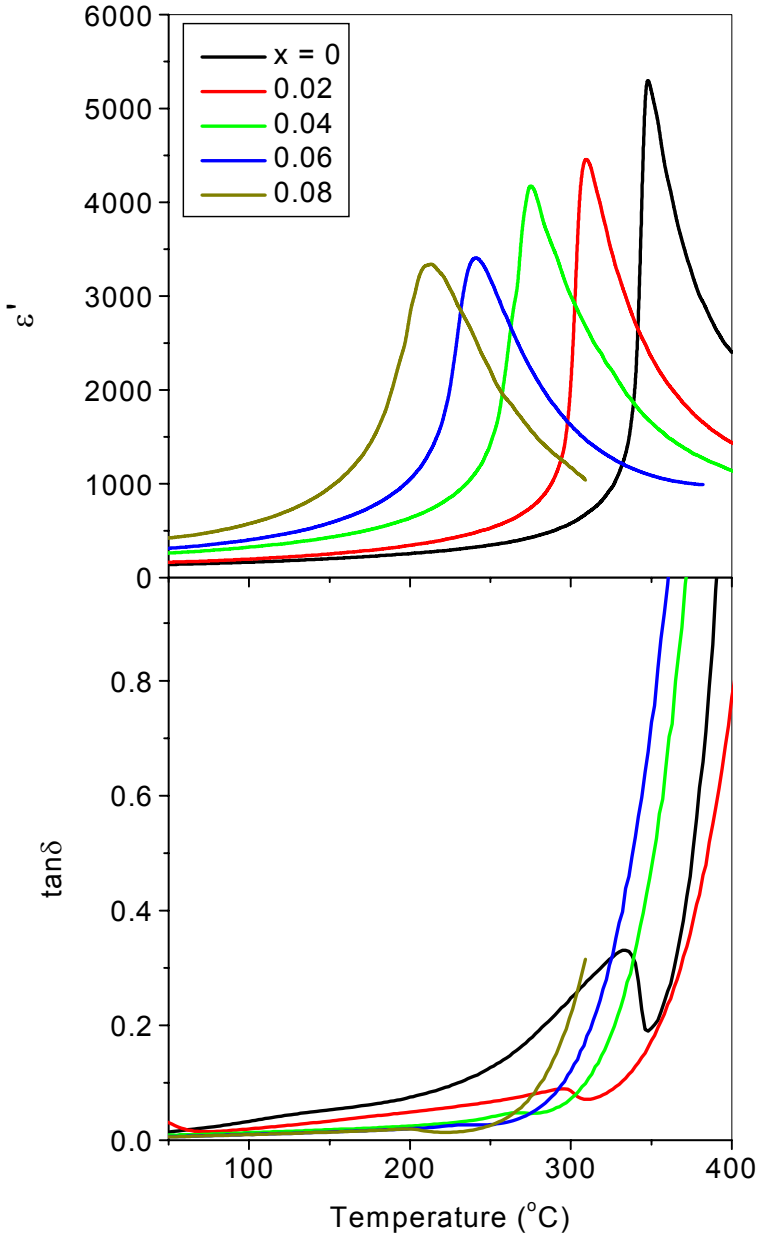

Fig. 4.14: Temperature variation of ε' and tanδ for series D at 10 kHz

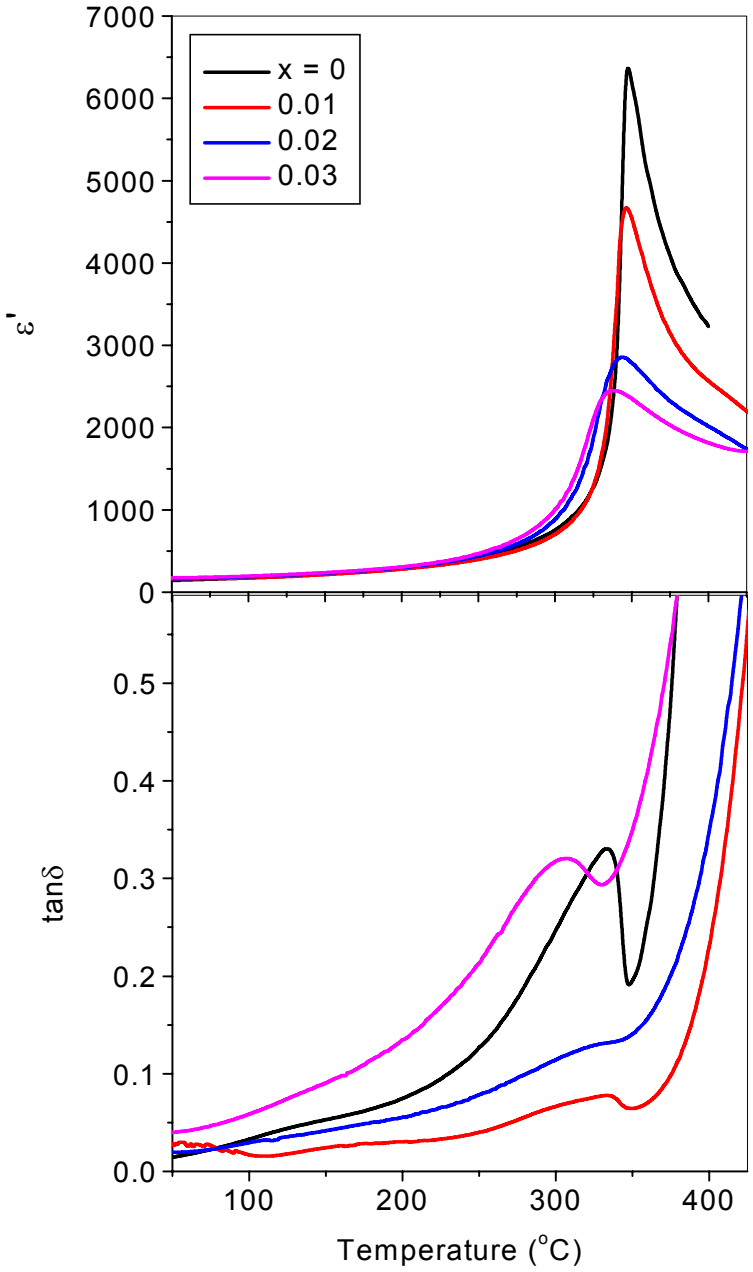

Fig. 4.15: Temperature variation of ε' and tanδ for series E at 10 kHz

Table - 4.1

Variation of transition temperature (T_c) with different x

T_c (^oC)						
	Series A	Series B	Series C	Series D	Series E	
x					x	
0	348	348	348	348	0	348
0.02	331	317	312	310	0.01	346
0.04	289	274	281	274	0.02	344
0.06	247	237	251	242	0.03	340
0.08	211	192	219	213	-	-

4.3 Diffusivity Study

A broadening of phase transition peak was observed with the increase in the amount of Sm, La and Ta in the pure PCT ceramics, as it is clear from the fig. 4.11-4.15. This broadening depends on the composition fluctuations and structural disorder [4]. The structural disorder in the compounds arises due to the presence of a number of voids and impurities of different sizes. Here in the present work, the degree of disorder or diffusivity (γ), in all the compositions was calculated using the expression [5]

$$\ln (1/\varepsilon'-1/\varepsilon'_{max}) = \gamma \ln(T-T_c) + a \qquad \textbf{…4.1}$$

where ε'_{max} is the value of ε' at T_c. The value of γ is the degree of diffusiveness, which lies in the range of $1 < \gamma \leq 2$, where $\gamma = 1$ represents ideal Curie-Weiss behaviour while γ between 1 and 2 indicates diffused transition [5]. The value of γ, calculated from the slope of graphs (fig. 4.16-4.20), is given in table 4.2 and was found to increase with increasing the substituting elements.

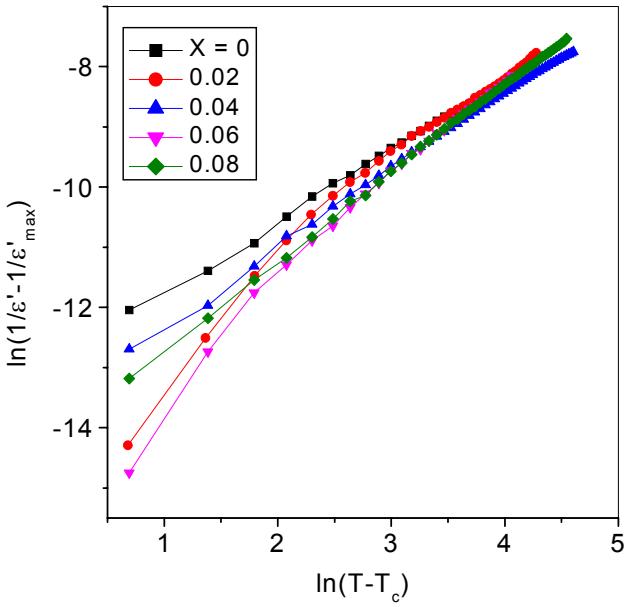

Fig. 4.16: Variation of ln $(1/\varepsilon'-1/\varepsilon'_{max})$ vs. ln $(T- T_c)$ for series A at 10 kHz

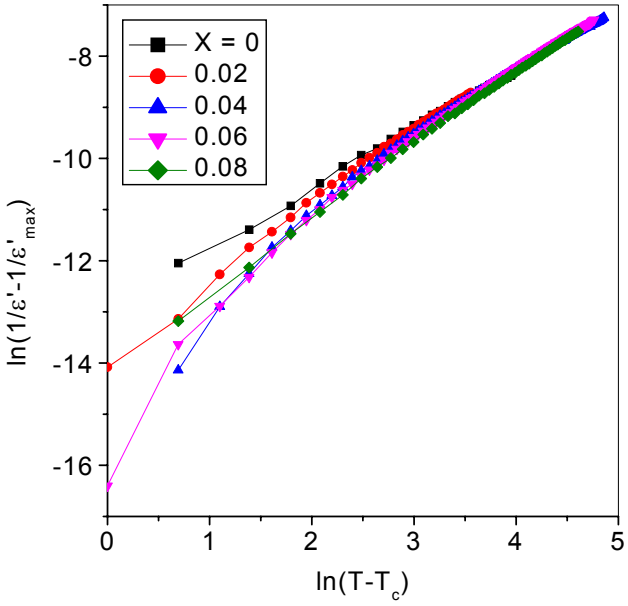

Fig. 4.17: Variation of ln $(1/\varepsilon'-1/\varepsilon'_{max})$ vs. ln $(T- T_c)$ for series B at 10 kHz

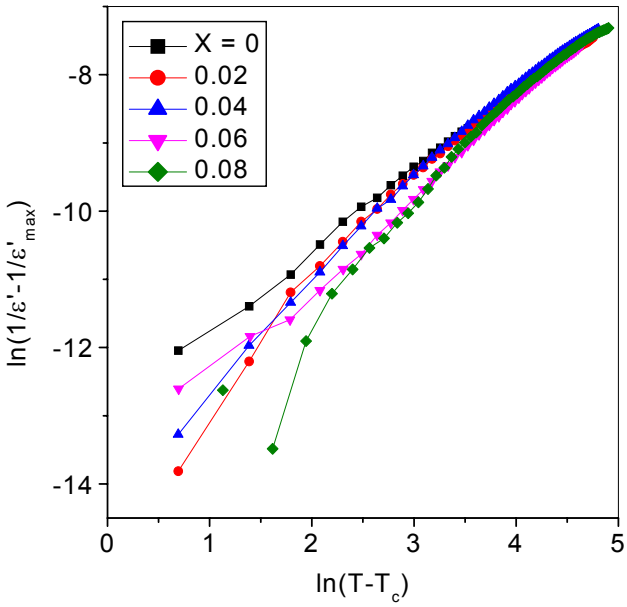

Fig. 4.18: Variation of ln $(1/\varepsilon'-1/\varepsilon'_{max})$ vs. ln $(T- T_c)$ for series C at 10 kHz

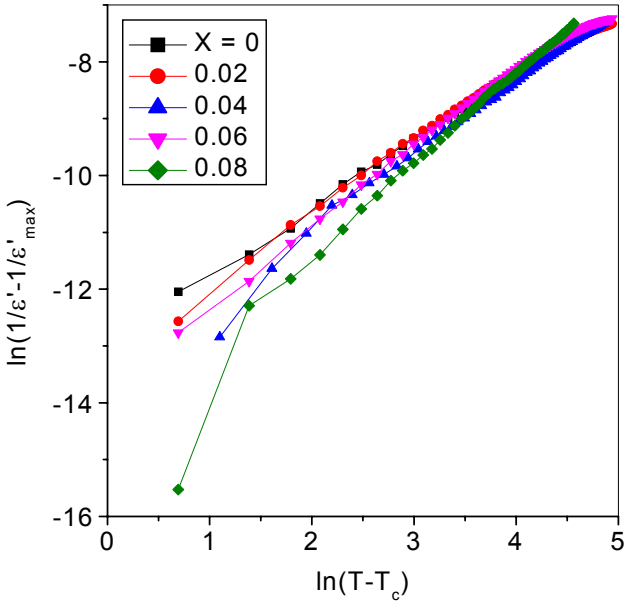

Fig. 4.19: Variation of ln $(1/\varepsilon'-1/\varepsilon'_{max})$ vs. ln $(T- T_c)$ for series D at 10 kHz

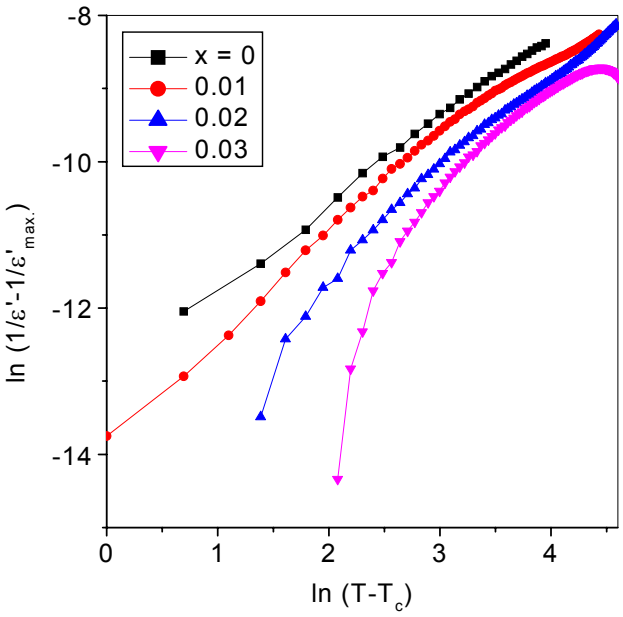

Fig. 4.20: Variation of ln $(1/\varepsilon'-1/\varepsilon'_{max})$ vs. ln $(T- T_c)$ for series E at 10 kHz

Table - 4.2

Variation of diffusivity (γ) with different x

γ						
	Series A	Series B	Series C	Series D	Series E	
x					x	
0	0.94	0.94	0.94	0.94	0	0.94
0.02	1.0	1.1	1.15	1.2	0.01	1.1
0.04	1.2	1.2	1.21	1.25	0.02	1.15
0.06	1.26	1.3	1.24	1.38	0.03	1.22
0.08	1.34	1.4	1.34	1.42	-	-

4.4 Typical Dilatometric Behaviour of Sintered Samples

The tetragonal to cubic transition at Curie temperature (T_c) was also determined by heating the sintered samples in dilatometer. Typical plot for the one composition from each series is shown in fig. 4.21-4.25. All the plots clearly indicate the tetragonal to cubic phase transformation as we pass through the Curie temperature. The value of T_c obtained from both dilatometric heating and dielectric study are compared and it is observed that both values are in good agreement with each other.

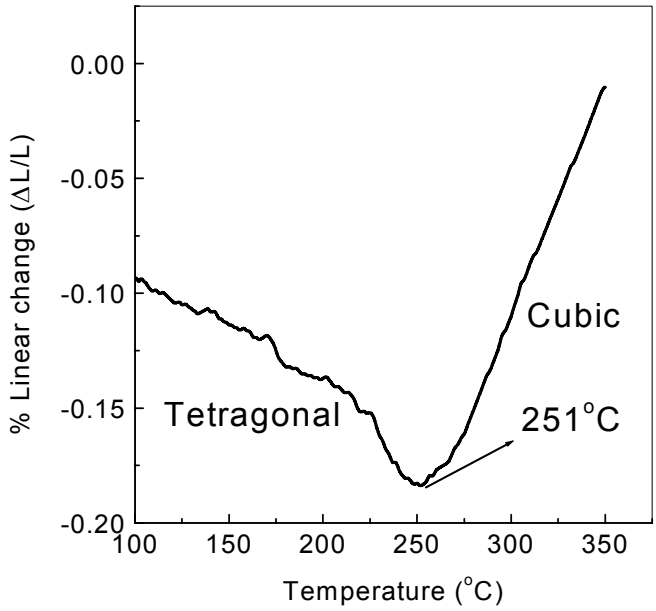

Fig. 4.21: Typical dilatometric plot of sintered sample (x = 0.06) of series A

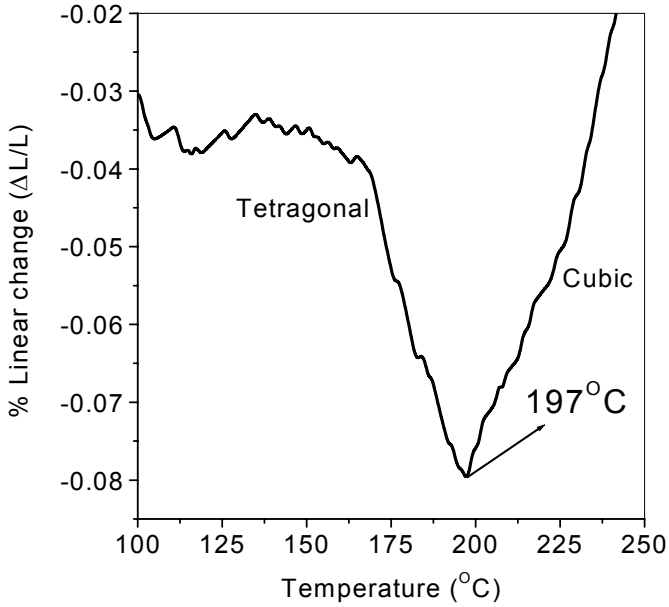

Fig. 4.22: Typical dilatometric plot of sintered sample (x = 0.08) of series B

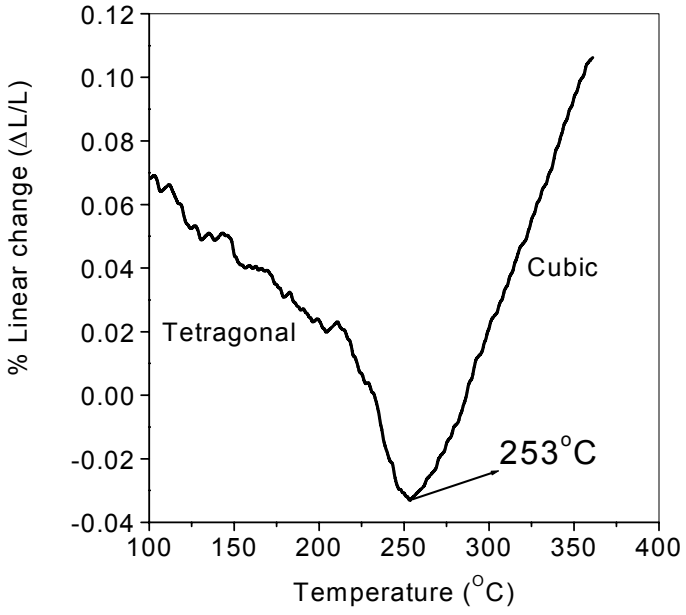

Fig. 4.23: Typical dilatometric plot of sintered sample (x = 0.06) of series C

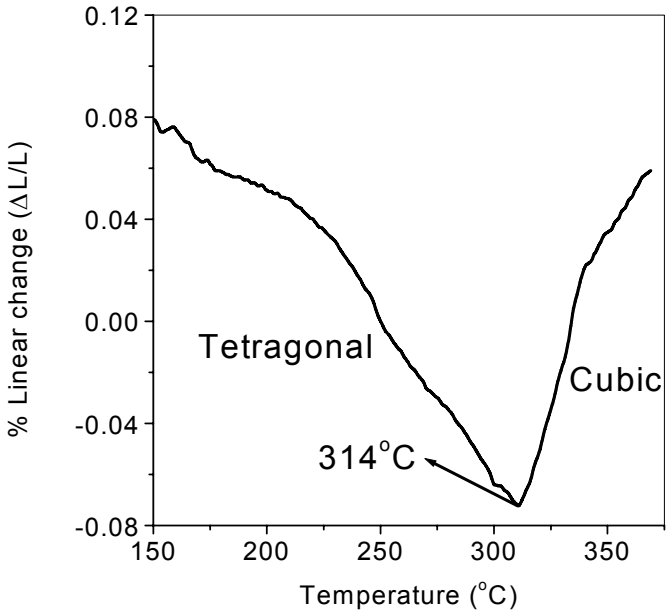

Fig. 4.24: Typical dilatometric plot of sintered sample (x = 0.02) of series D

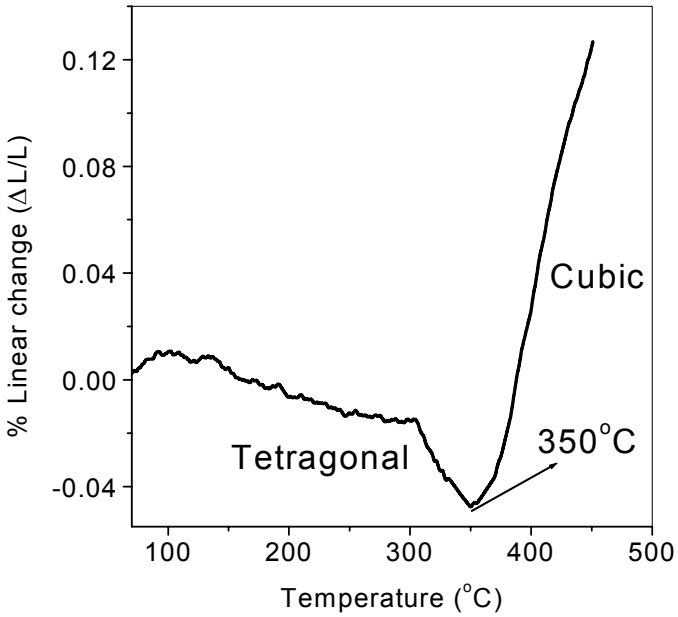

Fig. 4.25: Typical dilatometric plot of sintered sample (x = 0.01) of series E

4.5 Ferroelectric Properties

Another important characteristic of ferroelectrics is the ferroelectric hysteresis loop i.e., the polarization, P, is a double-valued function of the applied electric field, E. It can be observed by means of a Sawyer-Tower circuit [6].

Polarization vs. electric field (P-E) loops were observed for all the compositions except the samples substituted with tantalum because of high porosity and low resistivity. The results are shown in figures 4.26-4.29. Well-defined ferroelectric behaviour is observed. The values of coercive field (E_c) and remnant polarization (P_r) were determined from the P-E loops and are given in table 4.3 for the samples of series A, B, C and D. The results of E_c and P_r are correlated with the average grain size and the amount of substituent, respectively. For all the four series, a large increase in remnant polarization (P_r) was observed from 0-8 mol% substitutions. This may be due to the softening effect of substituting elements, which also results in reduction in tetragonality. In series A, P_r first decreases up to 4 mol% Sm followed by increasing trend up to 8 mol% substitution. This may be due to the smaller atomic displacement of the cell content [7]. Further increase in P_r may be resulted from the dominating effect of Sm amount, which results in large decrease in tetragonality. Further, for series B, C and D, a large increase in the value of P_r after 4 mol% Sm and La substituted samples may be resulted from the favourable effect of average grain size in addition to the substituent amount.

For series A, it can be seen that there is a decrease in the value of coercive field (E_c) up to 2 mol% Sm followed by the increase up to 6 mol%. This behaviour can be explained with the average grain size variation (values given in table 3.5 of section 3.3), which also show increase up to 2 mol% Sm followed by the decrease with further increasing Sm content up to 6 mol%. It is well reported in the literature that with increase in grain size, E_c decreases as each grain is mechanically clamped by its surrounding. This clamping effect, in addition to the mechanical stresses accompanying 90^o domain rotations, tends to impede the polarization reversal process, and hence, apparently increases E_c [8]. The value of E_c further decreases for 8 mol% Sm substitution as for this sample, the grain size again increases and more uniformity was observed in the microstructure.

For series B, the sample with 8 mol% Sm gives maximum value of P_r, which is 30 $\mu C/cm^2$. Also coercive field (E_c) for 6 mol% Sm sample is higher than the 8 mol%, which

may be due to the increase in grain size for 8 mol% Sm substituted sample. The remnant ratio defined by P_r/P_{sat} is found to be maximum for 6 and 8 mol% Sm and La substituted samples, respectively and it is ~ 0.76-0.80. For series C and series D, it can be seen that coercive field (E_c) decreases for 2 mol% La followed by the increase for 4 mol% and then again decrease with further substitution of lanthanum. This behaviour can be explained on the same lines as in case of series A, where the results of E_c are correlated with average grain size variation. Also if we compare the two series of Sm (series A and B) and two series of La (series C and D) with each other, then it is observed that the change in the values of E_c and P_r is more for the Sm substituted series as compared to the La substituted series, which may be due to the significant change in the lattice anisotropy as in case of Sm substitutes series, this change is significant as described in the section 3.1. Conclusively, Sm^{3+} and La^{3+} substituents for Pb^{2+} in PCT ceramics act as donor resulting in creation of A-site vacancies and the material becomes soften. This results in the enhancement of domain reorientation, lowering of coercive field and increase in remnant polarization.

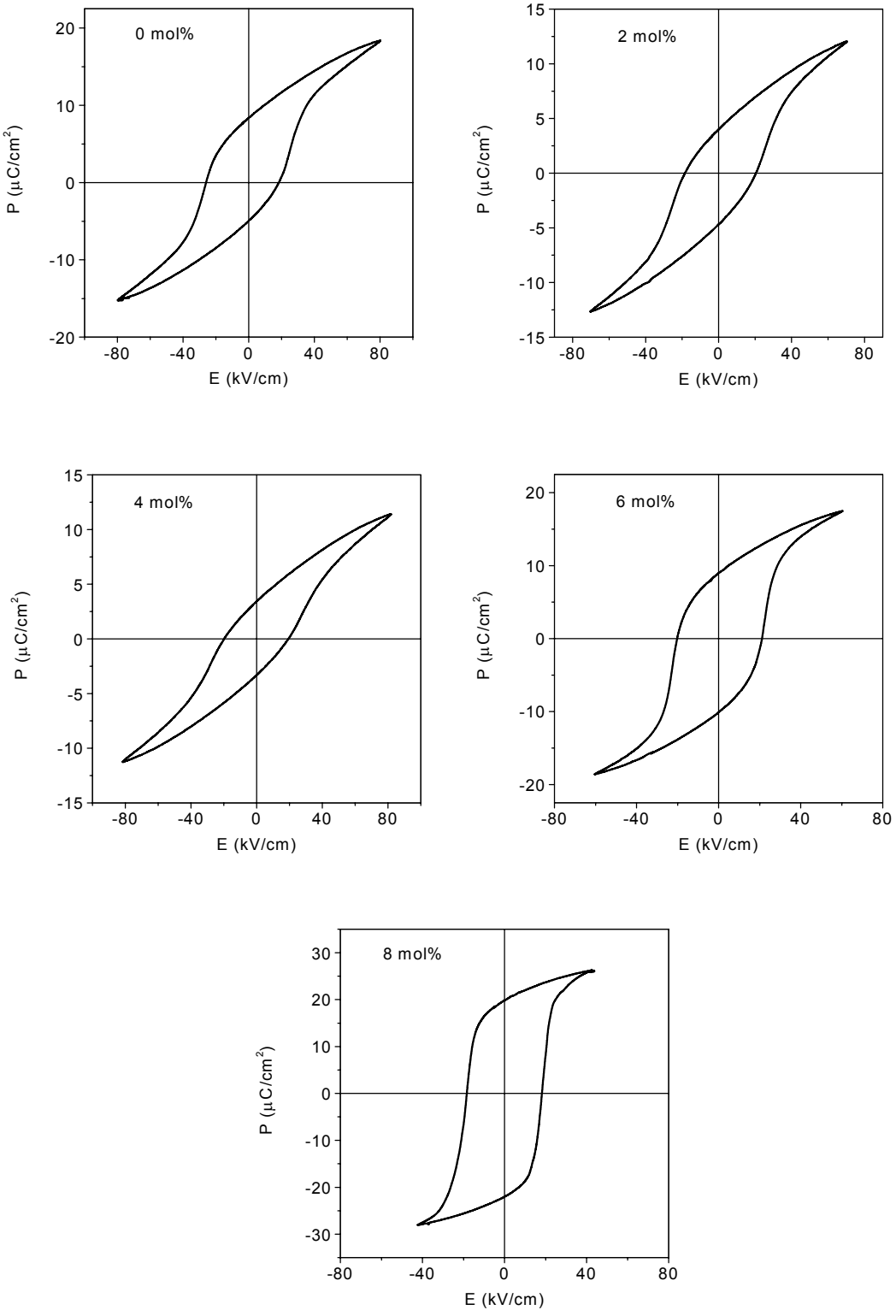

Fig. 4.26: Room temperature P – E hysteresis loops for series A

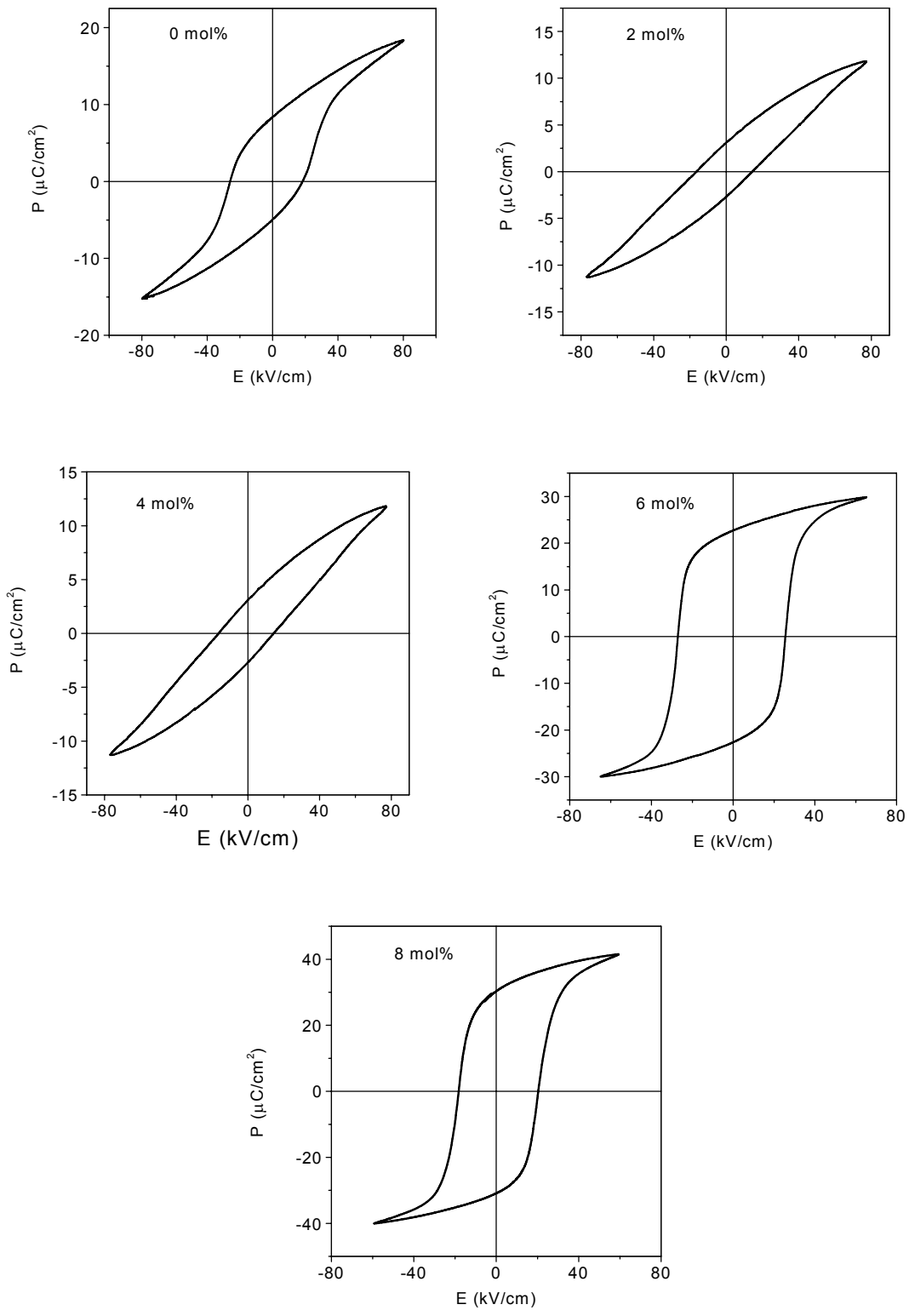

Fig. 4.27: Room temperature P – E hysteresis loops for series B

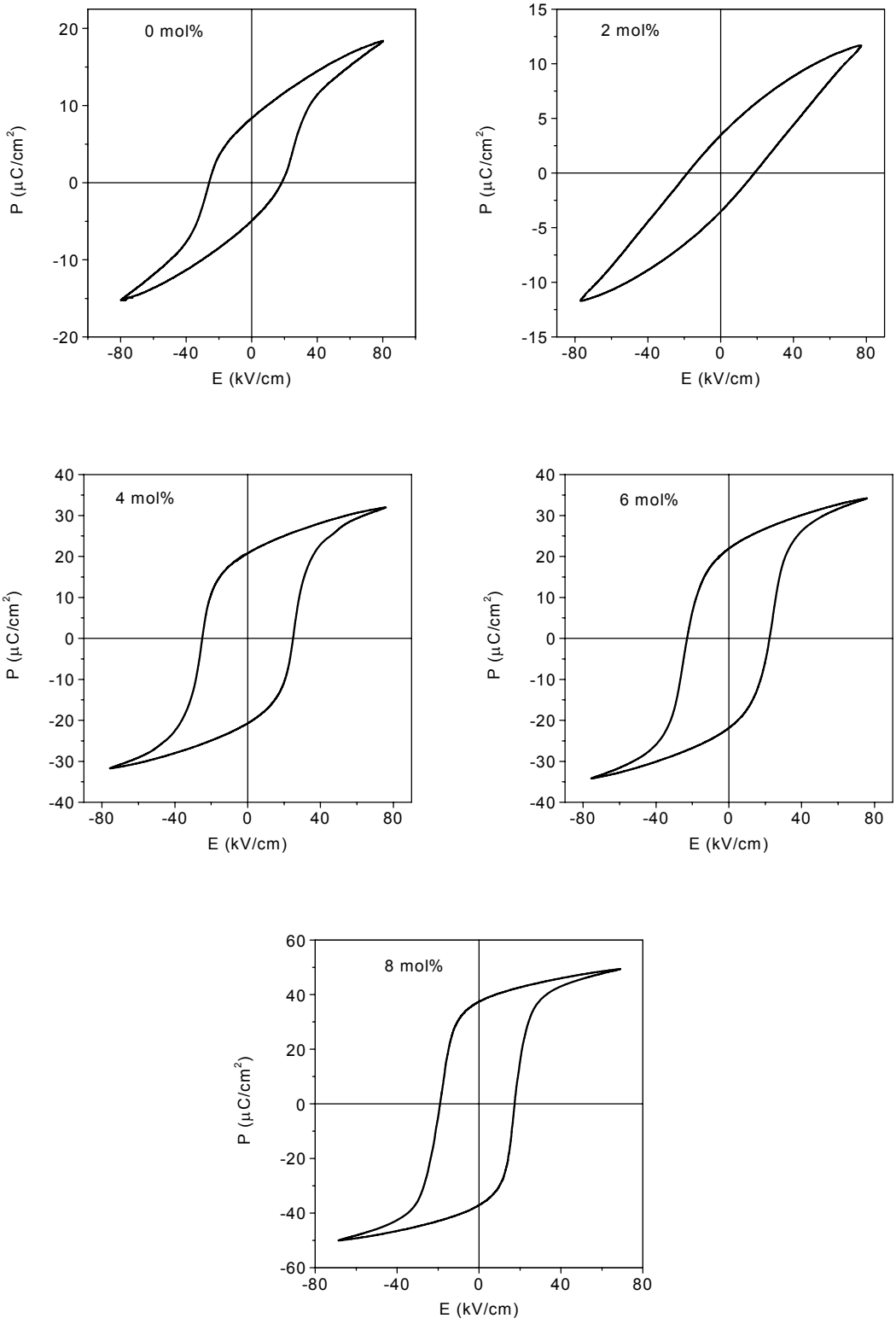

Fig. 4.28: Room temperature P – E hysteresis loops for series C

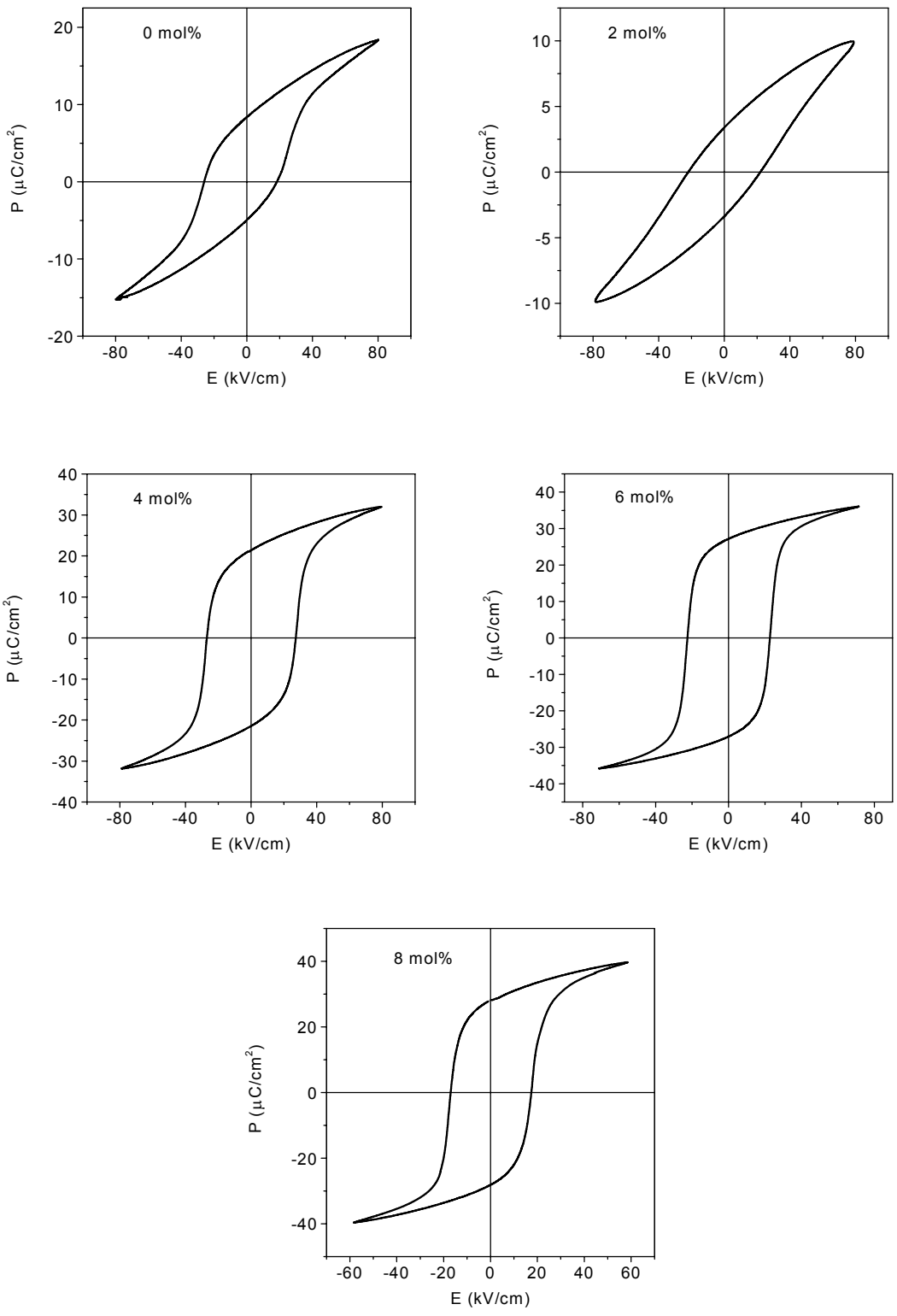

Fig. 4.29: Room temperature P – E hysteresis loops for series D

Table - 4.3

Variation of Coercive field, E_c (kV/cm) and Remnant polarization, P_r ($\mu C/cm^2$) with different x

	Series A		Series B		Series C		Series D	
x	E_c	P_r	E_c	P_r	E_c	P_r	E_c	P_r
0	22.2	6.7	22.2	6.7	22.2	6.7	22.2	6.7
0.02	19.5	4.4	14.9	7.3	18.4	3.5	21.5	3.4
0.04	19.6	3.4	15.4	2.9	24.9	20.7	27.2	21.4
0.06	20.7	9.5	26.3	22.6	22.7	21.9	22.6	27.1
0.08	18.3	21.7	19.0	30.6	18.2	37.3	17.2	27.8

References

1. J. Mal and R.N.P. Choudhary, Phase Transitions, **62** (1997) 19.
2. N.K. Mishra, R. Sati and R.N.P. Chaoudhary, Mater. Lett., **24** (1995) 313.
3. K. Okazaki, Ceram. Bull., **63** (1984) 1150.
4. F. Chu, I.M. Reaney and N. Setter, J. Am. Ceram. Soc., **78** (1995) 1947.
5. S.M. Pilgrim, A.E. Sutherland and S.R. Winzer, J. Am. Ceram. Soc., **73** (1990) 3122.
6. Y. Xu, Ferroelectric Materials and Their Applications, Elsevier Science Pub. Co. New York, USA (1991).
7. J. Mendiola, B. Jimenez, C. Alemany, L. Pardo and L.D. Olmo, Ferroelectrics, **94** (1989) 183.
8. K. Carl, Ferroelectrics, **9** (1975) 23.

Chapter V

PIEZOELECTRIC PROPERTIES

Lead titanate ceramics with samarium substitution are reported to exhibit excellent electromechanical anisotropy [1]. Large piezoelectric anisotropy (d_{33}/d_{31}) results in an impressive hydrostatic piezoelectric coefficient for modified PT ceramics [2]. Beside other applications, modified lead titanate ceramics also find use in hydroacoustic pressure sensor. In case of these ceramics, the large anisotropy of piezoelectric properties implies that longitudinal piezoelectric constant, d_{33}, is much larger in magnitude than the lateral piezoelectric constant, d_{31}, (which is negative) so that the hydroacoustic piezoelectric coefficient

$$d_h = d_{33} + 2d_{31} \qquad \textbf{…5.1}$$

is slightly smaller than d_{33}. Also, d_{31} is roughly 10% of the d_{33} in lead titanate ceramics. Therefore, the d_h of $PbTiO_3$ ceramics is about twice that of PZT ceramics despite the fact that d_{33} of PZT is four times larger. This large anisotropy of lead titanate consequently allows transducer designs with simple flat plates of piezoelectric material as opposed to the hollow cylindrical or spherical geometries commonly used with PZT ceramics [3]. This is important for high-pressure hydrophone designs where cylindrical or spherical geometries are impractical. These materials may also have some uses in underwater projectors, but the applications would be much more specialized. Also lower dielectric constant of these ceramics is advantageous in some sonar applications since the voltage sensitivity, g_h, is related to the hydroacoustic charge coefficient by the expression,

$$g_h = d_h/\varepsilon'\varepsilon_0 \qquad \textbf{…5.2}$$

The ability to change the dielectric constant by modifying the chemistry of these materials allows values of g_h and d_h to be adjusted for particular applications.

This chapter discusses the piezoelectric properties [like piezoelectric charge coefficients (d_{33}, d_{31}), voltage coefficients (g_{33}, g_{31}), piezoelectric anisotropy (d_{33}/d_{31}, g_{33}/g_{31}), thickness electromechanical coupling coefficient (k_t), planar electromechanical coupling coefficient (k_p) and electromechanical anisotropy (k_t/k_p)] at room temperature for all the samples synthesized by conventional dry ceramic technique. The effect of various substituted elements on the behaviour of these properties is explained.

The values of piezoelectric charge coefficients (d_{33}, d_{31}), piezoelectric voltage coefficients (g_{33}, g_{31}), hydrostatic coefficients (d_h, g_h), electromechanical coupling coefficients (k_p, k_t) are given in tables 5.1-5.10. Both d_{33} and $-d_{31}$ shows an increasing trend with increasing Sm and La substitution in modified PCT series whereas they show opposite trend for Ta substituted PCT series. The increase in d_{33} value may be due to the reorientation of domains, which is facilitated by decrease in crystal tetragonality [4]. In case of Ta substitution, the decreasing trend of d_{33} may be due to the dominating effect of relative density of the modified PCT samples on the small decrease in crystal tetragonality.

Piezoelectric voltage coefficients (g_{33}, g_{31}) were calculated by using expression [5]

$$g_{33} = (d_{33}) / (\varepsilon_0 \varepsilon') \qquad \textbf{…5.3}$$

$$g_{31} = (d_{31}) / (\varepsilon_0 \varepsilon') \qquad \textbf{…5.4}$$

The value of g_{33} and $-g_{31}$ effectively decreases with the substitution of Sm, La and Ta, which may be due to the relatively large increase in dielectric constant (relative permittivity) at room temperature. The hydroacoustic charge coefficient (d_h) and hydroacoustic voltage coefficient (g_h) show the same trend as d_{33} and g_{33}, respectively for all the series. A high value of piezo-figure of merit, $d_h.g_h$ is observed for all the modified PCT samples. Also relatively large values (in thousands) of $d_h.g_h$ are observed for Sm and La substituted PCT samples as compared to the values (in hundreds) for Ta substituted samples. This high value may be attributed to the large anisotropy in charge coefficients (d_{33}/d_{31}) and voltage coefficients ($-g_{33}/g_{31}$). The highest value (~ 2733) was observed for the sample of series A with 6 mol% Sm substitution. For series A and B, the samples with 6 mol% Sm substitution give maximum value of the piezo-figure of merit. For series

C and D, the samples with 8 mol% La substitution give maximum value of the piezo-figure of merit. Piezo-coefficients appear to be composition dependent. Apart from this, extrinsic parameters, like grain size, electronic and ionic objects [6] also play a part in the behaviour of these coefficients. The compositional dependence of the piezo-coefficients is because the composition influences dielectric constant [7].

The behaviour of planar (k_p) and thickness (k_t) electromechanical coupling coefficients and their ratios for all the series is given in table 5.6. Fig. 5.1 (a, b) shows the typical plots of admittance vs. frequency for the calculation of planar electromechanical coupling factor (fig. 5.1a) and thickness electromechanical coupling factor (fig. 5.1b). K_p is observed to show slight variation in all the samples whereas k_t is greatly influenced by the substituting elements (Sm, La and Ta). Also Ta substituted samples show a relatively less values of electromechanical anisotropy as compared to the Sm and La substituted PCT samples. The highest value of electromechanical anisotropy (k_t/k_p) was observed ~ 52 for 6 mol% samarium substituted PCT sample of Series A, which is desirable for high frequency applications. The trend of k_p shows a little agreement with the trend of average grain size (values given in section 3.3). Different mechanisms have suggested by different workers for the origin of electromechanical anisotropy. However, the exact origin has not been clearly established. It has been suggested that the increase in 90^o domain wall reorientation by poling reduces k_p and enhances anisotropy [8]. Also strong clamping caused by 90^o domain reorientation is attributed to vanishing of k_p [9].

Table - 5.1

Variation of piezo - coefficients for series A

x	d_{33} (pC/N)	$-d_{31}$ (pC/N)	$-d_{33}/d_{31}$	g_{33} ($x10^{-3}$ Vm/N)	$-g_{31}$ ($x10^{-3}$ Vm/N)	d_h (pC/N)	g_h ($x10^{-3}$ Vm/N)	$d_h.g_h$ ($10-^{12}m^2N^{-1}$)
0	45	2.0	22.5	34	1.5	41	31	1271
0.02	56	2.2	25.5	33.2	1.3	52	30.6	1580
0.04	67	2.5	26.8	33.4	1.3	62	30.8	1916
0.06	83	3	27.6	38.3	1.4	77	35.5	2733
0.08	92	6	15.3	33.4	2.2	80	29	2320

Table - 5.2

Variation of piezo - coefficients for series B

x	d_{33} (pC/N)	$-d_{31}$ (pC/N)	$-d_{33}/d_{31}$	g_{33} ($x10^{-3}$ Vm/N)	$-g_{31}$ ($x10^{-3}$ Vm/N)	d_h (pC/N)	g_h ($x10^{-3}$ Vm/N)	$d_h.g_h$ ($10-^{12}m^2N^{-1}$)
0	45	2.0	22.5	34	1.5	41	31	1271
0.02	55	2.13	25.8	31.5	1.22	45.7	29.6	1353
0.04	62	2.35	26.4	30.1	1.17	57.2	27.8	1590
0.06	70	2.60	26.9	29.6	1.09	64.7	27.4	1772
0.08	76	2.71	28	22.1	0.78	70.6	20.5	1447

Table - 5.3

Variation of piezo - coefficients for series C

x	d_{33} (pC/N)	$-d_{31}$ (pC/N)	$-d_{33}/d_{31}$	g_{33} ($x10^{-3}$ Vm/N)	$-g_{31}$ ($x10^{-3}$ Vm/N)	d_h (pC/N)	g_h ($x10^{-3}$ Vm/N)	$d_h.g_h$ ($10-^{12}m^2N^{-1}$)
0	45	2.0	22.5	34	1.5	41.0	31.0	1271
0.02	54	2.2	24.4	34.4	1.41	49.6	31.6	1567
0.04	60	2.4	25.0	28.4	1.14	55.2	26.1	1440
0.06	75	2.6	26.9	25.1	0.87	69.8	23.4	1633
0.08	85	3.0	28.3	24.6	0.28	79.0	24.1	1903

Table - 5.4

Variation of piezo - coefficients for series D

x	d_{33} (pC/N)	$-d_{31}$ (pC/N)	$-d_{33}/d_{31}$	g_{33} ($x10^{-3}$ Vm/N)	$-g_{31}$ ($x10^{-3}$ Vm/N)	d_h (pC/N)	g_h ($x10^{-3}$ Vm/N)	$d_h.g_h$ ($10-^{12}m^2N^{-1}$)
0	45	2.0	22.5	34	1.5	41.0	31.0	1271
0.02	57	2.3	24.4	27.7	1.12	52.4	25.5	1336
0.04	70	2.6	26.9	29.8	1.11	64.8	27.6	1788
0.06	85	2.8	30.3	26.7	0.88	79.4	24.9	1977
0.08	95	3	31.6	26.4	0.83	89	24.7	2198

Table - 5.5

Variation of piezo - coefficients for series E

x	d_{33} (pC/N)	$-d_{31}$ (pC/N)	$-d_{33}/d_{31}$	g_{33} ($x10^{-3}$ Vm/N)	$-g_{31}$ ($x10^{-3}$ Vm/N)	d_h (pC/N)	g_h ($x10^{-3}$ Vm/N)	$d_h.g_h$ ($10-^{12}m^2N^{-1}$)
0	45	2	22.5	34	1.5	41	31	1271
0.01	38	2.1	18.1	30	1.6	34	27	918
0.02	36	1.2	30	30	1	33	26	858
0.03	30	1	30	27	1	28	25	700

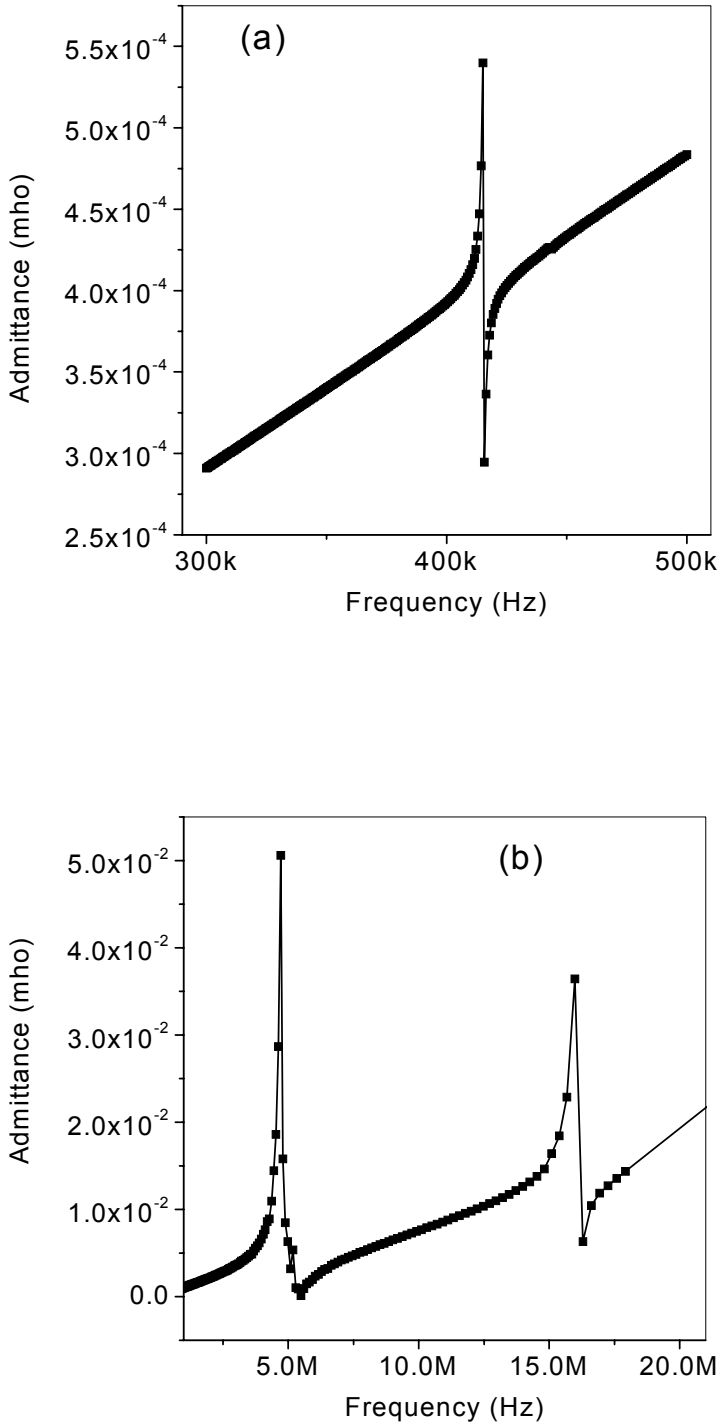

Fig. 5.1: Typical admittance spectra for the calculation of (a) k_p and (b) k_t

Table - 5.6

Variation of electromechanical coupling coefficients (k_p, k_t) and their anisotropy (k_t/k_p) with different x

	Series A			Series B			Series C			Series D			Series E			
x	k_t	k_p	k_t/k_p	k_t	k_p	k_t/k_p	k_t	k_p	k_t/k_p	k_t	k_p	k_t/k_p	x	k_t	k_p	k_t/k_p
0	27	2.3	11.7	27	2.3	11.7	27	2.3	11.7	27	2.3	11.7	0	27	2.3	11.7
0.02	36	3.4	10.6	36	3.0	12	40	5	8.00	32	3	10.6	0.01	25	2.5	10
0.04	45	2.2	20.6	42	2.8	15	42	4	10.5	45	3.5	13	0.02	23	2.6	8.8
0.06	57	1.1	51.8	50	2.5	20	51	1.9	26.8	50	2.2	23	0.03	20	3	6.7
0.08	55	1.8	30.5	54	2.0	27	46	2.5	18.4	52	2	26		-		

References

1. H. Takeuchi, Ceram. Bull., **71** (1992) 974.
2. L.M. Toroilo, D. Damjanovic and R.E. Newnham, J. Am. Ceram. Soc., **77** (1994) 857.
3. K.M. Rittenmyer and R.Y. Ting, Ferroelectrics, **110** (1990) 171.
4. J.D. Frutos and B. Jimenez, Ferroelectrics, **126** (1992) 341.
5. H. Jaffe, IRE standards on piezoelectric ceramics, Proc. IRE, **49** (1961) 1161.
6. D. Damjanovic, T.R. Gururaja and L.E. Cross, Ceram. Bull., **66** (1987) 699.
7. W. Wersing, K. Lubitz and J. Mohaupt, IEEE Trans. On Ultrasonics, Ferroelectrics and Frequency Control, **36** (1989) 424.
8. H. Takeuchi, S. Jyomura, E. Yamamoto and Y. Ito, J. Acoust Soc. Am., **72** (1982) 1114.
9. B. Jimenez, J. Mendiola, C. Alemany, D. Olmo, L. Pardo and E. Maurer, Ferroelectrics, **87** (1988) 97.

Chapter VI

NOVEL TECHNIQUES

6.1 Microwave Sintering

Microwave sintering of ceramic materials has been studied by various researchers [1-5] and was reported to be superior to conventional sintering by possessing rapid heating, significant reduction in manufacturing costs due to energy savings and shorter processing times, enhanced densification rate, less sintering active energy and improved microstructures. The reason may be attributed to different heating mechanism for microwave sintering, which shows electromagnetic waves interacting with ceramic materials leading to volumetric heating by dielectric loss. Microwave heating is a function of materials being processed, and there is almost 100% conversion of absorbed electromagnetic energy into heat, largely within the sample itself, unlike with conventional heating where there are significant thermal energy losses. Here in this section, we report the synthesis of PSCT system, $Pb_{0.76-3x/2}Sm_xCa_{0.24}Ti_{0.98}Mn_{0.02}O_3$; x = 0-0.08, using novel microwave sintering technique and detailed investigation of the structural, dielectric and piezoelectric properties. Also a comparison between the hysteresis behaviour, dielectric and piezoelectric properties and microstructures of one of the composition from the above mentioned series with x = 0.08 is presented for both microwave and conventional sintering techniques.

6.1.1 System Properties

6.1.1a Structural Properties

Fig. 6.1 shows the typical time-temperature profile for the samples sintered by microwave sintering technique. Total time for the whole run was only 135 minutes which includes heating and cooling rates of 20^oC/min and 10^oC/min, respectively with soaking time of 30 min. With this sintering schedule, we could get samples with relative density of the order of 99%. Fig. 6.2 shows the XRD patterns of the Sm modified PCT ceramics. Analysis confirmed a single-phase formation with tetragonal structure for all the samples. From the observed d values, lattice parameters ‘c’ and ‘a’ were determined and

tetragonality (c/a ratio) that represents the distortion of the cubic structure [6] was computed. The trend is given in fig. 6.3.

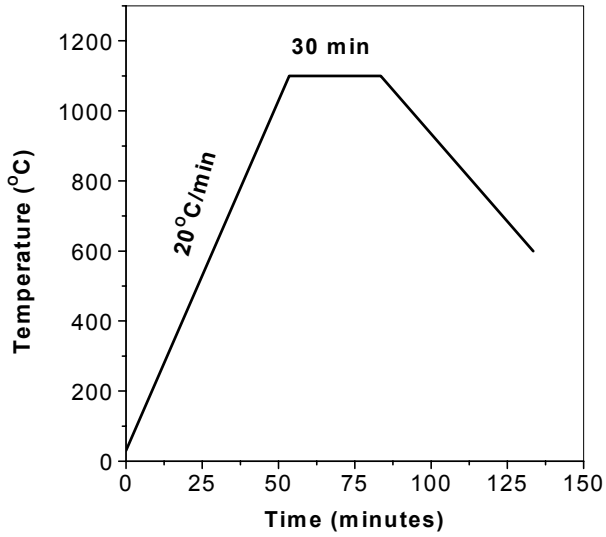

Fig. 6.1: Typical time-temperature profile for microwave sintering

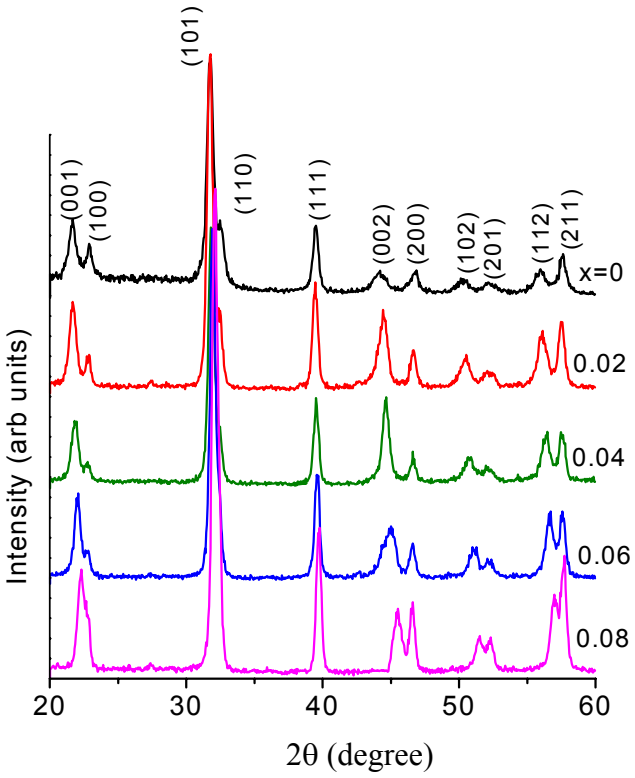

Fig. 6.2: XRD patterns for $Pb_{0.76-3x/2}Sm_xCa_{0.24})(Ti_{0.98}Mn_{0.02})O_3$ composition

The value of ‘c’ decreases faster whereas ‘a’ increases very slowly. The decrease in tetragonality confirms the approachness of the compounds towards cubic structure. The lesser the crystal anisotropy, the lesser are the mechanical stresses that arise in the ceramic [7-11] thus with increasing the Sm substitution, the mechanical strength of the microwave sintered PCT ceramics increases.

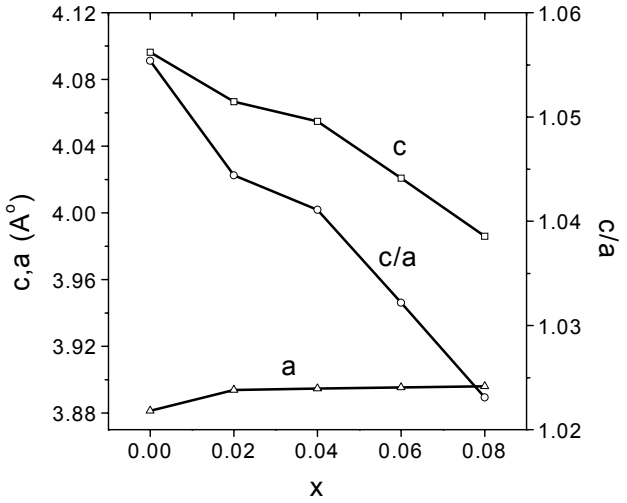

Fig. 6.3: Variation of lattice constants (c, a) and lattice anisotropy (c/a) with the samarium substitution (x)

In order to estimate the degree of densification, we calculated the theoretical density for these samples, using the values of the lattice constants ‘c’ and ‘a’. Table 6.1 shows the variation of relative density (%) with the increase in the amount of samarium in PCT ceramics. This shows an increasing trend and the sample with 8 mol% Sm shows the highest (99%) relative density.

Fig. 6.4 shows the microstructures of freshly broken fractured surfaces of microwave sintered PSCT samples. Nearly uniform distribution of grain size and also dense microstructures were observed for all the samples.

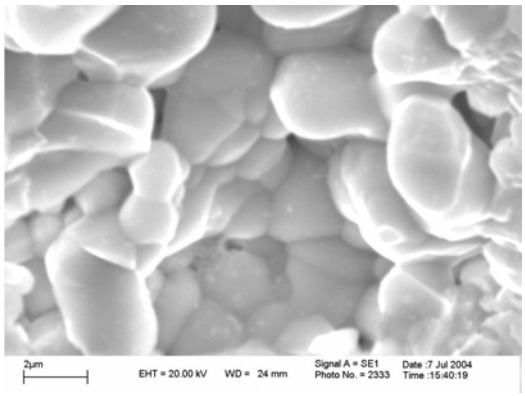

x = 0

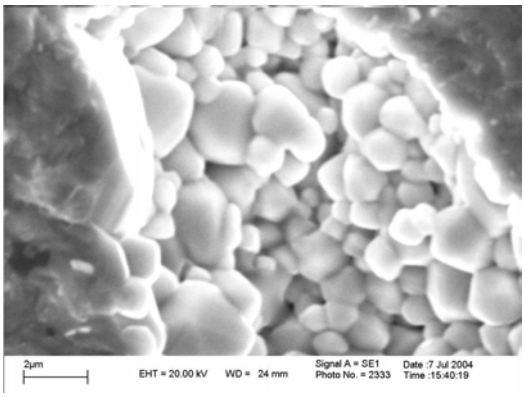

x = 0.02

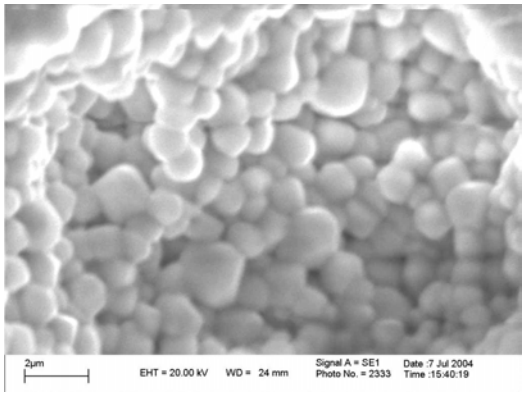

x = 0.04

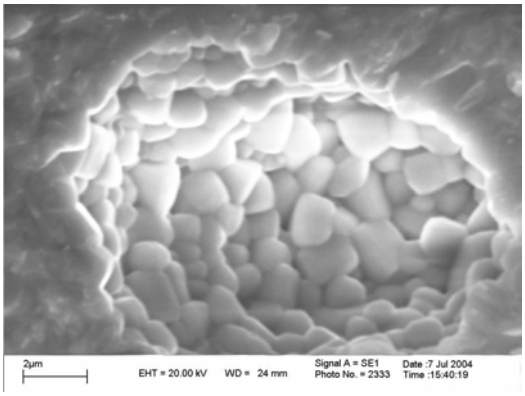

x = 0.06

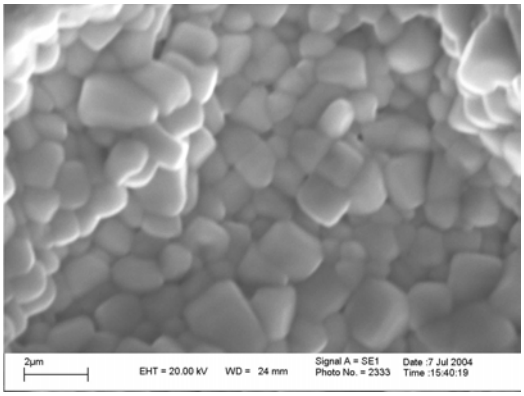

x = 0.08

Fig. 6.4: Scanning Electron Micrographs for 0-8mol% Sm-modified PCT ceramics

The average grain size lies between 1.4-2 μm. It means the rate of grain growth was markedly enhanced without inducing abnormal grain growth, which is desired to get the better electrical and electromechanical properties. The variation of average grain size for all the samples with increase in Sm content is shown in table 6.1.

6.1.1b Dielectric Properties and Hysteresis Behaviour

Fig. 6.5 shows the room temperature variation of dielectric constant (ε') and loss (tanδ) as a function of frequency (100 Hz - 1 MHz) for various concentrations of Sm (0-8 mol%) in PCT ceramics. Small decrease in ε' is observed with respect to frequency for all the samples whereas pronounced dispersion was observed at lower frequency region for tanδ. The decrease is because at higher frequencies, the ions cannot respond to the field quickly enough resulting in the decrease of dielectric constant. Also the dielectric constant (ε') increases correspondingly with the increase of amount of Sm (values at 1 kHz are given in table 6.1) at room temperature because the Curie temperature (T_c) of the PCT system decreases as Sm concentration increases (the behaviour of T_c is explained in coming results. Dielectric loss, tanδ (values at 1 kHz are given in table 6.1) showed a decreasing trend with increase in Sm amount which may be due to the increase in the density of PCT ceramics with the increment in the amount of samarium.

The variation of ε' and tanδ as a function of temperature at different frequencies (1 kHz, 10 kHz and 100 kHz) was done for all the samples. Fig. 6.6 shows this behaviour for one typical composition with x = 8 mol%. It was observed that as the temperature increases, the value of dielectric constant increases and passes through a maximum (transition temperature), and then decreases. The dissipation factor also exhibits slightly broad maxima around the transition temperature. This is because higher temperatures will facilitate the charge transport down grain boundaries. This increased charge mobility will subsequently increase the loss in a material under an applied field or we can say that the increase in the losses at elevated temperatures is caused by a corresponding conductivity increase [12].

Fig. 6.7 shows the temperature variation of dielectric constant and loss for different concentrations of samarium in PCT ceramics at 10 kHz. Transition temperature also

found to decrease with the increase in the Sm amount (values are reported in table 6.1). This can be attributed to the decrease in crystal tetragonality caused by Sm substitution, which reduces the internal stress and which in turn reduces the transition temperature [13]. Also there is broadening of the peak increases with increase in Sm substitution. This may be due to the disorder in the arrangement of rare earth (samarium) and other atoms, leading to a microscopic heterogeneity in the composition, and thus a distribution of different local Curie points [14]. The structural disorder in the compounds arises due to the presence of a number of voids and impurities of different sizes. The degree of disorder or diffusivity (γ), in all the three compositions was calculated using the expression [15],

$$\ln (1/\varepsilon'-1/\varepsilon'_{max}) = \gamma \ln(T-T_c) + a \qquad \textbf{…6.1}$$

where ε'_{max} is the maximum value of ε at T_c. The value of γ is the degree of diffusiveness, which lies in the range of $1 < \gamma \leq 2$, where $\gamma = 1$ represents ideal Curie-Weiss behaviour while γ between 1 and 2 indicates diffused transition [16] The values of γ, calculated from the slope of graphs (fig. 6.8), were found to increase with the substitution of samarium (table 6.1), which may be due to the compositional fluctuations and structural disordering in the arrangement of cations in one or more crystallographic sites in the structure that finally results in a microscopic heterogeneity in the samples with local curie points [17,18].

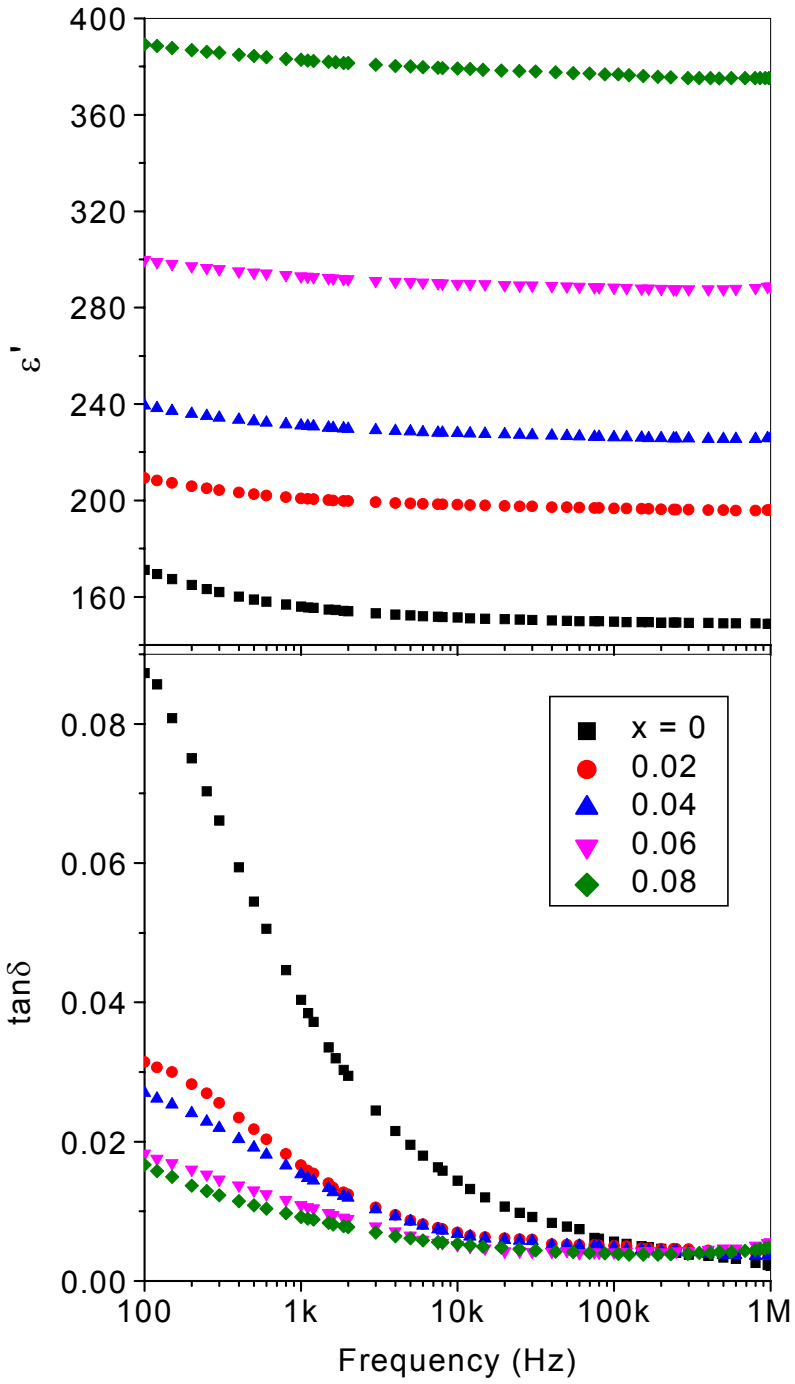

Fig. 6.5: Variation of ε' and tanδ with frequency for different amounts of samarium at room temperature

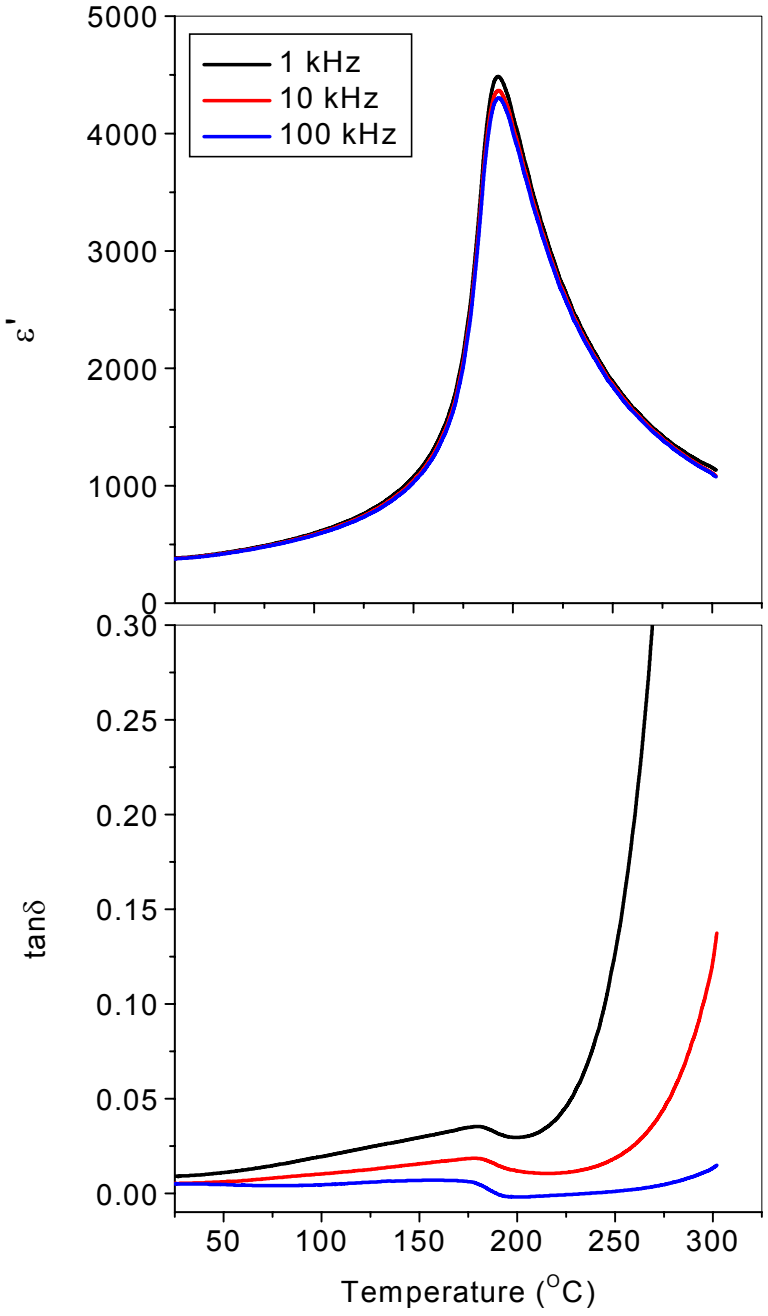

Fig. 6.6: Temperature variation of ε' and tanδ for the sample (x = 0.08) at different frequencies

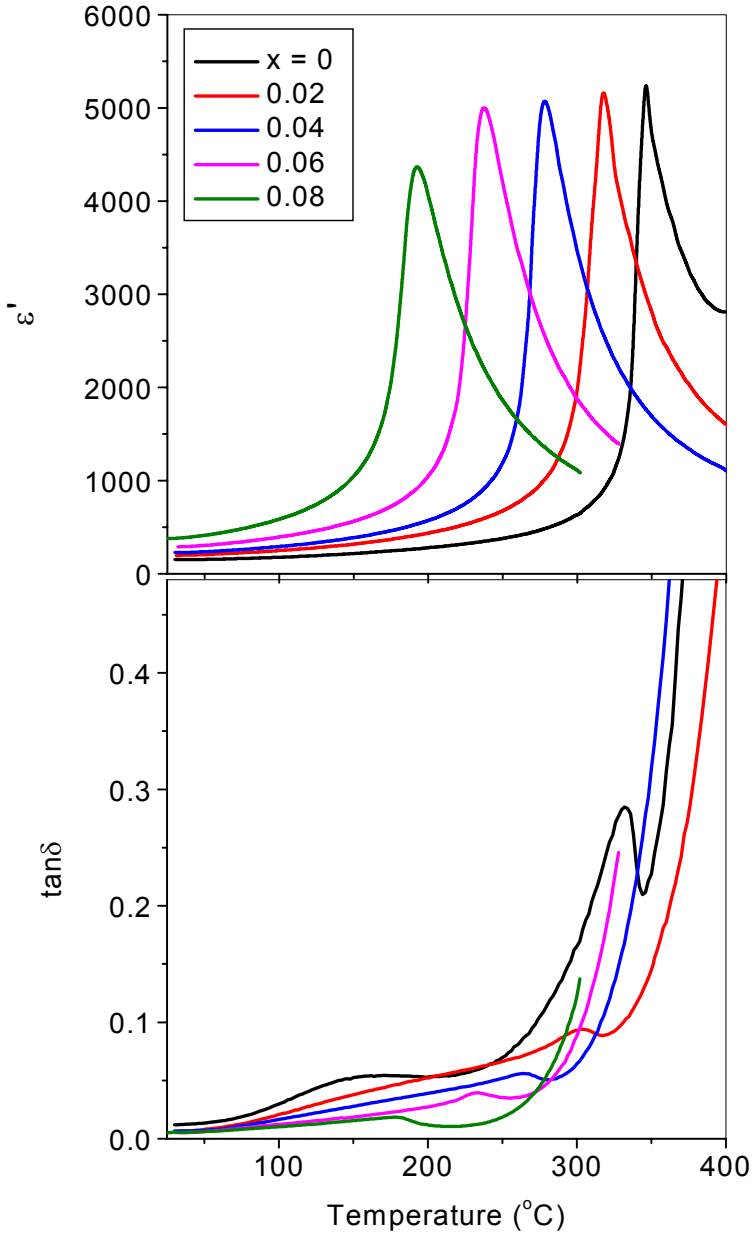

Fig. 6.7: Temperature variation of ε' and tanδ for different amounts of samarium at 10 kHz

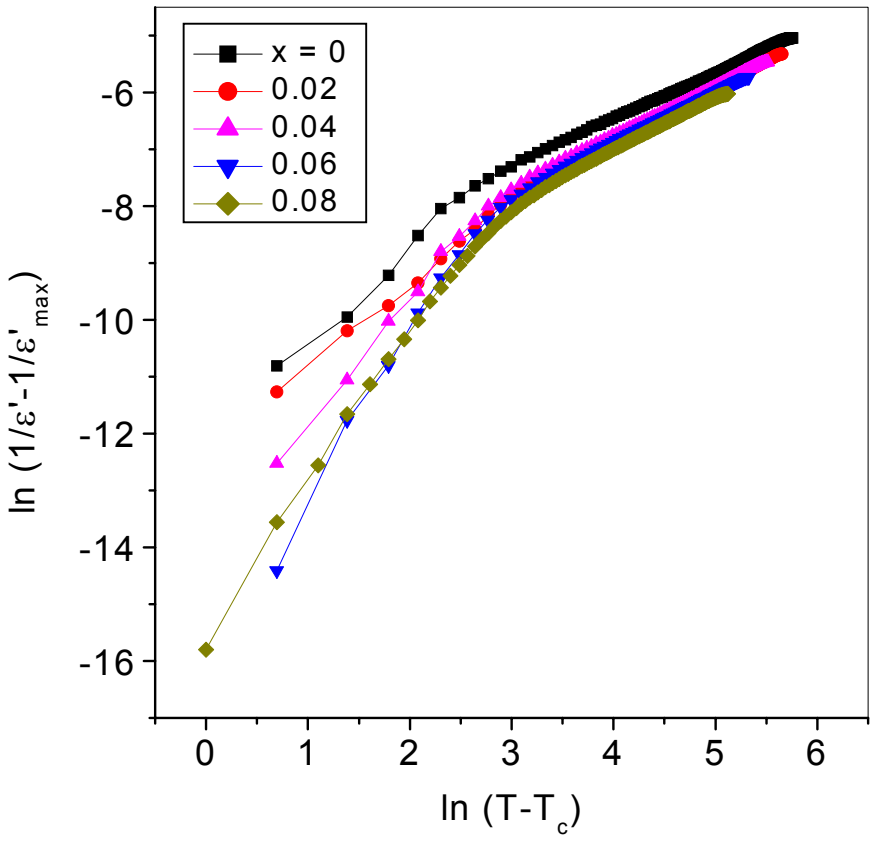

Fig. 6.8: Variation of ln ($1/\varepsilon'-1/\varepsilon'_{max}$) vs. ln ($T-T_c$) at 10 kHz

Fig. 6.9 illustrates P-E hysteresis loops for all the compositions, which show well-defined ferroelectric behaviour. The values of and coercive field (E_c) and remnant polarization (P_r) determined from the P-E loops are given in table 6.1. From the trend, it can be seen that there is an increase in the value of coercive field (E_c) up to 6 mol% Sm followed by the decrease for 8 mol%. This behaviour can be explained with the grain size variation, which also show decrease up to 6 mol% Sm followed by the increase with further increase in Sm content for 8 mol%. It is well reported in the literature that with decrease in grain size, E_c increases as each grain is mechanically clamped by its surrounding. This clamping effect, in addition to the mechanical stresses accompanying 90^0 domain rotations, tends to impede the polarization reversal process, and hence, apparently increases E_c [19].

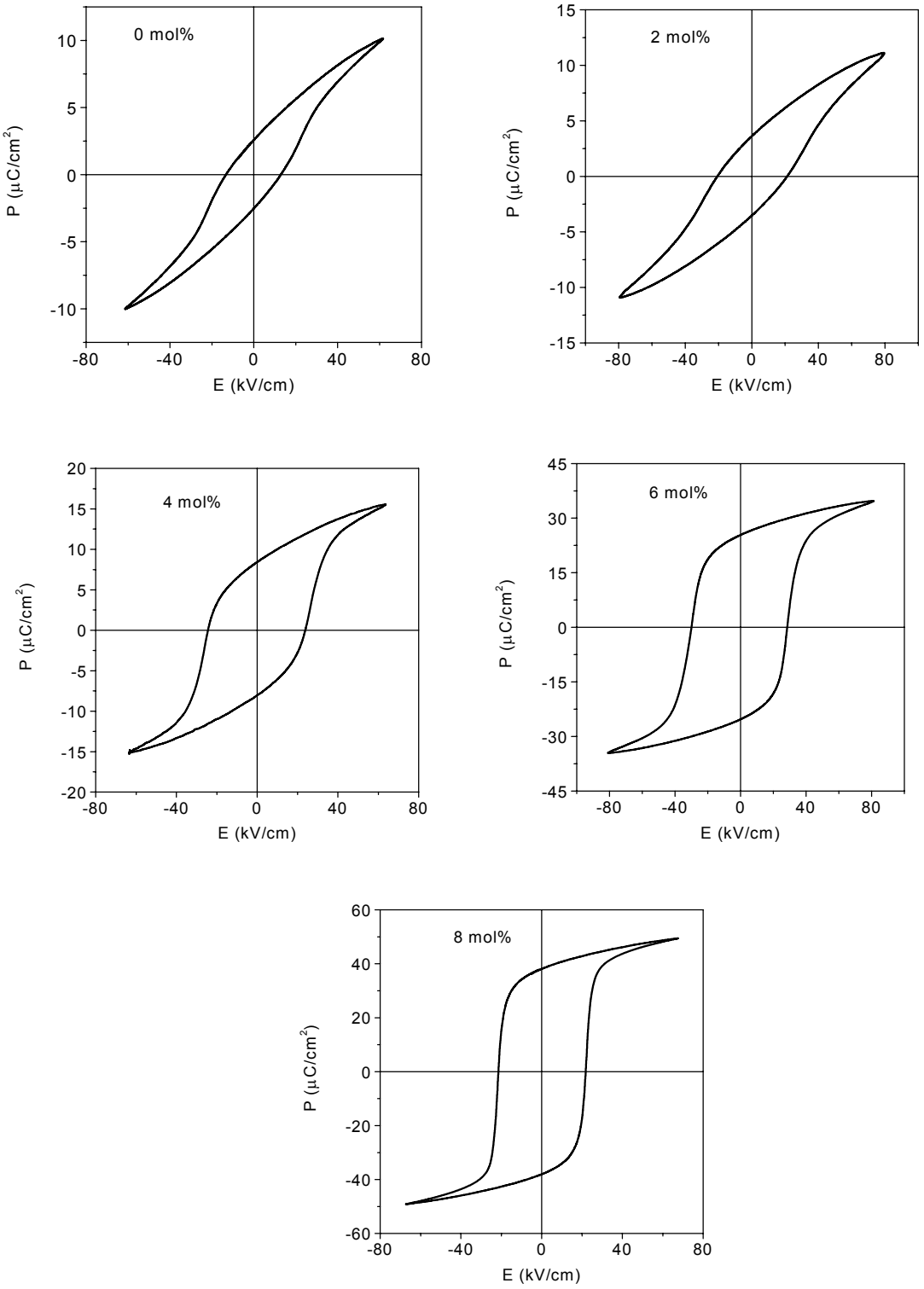

Fig. 6.9: Room temperature P – E hysteresis loops for different amounts of samarium

Also there is increase in the remnant ratio (P_r/P_s) for 8 mol% Sm (~ 0.77) as compared to the composition with 6 mol% Sm (~ 0.73). Major contribution for increase in P_r is due to softening effect of Sm substitution, which also results in reduction of tetragonality. Another factor contributing to observed increase in P_r might be due to the increase in the relative density with the increase in samarium substitution.

6.1.1c Piezoelectric Properties

Samarium modified PT ceramics are reported to exhibit excellent electromechanical anisotropy [20]. Large piezoelectric anisotropy (d_{33}/d_{31}) results in an impressive hydrostatic piezoelectric coefficient for modified PT ceramics [21]. The values of piezoelectric charge coefficients (d_{33} and d_{31}), piezoelectric voltage coefficients (g_{33} and g_{31}) and hydrostatic coefficients (d_h and g_h) are given in table 6.2. An increase in d_{33} is observed with increase in Sm substitution. The sample with 8 mol% Sm gives highest value of d_{33} 78 pC/N. This increase in d_{33} may be due to the reorientation of domains, which is facilitated by decrease in crystal tetragonality [22].

The transverse piezoelectric charge coefficient (d_{31}) exhibits a limited variation with the samarium substitution. The value of d_{31} varies between -2.5 to -4 pC/N. Piezoelectric voltage coefficient (g_{33}) was calculated by using expression [23],

$$g_{33} = (d_{33}) / (\varepsilon_0 \varepsilon') \qquad \textbf{…6.2}$$

The value of g_{33} decreases with the Sm substitution, which may be due to the large increase in dielectric permittivity. The value of g_{31} also shows the decreasing trend. The hydroacoustic charge coefficient (d_h) is found to increase with increase in samarium substitution. The value for 0 mol% Sm substituted composition is 42 pC/N and attains a maximum value of 73 pC/N in case of 8 mol% substitution. The voltage sensitivity coefficient, g_h decreases with the increase in samarium. This may be due to the more number of Pb^{2+} vacancies with the substitution of Sm.

The behaviour of planar (k_p) and thickness (k_t) electromechanical coupling coefficients with the increase in samarium content has been shown in table 6.3. k_p is observed to show slight variation whereas k_t is greatly influenced by samarium substitution. It has been

observed that k_t increases from 30% to 60% and k_p decreases form 3% to 1.2% with the substitution of samarium. As a result, highest value of electromechanical anisotropy (k_t/k_p) was observed to be 50 for 8 mol% samarium substitution. Different mechanisms have been suggested by different workers for the origin of electromechanical anisotropy. However, the exact origin has not been clearly established. It has been suggested that the increase in 90^o domain wall reorientation by poling reduces k_p and enhances anisotropy [7]. Also strong clamping caused by 90^o domain reorientation is attributed to vanishing of k_p [24]. Porosity in ceramics and wider grain boundaries reduce the intergranular stress caused by spontaneous strain during para-ferroelectric transition [25]. The pressure acting on the 90^o domain walls is lower in less dense ceramics than those with compact microstructures. If such ceramics, having appropriate microstructures, are poled to achieve relatively higher 90^o domain reorientation, the k_p should become zero, although specific mechanism, which attributes to this behaviour is not understood. In our case, the density shows the increasing trend with the increase in the amount of samarium and we got the dense microstructures by microwave sintering process. The intergranular stress produced by 90^o domain reorientation results in the increase in tendency of 90^o domains to come back to their initial orientation, i.e. domains which were reoriented by the poling field. If the intergranular stress is removed, the tendency of these domains to relax back will diminish and if these 90^o domains are permanently reoriented by poling field then their contribution to planar coupling coefficients will decrease and may also vanish if the reorientation achieved is very high [26]. Also the increase in the substitution of samarium may be one of the reasons for the increase in electromechanical anisotropy, which has direct effect on electrostrictive coefficients and permittivity on one hand and the coercive field on the other hand.

Table - 6.1

Variation of structural and dielectric properties for Sm modified PCT ceramics using microwave sintering technique

x	Relative density (%)	Average grain size (μm)	ε' (1kHz)	tanδ (1kHz)	T_c (^oC)	γ	E_c (kV/cm)	P_r ($\mu C/cm^2$)
0	96.0	2	155	0.040	346	0.94	13	2.5
0.02	97.2	1.7	200	0.016	317	1.05	21	3.6
0.04	98.3	1.5	230	0.015	278	1.21	24	8.2
0.06	99.0	1.3	295	0.011	238	1.3	29	25
0.08	99.1	1.4	385	0.009	192	1.4	22	38

Table - 6.2

Variation of piezo-coefficients with different x

x	d_{33} (pC/N)	$-d_{31}$ (pC/N)	$-d_{33}/d_{31}$	g_{33} ($x10^{-3}$ Vm/N)	$-g_{31}$ ($x10^{-3}$ Vm/N)	d_h (pC/N)	g_h ($x10^{-3}$ Vm/N)
0	50	4.1	13	34	2.73	41.8	28.5
0.02	52	3.5	15	28	1.91	45.0	24.2
0.04	65	3.4	19	31	1.63	58.2	27.7
0.06	75	3.2	23	28	1.20	68.6	25.6
0.08	78	2.5	31	23	0.77	73.0	21.5

Table - 6.3

Variation of electromechanical coupling coefficients (k_p, k_t) and their anisotropy (k_t/k_p) with different x

x	k_t (%)	k_p (%)	k_t/k_p
0	30	3	10
0.02	35	2.5	14
0.04	45	2	22.5
0.06	54	1.5	36
0.08	60	1.2	50

6.1.2 Comparative Study of Microwave Sintering and Conventional Dry Ceramic Method

Here, we report a comparative study on synthesis and properties of $Pb_{0.66}Sm_{0.08}Ca_{0.24}Ti_{0.98}Mn_{0.02}O_3$ (PSCT) system by conventional and microwave sintering techniques.

Fig. 6.10 compares the time-temperature profiles between microwave and conventional synthesis of PCT ceramics and sintering temperature and duration are listed in table 6.4. The total cycle time was 575 and 135 minutes for conventional sintering (CS) and microwave sintering (MS) samples, respectively. This indicates, unambiguously, the energy and time efficiency of MW processing over conventional one.

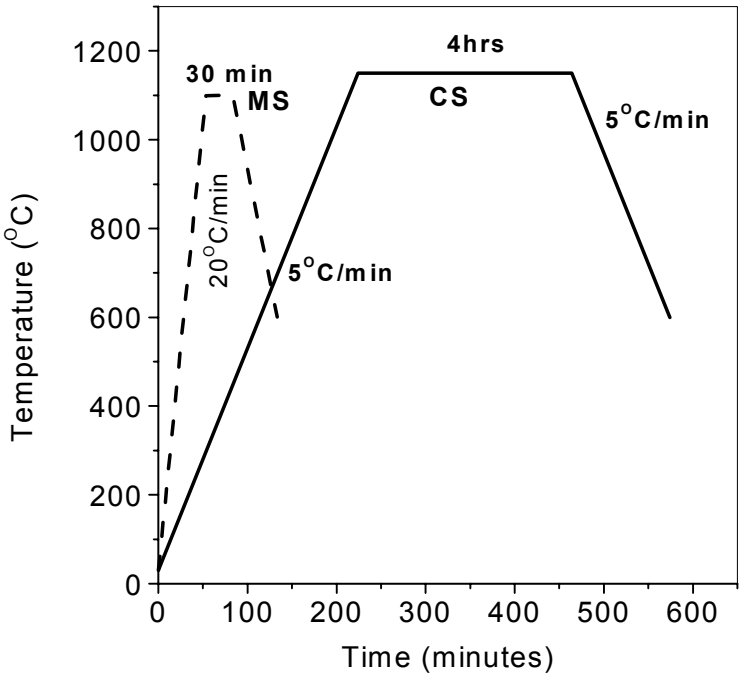

Fig. 6.10: Comparison of the time-temperature profiles for modified PCT ceramics prepared by microwave and conventional process

Fig. 6.11 shows the XRD patterns for conventionally and microwave sintered PSCT samples. Both the specimens reveal a single-phase formation with a tetragonal structure.

The lattice parameters (c, a) and 'c/a' ratio were calculated using 'XLAT' software and the values are given in table 6.4.

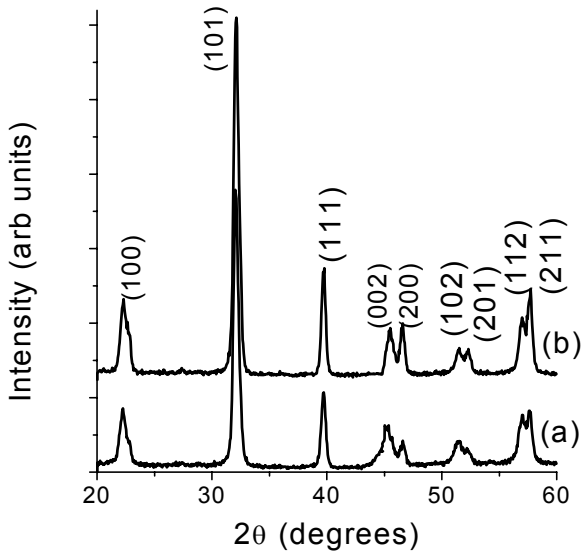

Fig. 6.11: XRD patterns for (a) Conventional (CS) and (b) microwave sintered (MS) samples

From lattice parameters, theoretical density (d_{th}) was calculated. The result implies that the microwave sintering process enhances the densification rate of Sm modified PCT ceramics as the sintering time needed is markedly shortened and lower sintering temperature could be sufficient to achieve the higher density of around 99% of the theoretical density. On the other hand, lower sintering temperature and less time facilitates to avoid the lead loss during sintering [27]. Structural anisotropy, c/a, found to be slightly higher for MS sample indicating enhanced sinterability [28]. The unit cell volume was found to decrease slightly from 60.54 to 60.48 $(Å)^3$ for MS sample.

Fig. 6.12 shows the microstructures of conventionally and microwave sintered PCT ceramics. The grain size distribution for MS sample is more uniform than that for CS sample. It means the rate of grain growth was markedly enhanced without inducing abnormal grain growth, which is desired to get the better electrical and electromechanical

properties. Also, the average grain size is smaller for MS sample as compared to that for CS sample.

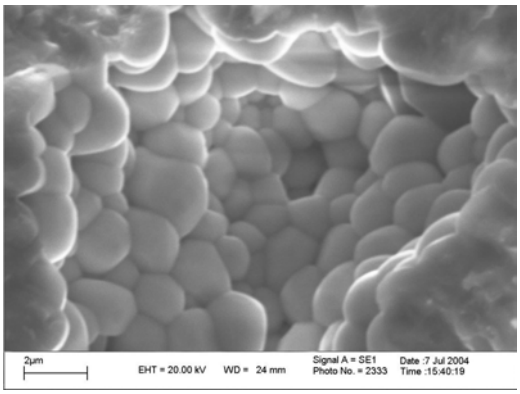

(a)

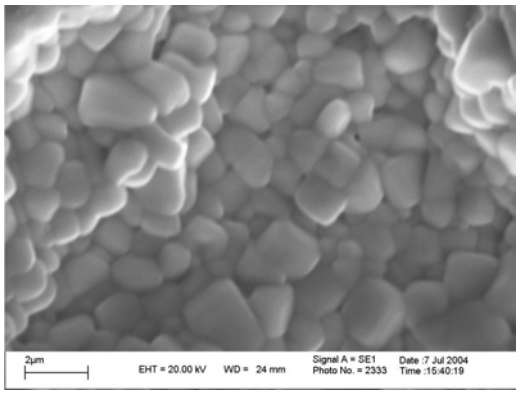

(b)

Fig. 6.12: Scanning electron micrographs for (a) CS and (b) MS samples

Fig. 6.13 shows the comparison of temperature dependence of dielectric constant (ε') and loss (tanδ) at 10 kHz for both the samples. It is observed that the value of dielectric constant at maxima decreases for MS sample. The Curie temperature was found to be 192^{o}C, which is hardly affected by processing techniques. The peak is sharp for both the samples. Dissipation factor also passes through maxima at T_c and then sharply increases due to conduction losses.

Room temperature values of dielectric constant and dissipation factor measured at 1 kHz are given in table 6.4. Dielectric constant is slightly less for MS sample as compared to CS sample, which may be due to the change in the microstructure. Dissipation factor (tanδ) is almost same for both the samples.

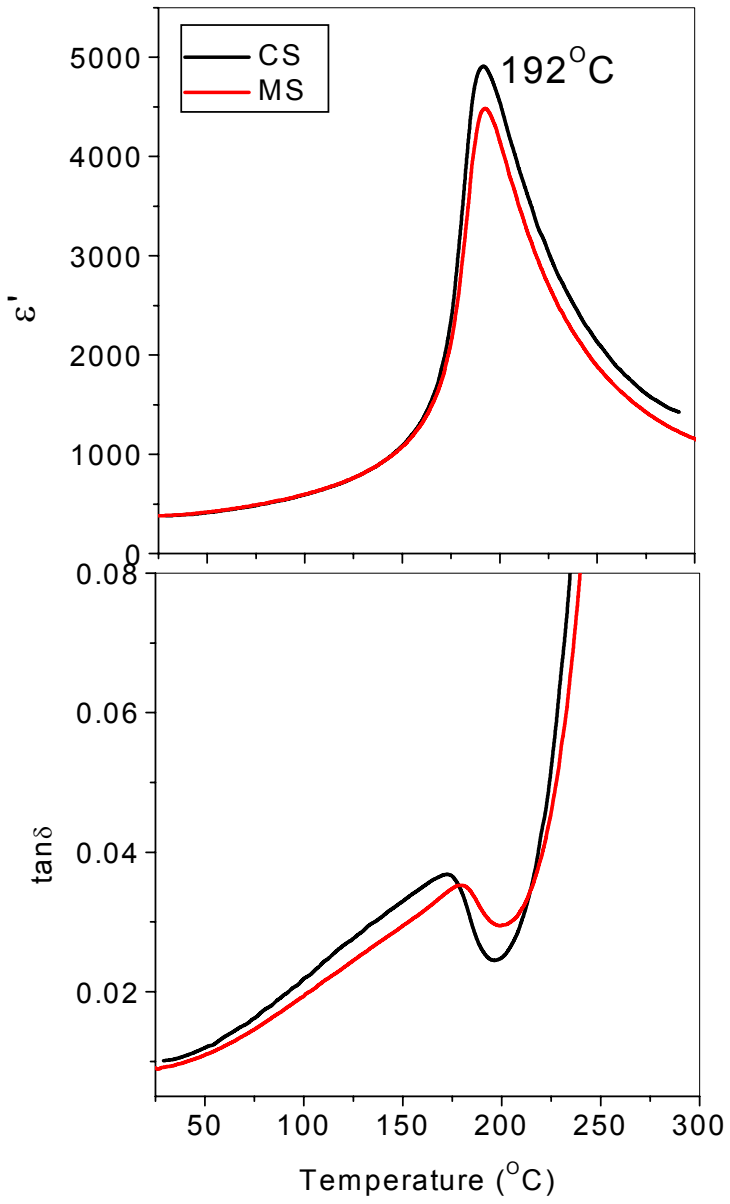

Fig. 6.13: Temperature dependence of ε' and tanδ for CS and MS samples at 10 kHz

The P-E hysteresis loops were recorded at room temperature at 50 Hz and the results are shown in fig. 6.14. Coercive field (E_c) and remnant polarization (P_r) were determined from the P-E loop and listed in table 6.4. It is observed that E_c is slightly higher for MS sample, which may be due to the smaller grain size restraining the domain switching. This can be further described as: In a ceramic material, each grain is mechanically clamped by its surroundings. This clamping effect in addition to the mechanical stresses accompanying 90^o domain rotations tends to impede the polarization reversal process, and, hence, apparently increase E_c [19]. The value of P_r is 38 $\mu C/cm^2$ for MS sample whereas it is 30 $\mu C/cm^2$ for conventional one.

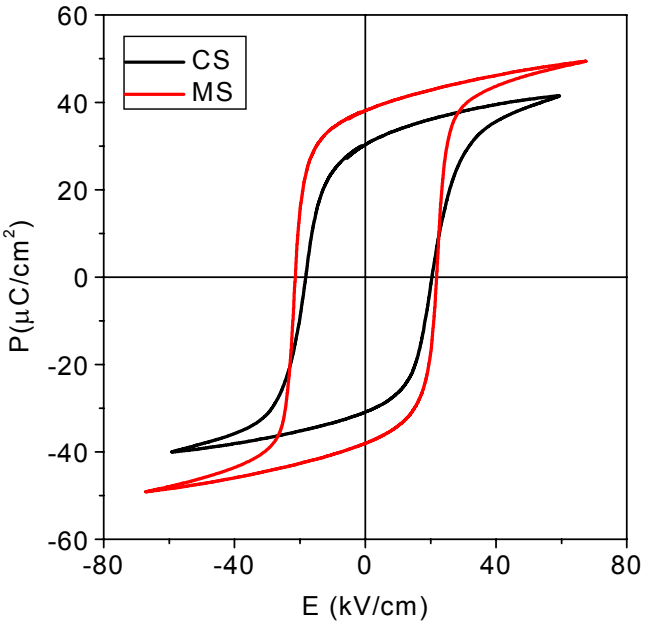

Fig. 6.14: The typical P - E hysteresis loops for CS and MS samples

The values of piezoparameters, d_{33}, k_p, k_t and k_t/k_p are given in table 6.4. There is little change seen in the value of d_{33} for MS and CS samples. It is observed that the value of k_t increases slightly and k_p decrease to the value of 0.012 resulting in an increase in electromechanical anisotropy (k_t/k_p) in case of microwave-sintered sample. This increase may be attributed to the change in the microstructure in case of microwave sintered

sample [29]. Table 6.5 shows the comparison of k_t and k_p for our MS and CS samples with the values reported by others. Although k_t for our CS sample is slightly lesser than the value observed by S.Y. Chu et al., but k_p is also less resulting in the increase in k_t/k_p ratio. Also for MS sample, k_t and k_p shows the higher and lesser values respectively as compared to the values obtained by C.S. Chen et al. using microwave sintering.

Table - 6.4

Various parameters obtained for conventional and microwave sintered Sm modified PCT ceramics

Parameters		Conventional Sintering (CS)	Microwave Sintering (MS)
Sintering temperature (^oC)		1150 / 4 hrs	1100 / (1/2) hr
Total Cycle time (minutes)		575	134
Lattice parameters	c (Å)	3.986 ± 0.0033	3.986 ± 0.0027
	a (Å)	3.897 ± 0.0019	3.896 ± 0.0011
	c/a	1.0229 ± 0.0010	1.0231 ± 0.0007
	Volume $(Å)^3$	60.542 ± 0.0761	60.482 ± 0.0533
Theoretical Density (d_{th}) (g/cc)		6.98	6.985
Expt. Density (d_{exp}) (g/cc)		6.88	6.92
Relative density (d_{exp}/d_{th}) (%)		98.4	99.1
Average grain size (μm)		2.2	1.4
Dielectric Constant (ε') (1 kHz)		390	385
Dissipation factor (tanδ) (1 kHz)		0.01	0.009
Curie temperature (^oC)		192	192
E_c (kV/cm)		19.32	21.62
P_r ($\mu C/cm^2$)		30	38
d_{33} (pC/N)		76	78
k_p (%)		2	1.2
k_t (%)		54	60
k_t/k_p		27	50

Table - 6.5

The comparative study of k_t and k_p with earlier results of PT - based systems

Compositions	Conventional Sintering (CS)			Microwave Sintering (MS)			
	Sintering Temperature (^oC)	k_t (%)	k_p (%)	Sintering temperature (^oC)	k_t (%)	k_p (%)	Ref.
$(Pb,Ca)(Co,W)TiO_3$	1200	52	5-20	-	-	-	[30]
$(Pb,Sr)(Co,W)TiO_3$	1200	45	10-20	-	-	-	[30]
$(Pb,Ba)(Co,W)TiO_3$	1200	36	10-20	-	-	-	[30]
$(Pb,Sm)(Ti,Mn)O_3$	1240-1280	50	3-5	-	-	-	[7, 31, 32, 29]
$(Pb,La)(Ti,Mn)O_3$	1280	47	9	-	-	-	[7]
$(Pb,Nd)(Ti,Mn)O_3$	1280	46	6.5	-	-	-	[7]
$(Pb,Gd)(Ti,Mn)O_3$	1280	49	5	-	-	-	[7]
$(Pb,Cd_{0.13},Sm)(Ti,Mn)O_3$	1150	56.2	3.8	-	-	-	[33]
$(Pb,Ca)(Co,W)TiO_3$	1200	52	-	1150	48	-	[27]
$(Pb,Sm_{0.08},Ca)(Ti,Mn)O_3$	1150	54	2	1100	60	1.2	Our sample

6.2 Comparative Study of Mechano-chemical Alloying and Conventional Dry Ceramic Method

Mechano-chemical alloying (MCA), which is also known as high-energy ball milling, was invented with an initial attempt as a method to develop dispersion-strengthened high temperature alloys and now a these days, it is also finding use for synthesizing lead titanate powders [34]. The most important advantage of the mechano-chemical alloying is that it can be used to synthesize designed compound at room temperature with a grain size in the nanometer scale. This characteristic is especially important to lead containing materials, because the lead oxide has a great volatility at an elevated temperature and is toxic. The volatility of lead makes the composition of the designed materials deviate from its stoichiometry.

Hence, in this section, we report an alternative approach to synthesize Sm modified PCT ceramics with compositional formula $Pb_{0.70}Sm_{0.06}Ca_{0.24}Ti_{0.98}Mn_{0.02}O_3$ (PSCT) via reaction sintering of a partially reacted oxide mixture produced by mechano-chemical alloying and their structural, dielectric and electromechanical properties have been discussed and compared with those prepared by conventional technique.

6.2.1 Structural Properties

Table 1 shows the values of particle size of the wet milled and dry milled powders. It was observed that after dry milling (30 min), the average particle size was 0.74 μm as compared to the wet milled powder having the particle size of 1.3 μm. This reduction in the particle size can be explained as follows: During mechano-chemical process, mechanical energy was subjected to milled powders by high strength collision and high-pressure impact between the milling media and the milled powder. This high-pressure is enough to break down the particles of the powders and further refine the grains. Even though the overall temperature of the high-energy ball milling system does not exceed 70^oC [34, 35, 36], the temperature of the localized point of collision may be much higher than 70^oC, which is sufficient to initiate the phase formation. XRD pattern showing the initiation of perovskite phase formation in our MCA powder is depicted in the fig. 6.15. The high-energy ball milling also induces structural defects and disorder. All these

factors favour diffusion and atomic rearrangements of the milled powder at very low temperature [35].

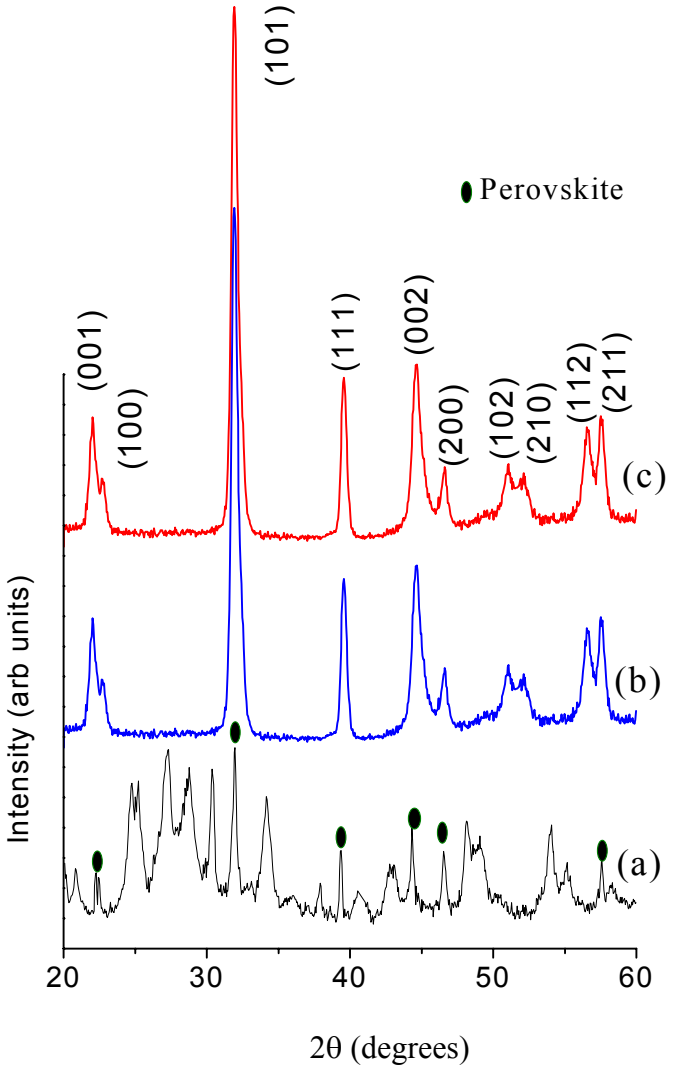

Fig. 6.15: XRD patterns of (a) MCA sample before sintering (b) MCA sample after sintering and (c) Conventional sample after sintering

XRD patterns for the sintered samples prepared with conventional and MCA processes are shown in fig. 6.15. Both the specimens reveal a single-phase formation with a tetragonal structure. MCA sample showed higher peak intensities as compared to the normal one. The

lattice parameters (c, a) and c/a ratio were calculated using 'XLAT' software and the values are given in table 6.6. Lattice anisotropy, c/a ratio, found to be slightly higher for MCA sample, which may be due to the enhanced reaction kinetics.

Fig. 6.16 shows the SEM results of the fractured surface of modified PCT ceramics (a) with conventional and (b) MCA sintered at 1150^{o}C for 4 hrs. There is an obvious difference in the microstructures of both the samples. MCA sample has relatively better uniformly developed grains as compared to conventionally prepared sample. Also, there is a minor improvement in relative density for MCA sample as shown in table 6.6. The average grain size for the MCA sample (~ 1.4 μm) was lower than the grain size of the sample prepared by normal milling, which was ~ 2.2 μm.

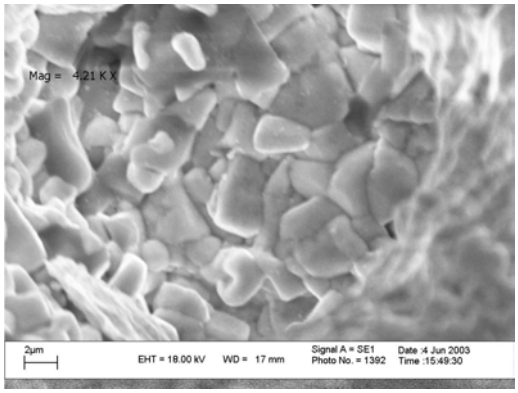

Conventional

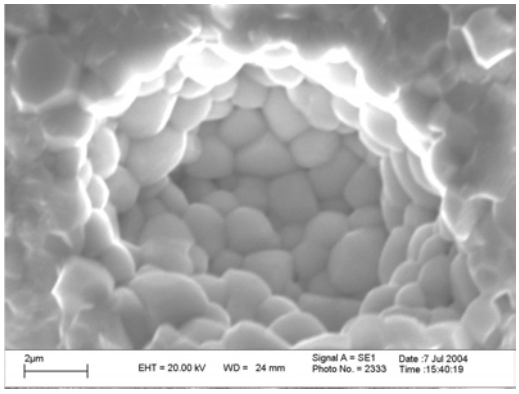

MCA

Fig. 6.16: Scanning Electron Micrographs of fractured surfaces of conventional and MCA samples

6.2.2 Dielectric and Hysteresis Behaviour

The temperature variation of dielectric constant (ε') and dissipation factor (tanδ) for conventional and a MCA sample at different frequencies is shown in fig. 6.17 and 6.18. The dielectric constant for MCA sample reaches to 5725 at a Curie temperature of 234^{o}C and 4848 at a Curie temperature of 247^{o}C for conventionally prepared sample at 1 kHz. There is no obvious frequency dispersion in the dielectric constant variation. Value of ε'_{max} for MCA sample is higher as compared to the ε'_{max} for the normal sample. The peak width also decreased slightly for MCA sample, which may be due to better compositional homogeneity. There is a decrease in the dielectric loss at T_c for MCA prepared sample. The dispersive loss at higher temperature is probably due to localized ionic conductivity [37]. Dielectric constant at room temperature (ε'_{rt}) is higher for MCA sample than that for normal one. This increase in dielectric constant may be due to the decrease in the grain size. Decrease in the dielectric constant with the increase in grain size has been reported by Kang et al. [38] where the grain size was smaller than 2.7 μm and similar results are reported for polycrystalline ferroelectric ceramics such as $BaTiO_3$ and PLZT [39].

Fig. 6.19 shows typical hysteresis loops obtained on the specimen prepared by conventional and MCA methods. The values of saturation polarization (P_{sat}), remnant polarization (P_r), coercive field (E_c) and remnant ratio of the Sm modified PCT are given in table 6.6. For the conventionally processed sample, the remnant polarization value (P_r) is 10 μC/cm^2, while the coercive field (E_c) and P_{sat} are 21 kV/cm and 18 μC/cm^2, respectively. The value of P_r and E_c increase to 21 μC/cm^2 and 26 kV/cm, respectively, for the MCA prepared sample. The higher value of E_c for MCA sample can be attributed to the decrease in grain size. The remnant ratio (P_r/P_{sat}) is ~ 0.7 for the MCA prepared sample whereas it is ~ 0.55 for the normal one.

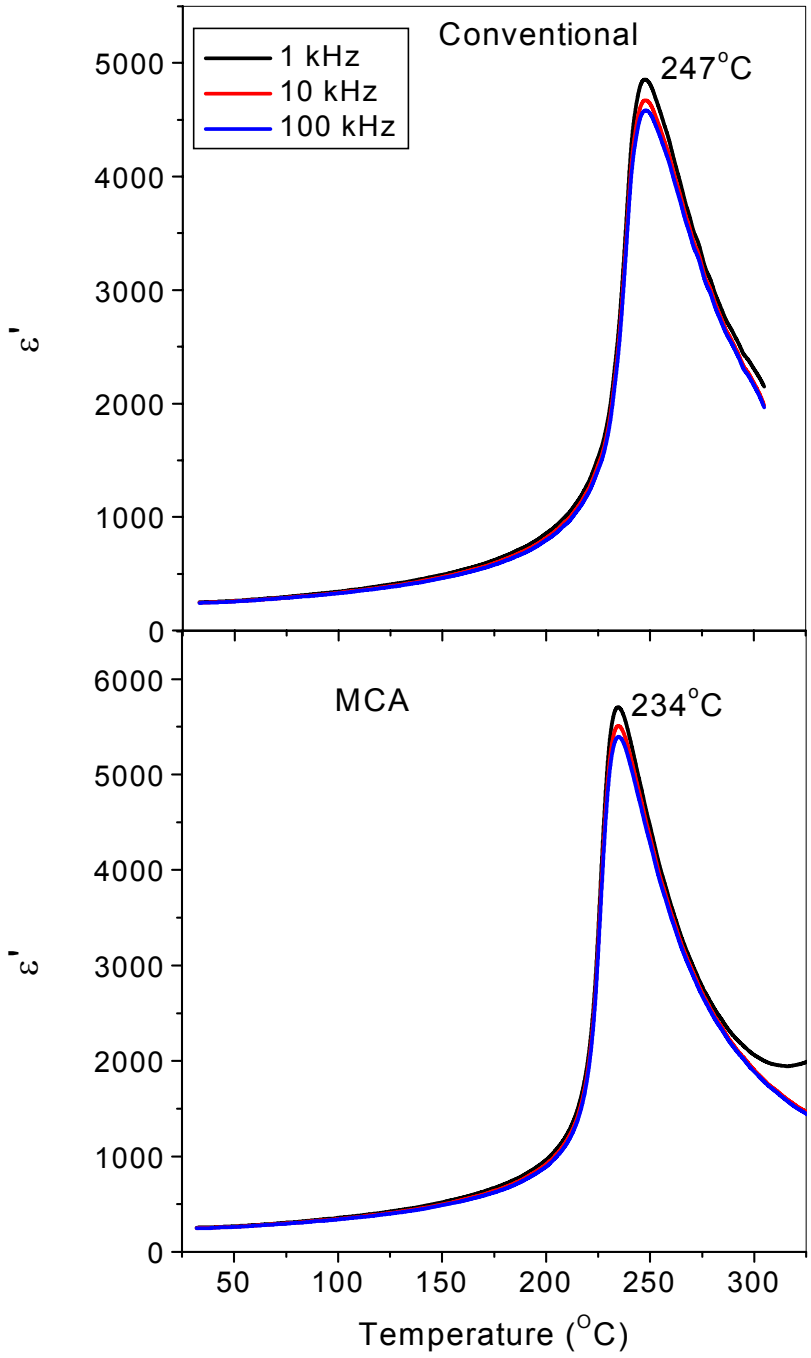

Fig. 6.17: Temperature dependence of ε' at different frequencies for the samples prepared by conventional and MCA methods

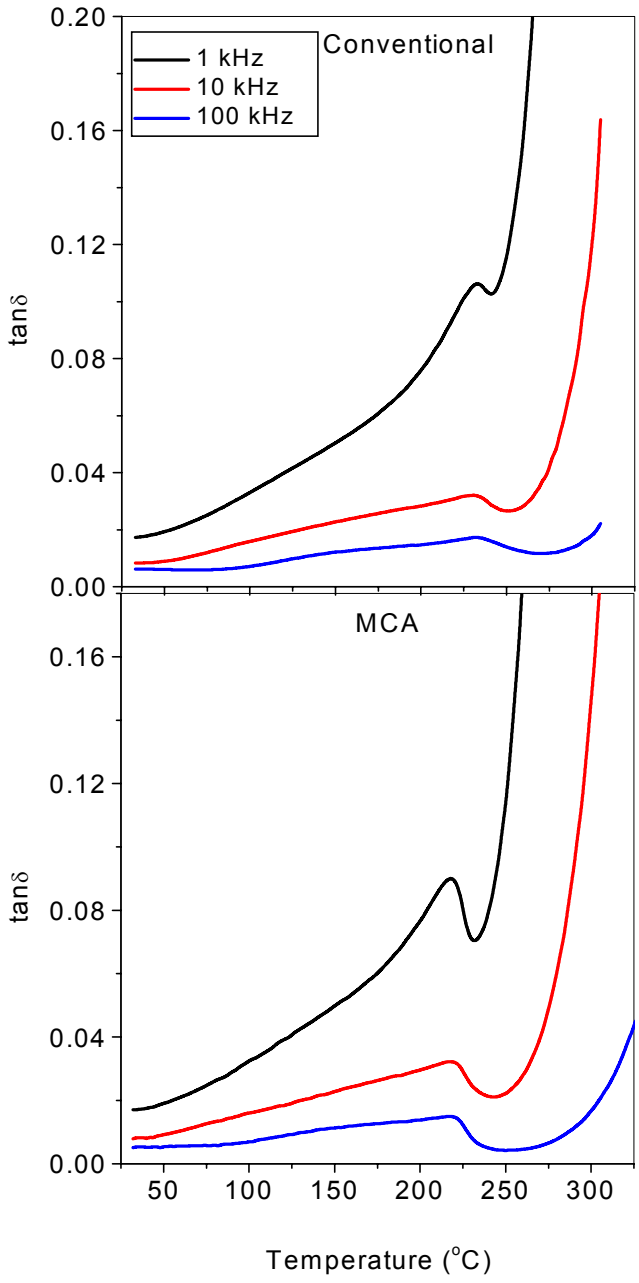

Fig. 6.18: Temperature dependence of tanδ at different frequencies for the samples prepared by conventional and MCA methods

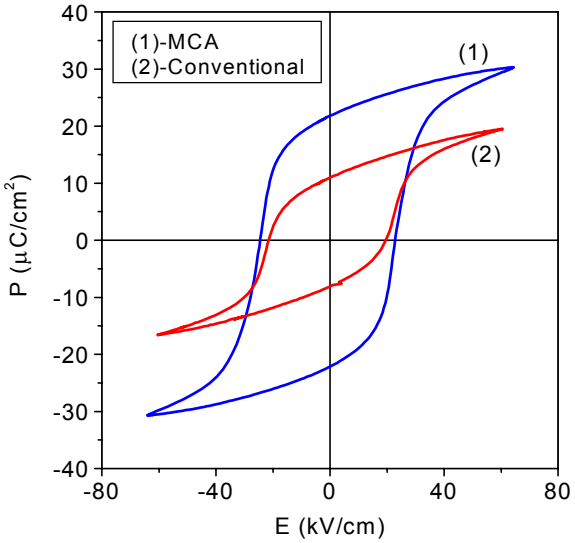

Fig. 6.19: The typical P - E hysteresis loops for conventional and MCA prepared samples

6.2.3 Piezoelectric Properties

The piezoelectric coefficients (d_{33}, d_{31}, g_{33}, g_{31}, d_h and g_h) and piezoelectric anisotropy (d_{33} / d_{31}) of conventional and MCA samples was measured and included in table 6.6. The sample prepared by MCA gives d_{33} value ~ 120 pC/N, which is higher than the value obtained for conventionally prepared sample having a value of ~ 83 pC/N. MCA prepared sample shows higher piezoelectric anisotropy as compared to normal one. This property is advantageous for low frequency applications like hydroacoustic pressure sensors as well [40]. The values of d_h and g_h were also determined and shown in table 1. Both the samples not only show comparable but also higher values as compared to the maximum values obtained by Rittenmyer et al. [31]. Also MCA prepared sample gives the better values of both d_h and g_h as compared to the normal sample. The electromechanical coupling coefficients, k_t and k_p and their ratio k_t/k_p are given in table 1 for both the samples. The planar coupling coefficient, k_p, is almost same, but the thickness coupling coefficient, k_t shows an increase with a value of 62% resulting higher

k_t/k_p ratio as compared to normal sample. This increase in anisotropy in the piezoelectric and electro-mechanical coupling coefficients, d_{ij}, k_p and k_t for MCA sample may be attributed to the increase in tetragonal distortion (c/a), better densification and fine and uniform grain size [41]. Table 6.6 shows the comparison of k_t and k_p for our MCA and normally prepared samples with the values reported by others. k_t and k_p for our normal sample are higher and lower respectively, than the values observed by others resulting in the increase in k_t/k_p ratio. Also for MCA sample, the electromechanical anisotropy is much higher than the normal one.

Table - 6.6

Various parameters obtained for MCA and Conventionally prepared PSCT ceramics

Parameters		Conventional	MCA
Sintering temperature (^oC)		1150	1150
Lattice parameters	c (Å)	4.046	4.047
	a (Å)	3.898	3.891
	c/a	1.037	1.040
	Volume $(Å)^3$	61.497	61.281
Average particle size (μm)		1.3	0.74
Theoretical Density (d_{th}) (g/cc)		7.12	7.15
Expt. Density (d_{exp}) (g/cc)		6.94	7.00
Relative density (%)		97.4	98
Average grain size (μm)		2.2	1.4
Dielectric Constant (ε') (1 kHz)		250	260
Dissipation factor (tanδ) (1 kHz)		0.018	0.017
Curie temperature (^oC)		247	234
E_c (kV/cm)		21	26
P_r ($\mu C/cm^2$)		10	21
P_s ($\mu C/cm^2$)		18	30
d_{33} (pC/N)		83	120
$-d_{31}$ (pC/N)		3.23	4.14
$-d_{33}/d_{31}$		25.69	28.98
g_{33} ($x10^{-3}$ Vm/N)		36	41
$-g_{31}$ ($x10^{-3}$ Vm/N)		1.31	1.72
d_h (pC/N)		77	112
g_h ($x10^{-3}$ Vm/N)		34	48
k_p (%)		1.1	1
k_t (%)		57	62
k_t/k_p		51.8	62

Table - 6.7

The comparative study of k_t and k_p with earlier results of PT-based systems

Compositions	Conventional			MCA			
	Sintering Temperature (^oC)	k_t (%)	k_p (%)	Sintering temperature (^oC)	k_t (%)	k_p (%)	Ref.
$(Pb,Ca)(Co,W)TiO_3$	1200	52	5-20	-	-	-	[30]
$(Pb,Sr)(Co,W)TiO_3$	1200	45	10-20	-	-	-	[30]
$(Pb,Ba)(Co,W)TiO_3$	1200	36	10-20	-	-	-	[30]
$(Pb,Sm)(Ti,Mn)O_3$	1240-1280	50	3-5	-	-	-	[30, 31, 32, 29]
$(Pb,La)(Ti,Mn)O_3$	1280	47	9	-	-	-	[7]
$(Pb,Nd)(Ti,Mn)O_3$	1280	46	6.5	-	-	-	[7]
$(Pb,Gd)(Ti,Mn)O_3$	1280	49	5	-	-	-	[7]
$(Pb,Cd_{0.13},Sm)(Ti,Mn)O_3$	1150	56.2	3.8	-	-	-	[33]
$(Pb,Sm_{0.06},Ca)(Ti,Mn)O_3$	1150	57	1.1	1150	62	1	Our sample

References

1. R. Roy, S. Komarneni and J.L. Yang, J. Am. Ceram. Soc., **68** (1985) 392.
2. S. Komarneni and R. Roy, Mater. Lett., **4** (1986) 107.
3. Jr. W.B. Snyder, W.H. Sutton, M.F. Iskander and D.L. Johnson, Materials Research Society Proceedings, vol. 189, 1990, USA.
4. R.L. Beatty, W.H. Sutton and M.F. Iskander, Materials Research Society Proceedings, vol. 269, 1992, USA.
5. D.E. Clark, W.R. Tinga and Jr. J.R. Laia, Ceram. Trans., **36** (1993) 110.
6. P. Yung, W.J. Lee and H.G. Kim, J. Phys. Condens. Matter, **9** (1977) 9445.
7. H. Takeuchi, S. Jyomura, E. Yamamoto and Y. Ito, J. Acoust. Soc. Am., **72** (1982) 1114.
8. H. Takeuchi, D. Damjanovic, T.R. Gururaja, S.J. Jang and L.E. Cross, in proceedings of the Sixth ISAF IEEE, 1986 pp. 402.
9. J. Shenglin, Z. Xuli, W. Xiaozhen and W. Xianghong, Piezoelect. Acoust., **17** (1995) 26.
10. I. Ueda and S. Ikegami, Jpn. J. Appl. Phys., **7** (1968) 236.
11. Y. Yamashita, K. Yokoyama, H. Honda and T. Takahashi, Jpn. J. Appl. Phys. Suppl., **20** (1981) 183.
12. O.P. Thakur and C. Prakash, Phase transition, **76** (2003) 567.
13. K. Okazaki, Ceram. Bull., **63** (1984) 1150.
14. M.E. Lines and A.M. Glass, Principles and Applications of Ferroelectrics and Related Materials, Oxford, Clarendon (1979).
15. S.M. Pilgrim, A.E. Sutherland and S.R. Winzer, J. Am. Ceram. Soc., **73** (1990) 3122.
16. K. Prasad, Indian J. Eng. Mater. Sci., **7** (2000) 446.
17. L.E. Cross, Ferroelectrics, **76** (1987) 241.
18. C. Schmidt, Ferroelectrics**, 78** (1988) 199.
19. K. Carl, Ferroelectrics, **9** (1975) 23.
20. H. Takeuchi, Ceram. Bull*.,* **71** (1992) 974.
21. L.M. Toroilo, D. Damjanovic and R.E. Newnham, J. Am. Ceram. Soc., **77**

(1994) 857.

22. J.D. Frutos and B. Jimenez, Ferroelectrics, **126** (1992) 341.
23. H. Jaffe, IRE standards on piezoelectric ceramics, Proc. IRE, **49** (1961) 1161.
24. B. Jimenez, J. Mendiola, C. Alemany, D. Olmo, L. Pardo and E. Maurer, Ferroelectrics, **87** (1988) 97.
25. L. Pardo, J. Mendiola, A.M. Gonzalez and J.D. Frutose, Ferroelectrics, **94** (1989) 189.
26. J. Mendiola, L. Pardo, F. Carmona and A.M. Gonzalez, Ferroelectrics, **109** (1990) 125.
27. C.S. Chen, S.K. Lin, C.C. Chou and C.S. Chen, Integ. Ferroelectrics, **53** (2003) 443.
28. H. Zhang, S. Ouyang, H. Iiu and Y. Li, in proceedings of the Materials Research Society, Pittsburgh, PA. P. 447.
29. D. Damjanovic, T.R. Gururaja and L.E. Cross, Ceram. Bull., **66** (1987) 699.
30. T. Takahashi, Ceram. Bull., **69** (1990) 691.
31. K.M. Rittenmyer and R.Y. Ting, Ferroelectrics, **110** (1990) 171.
32. J.N. Kim, M.J. Haun, S.J. Jang, L.E. Cross and X.R. Xue, IEEE Trans. Ultrason. Ferroelect. Freq. Contr., **36** (1989) 389.
33. S.Y. Chu and T.Y. Chen, Mater. Lett., 57 (2003) 2780.
34. L.B. Kong, W. Zhu and O.K. Tan, Mater. Lett., **42** (2000) 232.
35. J. Xue, D. Wan, S.E. Lee and J. Wang, J. Am. Ceram. Soc., **82** (1999) 1687.
36. L. Takacs, Appl. Phys. Lett., **69** (1996) 436.
37. C.L. Fan, D. Ciardullo and W. Huebner, Mater. Sci. Engg. B, **100** (2003) 1.
38. B.S. Kang, G.C. Dong and S.K. Choi, J. Mater. Sci. Lett., **9** (1998) 139.
39. H.T. Chung, J.H. Cho and H.G. Kim, Jpn. J. Appl. Phys., **37** (1998) 2548.
40. K.M. Rittenmyer, R.Y. Ting and T. Henriquez, J. Acoust. Soc. Am., **79** (1986) 2073.
41. W. Wersing, K. Lubitz and J. Mohaupt, IEEE Trans. On Ultrasonics Ferroelectrics and Frequency Control, **36** (1989) 424.

Chapter VII

THIN FILMS

As there is lot of work going on ferroelectric materials in bulk form, but there are some limitations to these materials owing to the high operating voltages required, advances in thin-films fabrication technology have led to an interest in the ferroelectric thin film area. Thin films of ferroelectric are being considered for applications in numerous electronic and electro-optic devices e.g. non-volatile memories, optical waveguides, multilayer capacitors, surface acoustic wave devices and ultrasonic transducers [1-7]. Hence, in the present study, thin film of one typical composition ($Pb_{0.66}Sm_{0.08}Ca_{0.24}Mn_{0.02}Ti_{0.98}O_3$) was also attempted by laser ablation technique using the conditions mentioned in table 2.1. This chapter deals with the growth and characterization of thin films of samarium modified lead calcium titanate (PSCT) ceramics. Optimization of annealing temperature and single perovskite phase formation, structural, I-V and C-V characteristics and ferroelectric hysteresis behaviour have been described in this chapter.

7.1 X-ray Diffractions (XRD) Study

Fig. 7.1 shows the perovskite phase formation of the PSCT films with annealing temperature. PSCT films were first deposited at 450^oC, 250 mJ incident laser energy pulses. The substrate was $Pt/TiO_2/SiO_2/Si$. Films were found to be amorphous as seen in XRD. Then the films were annealed to 650^oC with an interval of 50^oC for two hours and XRD was done subsequently. It was found that there was no phase formation up to 550^oC, but at 600^oC the phase formation starts. The films were further annealed at 650^oC for two hours and XRD analysis confirmed the single perovskite phase formation. Thus, this temperature was assumed as optimized temperature for further growth of the PSCT films.

Then the PSCT films were further deposited at different incident laser energy pulses and at a constant temperature of 450^oC. The films were then annealed at 650^oC for two hours and the normalized XRD patterns of the films are showed in fig. 7.2. From the figure, it was observed that there is <110> oriented growth of the film at 150 mJ. At 50 mJ energy

pulses, the phase formation of the PSCT starts with some additional peaks (marked by 'x'), which diminishes as the incident energy is increased. After 150 mJ, the <110> orientation of the film started diminishing and <100> orientation of the PSCT film was favoured.

Further, PSCT films were deposited at different energy pulses and at a constant temperature of 650^{o}C in-situ and single perovskite phase was again observed for all the samples as shown in fig. 7.3.

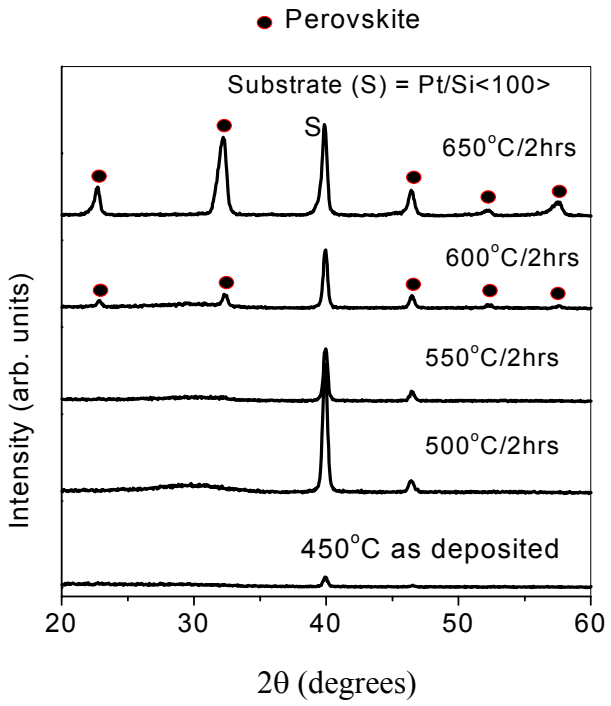

Fig. 7.1: Phase progression of PSCT films at different annealing temperatures

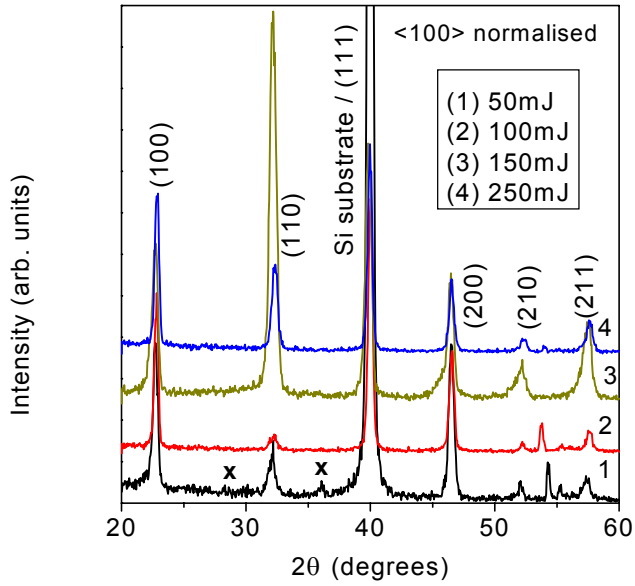

Fig. 7.2: XRD patterns of PSCT films deposited at different laser energies and annealed at 650°C

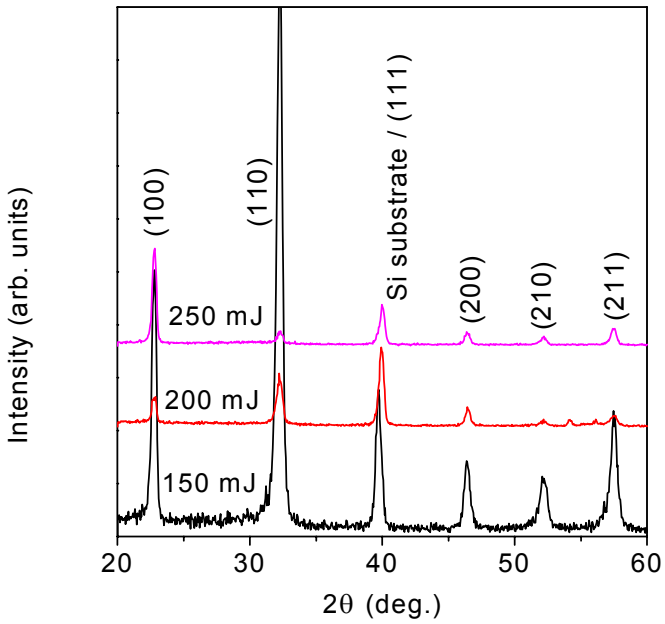

Fig. 7.3: XRD patterns of PSCT films deposited in-situ at 650°C and at different laser energies

Bottom electrodes of the films on Pt/Si substrates were created by etching the films in 10% HF solution. A metal-ferroelectric-metal (MFM) structure was made for all the films by depositing a gold electrode of 500 μm dia for electrical characterization. It was observed that out of all the films, which showed single perovskite phase, only four showed a thickness sufficient for I-V and C-V measurements. The thickness values of the four films; named as 1, 2, 3 and 4 are given in table 7.1. Other films were showing a conducting behaviour on the application of an applied voltage.

Table - 7.1
Deposition conditions and thickness of PSCT films

Film No.	Deposition parameters	Thickness (Å)
1	150 mJ, annealed at 650^{o}C	2780
2	250 mJ, annealed at 650^{o}C	3000
3	200 mJ, in-situ at 650^{o}C	2695
4	250 mJ, in-situ at 650^{o}C	4500

7.2 Current-Voltage (I-V) Characteristics

Fig. 7.4 (a-d) showed the typical Current-voltage (I-V) curves of the films deposited in different conditions as mentioned in the table 1. As seen from the fig. 7.4a & 7.4b, there is no shift in current near the zero bias. However, a shift near the zero field is seen for the films deposited in-situ at 650^{o}C. This shift may be due to the presence of space-charge regions (SCR) between the electrode and the PSCT. Here again the bottom electrode is Pt and the top electrode is Au. This MFM structure should be considered in terms of two back-to-back Schottky diodes with a ferroelectric material in between [8]. Also, the I-V curves are asymmetric and are similar as reported [9].

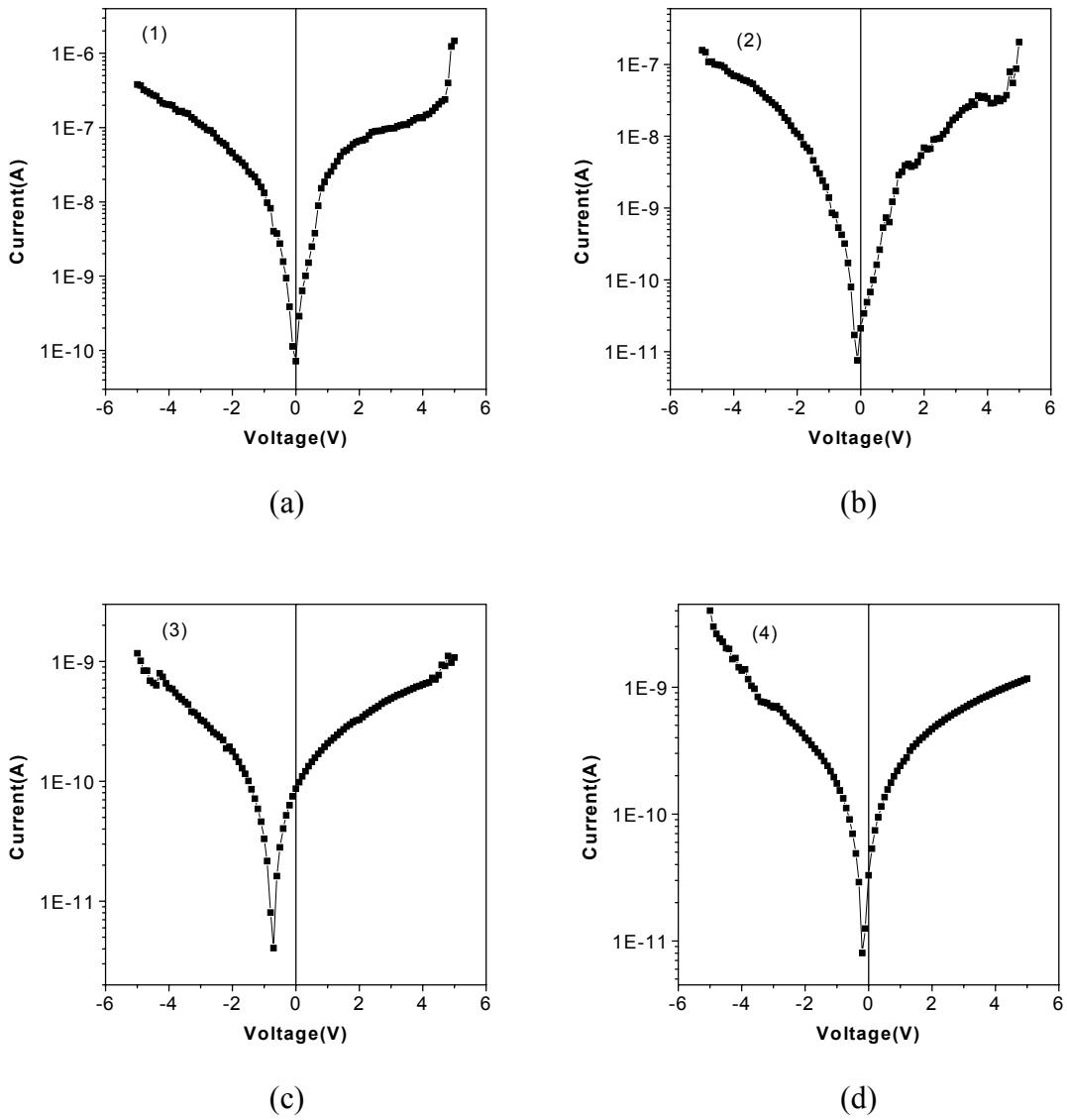

Fig. 7.4: I-V characteristics of an Au/PSCT/Pt MFM structure

7.3 Microstructural Study

Fig. 7.5, 7.6 and 7.7 show the AFM micrographs for the substrate (3-D view) used to deposit the films, 2-D and 3-D views of the films, respectively deposited by laser ablation technique under various conditions. AFM images are characterized by average surface roughness (R_a) with a uniform crack free, densely packed microstructure. The surface roughness of the PSCT films is calculated using the equipment's software. All the films

have shown nano-size average surface roughness (R_a). The values of surface roughness are given in table 7.2. The surface roughness of the substrate was observed as 3.57 nm. The lowest value of R_a was observed for the film 3, which was deposited in-situ at 650^{o}C and at 200 mJ incident laser energy pulses. The Crystallinity of the films has improved for the films deposited in-situ. It is clearly seen that deposition of the films are dependent on the microstructure of the substrate. The films 1 & 2 however, show smooth surface morphology and nucleation of the film. In the case of films 3 & 4, the microstructure is clear and distinct and thickness of the film looks uniform through out. The string like pattern in the film 3 & 4 is basically the substrate effect as is clear from the substrate AFM. From the 2-D (Plane view) micrograph the value of grain size was estimated as (1) 0.7 μm, (2) 0.9 μm, (3) 0.25 μm and (4) 1.1 μm. The values obtained in the present case are consistent with the values reported earlier [10].

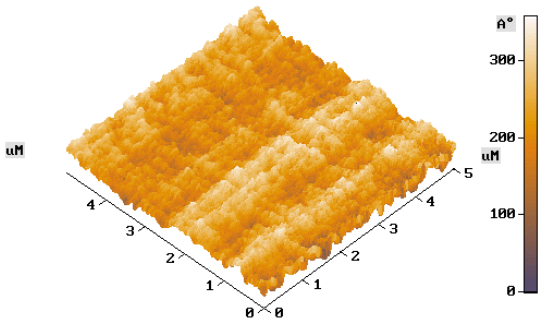

Fig. 7.5: Atomic Force Micrographs (3-D view) of Pt/TiO_2/SiO_2/Si substrate

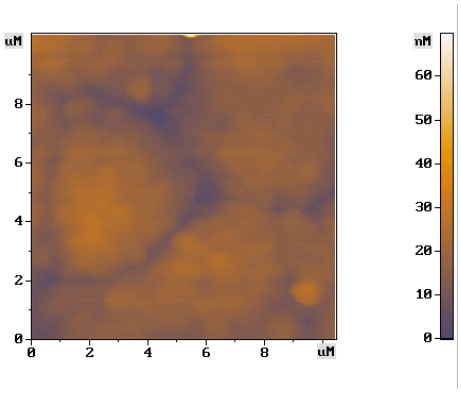

(a) Film No. 1

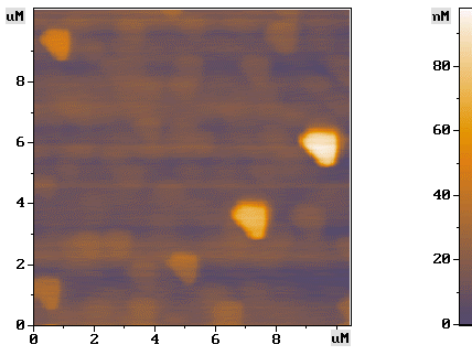

(b) Film No. 2

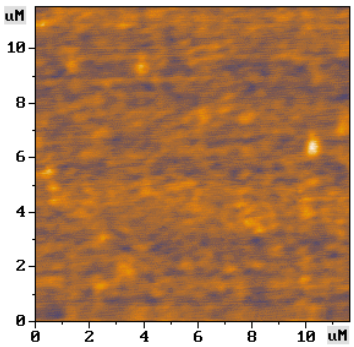

(c) Film No. 3

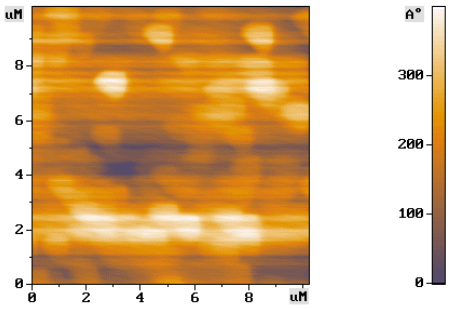

(d) Film No. 4

Fig. 7.6: Atomic Force Micrographs (2-D views) of PSCT films

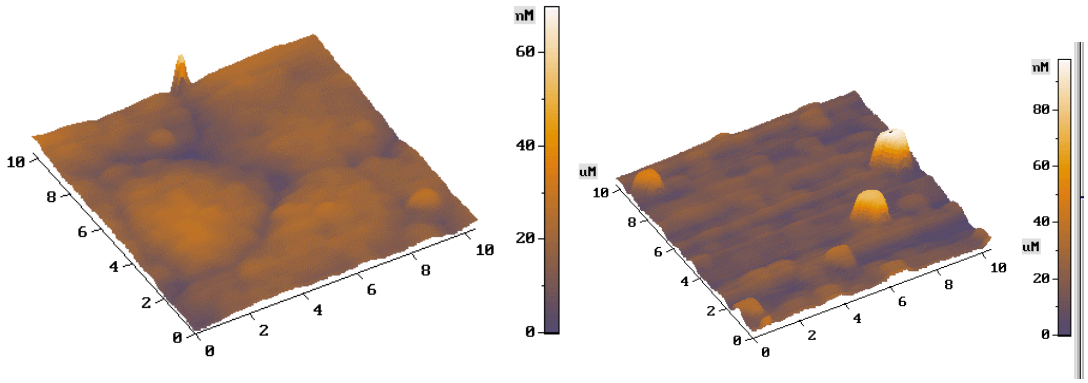

(a) Film No. 1 (b) Film No. 2

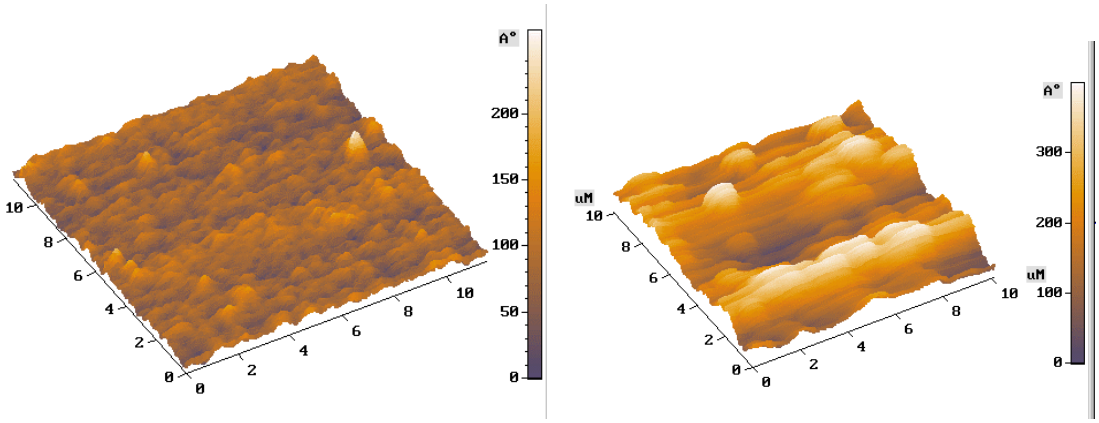

(c) Film No. 3 (d) Film No. 4

Fig. 7.7: Atomic Force Micrographs (3-D views) of PSCT films

7.4 Ferroelectric Hysteresis Behaviour

The ferroelectric hysteresis loops of PSCT thin films are shown in fig. 7.8 (a-d). The values of remnant polarization (P_r) and Coercive field (Ec) of the films are given in table 7.2. It was found that the film 1, which was deposited at 450^{o}C at 150 mJ and annealed at 650^{o}C, shows good ferroelectric properties with highest value of P_r and lowest value of Ec as compared to other films. It is reported that the value of P_r increases with decrease in surface roughness [11]. Further a decrease in the Pr may be attributed to the formation of space charge region (SCR) [8]. Film 4 shows lossy behaviour. The actual reason for this lossy behaviour is not understood but this behaviour may be due to relatively larger surface roughness, thickness and SCR. Also as it can be seen from the figure 7.8, the hysteresis curves for all the films show shift along polarization as well as field axes. The shift in the coercive field in the films suggests the presence of some internal bias due to different electrode interfaces (different work functions, probably different densities of interface states acting as traps) [12].

Table - 7.2

Coercive field (E_c), remnant polarization (P_r) and surface roughness (R_a) of the PSCT films grown by laser ablation technique

Film No.	Ec (kV/cm)	P_r ($\mu C/cm^2$)	R_a (nm)
1	170	11.5	3.6
2	120	4.0	5.4
3	155	6.5	1.9
4	220	9.0	6.0

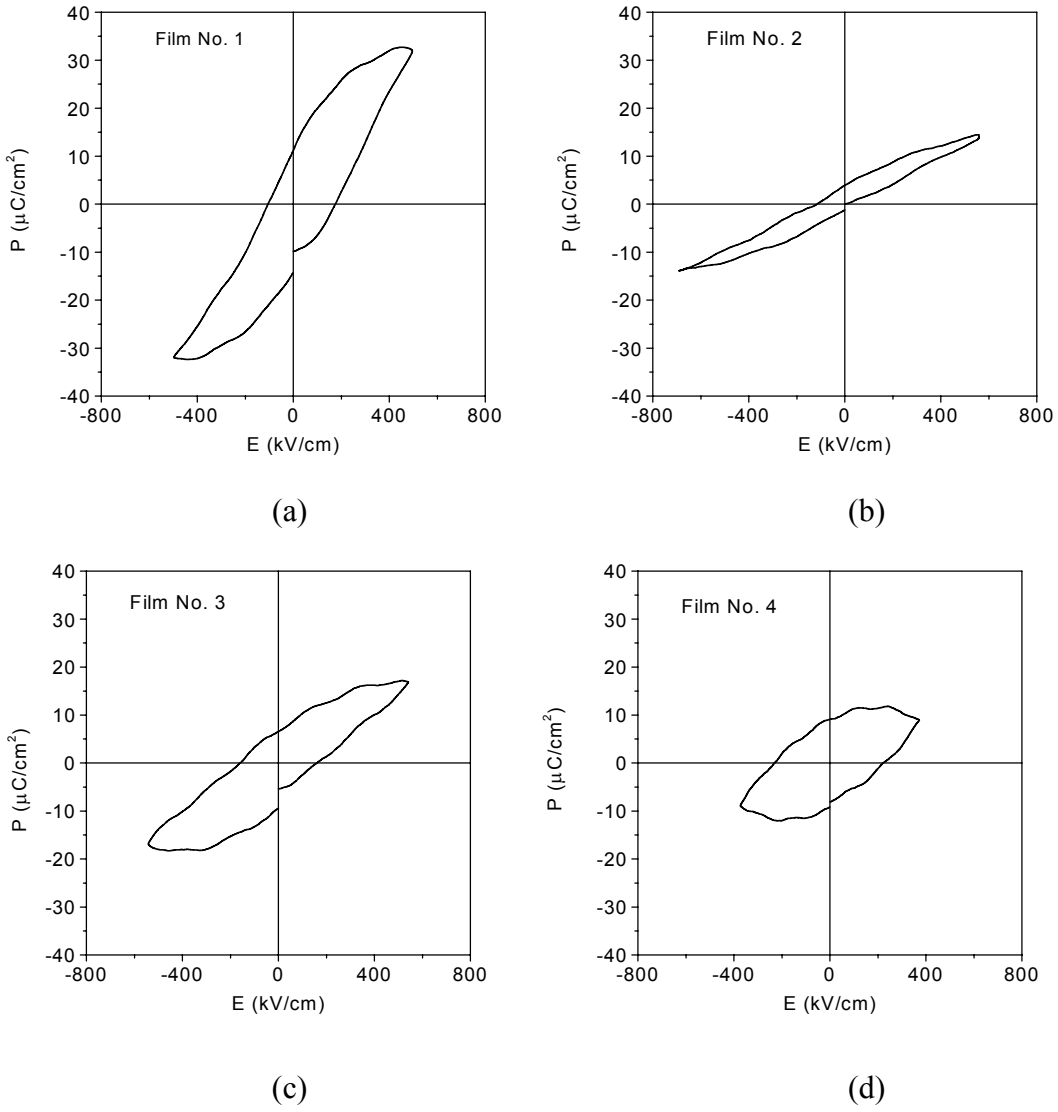

Fig. 7.8 (a-d): P-E hysteresis loops of Au/PSCT/Pt capacitor structure

7.5 Capacitance-Voltage (C-V) Characteristics

The C-V curves for the films are shown in fig. 7.9 and 7.10. All curves have the typical butterfly shape with two maxima that should correspond to the coercive filed values [13] however, in case of film 2, the change in the capacitance with the application of voltage is very small in the region from –0.75V to +0.75V. Also, the values of coercive field obtained from C-V curves found to be much lower than the values obtained from P-E curves (table 7.3). At this point, it is worth noting that the C-V curve is measured applying a dc bias (the ac testing signal is small), which means that space-charge regions may develop near the contacts and follow the bias even if the kinetics of this process is slow. If this happens, the internal electric field present in SCR can impede the polarization reversal. Thus, the film thickness acting as a real ferroelectric should be considerably reduced [8].

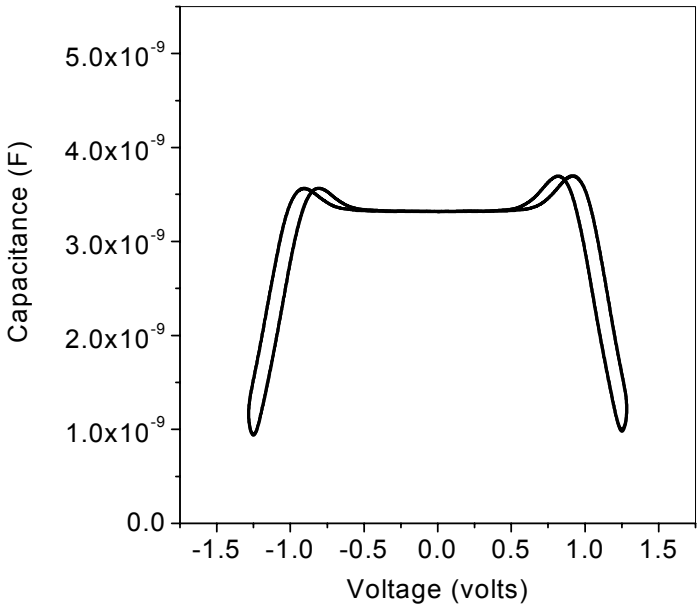

(a)

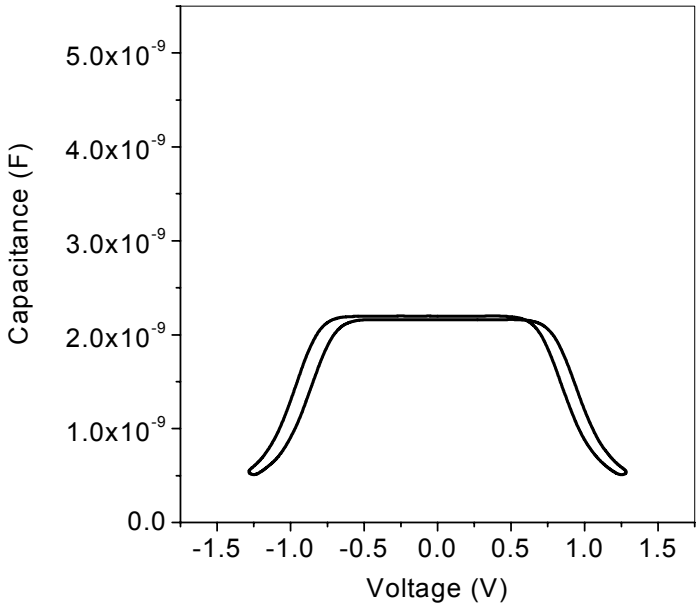

(b)

Fig. 7.9: C-V characteristics for Au/PSCT/Pt capacitor of (a) film no. 1 and (b) film no. 2

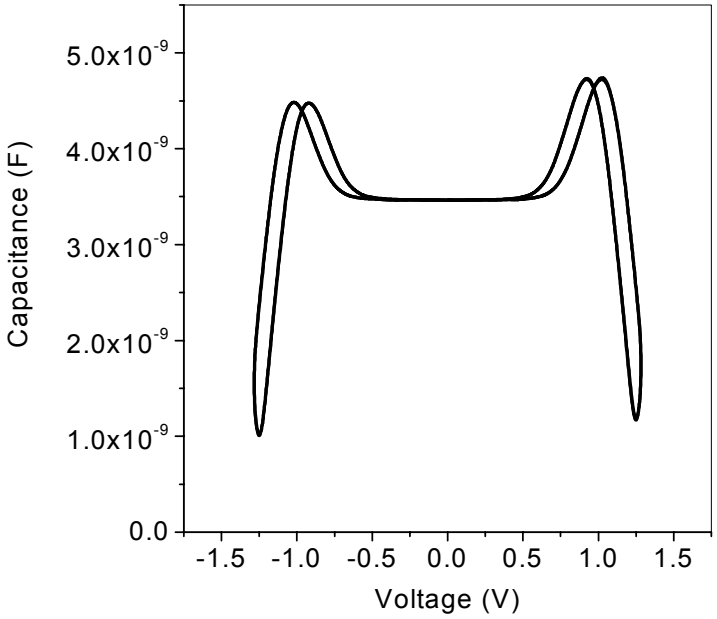

(c)

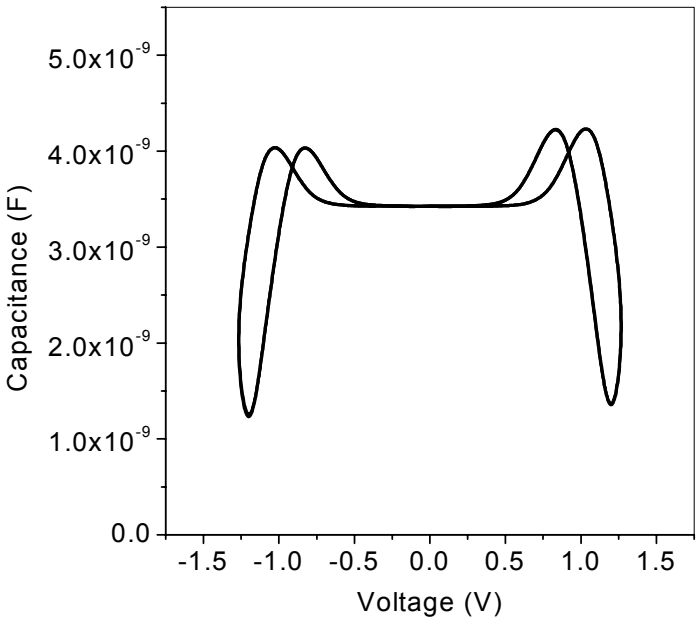

(d)

Fig. 7.10: C-V characteristics for Au/PSCT/Pt capacitor of (a) film no. 3 and (b) film no. 4

Table 7.3

A comparison of the values of E_c obtained from the C-V and P-E curves for the PSCT films deposited at different conditions

Film No.	E_c (kV/cm) from C-V curve	E_c (kV/cm) from P-E curve
1	65	170
2	55	120
3	46	155
4	72	220

References

1. E. Cattan, T. Haccart, G. Velu, D. Remiens, C. Bergaud and L. Nicu, Sens. and Actuat., **74** (1999) 60.
2. T. Kanda, T. Morita, M.K. Kurosawa and T. Higuchi, Sens. and Actuat., **83** (2000) 67.
3. D.L. Polla, Microelectron. Engg., **29** (1995) 51.
4. M. Kochli, C. Wuethrich, K. Brooks, B. Willing, M. Forster, P. Muralt, N. Setter and P. Ryser, Sens. and Actuat. A, **61** (1997) 147.
5. D.S. Paik, A.V. Prasadarao and S. Komarneni, Mater. Lett., **32** (1997) 97.
6. A. Kholkin, A. Seifert and N. Setter, Appl. Phys. Letter., **72** (1998) 3374.
7. S.R. Shannigrahi, R.N.P. Choudhary and H.N. Acharya, J. Appl. Phys., **85** (1999) 1713.
8. I. Boerasu, L. Pintilie, M. Pereira, M.I. Vasilevskiy and M.J.M. Gomes, J. Appl. Phys., **93** (2003) 4776.
9. C. Shudhama, A.C. Campbell, P.D. Maniar, R.E. Jones, R. Moazzami, C.J. Mogab and J.C. Lee, J. Appl. Phys., **75** (1994) 1014.
10. S. Chopra, Ph.D. Thesis, IIT Delhi, 2004.
11. S.K. Pandey, A.R. James, C. Prakash, T.C. Goel and K. Zimik, Mater. Sci. Engg. B, **112** (2004) 96
12. J. Lee, C.H. Choi, B.H. Park, T.W. Noah and J.K. Lee, Appl. Phys. Lett., **72** (1998) 3380.
13. R.T. Liang, Z.L. Tao, L.L. Tian and L.Z. Jian, J. Phys. D: Appl. Phys., **33**, (2000) L77.

Chapter VIII

CONCLUSIONS AND RECOMMENDATIONS

Present work deals with the synthesis and characterization of modified PCT ceramics both in bulk and thin film forms. The modification of these ceramics was carried out by substituting Sm^{3+} and La^{3+} ions in A site and Ta^{5+} ions in B site. This substitution was undertaken with a view to know the suitability of the substituting elements for the enhancement of various structural, dielectric, ferroelectric and piezoelectric properties of PCT ceramics. The samples in bulk form were synthesized by conventional dry ceramic method and also by using novel techniques namely; microwave sintering and mechanochemical alloying. The advantages of the novel techniques over conventional method are also discussed. Thin films of typical composition ($Pb_{0.66}Sm_{0.08}Ca_{0.24}Mn_{0.02}Ti_{0.98}O_3$) were prepared by pulsed laser deposition process and characterized for their structural and electrical properties. Characterization results are suggestive of the suitability of modified PCT ceramics for various applications. The conclusions drawn from the present investigations as follows: -

8.1 Conclusions

- For Sm and La modified PCT series, relative density increases from ~ 95% to ~ 98.5% of the theoretical density at relatively lower sintering temperature of 1150^{o}C with soaking time of 4 hrs for increase in their concentrations in PCT ceramics. Also there is a little change observed in the relative densities of two different La substituted series whereas no significant change is observed if we compare the Sm substituted series made by two different formulations (mentioned in section 2.4.1a). An opposite trend is observed in the case of Ta substitution where relative density decreases from ~ 95% to ~ 79% of the theoretical density.
- XRD studies at various calcination temperatures confirm the onset of perovskite phase at 450^{o}C and complete phase stabilization at a calcination temperature of 850^{o}C with 4 hrs soaking time for modified PCT ceramics.

- XRD studies confirm the single perovskite phase with tetragonal structure for 0-8 mol% Sm and La substitution in PCT ceramics whereas Ta substituted PCT ceramics show single-phase with tetragonal structure up to 3 mol%.
- The value of lattice constant 'c' decreases and that of lattice constant 'a' increases with increase of Sm, La and Ta amount in PCT ceramics, which results in decrease in tetragonality (c/a) as revealed form the XRD studies. Also relatively large decrease in tetragonality is observed for Sm and La substitution as compared to Ta substitution.
- Microstructural study reveals that almost uniform grain growth and grain compaction with well-defined grain boundaries is observed with the increase in substitution of Sm and La in PCT ceramics whereas for Ta substituted PCT series microstructure is indicative of porous material. The average grain size varies between 1.2-3.2 μm for series A, 1.2-2.2 μm for series B, 1.2-2.5 μm for series C, 1.2-2.3 μm for series D and 1.2-0.9 μm for series E.
- Dilatometric study can be one of the tools for optimising the sintering temperature and soaking duration.
- Dilatometric studies of green samples show that relatively more shrinkage (~ 16-20%) was observed for the Sm and La substituted PCT samples as compared to the shrinkage (~ 10%) observed in Ta substituted samples. Also it is observed that viscous flow of matter and volume diffusion from grain boundaries are the dominating shrinkage mechanisms in the first 10 minutes and rest of the period of isothermal shrinkage, respectively.
- XRD studies can be correlated to the dilatometric behaviour for the study of perovskite phase progression in modified PCT ceramics.
- Both dielectric constant (ε') and loss (tanδ) show decreasing trend with increase in frequency for Sm, La and Ta substituted PCT series at room temperature.
- Room temperature dielectric constant shows an increasing trend as we increase the amount of various substituents (Sm, La and Ta) in pure PCT ceramics. Curie transition temperature found to decrease with the increase in the amount of Sm, La and Ta. In contrast to Sm and La substituted PCT samples, no significant decrease in T_c is observed with the increase in the amount of Ta, as there is little increase in the dielectric constant in the Ta substituted PCT series at room temperature.

- In contrast to the increase of dielectric constant, the room temperature loss factor (tanδ) shows a decreasing trend with increasing amount of Sm and La in PCT ceramics, whereas it increases for Ta substitution.
- As typical of normal ferroelectrics, dielectric constant increases gradually with increment in the temperature and passes through a maximum (Curie temperature, T_c) and then decreases due to the phase transition from ferroelectric to the paraelectric phase in Sm, La and Ta substituted PCT ceramics.
- On the comparison of the two series of Sm (Series A and B) and two series of La (series C and D) with each other, it is observed that the change in Curie temperature is significant for the Sm substituted series as compared to the La substituted series, which may be due to the significant change in the lattice anisotropy in the two Sm substitutes series.
- The value of diffusivity, γ, is found to increase with the increase in the amount of Sm, La and Ta in the PCT ceramics.
- The value of Curie temperature obtained from both dilatometric heating and dielectric study are compared and it is observed that both values are in good agreement with each other for Sm, La and Ta in the PCT ceramics.
- Polarization vs. electric field (P-E) loops are obtained for all the compositions except the samples substituted with Ta because of their high porosity and low resistivity. Well-defined ferroelectric behaviour is observed. The values of coercive field (E_c) and remnant polarization (P_r) were determined from the P-E loops. The off-valent donors (Sm^{3+} and La^{3+}) are compensated by A site (Pb^{2+}) vacancies resulting in the softening of PCT material with low coercive field and high remnant polarization. Also on comparing the two series of Sm (series A and B) and two series of La (series C and D) with each other, then it is observed that the change in the values of E_c and P_r is more for the Sm substituted series as compared to the La substituted series.
- The values of piezoelectric charge coefficients (d_{33}, d_{31}), piezoelectric voltage coefficients (g_{33}, g_{31}), hydrostatic coefficients (d_h, g_h), electromechanical coupling coefficients (k_p, k_t) are obtained for all the samples. Both d_{33} and $-d_{31}$ shows an increasing trend with increasing Sm and La substitution in modified PCT series whereas they show opposite trend for Ta substituted PCT series. The value of g_{33} and

$-g_{31}$ effectively decreases with the substitution of Sm, La and Ta. Also relatively large values (in thousands) of piezo-figure of merit ($d_h.g_h$) are observed for Sm/La substituted PCT samples as compared to the values (in hundreds) for Ta substituted samples. The highest value (~ 2733) of $d_h.g_h$ is observed for the sample of series A with 6 mol% Sm substitution. Also this composition gives the highest value (~ 52) of electromechanical anisotropy (k_t/k_p) in conventionally sintered samples, which is desirable for high frequency applications.

- Both the novel techniques (microwave sintering and mechano-chemical alloying) show superior structural, dielectric, ferroelectric and piezoelectric properties than the conventionally sintered Sm modified PCT samples.
- Dense and crack free Sm modified PCT thin films have been fabricated on $Pt/TiO_2/SiO_2/Si$ substrate using laser ablation technique. XRD studies at various annealing temperatures confirm that complete perovskite-phase formation takes place at 650^{o}C. The XRD patterns for the PSCT films deposited at different incident laser energy pulses and at a constant temperature of 450^{o}C conclude that there is <110> oriented growth of the films at 150 mJ. After 150 mJ, the <110> orientation of the film started diminishing and <100> orientation of the PSCT film was favoured. Also single perovskite phase is again observed for all the PSCT films deposited at different energy pulses and at a constant temperature of 650^{o}C in-situ.
- Current-voltage (I-V) curves of the good quality PSCT films reveal that there is no shift in current near the zero bias for ex-situ annealed samples, however, a shift near the zero field is seen for the films deposited in-situ at 650^{o}C. This shift may be due to the presence of space-charge regions (SCR) between the electrode and the PSCT.
- AFM images show good microstructural quality of the films. All the films have shown nano-size average surface roughness (R_a).
- Ferroelectric hysteresis loops of PSCT films were obtained. Ferroelectric properties of the films are related with the surface roughness and space charge regions.
- Capacitance-voltage (C-V) characteristics of the films show a typical butterfly loop confirming the ferroelectric properties of these films.

8.2 Recommendations for the further work

Following recommendations for further extension of work are made: -

- For proper domain understanding, TEM study can be done.
- Dielectric and piezoelectric characterization of thin films can be made for their integration in memory devices.
- Novel techniques can be adopted for La and Ta modified PCT ceramics.
- X-ray diffraction can be studied at different temperatures.
- Dependence of grain size and other properties particularly piezoelectric parameters on sintering temperature can be studied.

ABOUT THE AUTHOR

Mr. Sarabjit Singh was born on 19th December 1976 at Naya Nangal, Punjab. He obtained his B.Sc. from H. P. University, Shimla in 1997 and M.Sc. (Materials Science) from Thapar Institute of Engineering and Technology (Deemed University), Patiala in 2000. He got Gold medal in M.Sc. He joined Solid State Physics Laboratory (SSPL), Defence Research and Development Organisation (DRDO), Delhi in 2001 as Junior Research Fellow. Presently, he is working as Senior Research Fellow at the Electroceramics Group, SSPL. His areas of research include: preparation and characterization of ferroelectric, piezoelectric and pyroelectric materials.